~~T-71-34150~~
N71-28934

Final Report

# FEASIBILITY AND CONCEPTUAL DESIGN STUDY - VIBRATION GENERATOR TRANSIENT WAVEFORM CONTROL SYSTEM

by

Jay M. LeBrun
John Favour

Prepared for

NATIONAL AERONAUTICS AND SPACE ADMINISTRATION

June 1969

Contract NAS5-15171

Technical Management
NASA Goddard Space Flight Center
Greenbelt, Maryland




Aerospace Group
THE BOEING COMPANY
Kent, Washington

Rqt 64776

# PREFACE

This report describes a feasibility and conceptual design study of a Vibration Generator Transient Waveform Control System performed by The Boeing Company from July 1968 to June 1969 under Contract NAS5-15171. The work was administered by Joseph P. Young, Structural Dynamics Branch, Test and Evaluation Division, NASA Goddard Space Flight Center.

Boeing personnel who participated in the investigation include: Darrell R. Harting, program manager; Jay M. LeBrun, principal investigator; and John Favour, research engineer. Program support was provided by: Charles Whitmore, computer programming; and James Brown, environmental laboratory operations.

The information contained in this report is also released as Boeing Document D2-114438-1.

# ABSTRACT

This report presents the results of a feasibility and conceptual design study for on-line transient waveform control of typically available electromagnetic and hydraulic vibrators. The control concept is implemented with modern digital computing algorithms and the reciprocal properties of the discrete Fourier transform using a time-invariant linear system approach. Compensation for frequency dependent distortion, due to the electrical and mechanical components of the vibration test system, produces the desired arbitrary complex transient-time history at the test article. Impulse techniques were used to define the test system transfer function. The study elements include:

1) Fourier integral transform error study;

2) Empirical results from a prototype control system;

3) Control system error analysis and test equipment limitations;

4) Conceptual design of a control system;

5) Cost estimate of the proposed system.

Successful control of an electromagnetic vibration test system initiated its immediate use to satisfy shock test requirements, per MIL 810-B specification.

CONTENTS


| | PAGE |
|---|---|
| INTRODUCTION | 1 |
| PRELIMINARY DISCUSSION | 4 |
| GENERAL OUTLINE OF APPROACH | 5 |
| FEASIBILITY STUDY RESULTS | 12 |
| Fourier Integral Transform Error Study | 12 |
| Experimental Investigation with a Transient Waveform Prototype Control System | 47 |
| Control System Empirical Error Study | 81 |
| Equipment Limitations | 112 |
| Nonlinearities | 114 |
| Conceptual Design of Control System | 129 |
| Cost Estimate of Proposed System | 132 |
| CONCLUSIONS AND RECOMMENDATIONS | 133 |
| REFERENCES | 136 |
| APPENDIX I - Error Analysis of a Transient Waveform Control System | I-1 |
| APPENDIX II - Vibration Test System Distortion Measurements | II-1 |
| APPENDIX III - Statistical Analysis of the Prototype Control System Performance | III-1 |

LIST OF ILLUSTRATIONS


| Figure | | Page |
|---|---|---|
| 1 | Transient Waveform Control Applied to Spacecraft Flight Transients | 2 |
| 2 | Transient Waveform Control Applied to MIL 810-B Shock Test Requirements | 3 |
| 3 | Transient Waveform Control, Logic Diagram | 7 |
| 4 | Terminal-Peak Sawtooth Pulse | 20 |
| 5 | Theoretical Transform-Terminal-Peak Sawtooth | 21 |
| 6 | Computed Zero-Frequency Components vs A/D Converter Word Size | 22 |
| 7 | Fourier Transform of the Terminal-Peak Sawtooth Sampled at 2,048 Samples/Second | 23 |
| 8 | Fourier Transform of Terminal-Peak Sawtooth with a Sample Record Length of 0.125 Second | 24 |
| 9 | Fourier Transform of Terminal-Peak Sawtooth with a Sample Record Length of 0.5 Second | 25 |
| 10 | Fourier Transform of Terminal-Peak Sawtooth with a Sample Record Length of 1.0 Second | 26 |
| 11 | Time History; Step-Decay Function | 27 |
| 12 | Theoretical Transform; Step-Decay Function | 28 |
| 13 | Fourier Transform of an 8-Bit Word Size Modified Step-Decay Pulse | 29 |
| 14 | Fourier Transform of a 10-Bit Word Size Modified Step-Decay Pulse | 30 |
| 15 | Fourier Transform of a 12-Bit Word Size Modified Step-Decay Pulse | 31 |
| 16 | Fourier Transform of a 14-Bit Word Size Modified Step-Decay Pulse Sampled at 16,384 Samples/Second | 32 |
| 17 | Fourier Transform of Modified Step-Decay Pulse Sampled at 2,048 Samples/Second | 33 |
| 18 | Fourier Transform of Modified Step-Decay Pulse Sampled at 4,096 Samples/Second | 34 |

LIST OF ILLUSTRATIONS (CONT)


| Figure | | Page |
|---|---|---|
| 19 | Fourier Transform of Modified Step-Decay Pulse with a Sample Record Length of 0.0078 Second | 35 |
| 20 | Shaker Impulse Response | 36 |
| 21 | Theoretical Transform of Shaker Impulse Response | 37 |
| 22 | Fourier Transform of an 8-Bit Word Size Shaker Impulse Response | 38 |
| 23 | Fourier Transform of a 10-Bit Word Size Shaker Impulse Response | 39 |
| 24 | Fourier Transform of a 12-Bit Word Size Shaker Impulse Response | 40 |
| 25 | Fourier Transform of a 14-Bit Word Size Shaker Impulse Response | 41 |
| 26 | Fourier Transform of an 8-Bit Word Size Shaker Impulse Response Utilizing the Unbias Routine | 42 |
| 27 | Fourier Transform of a 10-Bit Word Size Shaker Impulse Response Utilizing the Unbias Routine | 43 |
| 28 | Fourier Transform of 8-Bit Word Size Modified Step-Decay Pulse Utilizing the Unbias Routine | 44 |
| 29 | Fourier Transform of Shaker Impulse Response with Noise Added, With and Without Unbias Routine | 46 |
| 30 | Fourier Transforms of Shaker Impulse Response with Various Word Size, With Noise Added | 47 |
| 31 | Dynamic Data Analysis System Data Processing | 49 |
| 32 | Dynamic Data Analysis System | 50 |
| 33 | Remote Computer Test Station in Vibration Test Laboratory | 51 |
| 34 | Control System Signal Definition and Flow Diagram | 52 |
| 35 | Inter-Overlay Operational Logic versus Test Station Switch Position | 53 |
| 36 | Test System Calibration Pulse, $f(t)_i$ | 57 |

| Figure | | Page |
|---|---|---|
| 37 | Calibration Pulse, Fourier Transform Modulus, $F(\omega)_i$ | 58 |
| 38 | Calibration Pulse, Fourier Transform Phase Spectrum, $F(\omega)_i$ | 59 |
| 39 | Transient Calibration Output, $f(t)_o$ | 60 |
| 40 | Transient Calibration Output, Fourier Transform Modulus, $f(\omega)_o$ | 61 |
| 41 | Transient Calibration Output, Fourier Transform Pulse Spectrum, $F(\omega)_o$ | 62 |
| 42 | Inverse Transfer Function Modulus, $1/H(\omega) = F(\omega)_i/F(\omega)_o$ | 63 |
| 43 | Inverse Transfer Function Phase Spectrum, $1/H(\omega) = F(\omega)_i/F(\omega)_o$ | 64 |
| 44 | Required Transient Waveform, $f(t)_R$ | 65 |
| 45 | Required Transient Waveform, Fourier Transform Modulus, $F(\omega)_R$ | 66 |
| 46 | Required Transient Waveform, Fourier Transform Phase Spectrum, $F(\omega)_R$ | 67 |
| 47 | Synthesized Input Voltage, $f(t)_s$ | 68 |
| 48 | Synthesized Transient Waveform, $f'(t)_R$ | 69 |
| 49 | Synthesized Transient Waveform, Fourier Transform Modulus, $F'(\omega)_R$ | 70 |
| 50 | Synthesized Transient Waveform, Fourier Transform Phase Spectrum, $F'(\omega)_R$ | 71 |
| 51 | Synthesized Transient Waveform, $f'(t)_R$ | 72 |
| 52 | Synthesized Transient Waveform, Fourier Transform Modulus, $F'(\omega)_r$ | 73 |
| 53 | Synthesized Transient Waveform, Fourier Transform Phase Spectrum, $F'(\omega)_R$ | 74 |
| 54 | Required Transient Waveform, $f(t)_R$ | 75 |
| 55 | Required Transient Waveform, Fourier Transform Modulus, $F(\omega)_R$ | 76 |

LIST OF ILLUSTRATIONS (CONT)


| Figure | | Page |
|---|---|---|
| 56 | Required Transient Waveform, Fourier Transform Phase Spectrum, $F(\omega)_R$ | 77 |
| 57 | Synthesized Input Voltage, $f(t)_s$ | 78 |
| 58 | Synthesized Transient Waveform, $f'(t)_R$ | 79 |
| 59 | Synthesized Transient Waveform, Fourier Transform Modulus, $F'(\omega)_R$ | 80 |
| 60 | Synthesized Transient Waveform, Fourier Transform Phase Spectrum, $F'(\omega)_R$ | 81 |
| 61 | Baseline Impulse Response Function Derived from Sine Sweep | 91 |
| 62 | Vibration Control System Background Noise | 92 |
| 63 | Fourier Transform Modulus of Vibration Control System Noise | 93 |
| 64 | Time History of Transient Calibration Output $f(t)_o$ 9G Positive Peak | 94 |
| 65 | Fourier Modulus of Transient Calibration Output $f(t)_o$ 9G Positive Peak | 95 |
| 66 | Time History of Transient Calibration Output $f(t)_o$ 20.8G Positive Peak | 96 |
| 67 | Fourier Modulus of Transient Calibration Output $f(t)_o$ 20.8G Positive Peak | 97 |
| 68 | Time History of Transient Calibration Output $f(t)_o$ 32G Positive Peak | 98 |
| 69 | Fourier Modulus of Transient Calibration Output $f(t)_o$ 32G Peak | 99 |
| 70 | Unfiltered Square Wave Time History | 100 |
| 71 | Fourier Modulus of Unfiltered Square Wave with Aliasing | 101 |
| 72 | Filtered Square Wave Time History | 102 |
| 73 | Filtered (6-Pole Butterworth Filter) Square Wave Fourier Modulus | 103 |

| Figure | | Page |
|---|---|---|
| 74 | Transient Calibration Output $f(t)_o$ Truncated $\tau$ = 350 Data Points, 3,746 Zero Data Points | 104 |
| 75 | Transient Calibration Output $f(t)_o$ Truncated $\tau$ = 350 Data Points | 105 |
| 76 | Transient Calibration Output $f(t)_o$ Truncated $\tau$ = 800 Data Points, 3,296 Zero Data Points | 106 |
| 77 | Transient Calibration Output $f(t)_o$ Truncated $\tau$ = 800 Data Points | 107 |
| 78 | Transient Calibration Output $f(t)_o$ Truncated $\tau$ = 2,048 Data Points, 2,048 Zero Data Points | 108 |
| 79 | Transient Calibration Output $f(t)_o$ Truncated $\tau$ = 2,048 Data Points | 109 |
| 80 | Transient Calibration Output $f(t)_o$ Truncated $\tau$ = 4,096 Data Points, No Zero Data Points | 110 |
| 81 | Transient Calibration Output $f(t)_o$ Truncated $\tau$ = 4,096 Data Points | 111 |
| 82 | Error Model of Control System | 112 |
| 83 | Acceleration Nonlinearity Function of the G.S.F.C.-L.P.S. Hydraulic Vibrator | 118 |
| 84 | Fourier Transform of the Modified Step-Delay Pulse, Modified by the G.S.F.C.-L.P.S. Acceleration Nonlinearity Function | 119 |
| 85 | Velocity Nonlinearity Function of the G.S.F.C.-L.P.S. Hydraulic Vibrator | 120 |
| 86 | Fourier Transform of the Modified Step-Delay Pulse, Modified by the G.S.F.C.-L.P.S. Velocity Nonlinearity Function | 121 |
| 87 | Displacement Nonlinearity Function of the G.S.F.C.-L.P.S. Hydraulic Vibrator | 122 |
| 88 | Fourier Transform of the Modified Step-Delay Pulse, Modified by the G.S.F.C.-L.P.S. Displacement Nonlinearity Function | 123 |
| 89 | Acceleration Nonlinearity Function of the MB210/MB5140 System (G.S.F.C.) | 124 |

LIST OF ILLUSTRATIONS (CONT)


| Figure | | Page |
|---|---|---|
| 90 | Fourier Transform of the Shaker Impulse Response Modified by the Acceleration Nonlinearity Function of the MB210/MB5140 System | 124 |
| 91 | Acceleration Nonlinearity Function of the MB C125/MB 996A System | 125 |
| 92 | Fourier Transform of the Shaker Impulse Response Modified by the Acceleration Nonlinearity Function of the MB C125/MB 996A System | 126 |
| 93 | Acceleration Nonlinearity Function of Boeing-Ling 249/Ling PP-120/150 System | 127 |
| 94 | Fourier Transform of the Shaker Impulse Response Modified by the Acceleration Nonlinearity of the Boeing-Ling 249/Ling PP-120/150 System | 128 |
| 95 | Conceptual Design-Transient Waveform Control System | 130 |
| I-1 | Data Processing Error | I-21 |
| I-2 | Typical Fourier Transform Modulus | I-29 |
| II-1 | Vibration System Distortion | II-2 |
| II-2 | Vibration System Distortion | II-3 |
| II-3 | Vibration System Distortion | II-4 |
| II-4 | Vibration System Distortion | II-5 |
| II-5 | Vibration System Distortion | II-6 |
| II-6 | Vibration System Distortion | II-7 |
| III-1 | 19-Millisecond Comparison---"Required" and "Synthesized" Transient Waveform TAT/Agena-D Launch Vehicle (OGO-D Spacecraft), PL20 at T+234.5 | III-4 |
| III-2 | Fourier Transform Modulus of the PL-20 Required Waveform $F(\omega)_R$ | III-5 |
| III-3 | Fourier Transform Modulus of Synthesized Waveform PL-20, $F'(\omega)_R$ | III-6 |
| III-4 | Time History of Required Waveform PL-30, $f(t)_R$ | III-7 |

LIST OF ILLUSTRATIONS (CONT)


| Figure | | Page |
|---|---|---|
| III-5 | Fourier Transform Modulus of Required Waveform, $F'(\omega)_R$ | III-8 |
| III-6 | Time History of Synthesized Waveform, $f'(t)_R$ | III-9 |
| III-7 | Fourier Transform Modulus of Synthesized Waveform PL-30, $F'(\omega)_R$ | III-10 |

## SYMBOLS

| | |
|---|---|
| A | Scaling factor in (1) modified step-decay pulse ($24{,}576 \times 10^8$) and (2) shaker impulse response ($1.95 \times 10^8$) |
| a(f) | Fourier integral transform function of frequency |
| A(n) | Fast Fourier Transform function of n |
| $A_p$ | Discrete Fourier transform function of frequency |
| $A(\omega)$ | Anti-aliasing filter characteristics |
| A/D | Analog-to-digital converter |
| D/A | Digital-to-analog converter |
| e | Naperian base, 2.7182818,.. |
| $E(\omega)$ | Error term (frequency domain) in transient waveform control system |
| f | frequency |
| $f_1$ | First frequency increment before $f_R$ |
| $f_2$ | First frequency increment after $f_R$ |
| $f_R$ | Resonant response frequency observed on Fourier transform modulus plot |
| f(q)t | Quantized time history |
| f(t) | Time domain description of a function |
| $f(t)_i$ | Transient calibration input |
| $f(t)_o$ | Transient calibration output |
| $f(t)_R$ | Required waveform transient time domain description |
| $f(t)_s$ | Synthesized input voltage |
| $f_p(t)$ | Periodic function of time |
| $f_p(\omega)$ | Periodic function of frequency |
| $F_e(\omega)$ | Fourier transform error term |
| $F_q(\omega)$ | Fourier transform of quantized time history |
| $F(\omega)$ | Frequency domain description of a function |
| $F(\omega)_R$ | Frequency domain description of required waveform |
| g | Acceleration due to gravity |

| | |
|---|---|
| $h(t)$ | Impulse response function |
| $H(\omega)$ | Transfer function |
| $j$ | $\sqrt{-1}$ |
| $k$ | (1) Integer notation on Fast Fourier Transform<br>(2) $10^3$ as in 1 kHz |
| $K$ | Arbitrary constant |
| $M$ | Number of bits in a word |
| $N$ | Number of samples describing a discrete function |
| $Q$ | Number of quantizing levels |
| $R$ | Sampling rate |
| $S$ | LaPlace operator, $S = \sigma + j\omega$ |
| $T$ | Time duration of data sample |
| $X(k)$ | Fast Fourier Transform function of k |
| $x(t)$ | Fourier integral transform function of time |
| $\alpha$ | Parameter of modified step-decay function<br>$\alpha$ = 6,283 radians/sec |
| $\beta$ | Parameter of modified step-decay function<br>$\beta$ = 314.1 radians/sec |
| $\Delta$ | Small increment of a function |
| $\delta$ | Damping ratio |
| $\delta(t)$ | Impulse function |
| $\theta_1$ | Phase angle coincident with $f_1$ |
| $\theta_2$ | Phase angle coincident with $f_2$ |
| $\sigma$ | (1) rms value of a signal<br>(2) real part of LaPlace operator $S = \sigma + j\omega$<br>(3) arbitrary constant $\sigma$ = 1,758 |

SYMBOLS (CONT)

| | |
|---|---|
| $\sigma_e^2$ | Variance of error term |
| $\tau$ | Truncation length of data sample |
| $\tau_o$ | Time constant |
| $\omega$ | Radian frequency |

# INTRODUCTION

Spacecraft vibration is caused by two different sources. The first is characterized by a continuous process, such as launch booster noise or transonic buffet, and requires that the process be analyzed by harmonic analysis with a statistical consideration. The second is transient in nature and arises from impulses, such as engine starts and stops and staging operations. This type requires that the process be analyzed as a transient. The widespread practice of applying continuous sine-sweep vibration tests (generalized harmonic analysis) to spacecraft which experience transient excitation of high level is too conservative. The results of this study demonstrate that transient waveform control of electromagnetic vibration test equipment is feasible, and provides a better method of simulating a transient environment in a laboratory (Figures 1 and 2).

This final report covers the work performed under NASA Goddard Contract NAS5-15171, Feasibility and Conceptual Design Study - Vibration Generator Transient Waveform Control System. The purpose of the contract is to:

1) Perform a feasibility and conceptual design study of an on-line control system capable of operating in near real time;

2) Provide an analysis of the proposed system;

3) State considerations of adverse effects of possible nonlinearities on the control system performance;

4) Control transient waveforms at the test article, using either an electromagnetic or a hydraulic vibrator, with time duration from 0.1 millisecond to 2.0 seconds, and frequency content from 2 Hz to 5,000 Hz.

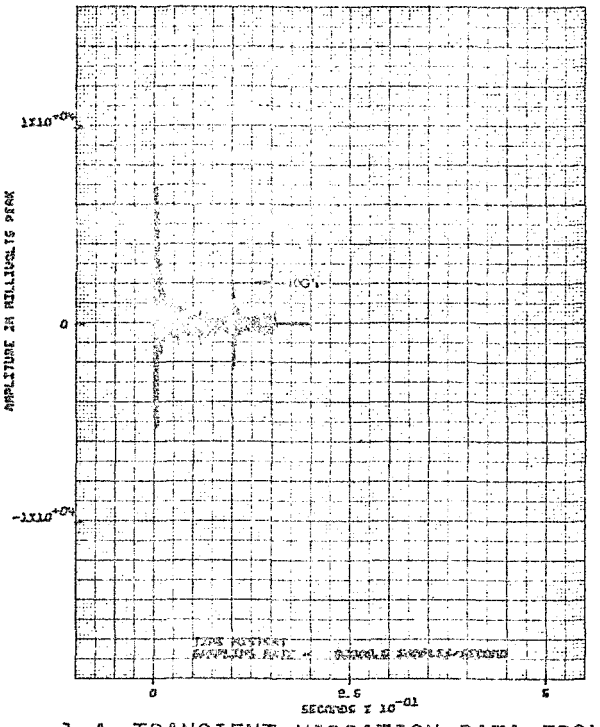


Figure 1-A: TRANSIENT VIBRATION DATA FROM THE TAT/AGENA-D LAUNCH VEHICLE (OGO-D Spacecraft), PL20 AT T+234.5

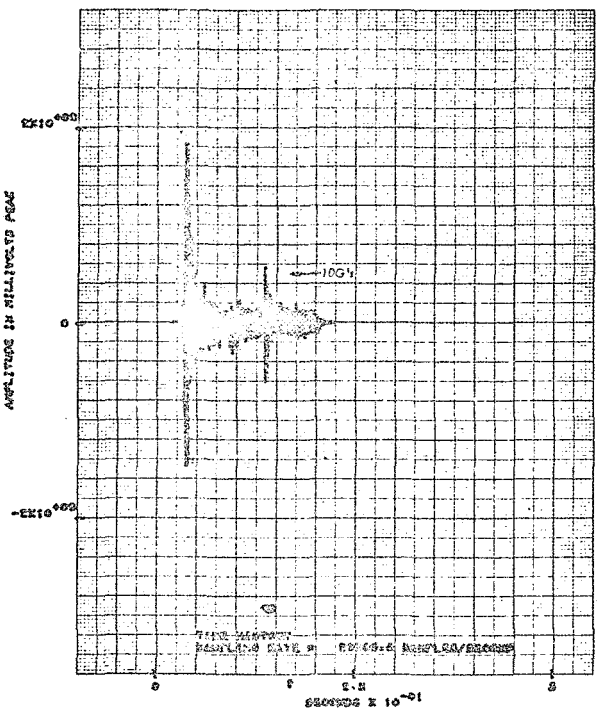


Figure 1-B: LABORATORY ELECTROMAGNETIC TEST EQUIPMENT SYNTHESIS OF OGO-D FLIGHT TRANSIENT

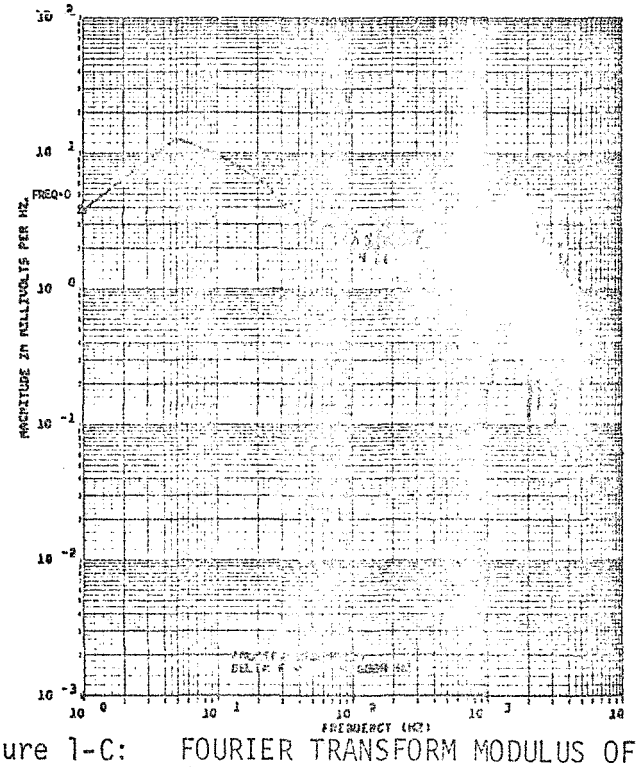


Figure 1-C: FOURIER TRANSFORM MODULUS OF OGO-D SPACECRAFT RESPONSE PL20 AT T+234.5

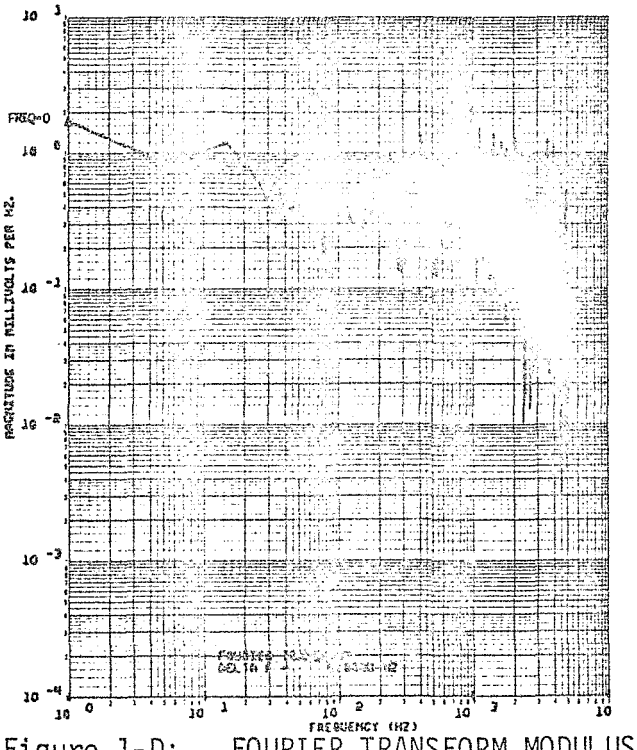


Figure 1-D: FOURIER TRANSFORM MODULUS OF LABORATORY SYNTHESIZED OGO-D FLIGHT TRANSIENT

Figure 1: TRANSIENT WAVEFORM CONTROL APPLIED TO SPACECRAFT FLIGHT TRANSIENTS
L249 Vibrator, PP120/150 Amplifier, Specimen Weight 450lb

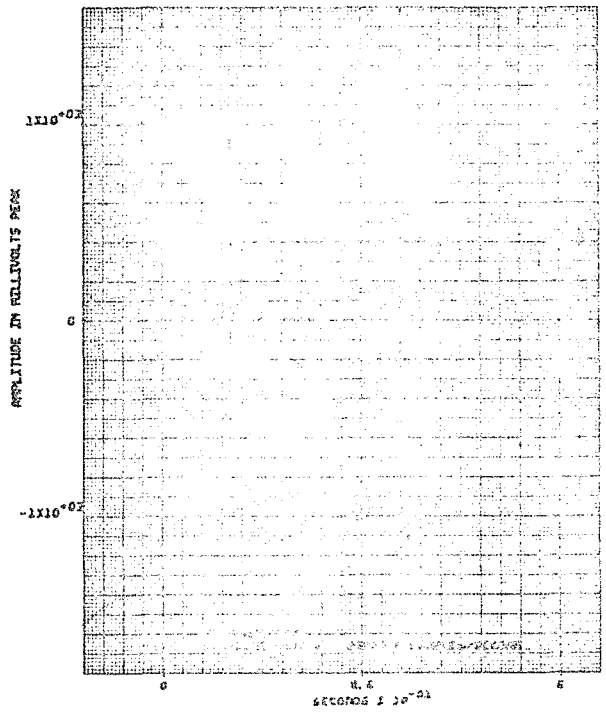


Figure 2-A: TERMINAL PEAK SAWTOOTH SPECIFICATION (MIL810-B) 50 MV/G

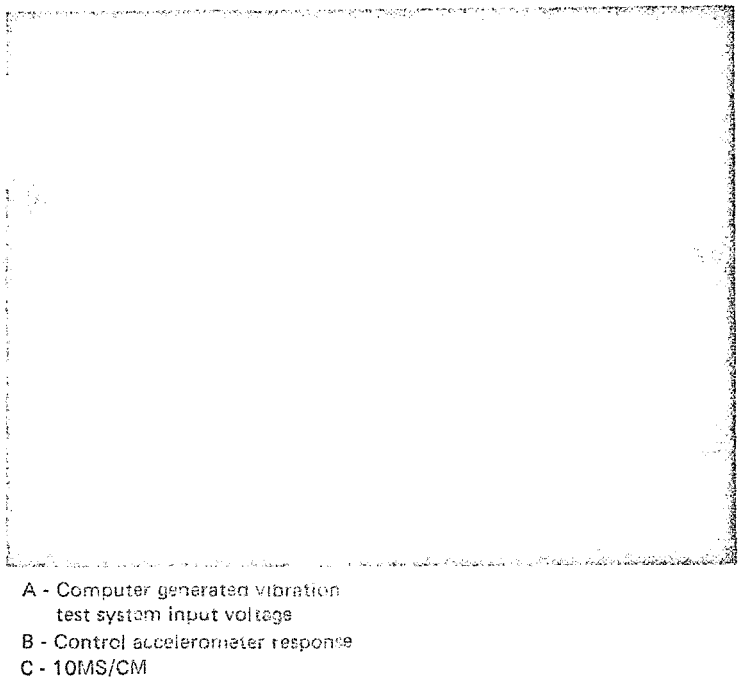



Figure 2-B: SHOCK SYNTHESIS ON VIBRATION TEST SYSTEM

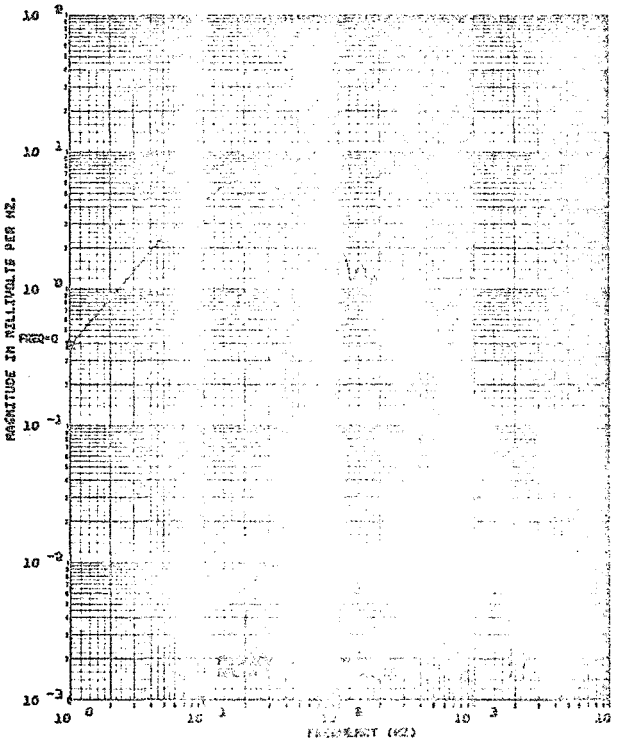


Figure 2-C: FOURIER TRANSFORM MODULUS OF SPECIFIED TERMINAL PEAK SAWTOOTH

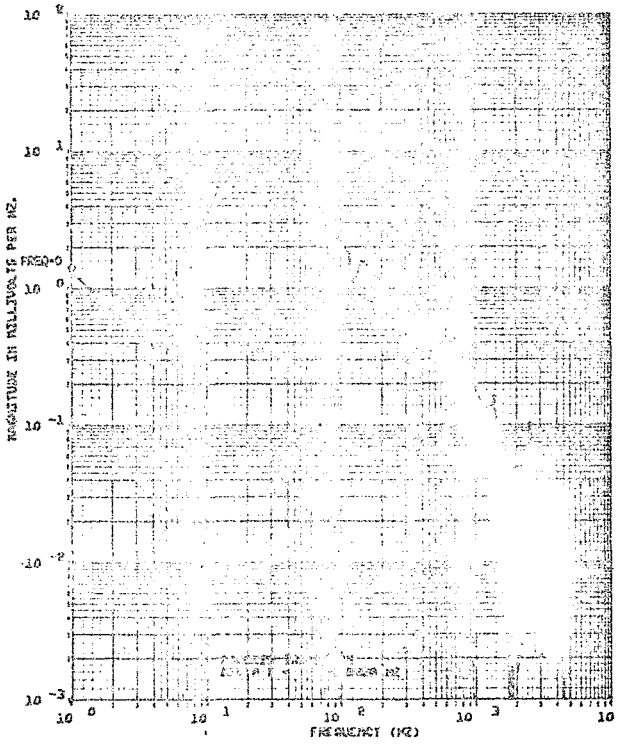


Figure 2-D: FOURIER TRANSFORM MODULUS OF SYNTHESIZED WAVEFORM (Control Accelerometer Response)

Figure 2: TRANSIENT WAVEFORM CONTROL APPLIED TO MIL810-B SHOCK TEST REQUIREMENTS

## PRELIMINARY DISCUSSION

The procedures and results of this investigation are presented in the following sections.

1) In the "General Outline of Approach" Section, the problem and proposed method of solution are presented with the practical difficulties involved in obtaining a solution.

2) In the "Fourier Integral Transform Error Study" Subsection, the results of an empirical analysis are directed at answering the question, "what is required to accurately represent a bounded-transient time function in the frequency domain?" The analysis in this section provides direction for the subsequent experimental work.

3) The results of experiments with a prototype digital control system are included in the "Experimental Investigation with a Transient Waveform Prototype Control System" Subsection. Both flight data from an OGO-D spacecraft and an analytic function were synthesized on typical vibration test apparatus using a laboratory general purpose computer.

4) The "Control System Empirical Error Study," "Equipment Limitations," and "Nonlinearities" Subsections include practical experience with the prototype system, analytic and empirical presentations of system errors, and equipment limitations with a concise commentary on the adverse effect of nonlinearities. A statistical definition of the control system performance is presented in Appendix III.

5) The requirements for implementing a Transient Waveform Control System in as near an on-line fashion as possible are included in the "Conceptual Design of Control System" and "Cost Estimate of Proposed System" subsections.

Particular emphasis was directed at using both time and frequency domain criteria for the adequacy of the controlled waveforms. The digital prototype control system has many print and plot options within the sequence of computation. A complete sequence is included with examples illustrating Fourier transform properties of transient data derived from digital calculations.

The graphs of the Fourier transform modulus carry a distinct error in the low frequency domain. The low frequency error sources have been isolated, evaluated, and corrective action outlined within the scope of this feasibility study is included in the text.

Appendix I, "Error Analysis of a Transient Waveform Control System," presents a detailed error model of the proposed control system. The analysis in this section was developed from a mathematical viewpoint and the notation is self contained. Its basic assumption of 'white' wide band stationary noise was invalidated with laboratory experience on the prototype control system. The "Control System Empirical Error Study" Section, included in the text, is semi-empirical, directly relating the findings of the feasibility study and conceptual design.

Appendix II, presents distortion data on both NASA-Goddard vibration equipment, to be used as a part of the Transient Waveform Control system, and a Boeing vibration system that has been used successfully to perform transient waveform control.

Appendix III, "Statistical Analysis of the Prototype Control System Performance," presents empirical evidence of transient waveform control with a time domain variance of less than 13 percent.

## GENERAL OUTLINE OF APPROACH

The objective of structural test programs has been to obtain data for correlation with analytic results. These tests generally fall into three categories---static, modal, and forced response. Laboratory test procedures are established to generate forced responses of a structure for sinusoidal and random excitations. Transient test procedures, such as shock spectra or tone burst for transient excitations, are currently subject to conjecture with universal acknowledgement that transient waveforms are difficult to reproduce on a vibration test system. The successful implementation of a Transient Waveform Control System for laboratory test apparatus has many ramifications that result in:

1) Reduced test costs;

2) Design based on transient response loads rather than loads developed in sine tests;

3) Reliability (i.e., no cumulative fatigue damage);

4) Virtual simulation of damage potential of a service environment;

5) Reproduction of past service environments.

The analysis of a control system is based on a transfer-function concept employing a block diagram representation of the system or its components. These block diagrams represent the flow of information and the functions performed by each component in the system. The dynamic characteristics of the functional block, in terms of a transfer function, are defined by the ratio of the Fourier transform of the output to the Fourier transform of the input. A transform or transformation process is a mathematical or physical tool to alter the problem into one that can be solved. It is important to recognize that transient waveforms and their frequency spectra are Fourier transforms of each other.

The general approach to this Transient Waveform Control System is to:

1) Develop an accurate definition of the test system inverse-transfer function, $1/H(\omega)$, in the frequency domain;

2) Multiply the frequency domain description of the required waveform by the inverse-transfer function of the test system;

3) Inverse transform this product into the time domain.

This computer-generated time domain function represents a voltage that, when applied as an input to the test system, will cause the required waveform to be generated at the control point. This concept is schematically illustrated in Figure 3.

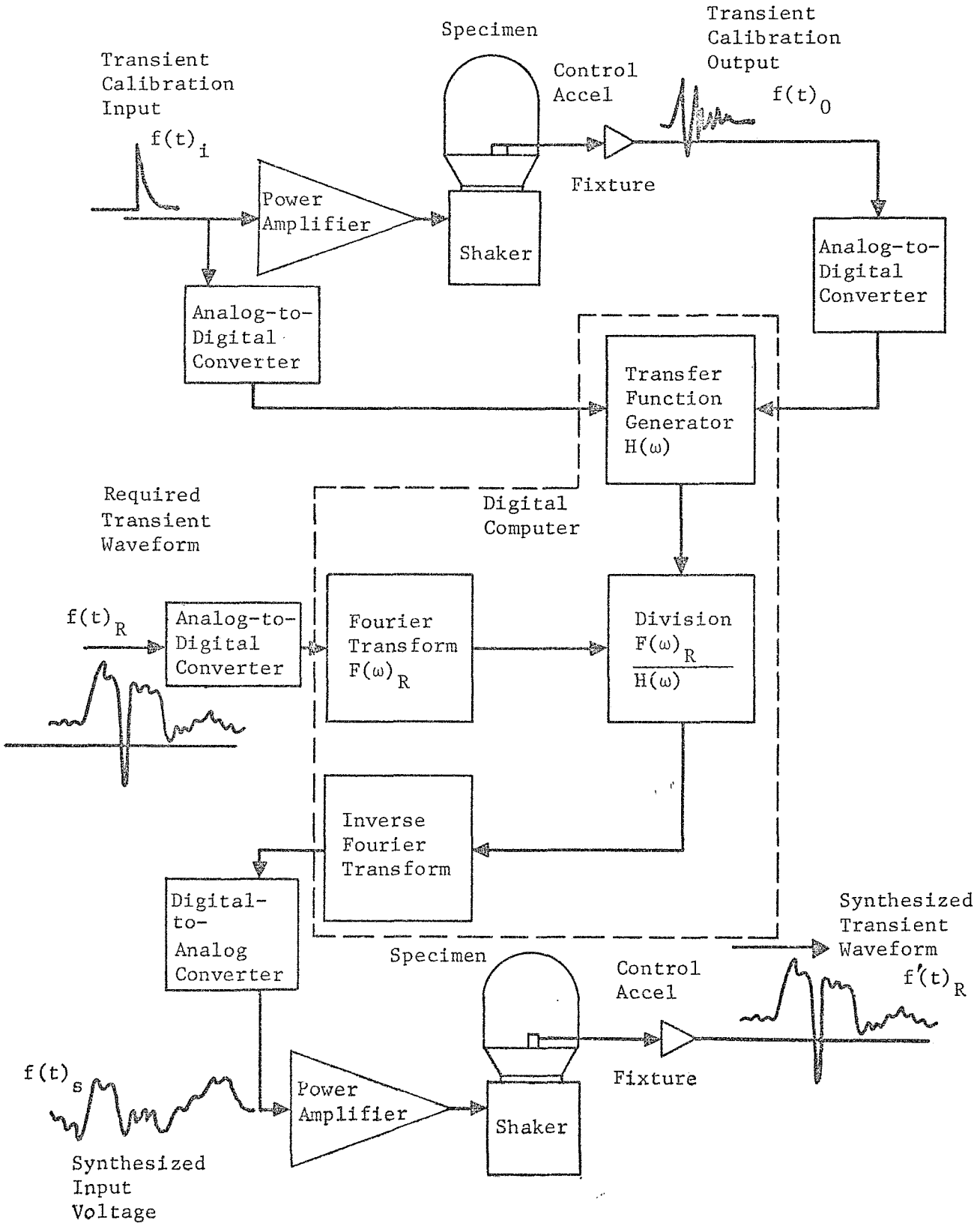



Figure 3: TRANSIENT WAVEFORM CONTROL, LOGIC DIAGRAM

A transient calibration pulse of the form is used

$$f(t)_i = 0, \quad t < 0$$
$$f(t)_i = K_e^{-t/\tau_o}, \quad t > 0 \tag{1}$$

This calibration pulse was chosen for two reasons: first, the Fourier transform of this pulse contains all frequencies within the system bandwidth, and provides sufficient energy at all frequencies to fully define the system transfer function. Second, the finite energy that this pulse puts into the test system does not jeopardize the test specimen from the standpoints of cumulative fatigue damage or destructive resonances of the test specimen. The magnitude of the calibration pulse can be adjusted to the approximate level of the required transient so that the transfer function of the system, if mildly nonlinear, can be most accurately described for that level pulse.

For transient control of vibration test equipment, the frequency domain representations of both the time history of the desired transient and the transfer function of the test equipment are required. Historically, representing a time function in the frequency domain has been performed exclusively with analog equipment with difficulty and limited success. The advent of digital computers has opened new methods for problem-solving, and for control techniques once considered impractical.

Fundamental to any frequency-domain analysis of transient time-domain data is the computation of Fourier integral transforms. The Fourier integral is defined for continuous data both in time and frequency, as

$$F(\omega) = \int_{-\infty}^{\infty} f(t)e^{-j\omega t}dt \tag{2}$$

$$F(\omega) = \int_{-\infty}^{\infty} f(t)(\cos\omega t - j\sin\omega t)dt.$$

The corresponding inverse Fourier transform is then defined as

$$f(t) = \frac{1}{2\pi} \int_{-\infty}^{\infty} F(\omega)e^{j\omega t}d\omega \tag{3}$$

$$f(t) = \frac{1}{2\pi} \int_{-\infty}^{\infty} F(\omega)(\cos\omega t + j\sin\omega t)d\omega.$$

If the time function, f(t), is sampled at N even time intervals of $\Delta t$ seconds, then the Fourier integral transform pair given, Equations (2) and (3), are redefined as the discrete Fourier transform

$$F_p(\omega) = \Delta t \sum_{n=0}^{N-1} f_p(t) e^{-j\omega n \Delta t} \tag{4}$$

and the inverse discrete Fourier transform is

$$f_p(t) = \frac{\Delta\omega}{2\pi} \sum_{n=0}^{N-1} F_p(\omega) e^{j\omega n \Delta t} , \tag{5}$$

where, in both cases,

$$n = 0, 1, 2, \ldots . N - 1.$$

The normal procedure for computing the Fourier transform of a sampled time function on the digital computer would use

$$F_p(\omega) = \Delta t \sum_{n=0}^{N-1} f_p(t)(\cos\omega n\Delta t - j\sin\omega n\Delta t). \tag{6}$$

The resulting Fourier transform is a complex quantity where the cosine terms are the real part and the sine terms are the imaginary part. The modulus of the Fourier transform is defined as the square root of the sum of the squares of the real and imaginary parts. The transform phase angle is the arctangent of the imaginary part divided by the real part.

If the sampled time funtion, $f_p(t)$, contains N data points, the computation of N values of $F_p(\omega)$ will require $N^2$ complex multiplication and additions.

In 1965, a new algorithm for computing a discrete Fourier transform was described by Cooley and Tukey[1]*. This algorithm is known as the Fast Fourier Transform (FFT). Calculating efficiencies are implemented via symmetry, efficient grouping, matrix operations, and fast difference equation methods. The FFT requires only $N\log_2 N$ complex operations to compute the transform that Equation 6 required $N^2$ operations to do. For example, if N equals 4,096 data points, the FFT computation would be about 341 times faster.

*Numbers in parenthesis refer to references at the end of the report.

The FFT is a discrete Fourier transform based upon reciprocal equations[2] of the Fourier transform,

$$A(n) = \frac{1}{N} \sum_{k=0}^{N-1} X(k) e^{-j2\pi nk/N} , \tag{7}$$

and the inverse Fourier transform,

$$X(k) = \sum_{n=0}^{N-1} A(n) e^{j2\pi nk/N} . \tag{8}$$

The quantities A(n) and X(k) represent number sets only. In this form, they are not restricted to a time-frequency domain relationship.

Equations (7) and (8) are used to compute discrete Fourier transforms, in units of time and frequency, by inclusion of the sampling increments, $\Delta t$ and $\Delta f$, and use of the following theorem[2].

If, x(t) (a continuous time function for $-\infty<t<\infty$) and a(f) (a continuous frequency function for $-\infty<f<\infty$) are a Fourier integral transform pair,

$$x(t) \longleftrightarrow a(f) , \tag{9}$$

then,

$$TX_p(k\Delta t),\ k = 0,\ 1,\ 2\ .\ .\ .\ .\ .\ N - 1 \tag{10}$$

and

$$A_p(n\Delta f),\ n = 0,\ 1,\ 2\ .\ .\ .\ .\ .\ N - 1 \tag{11}$$

are a discrete Fourier transform pair; where,

$$\Delta f = \frac{1}{N\Delta t} = \frac{1}{T} = \frac{\Delta\omega}{2\pi} . \tag{12}$$

The resulting transform pair are[2]

$$A_p(n\Delta f) = \Delta t \sum_{k=0}^{N-1} X_p(k\Delta t) e^{-j2\pi kn/N} \tag{13}$$

and

$$X_p(k\Delta t) = \Delta f \sum_{n=0}^{N-1} A_p(n\Delta f) e^{j2\pi kn/N}; \qquad (14)$$

where,

$A_p(n\Delta f)$ = nth complex frequency sample;

$X_p(k\Delta t)$ = kth time sample;

N = Total number of time/frequency samples,

$j = \sqrt{-1}$

One restriction on the FFT calculation process involves the transform resolution in the frequency domain, $\Delta f$. This is restricted to be the reciprocal of the total sample record length, T (Equation 12). For example, to accommodate a 2 Hz resolution in the frequency domain, the total sample length must equal 0.5 second. This restriction can be lifted only with a thorough understanding of the boundary conditions involved in Fourier transform theory. The technique of adding zero amplitude data points onto read data, thereby artificially increasing the sample record length is discussed in the "Control System Empirical Error Study" Section. The advantages of having equivalent discrete data points, both in the time and frequency domain, directed the use of FFT computation as the primary tool for mechanizing the control system design task.

When a physical quantity is represented numerically, a nonlinearity is inherently present in the form of quantization error. The value of the measurement is designated by an integer corresponding to the nearest number of units contained in the measured physical quantity. A control system incorporating this process is nonlinear, and difficult to deal with by any direct analytic procedure. A statistical analysis reduces the complexity, yielding average results that are adequate for system evaluation and design. An empirical approach reduces the complexity further by placing real bounds on the errors as a function of the quantizing variable. The control system prototype design, when subjected to the experimentation in this study, produced a significant argument for the necessary unbiasing of quantized data for the accurate definition (digital description) of a waveform.

In the sampling process, aliasing is a major consideration in correctly conditioning any data for frequency domain operations. Aliasing is a phenomena where different frequencies adopt the identity of one particular frequency. If the time interval between data samples is $\Delta t$, the sampling rate is $1/\Delta t$ samples per second. The real frequency content of the data can only be defined from 0 to $1/2\Delta t$ cycles per second and higher frequencies will be folded into the frequency range from 0 to $1/2\Delta t$ cycles per second. This cutoff frequency, $f_c = 1/2\Delta t$, is known as the Nyquist folding frequency.

Recognizing the inherent problems associated with digital representation of data and frequency domain calculation, the study plan called for an extensive investigation to define the errors associated with the computation of the Fourier integral transform, and the development of a prototype control system on a general purpose computer associated with a laboratory dynamic data analysis system.

The specific Fortran statements that perform the Fast Fourier Transform used in this study are contained in Reference (3).

## FEASIBILITY STUDY RESULTS

### Fourier Integral Transform Error Study

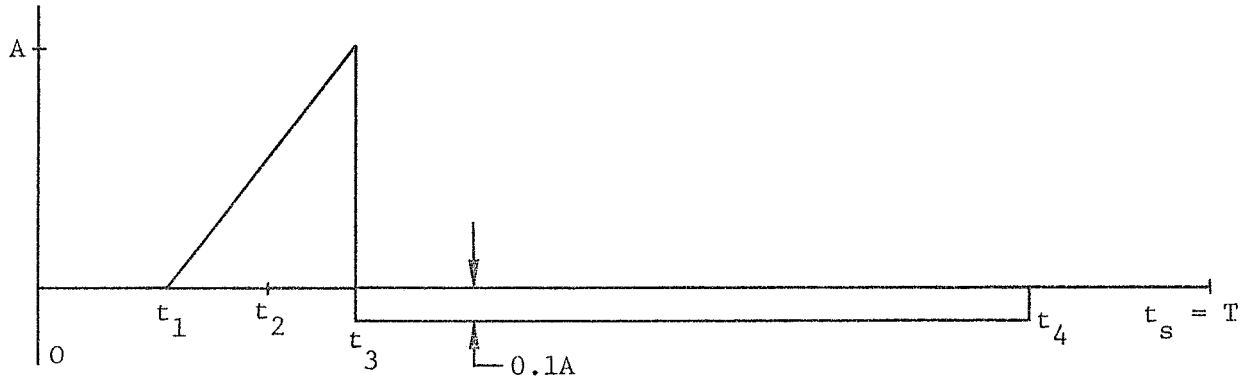
Three mathematically simulated analog data pulses were generated by the computer. These pulses were then sampled, according to a fixed plan, to simulate actual analog-to-digital (A/D) conversion. The sampling parameters were: (1) word size M (number of bits in A/D converter word); (2) sampling rate R (samples/second); and (3) sampled record length T (seconds). The Fast Fourier Transforms (FFT) of these sampled pulses were then computed and plotted. The plots were compared with the plot of the theoretical Fourier transform of the pulse to determine the errors involved in quantization, sample record length, and sampling rate variation. The effect was similarly studied by adding pseudo-random noise to the sampled pulses [1] and again comparing the transforms.

The simulated A/D converter word sizes used in the error study were M = 8 (8 bits plus sign), M = 10 (10 bits plus sign), M = 12 (12 bits plus sign), and M = 14 (14 bits plus sign). Also, for each word size (M = 8, 10, 12, and 14), the following matrix of sample record length (pulse duration), T, and sampling rate, R, was used in the error study.

| T \ R | $2^{11}$ | $2^{12}$ | $2^{14}$ | $2^{16}$ |
|---|---|---|---|---|
| $2^{-7}$ | | | ● | ● |
| $2^{-5}$ | | ● | ● | ● |
| $2^{-3}$ | ● | ● | ● | ● |
| $2^{-1}$ | ● | ● | ● | |
| $2^{1}$ | ● | ● | | |

First pulse, terminal peak sawtooth.-The terminal peak sawtooth pulse used in this study meets the basic shock test requirements specified in MIL.STD.810B. This pulse was chosen as a typical pulse. The actual pulse used contained a trailing negative block, of area equal to the positive sawtooth, such that the overall pulse would contain no d.c., or zero frequency, energy. This condition is necessary for operation on electromagnetic exciters. The pulse is described as follows (also, see Figure 4):

[1] During the noise study, the errors due to quantization, sample record length, and sampling rate were minimized.




The specified times are:

$t_1$ = 0.0044 second;

$t_2$ = 0.0099 second = $t_1 + \frac{t_3 - t_1}{2}$ ;

$t_3$ = 0.0154 second;

$t_4$ = 0.0704 second;

$t_5$ = T seconds;

$f(t) = 0$ (for $t < t_1$);

$f(t) = \frac{\Delta t}{(t_3 - t_1)} = \frac{\Delta t}{0.011}$ (for $t_1 \leq t \leq t_3$) and $f(t_1) = 0$

$f(t) = -0.1A$ (for $t_3 < t \leq t_4$);

$f(t) = 0$ (for $t_4 < t < T$);

$f(t) = 0$ (for $t > T$).

The Fourier integral transform of this pulse is

$$F(j\omega) = \frac{1}{j\omega} \left\{ [A \frac{\sin(\frac{\omega\tau}{2})}{(\frac{\omega\tau}{2})}] e^{j\omega t_2} - 1.1Ae^{-j\omega t_3} + 0.1Ae^{-j\omega t_4} \right\} \qquad (15)$$

where:

$\tau = t_3 - t_1$.

This Fourier integral transform is plotted directly from Equation 15 (Figure 5). Figures 4 through 10 illustrate the individual effects of separately varying M, R, and T for this pulse. These effects can be summarized as follows.

1) Quantization error. The zero frequency, (d.c.), component, signified by hash mark on the left margin of the figure, approaches zero (proper value) with increasing word size (Figure 6). There is no significant degradation of the transform, in the bandwidth from 2 to 5,000 Hz, due to word size as low as 8 bits.

2) Sampling rate. Insufficient sampling produces two effects. First, the Fourier transform is truncated at one-half the sampling frequency (Nyquist frequency). Second, as the transform approaches the Nyquist frequency, it increases[4] above the terminal slope in a "ski slope" manner (Figure 7). This is referred to as aliasing and in serious cases the errors carry back into the low frequency domain (refer to "Second Pulse, Modified Step Decay" Subsection).

3) Sample record length. The pulse duration, T, is varied by the addition of zero amplitude data values. The overall effect is to produce closer frequency resolution, $\Delta f$. The minimum value of T ($T = 2^{-3}$ seconds) produced a segmented, nonsmooth, transform[2]. The discrete frequencies. Since there were no sharp peaks in this transform, the lack of frequency domain resolution was not judged to be serious (Figures 8 through 10).

Second pulse, modified step decay[3].-The modified step-decay pulse was chosen to demonstrate the errors generated by quantization of analog data. This pulse was considered as a good test case because of the low exponential slope at a low amplitude. Quantization of this slope will convert it from a smooth continuous function into a distinct staircase function. A description of the pulse in the time domain is

$$f(t) = A\left\{\left[\frac{\beta}{(\beta-\alpha)^3}\right]e^{-\alpha t} - \left[\frac{\beta}{(\beta-\alpha)^2}\right]te^{-\alpha t} + \left[\frac{\alpha}{2(\beta-\alpha)}\right]t^2e^{-\alpha t} + \left[\frac{\beta}{(\alpha-\beta)^3}\right]e^{-\beta t}\right\}; \quad (16)$$

this time history is illustrated in Figure 11. The Fourier transform of this pulse is

$$F(\omega) = \left[\frac{j\omega}{(\alpha+j\omega)^3(\beta+j\omega)}\right] \quad (17)$$

and is illustrated in Figure 12.

[2] Due to straight line interpolation between discrete transform values.

[3] A step-decay pulse, $f(t) = \left[\frac{\alpha e^{-\alpha t} - \beta e^{-\beta t}}{(\alpha-\beta)}\right]$, was originally tried, but was not used for further analysis due to excessive energy above 5 kHz, which created aliasing problems.

The parameters of Equations 10 and 11 are:

A = scaling factor, $24{,}576 \times 10^8$;

$\beta$ = 314.1 radians/sec;

$\alpha$ = 6,283 radians/sec;

e = naperian base, 2.7182818....

The effects of quantization word size, sample record length, and sampling rate are summarized as follows.

1) Quantization error. Figures 13 through 16 illustrate three effects of inadequate word size. First, the zero frequency value should be equal to zero and only the large word-size computations approach the proper value. Second, for small word size (8 and 10 bit plus sign), the computed transform erroneously oscillates above and below the theoretical transform in the low frequency domain. Finally, small word-size conversion produces hash in the high frequency domain.

2) Sampling rate. Figures 16, 17, and 18 illustrate the effects of inadequate sampling rate. First, the transform is computed only to the Nyquist frequency (one-half the sampling rate). Second, aliasing occurs to such an extent (Figure 17 in particular) that the ski-slope effect occurs at both the low-frequency and high-frequency domain and the computed transform undershoots in the midfrequency domain.

3) Sample record length. Figure 19 illustrates the effect of insufficient sample record length, which is to eliminate the computation of frequency components below the inverse of the sample record length, T.

Third pulse, shaker impulse response.-The third pulse was designed to represent the impulse response of an electromagnetic exciter. The transfer function[4] of an electromagnetic exciter can be described(5), using LaPlace notation, as follows.

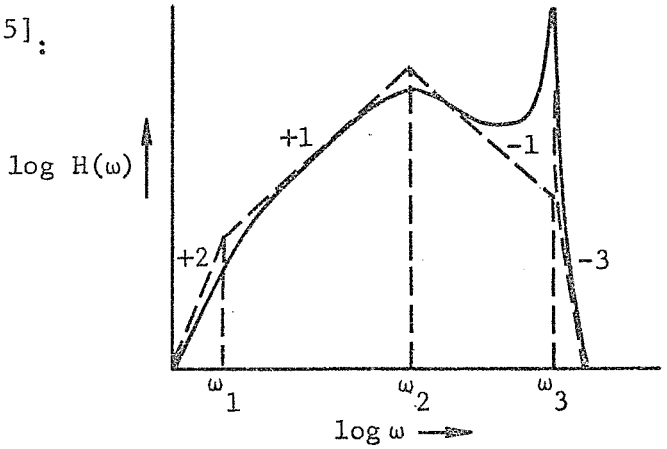
$$H(s) = \frac{K_1 S^2}{S^5 + K_2 S^4 + K_3 S^3 + K_4 S^2 + K_5 S + K_6} \quad . \tag{18}$$

[4] $H(s) = \ddot{X}(s)/E_1(s)$ (acceleration out/voltage in)

The factored form of this transfer function is,

$$H(s) = \frac{K_S^2}{(S+\omega_1)(S^2+2\delta_2 S\omega_2+\omega_2^2)(S^2+2\delta_3 S\omega_3+\omega_3^2)} \tag{19}$$

and is plotted[6] as[5]:




The break point at $\omega_1$ is due to the armature suspension and occurs at quite low frequency, less than 2 Hz. If the breakpoint at $\omega_1$ is ignored, the transfer function can be approximated by the product of

$$F_1(j\omega) = \frac{\omega_3}{[(\alpha^2+\omega_3^2) - \omega^2+j2\alpha\omega]}, \text{ and} \tag{20}$$

$$F_2(j\omega) = \frac{j\omega}{[(\sigma^2+\omega_2^2) - \omega^2+j2\sigma\omega]}.$$

Therefore,

$$F(j\omega) = \frac{(j\omega)\omega 3}{[(\alpha^3+\omega_3^2) - \omega^2+j2\alpha\omega]\,[(\sigma^2+\omega_2^2) - \omega^2+j2\sigma\omega]} \tag{21}$$

is the simulated transfer function and the impulse response of this function is the time domain convolution of

$$f_1(t) = e^{-\alpha t}\sin\omega_3 t \text{ , and} \tag{22}$$

$$f_2(t) = e^{-\sigma t}\left(\cos\omega_2 t - \frac{\sigma}{\omega_2}\sin\omega_2 t\right).$$

Therefore, $f(t) = f_1(t) * f_2(t)$. (23)

---

[5] In the theory of LaPlace Transforms, $S = \sigma+j\omega$. In this case, $\sigma = 0$.

The method of generation of this pulse was considerably different from that of the first two. The pulse information was generated in the frequency domain from Equation 21. The parametric values used in this equation were:

$\omega_2 = 628$ radians/sec;

$\omega_3 = 17{,}593$ radians/sec;

$\delta_2 = 2.8$;

$\delta_3 = 0.0187$;

$\sigma = \delta_2\omega_2 = 1{,}758$;

$\alpha = \delta_3\omega_3 = 330$.

Equation 21 was multiplied by a scaling factor,

$A = 1.95 \times 10^8$,

to yield a time history of suitable amplitude. The frequency domain information was then inverse transformed into the time domain to produce the desired shaker impulse response (Figure 20). Due to computer inaccuracies (24-bit significants in floating point words), the inverse transformation produced small imaginary components in the time domain. To facilitate working with the pulse these imaginary components were equated to zero for subsequent analysis. The theoretical transform was then generated by transforming the above data (time history pulse) back into the frequency domain using full computer accuracy (24 bits) (Figure 21). The zeroing of the imaginary components in the time domain resulted in a sharp "hole" at 8,192 Hz and integer multiples thereof. The shaker impulse response was sampled and transformed with various values of the control parameters, M, R, and T. The results are summarized as follows:

1) Quantization error. Figures 22 through 25 illustrate the effect of inadequate A/D converter word size. First, the zero frequency components, which should equal zero, were largest; therefore, in greatest error for the small bit-size words. Second, for the smaller bit-size words, serious aberrations occur in the low-frequency domain. In the case of the 8-bit word, these aberrations created a notch at 30 Hz. This type of phenomenon was previously experienced in analyzing real impulse response data from available shakers; it therefore indicated good modeling in this error study. Finally, the smaller bit-size words produced high frequency hash as previously shown. It must be noted that although the high frequency hash, produced by quantization error, is of relatively low amplitude, it is important because the actual transfer function of an exciter system is determined by ratioing two such Fourier transforms (output divided by input). Since both transforms will contain this hash, the ratio will seriously deteriorate in the high frequency domain.

2) Sampling rate. The sampling rates used on this pulse were $2^{14}$ and $2^{16}$ samples per second. Both produced excellent results out to 5 kHz.

3) Sample record length. The sample record lengths used were $2^{-3}$ and $2^{-1}$ seconds. Both record lengths are suitable, except that the $2^{-1}$ second record length yielded a smoother transform.

Additional investigation.-The results of the above error-study point to the problem of A/D converter word size, M. Sampling rate, R, and sample record length, T, are well defined by the upper and lower bandwidth requirements; i.e., if the lower frequency requirement is 2 Hz, then the sample record length must be of the inverse of 2 Hz (0.5 second); also, if the upper frequency is 5,000 Hz, the sampling rate, R, should be at least $2^{14}$ (16,384) samples per second and preferably four times the upper frequency or 20,000 samples/second. The quantization error problem can be solved by using a large word-size (14 bits plus sign) analog-to-digital converter. Since 10 bit plus sign converters are common and less expensive than 14 bit plus sign converters, the possibility of reducing the resulting quantization error through software techniques was investigated.

Since it was established that most A/D converters use a chop routine in the decision making process, as opposed to a rounding routine, a bias could therefore be placed on the resulting digital data. This is especially true when the routine chops toward either full scale value. In the error study, the simulated process chopped toward the negative full scale value. It was reasoned that if the analog data was evenly or uniformly distributed between quantization levels, then the bias could be removed by adding one-half quantization level size, or one-half bit, to each data value (synthetic zeros added to the pulse data would not be affected).

Special software, termed Unbias Routine, was generated and applied to the second and third pulses of the error study. The parametric values were:

$M = 8, 10, 12,$ and 14 bits;

$R = 2^{14}$ samples/second;

$T = 2^{-1}$ seconds.

Figures 26 and 27 (transforms of the Shaker Impulse Response), and Figure 28 (transforms of Modified Step Delay Pulse) illustrate the effectiveness of the Unbias Routine. Note how effectively the Unbias Routine draws the computed transform into agreement with the theoretical transform in the low-frequency domain. Also, note the dramatic reduction in the zero frequency (d.c.) component (theoretically it should be equal to zero). Also review Figure 6. Finally, note that the Unbias Routine in no way reduced the high-frequency hash that results from inadequate word size. From this the following conclusion is drawn. The Unbias Routine will help reduce the effect of quantization errors in the low-frequency domain only. It does not help the quantization error induced high-frequency hash. Therefore, inadequate word size will limit the effective bandwidth over which a transform may be defined. Consequently, a bandwith over which a transfer function (ratio of two transforms) can be accurately defined is also limited.

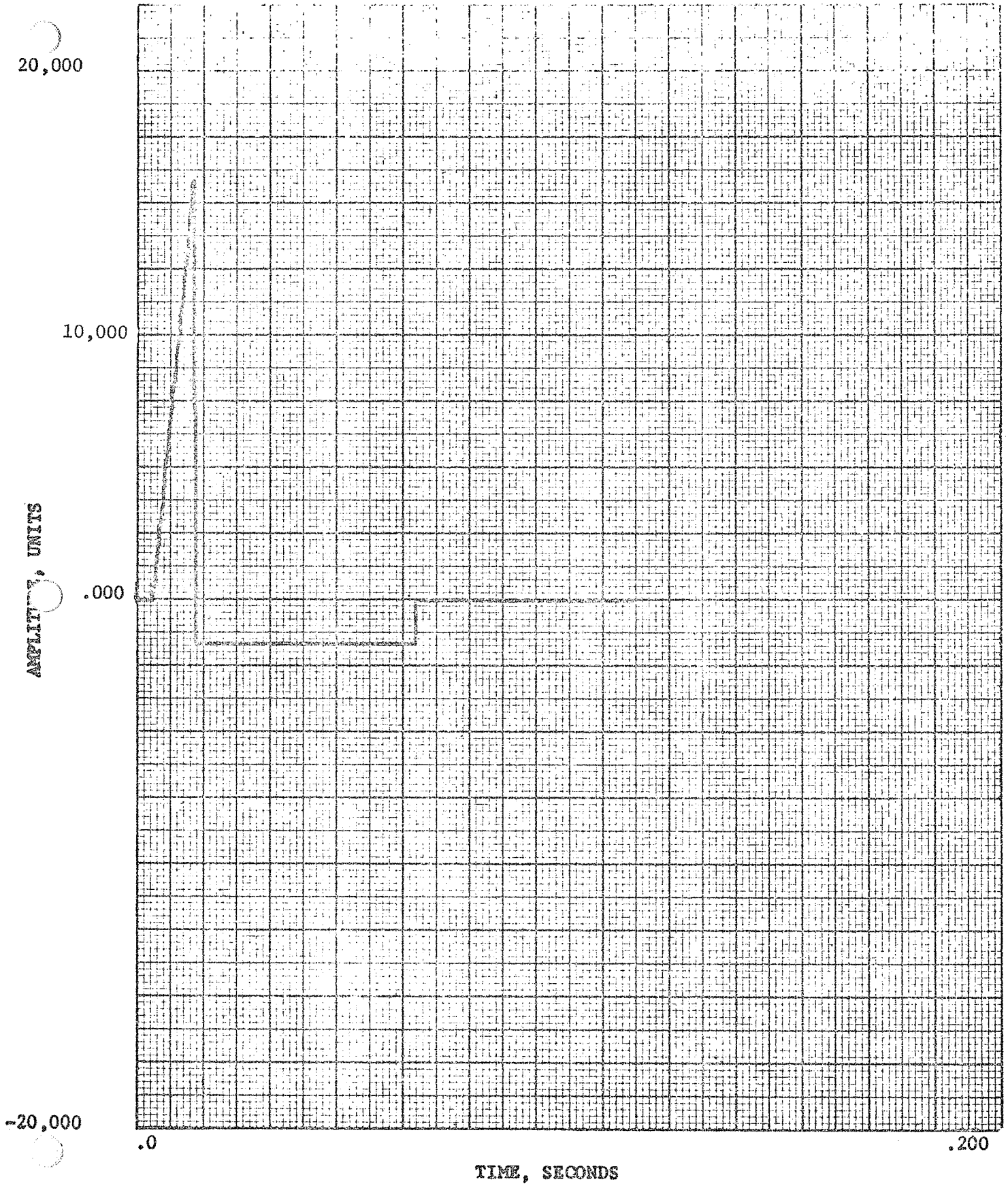



Figure 4: TERMINAL-PEAK SAWTOOTH PULSE

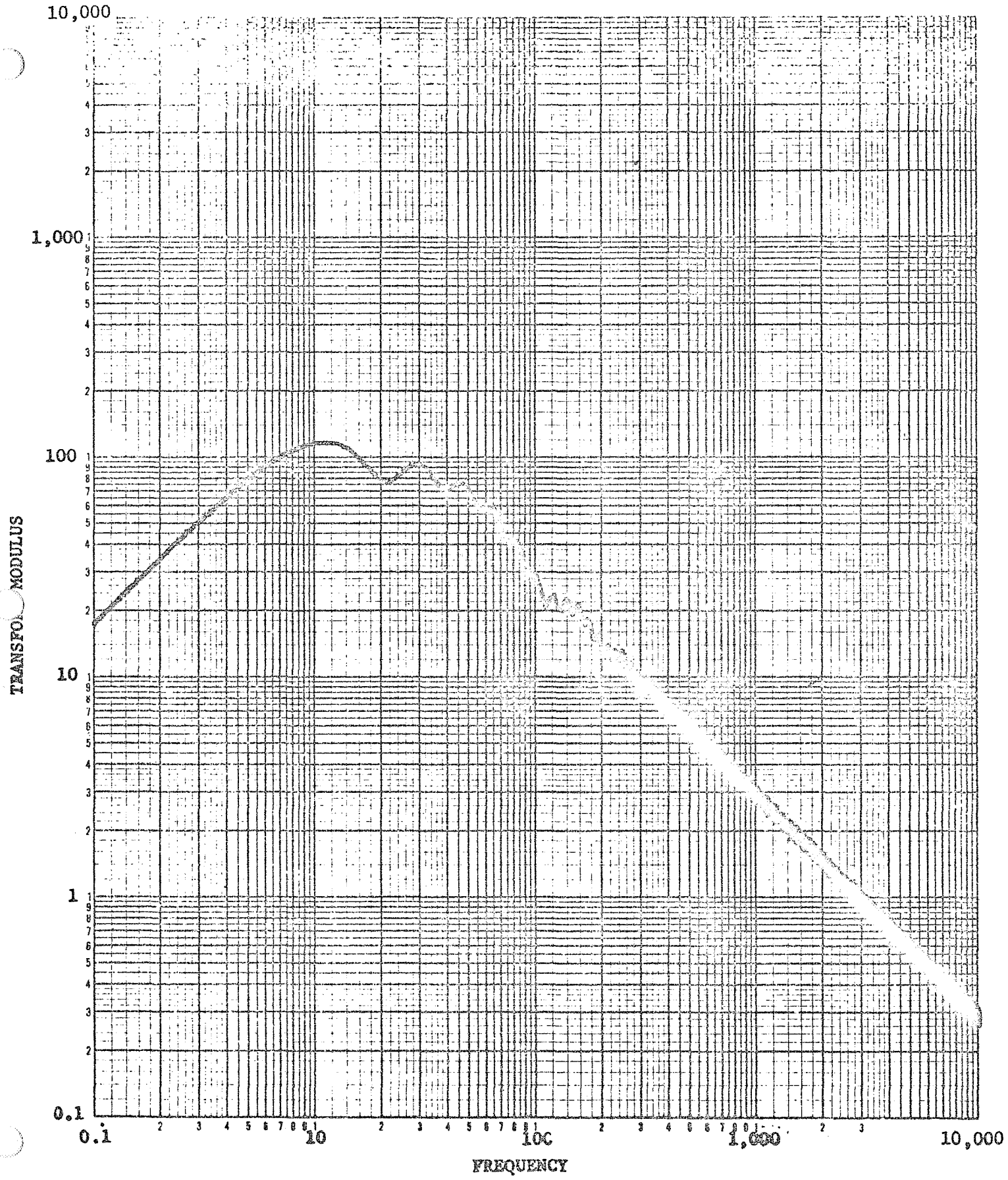



Figure 5: THEORETICAL TRANSFORM-TERMINAL-PEAK SAWTOOTH

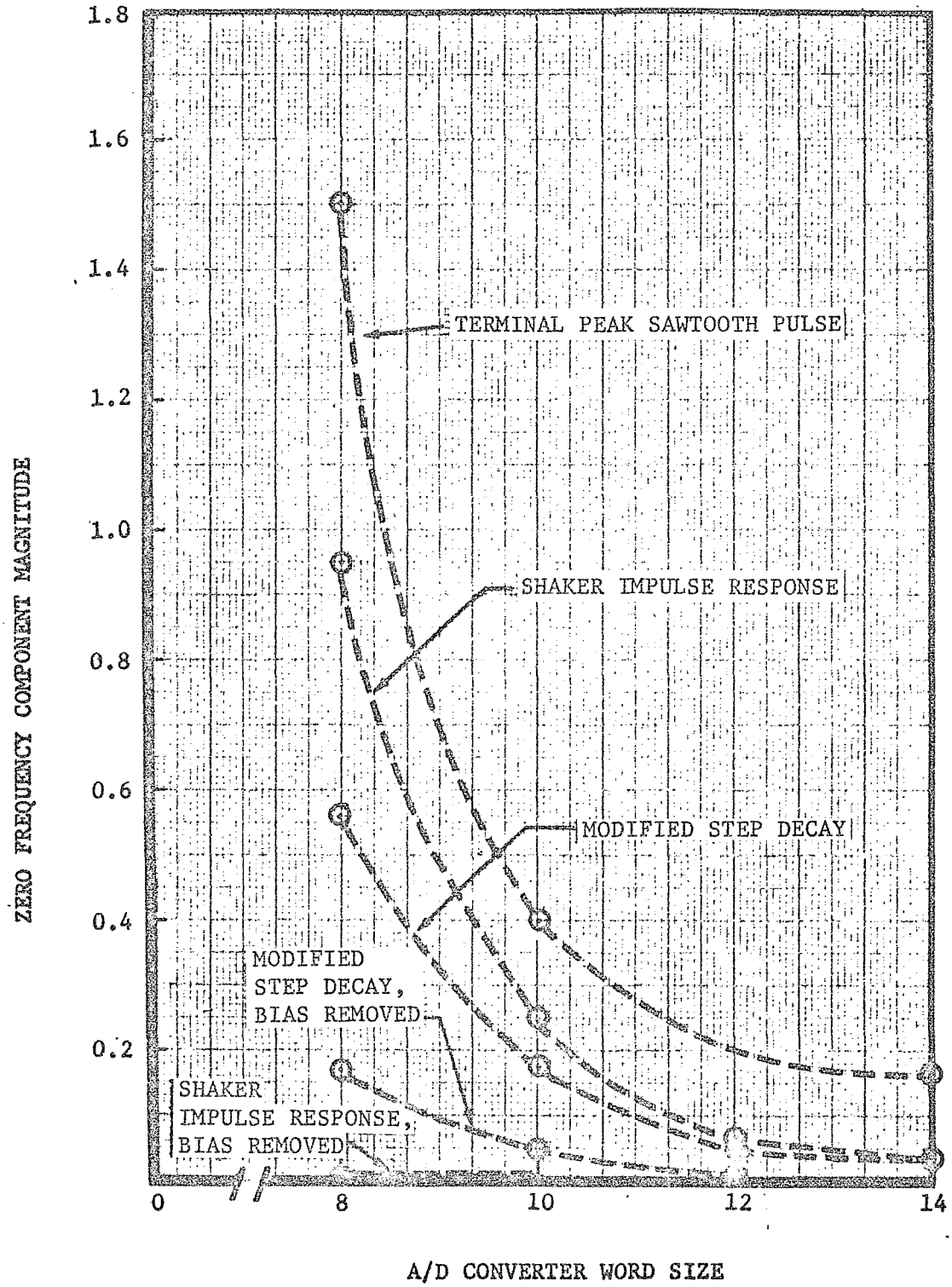



Figure 6: COMPUTED ZERO-FREQUENCY COMPONENTS VS A/D CONVERTER WORD SIZE

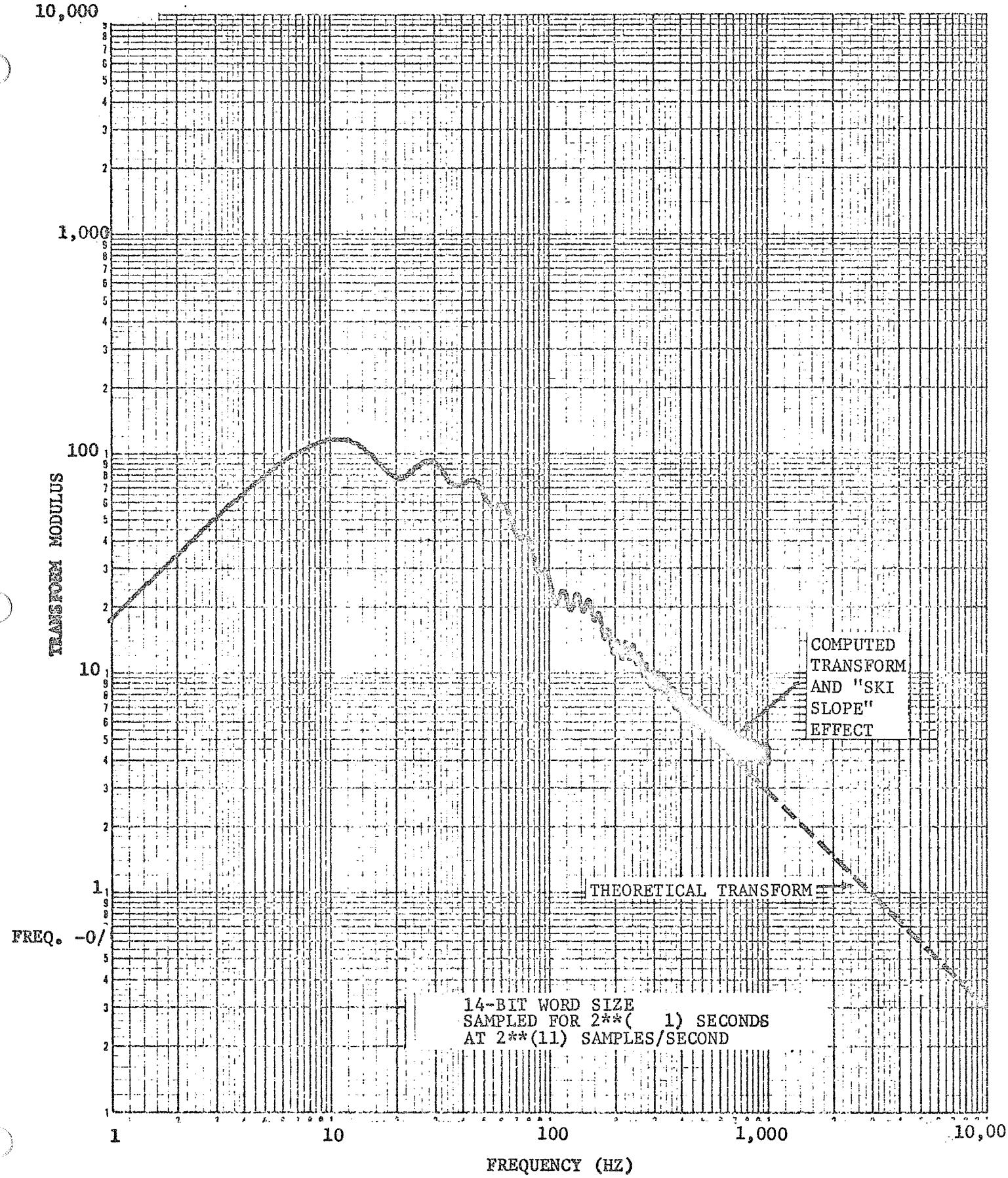



Figure 7: FOURIER TRANSFORM OF THE TERMINAL-PEAK SAWTOOTH SAMPLED AT 2,048 SAMPLES/SECOND

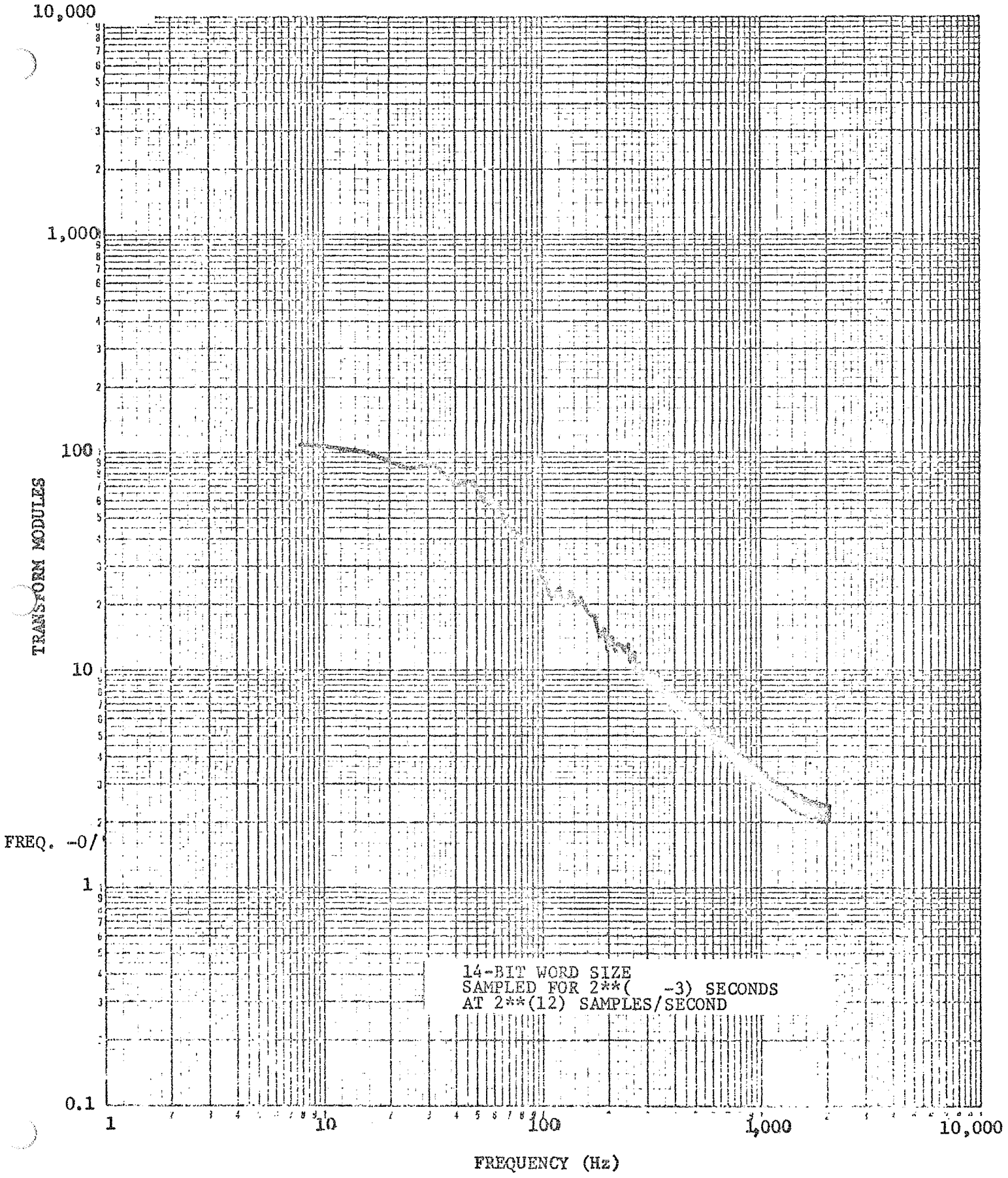



Figure 8: FOURIER TRANSFORM OF TERMINAL-PEAK SAWTOOTH WITH A SAMPLE RECORD LENGTH OF 0.125 SECOND

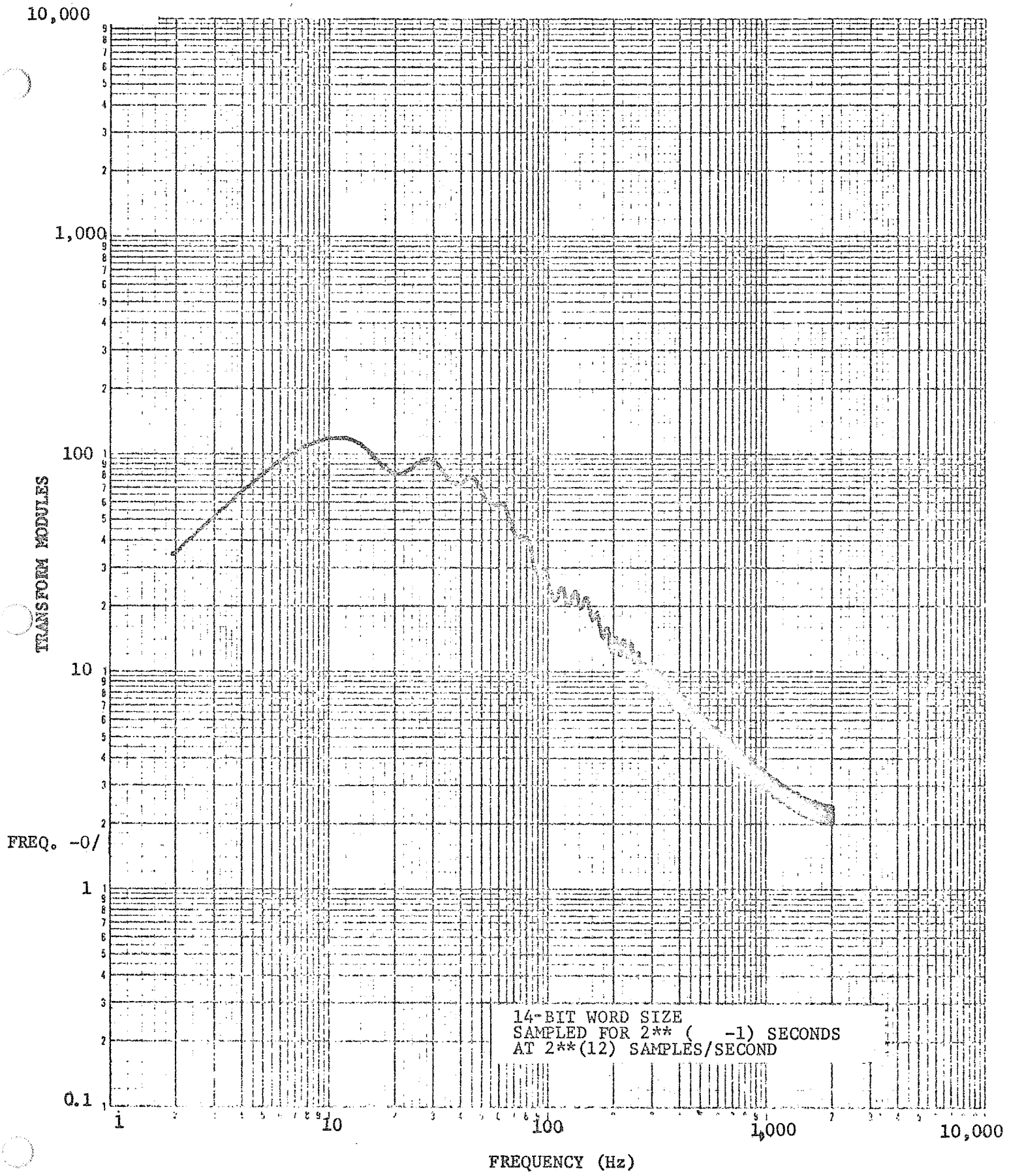



Figure 9: FOURIER TRANSFORM OF TERMINAL-PEAK SAWTOOTH WITH A SAMPLE RECORD LENGTH OF 0.5 SECOND

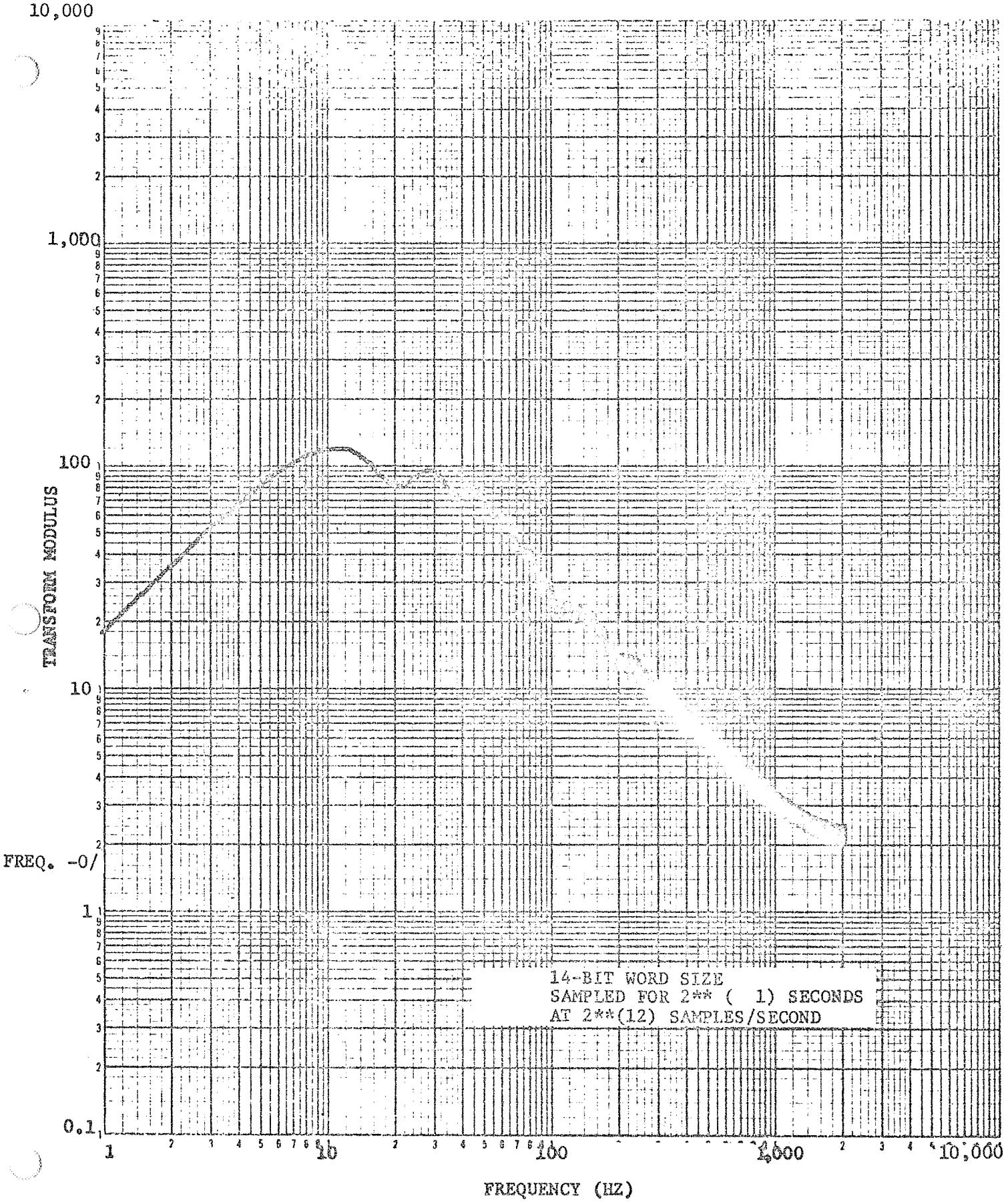



Figure 10: FOURIER TRANSFORM OF TERMINAL-PEAK SAWTOOTH WITH A SAMPLE RECORD LENGTH OF 1.0 SECOND

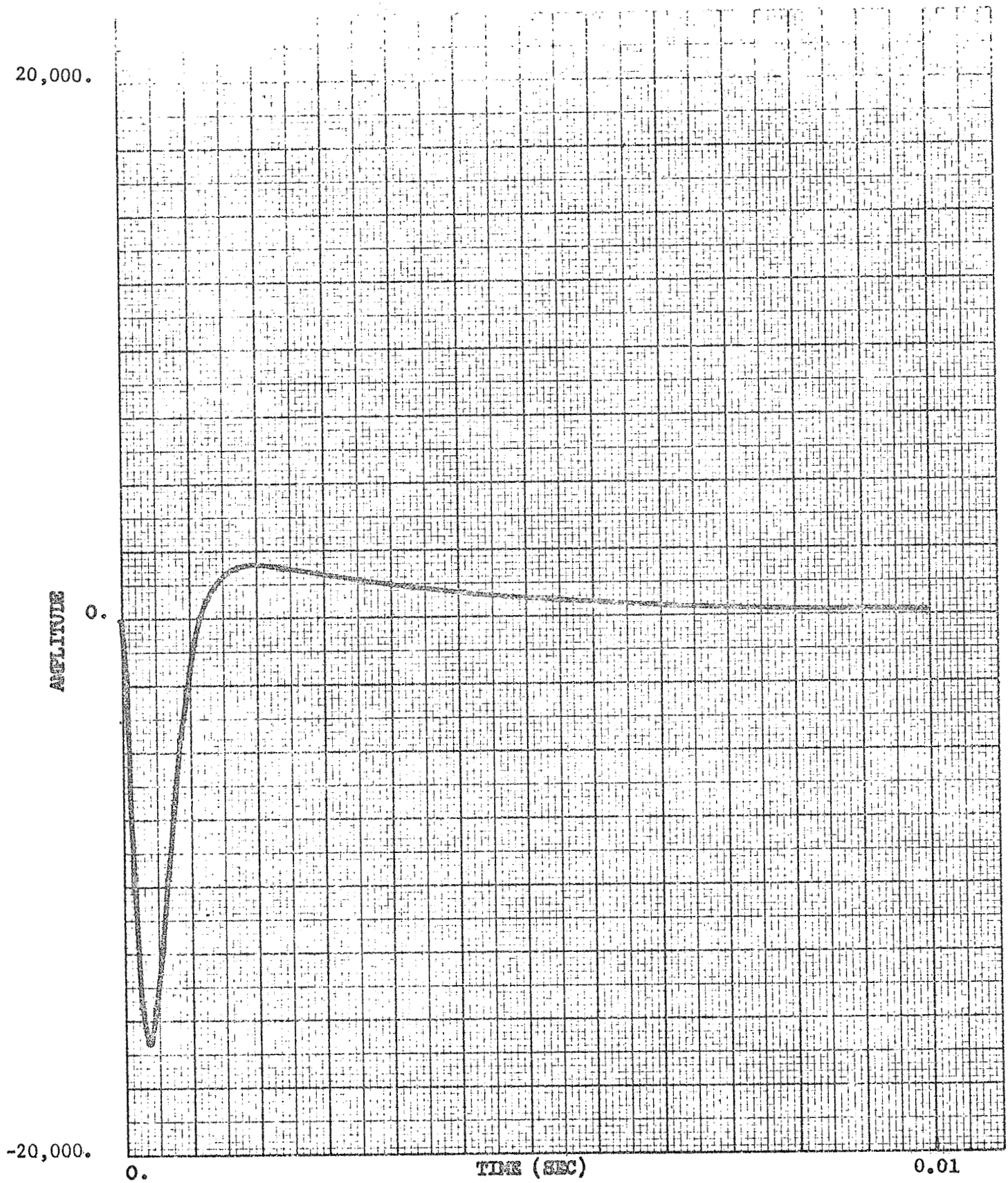



Figure 11: TIME HISTORY: STEP-DECAY FUNCTION

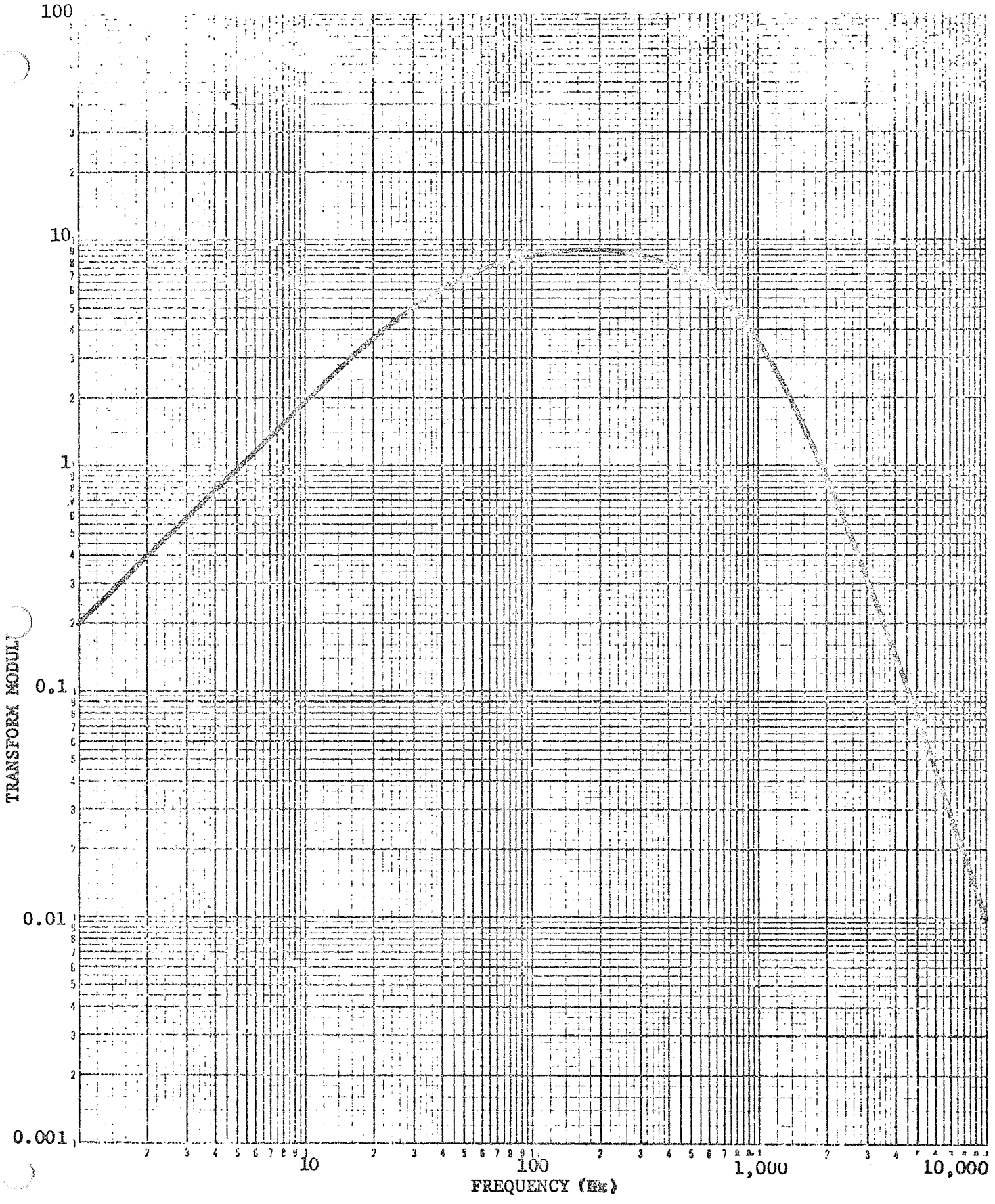



Figure 12: THEORETICAL TRANSFORM; STEP-DECAY FUNCTION

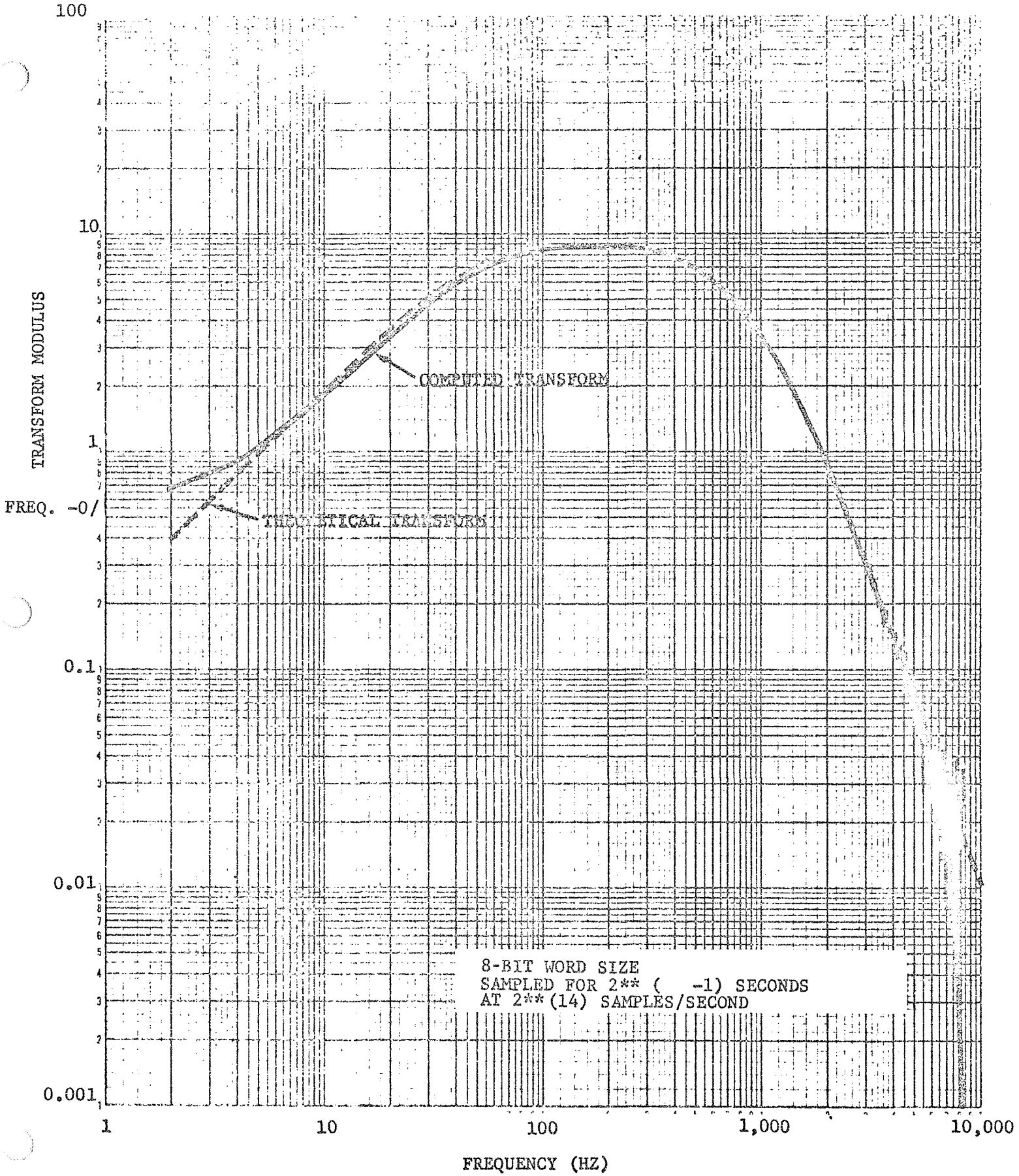



Figure 13: FOURIER TRANSFORM OF AN 8-BIT WORD SIZE MODIFIED STEP-DECAY PULSE

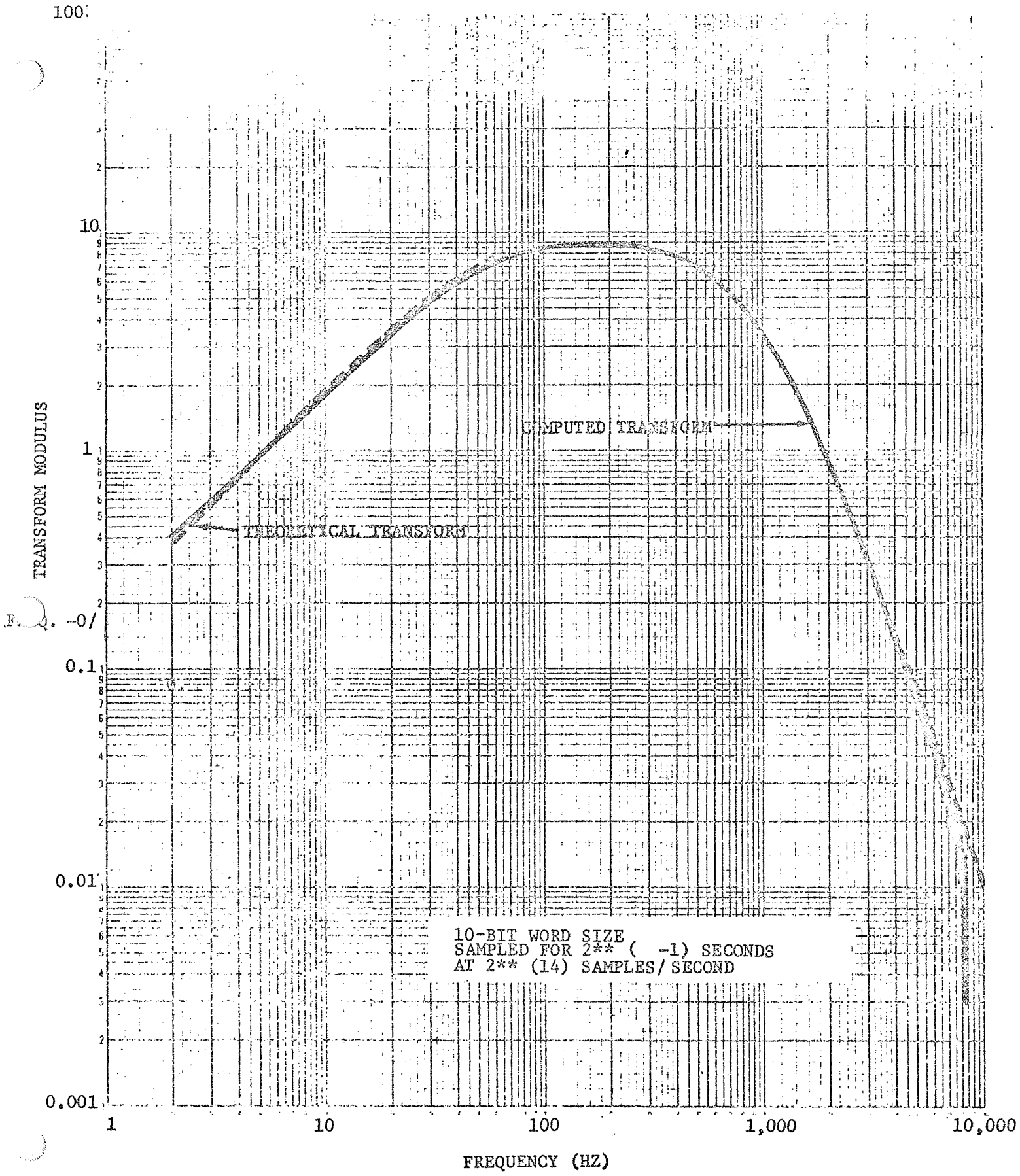



Figure 14: FOURIER TRANSFORM OF A 10-BIT WORD SIZE MODIFIED STEP-DECAY PULSE

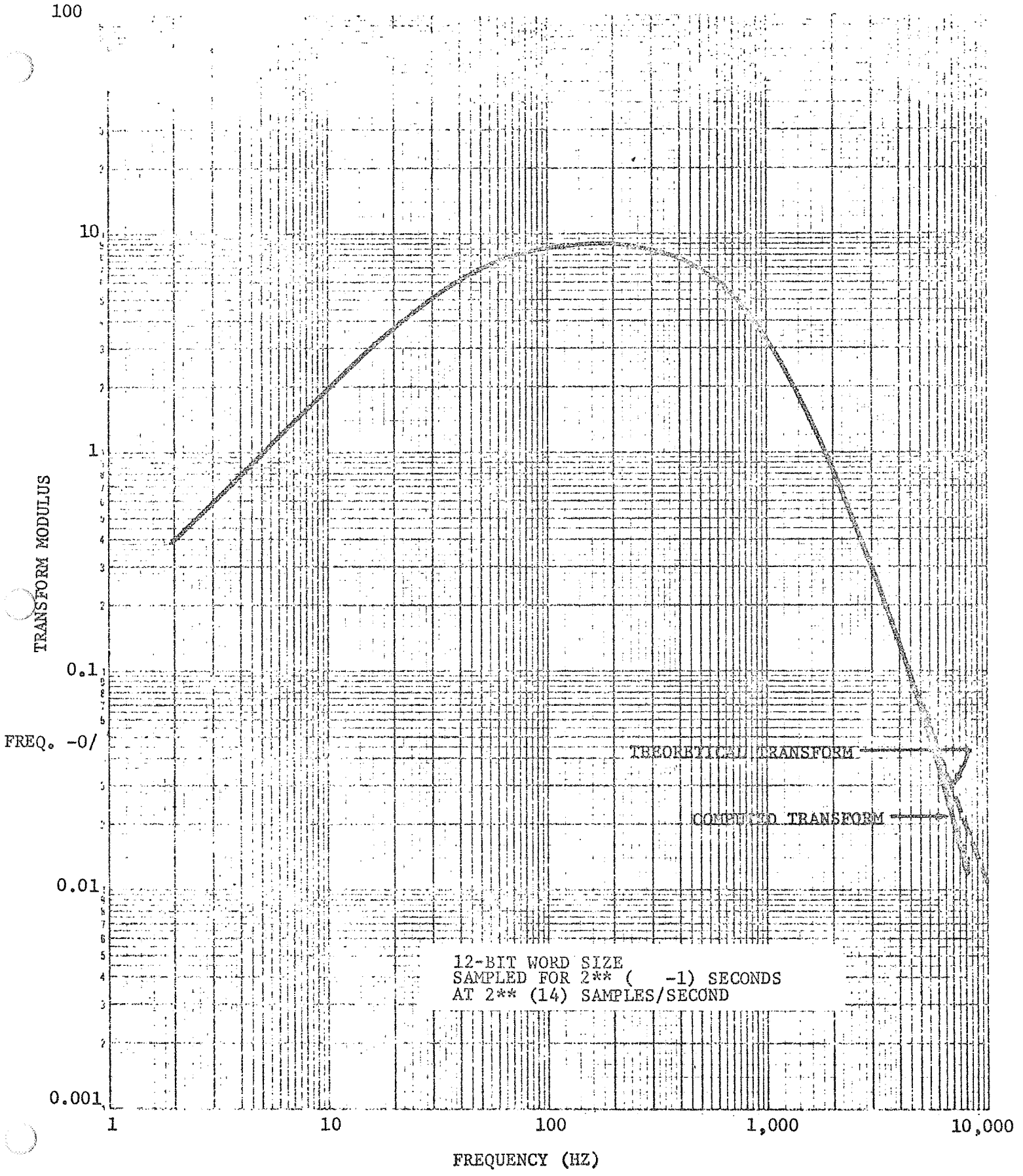



Figure 15: FOURIER TRANSFORM OF A 12-BIT WORD SIZE MODIFIED STEP-DECAY PULSE

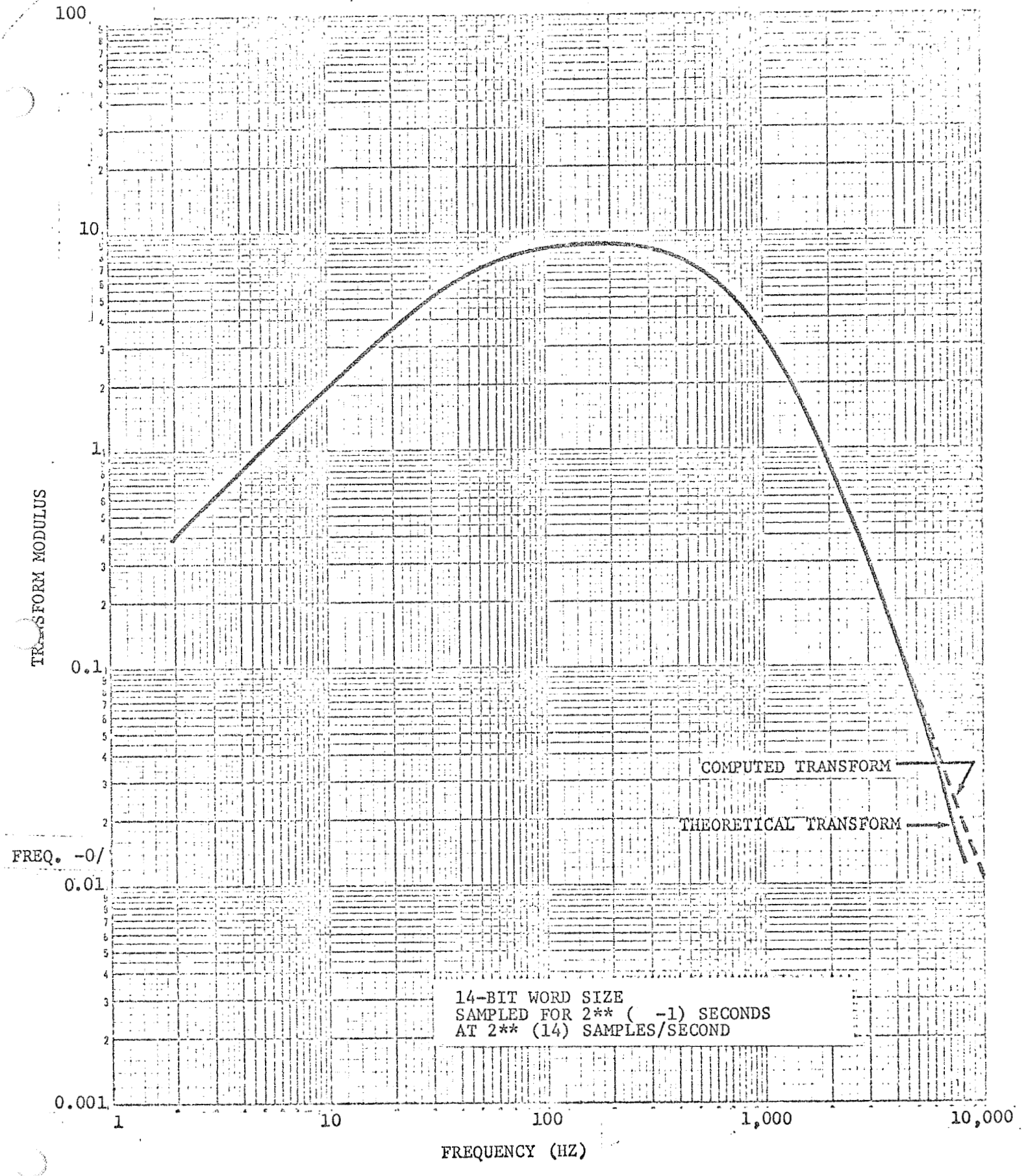



Figure 16: FOURIER TRANSFORM OF A 14-BIT WORD SIZE MODIFIED STEP-DECAY PULSE, SAMPLED AT 16,284 SAMPLES/SECOND

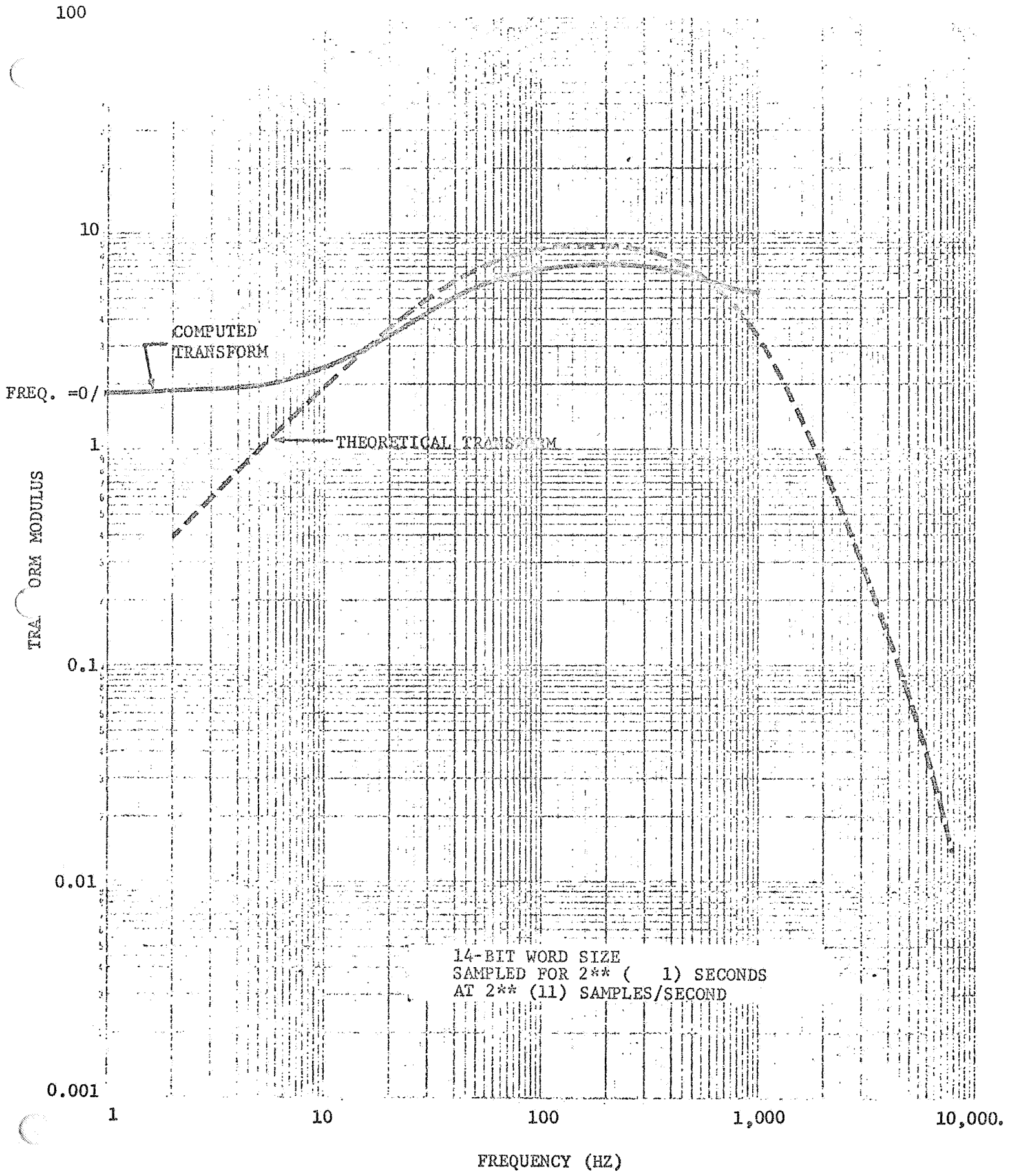



Figure 17: FOURIER TRANSFORM OF MODIFIED STEP-DECAY PULSE SAMPLED AT 2,048 SAMPLES/SECOND

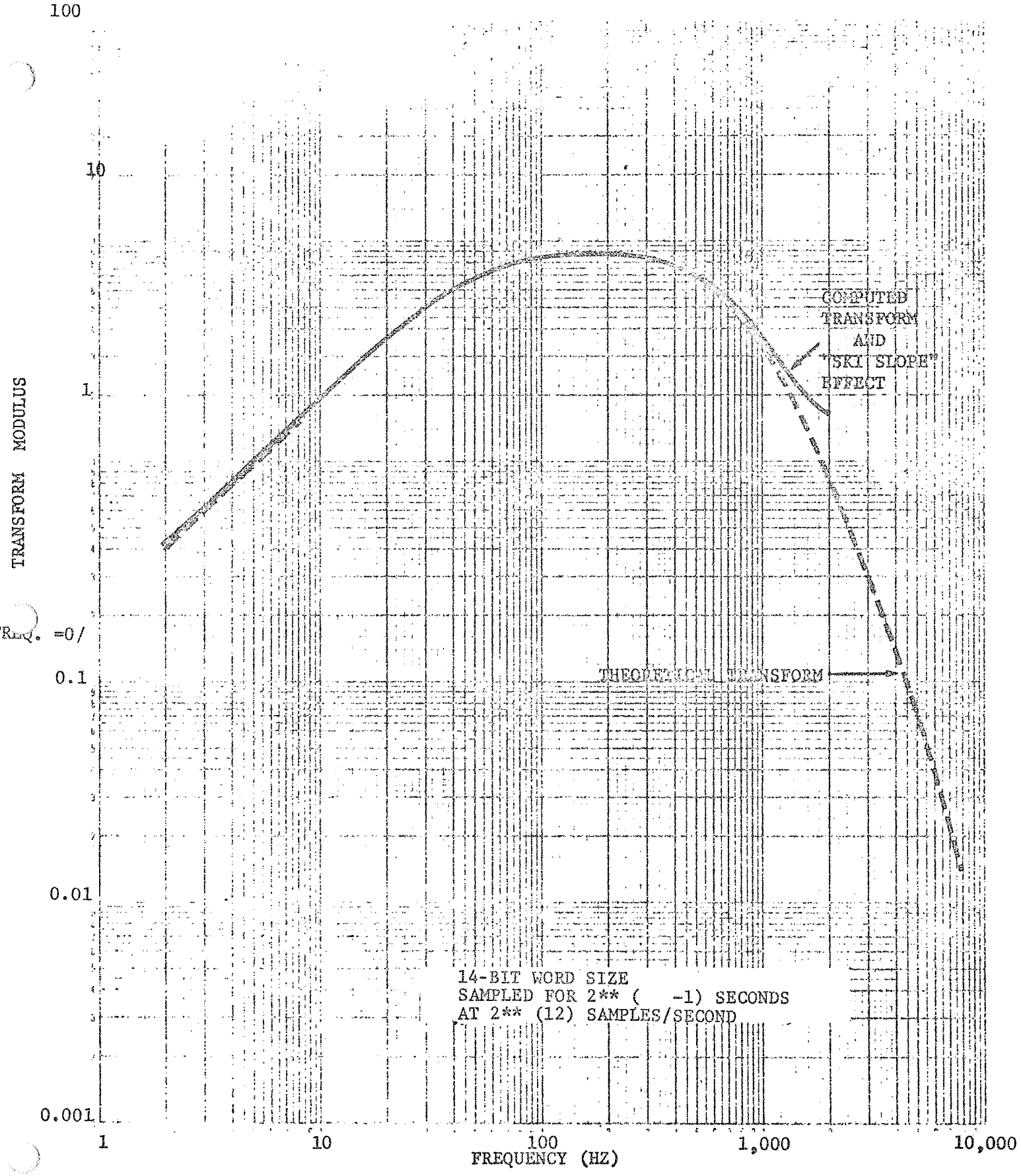



Figure 18: FOURIER TRANSFORM OF MODIFIED STEP-DECAY PULSE SAMPLED AT 4,096 SAMPLES/SECOND

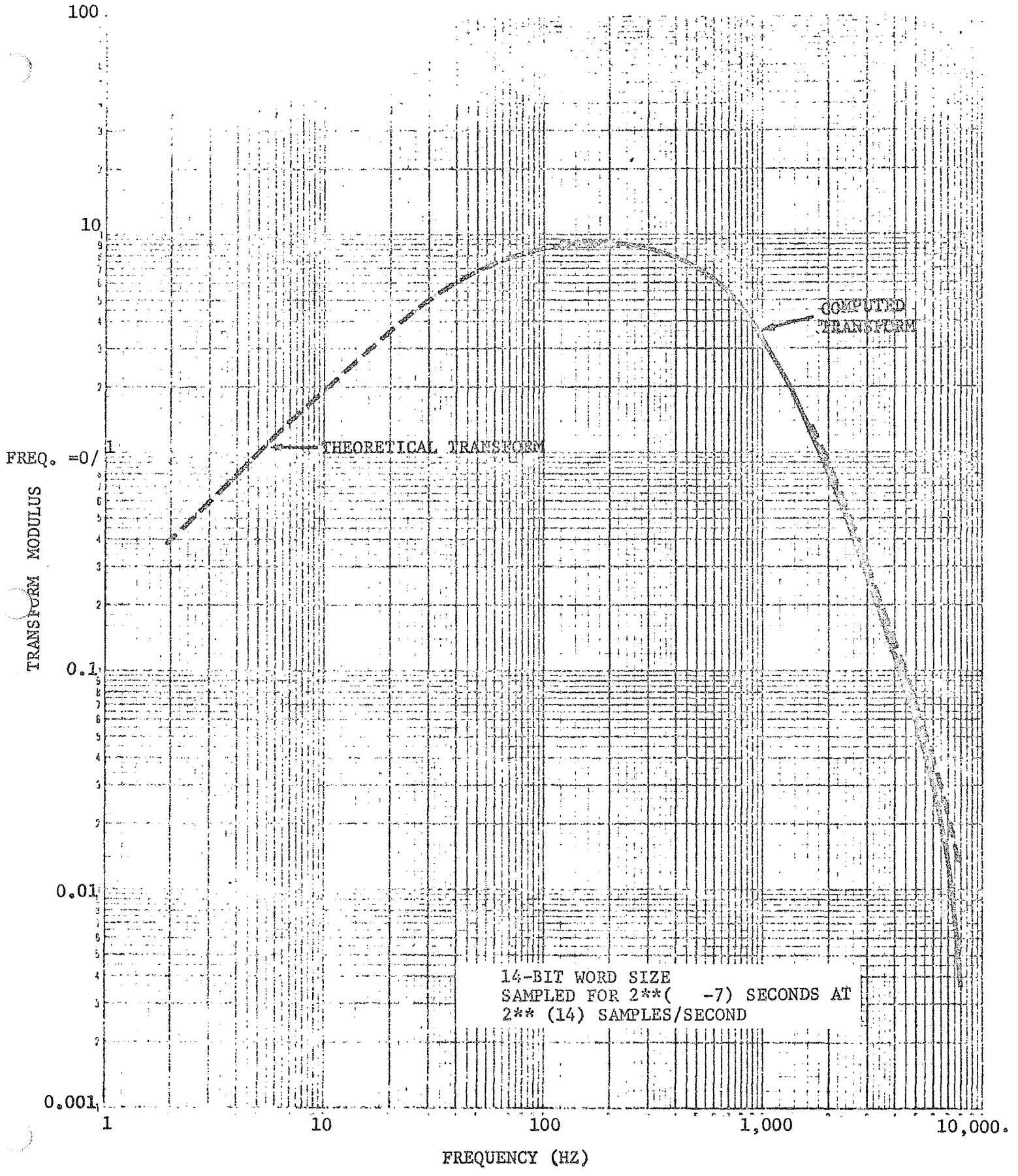



Figure 19 : FOURIER TRANSFORM OF MODIFIED STEP-DECAY PULSE WITH A SAMPLE RECORD LENGTH OF 0.0078 SECOND

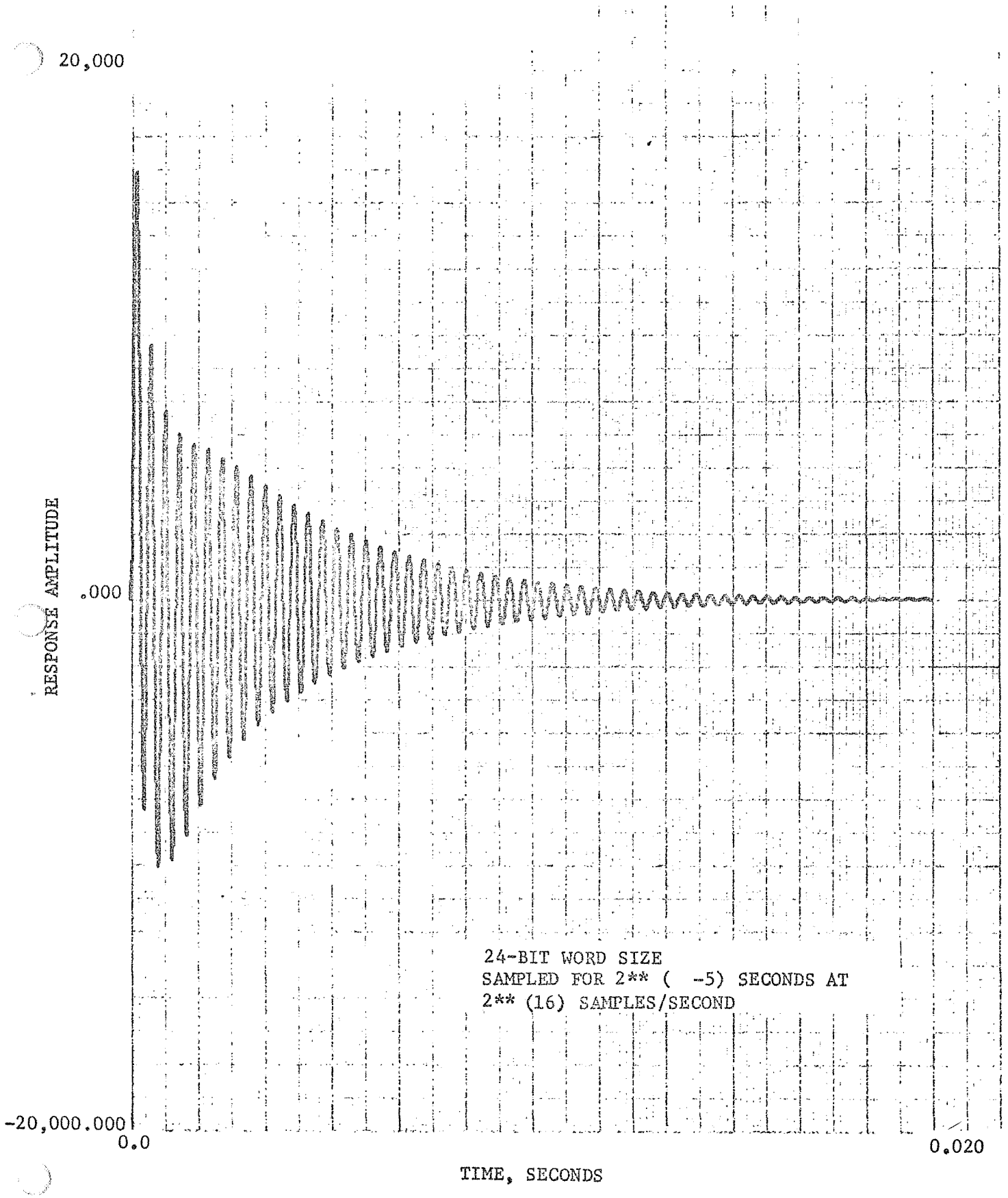



Figure 20 : SHAKER IMPULSE RESPONSE

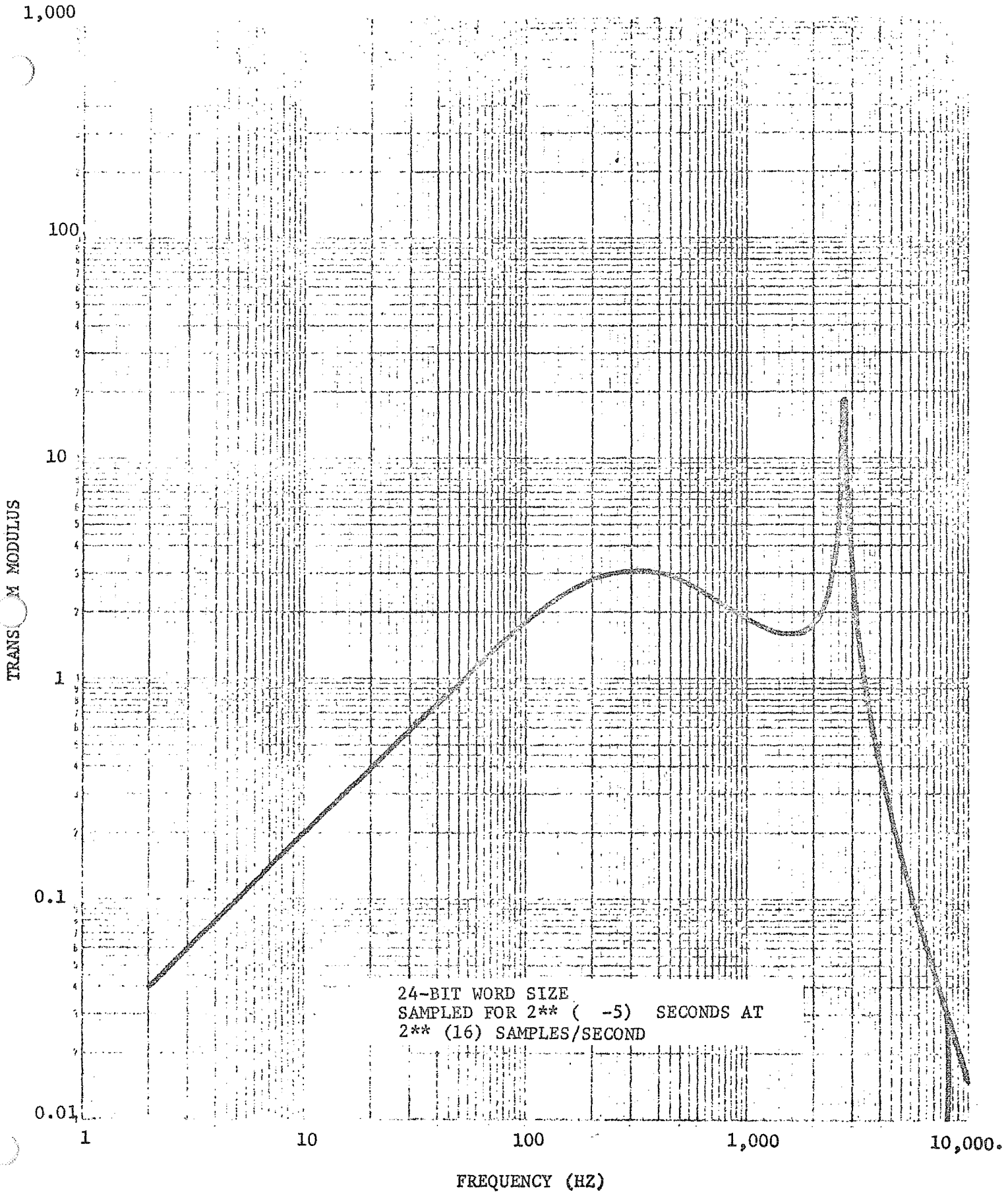



Figure 21: THEORETICAL TRANSFORM OF SHAKER IMPULSE RESPONSE

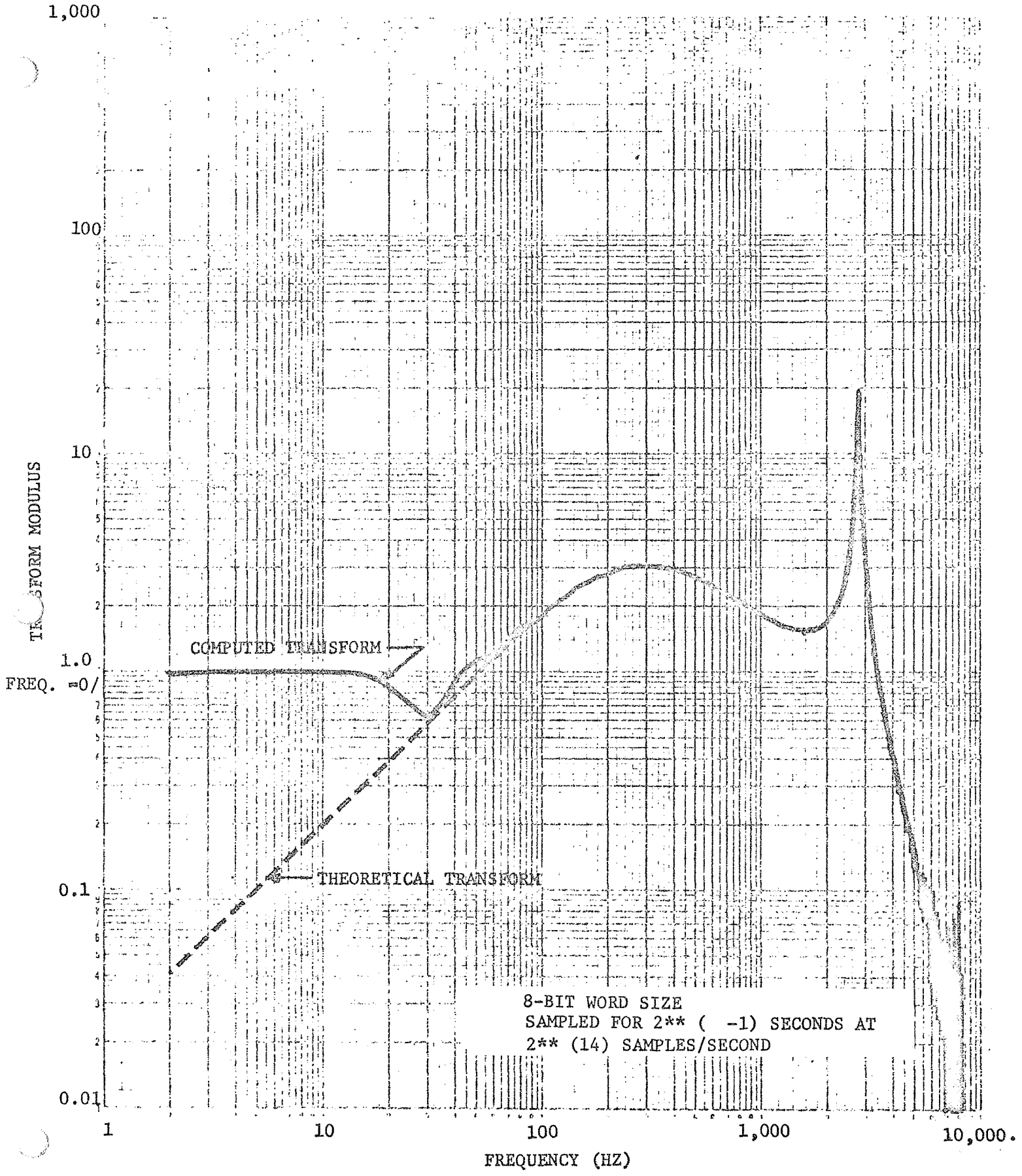



Figure 22: FOURIER TRANSFORM OF AN 8-BIT WORD SIZE SHAKER IMPULSE RESPONSE

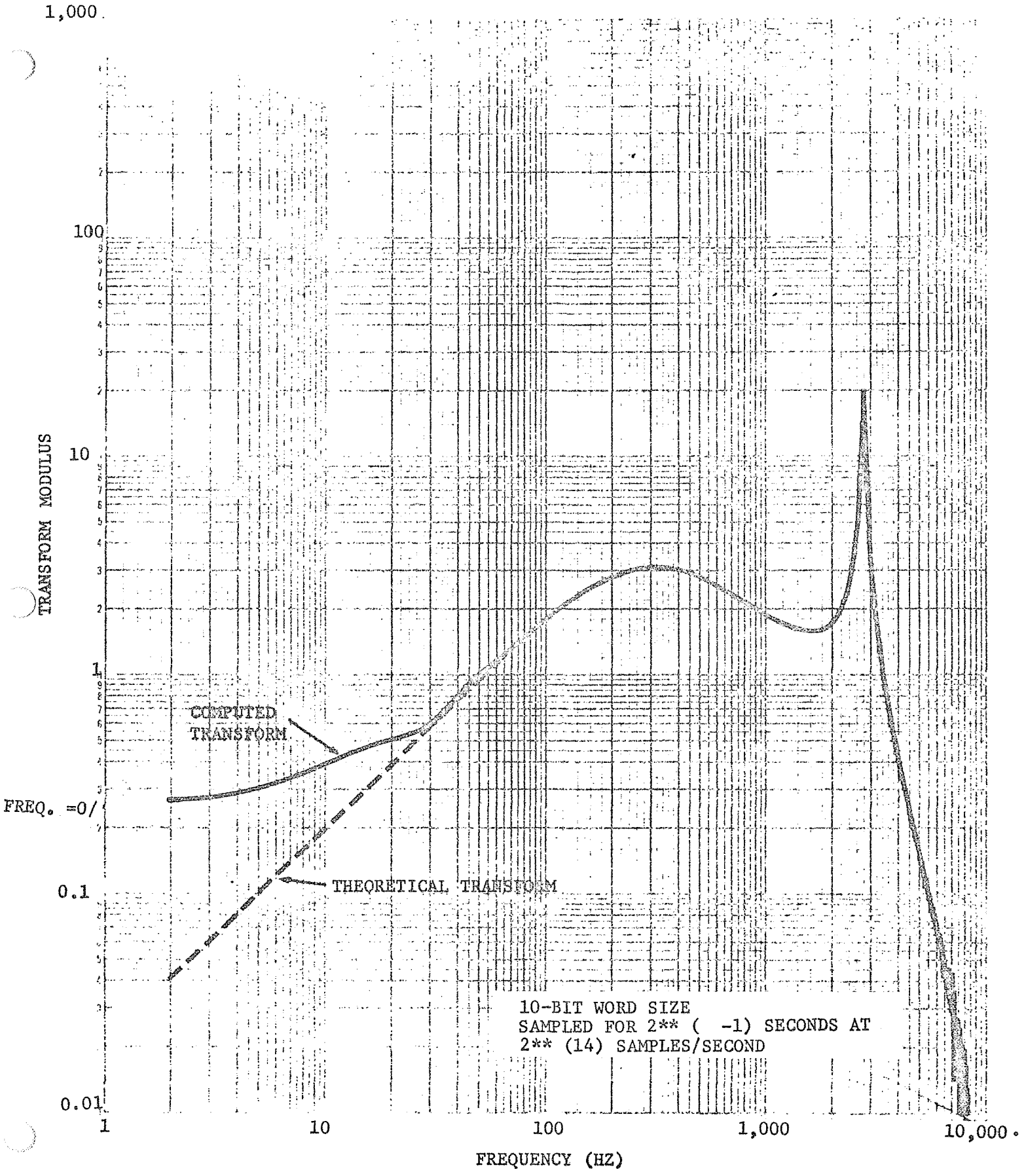



Figure 23: FOURIER TRANSFORM OF A 10-BIT WORD SIZE SHAKER IMPULSE RESPONSE

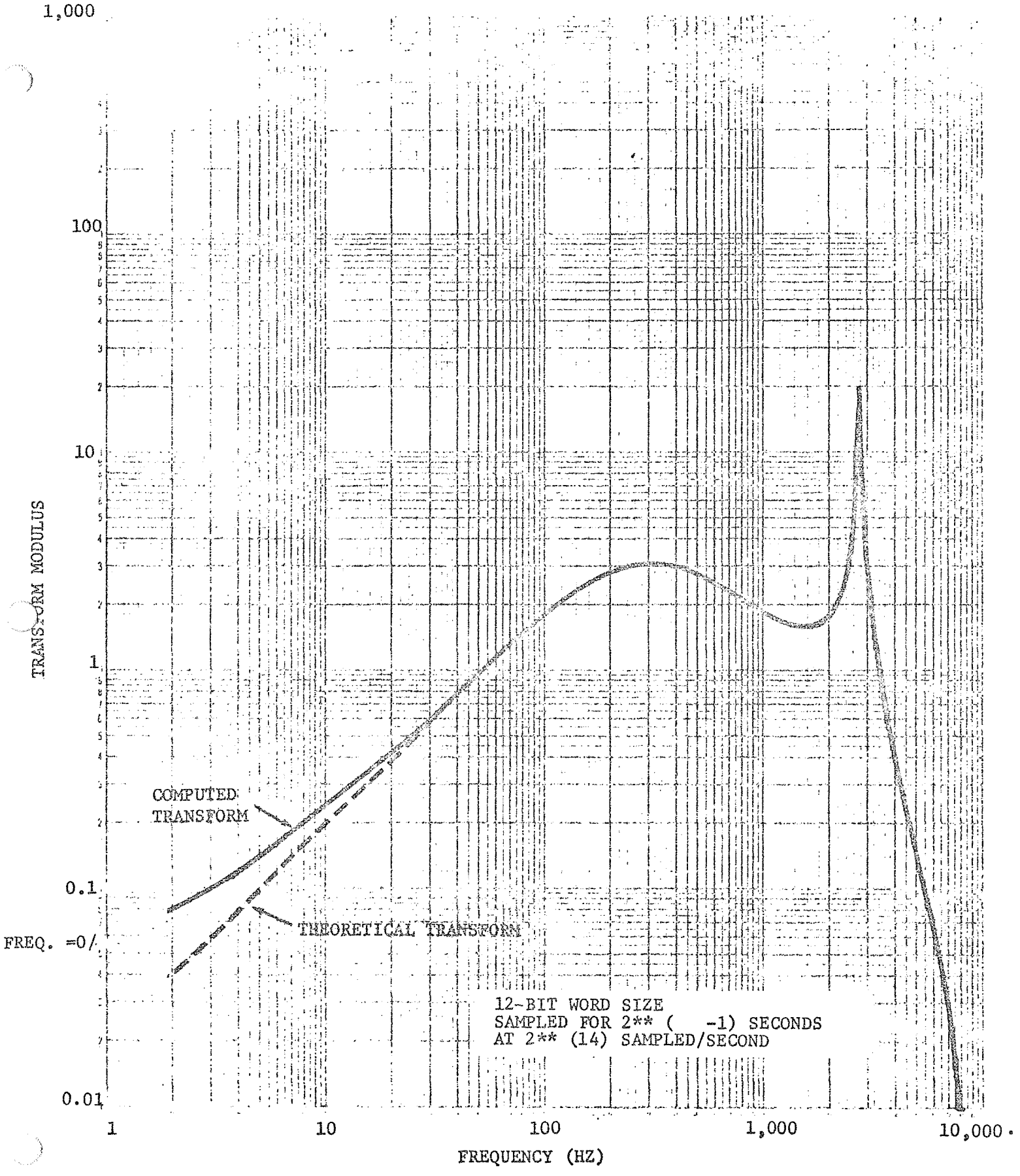



Figure 24: FOURIER TRANSFORM OF A 12-BIT PLUS SIGN SHAKER IMPULSE RESPONSE

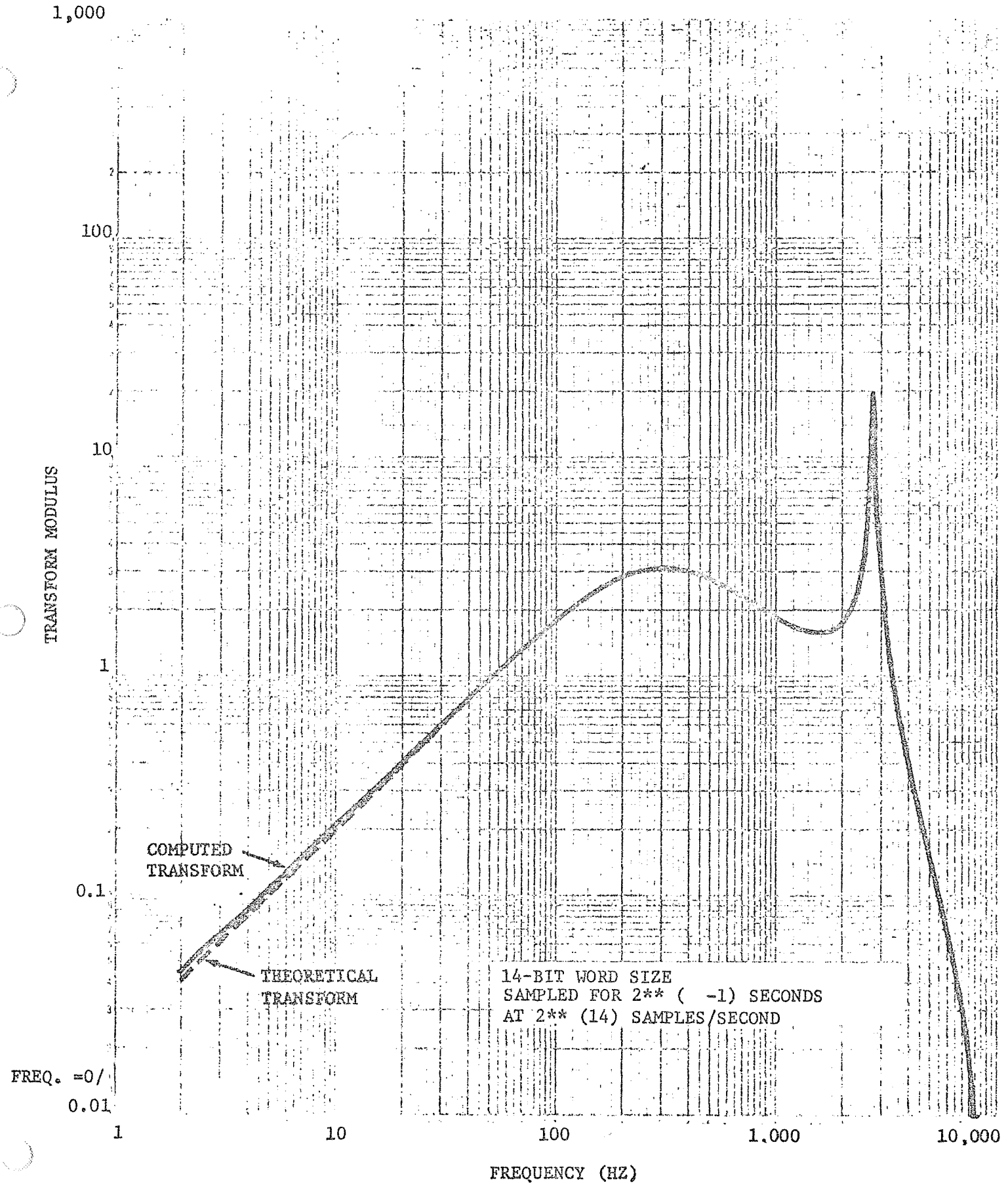



Figure 25: FOURIER TRANSFORM OF A 14-BIT WORD SIZE SHAKER IMPULSE RESPONSE

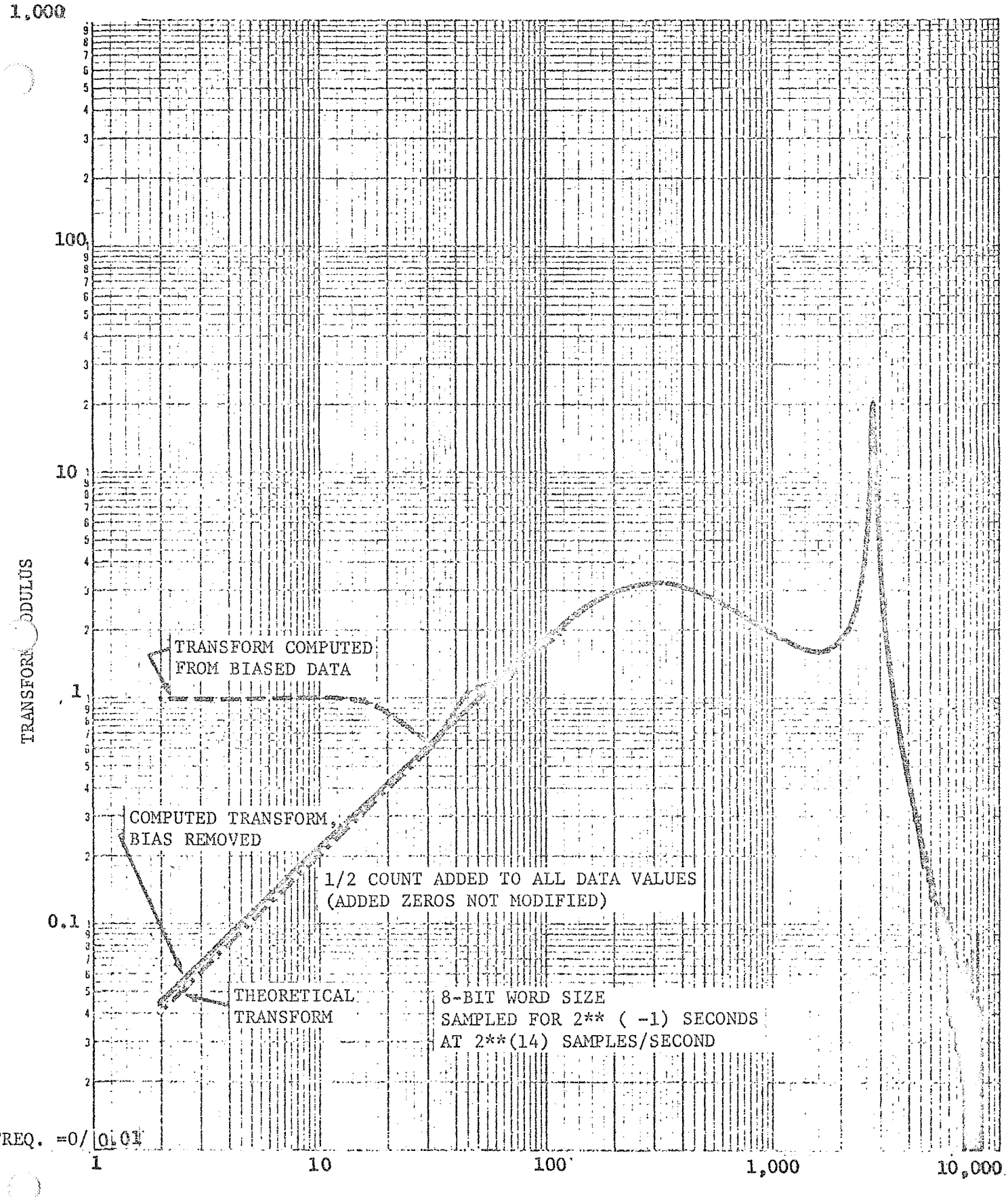



Figure 26: FOURIER TRANSFORM OF 8-BIT WORD SIZE SHAKER IMPULSE RESPONSE UTILIZING THE UNBIAS ROUTINE

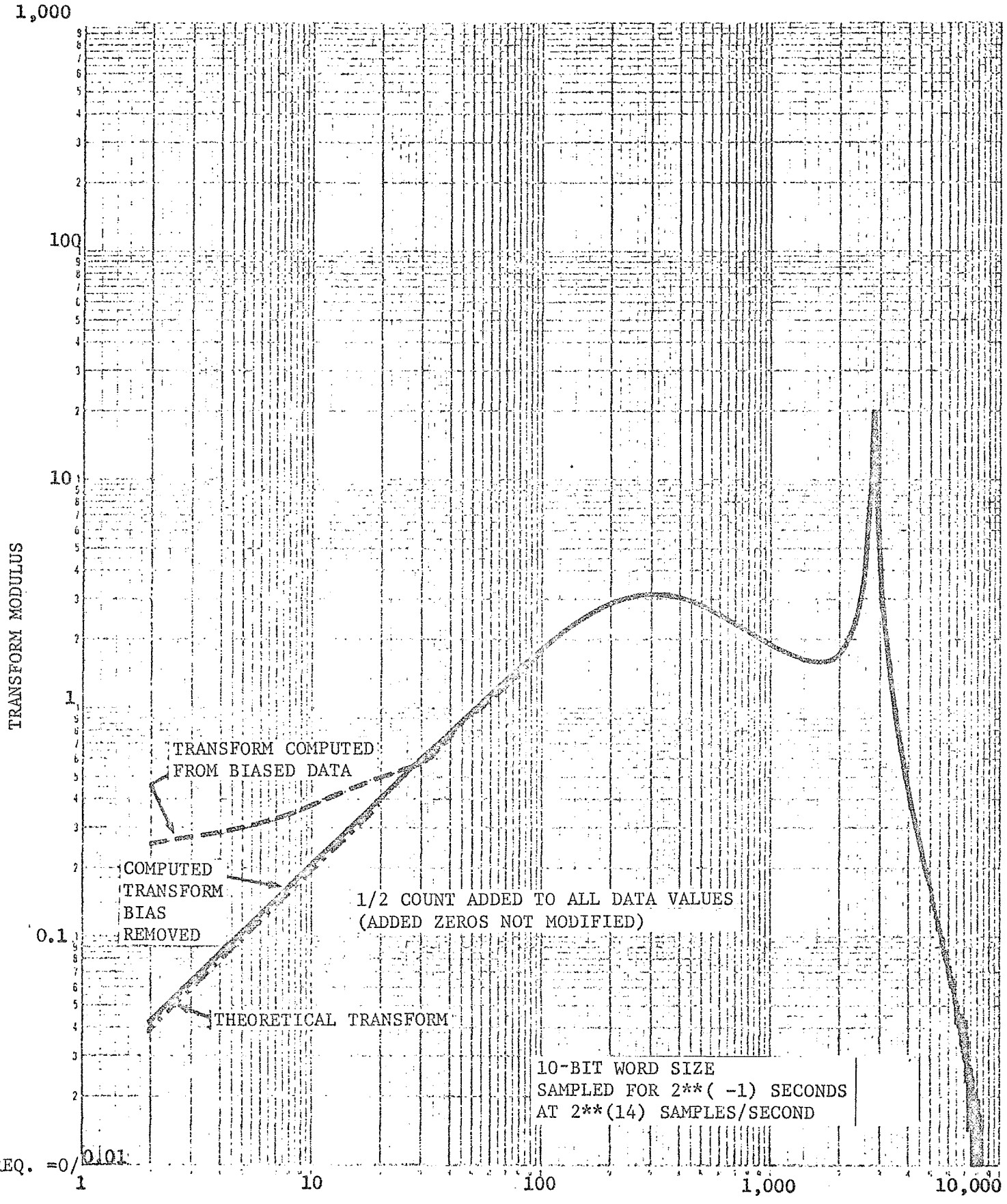



Figure 27: FOURIER TRANSFORM OF 10-BIT WORD SIZE SHAKER IMPULSE RESPONSE UTILIZING THE UNBIAS ROUTINE

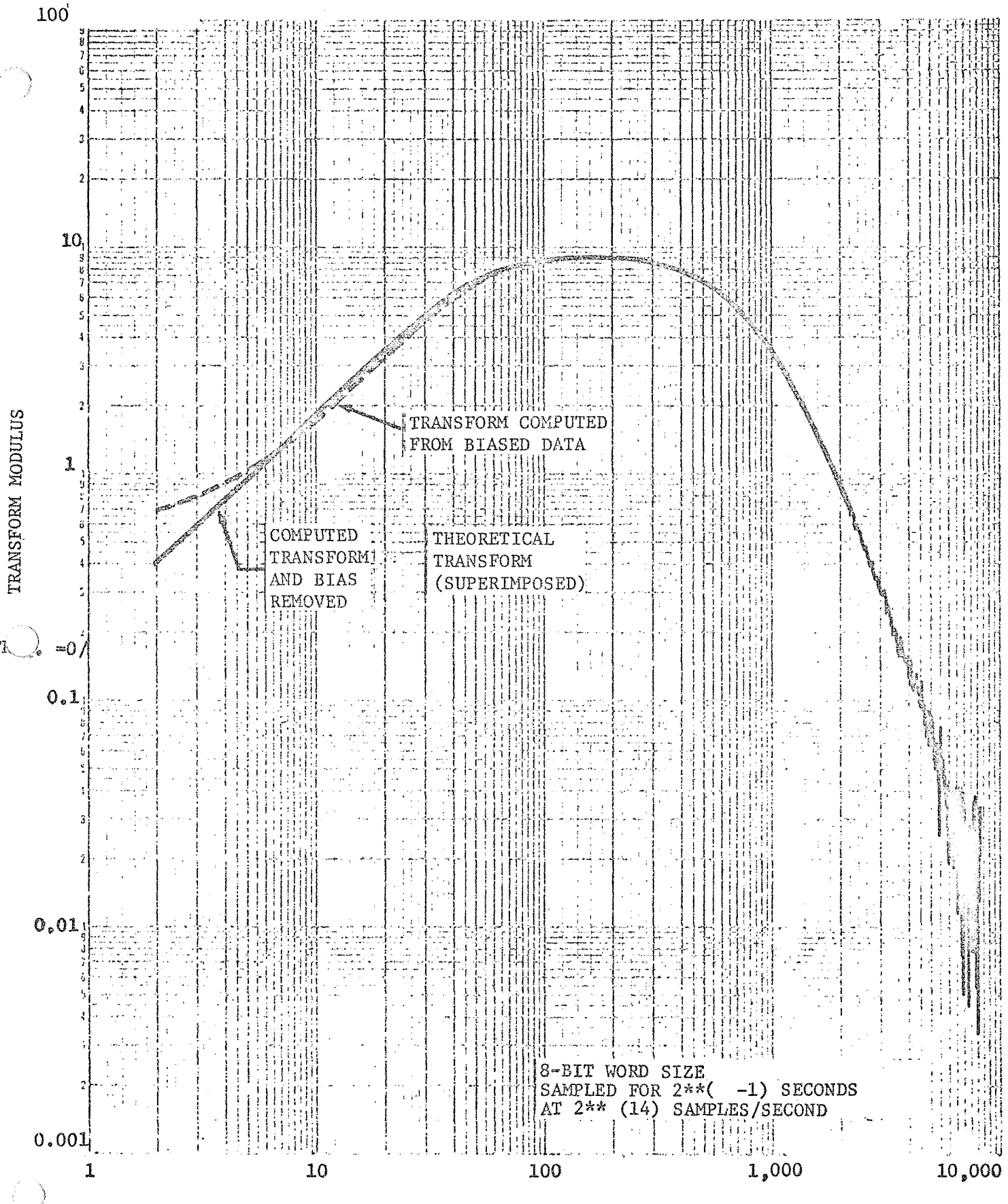



Figure 28: FOURIER TRANSFORM OF AN 8-BIT WORD SIZE MODIFIED STEP DECAY PULSE UTILIZING THE UNBIAS ROUTINE

Noise.-The problem of errors being introduced into the Fourier transform, due to noise riding on the actual data, was also studied. This was accomplished by adding pseudo-random noise, with a Gaussian distribution, to the shaker impulse response data. The distribution assumed a range from $-4\sigma$ to $+4\sigma$ with 100 discrete levels.

The shaker impulse response pulse was generated for 2,048 points. To each of these points, a random number was added. This was done for three different rms noise levels---82 units, 164 units, and 328 units.

An rms level of 82 units is equivalent to 0.5% of the full scale of 16,384 units. For a 14 bit plus sign word size, 1 unit makes up 1-digital count, and the rms noise level is 82 counts; for a 12 bit plus sign word size, 4 units make up 1-digital count, and the rms noise level is 20.5 counts; for 10 bit plus sign word size, 16 units make up 1-digital count, and the rms noise level is approximately 5.1 counts; and for the 8 bit plus sign word size, 64 units make up 1-digital count, and the rms noise level is approximately 1.3 counts.

Figures 29 and 30 illustrate the Fourier transform resulting from the superposition of noise[6] onto a signal. Referring to Figure 29, the hash in the high frequency domain is independent of word size (not quantization error) and is considerably larger than the hash produced by quantization error (Figure 22). From this, it is assumed to be the transform of the noise itself. Again, the effect of digital word size, in the A/D conversion, shows up in the low-frequency domain. The larger the word size transform, the closer is the match with the theoretical transform. Based on previous work, it is assumed that the 14 bit plus sign word size transform is equal to the transform of the noise superimposed onto the transform of the shaker impulse response transform. Figure 30 illustrates the effectiveness of applying the unbias routine to the data. In this figure, the transform of the 8-bit word size data with the unbias routine is compared with the transform of the 14-bit word size data without the unbias routine.

Two generalized conclusions are reached from this noise study. First, the existance of noise on a time-domain function limits the accuracy to which the Fourier transform of that function may be computed. When the noise is the limiting factor, increasing the digital word size will not help. This statement places a constraint upon the performance of equipment, in that the static-noise level must be held to an absolute minimum. It suggested that the rms level of noise, at the A/D converter, should be 1-digital count or less. Second, the unbias routine improves the accuracy of the transformation process, even in the presence of noise.

[6] Only the results of the 82 units rms level noise is presented here. The higher noise levels offer no new information.

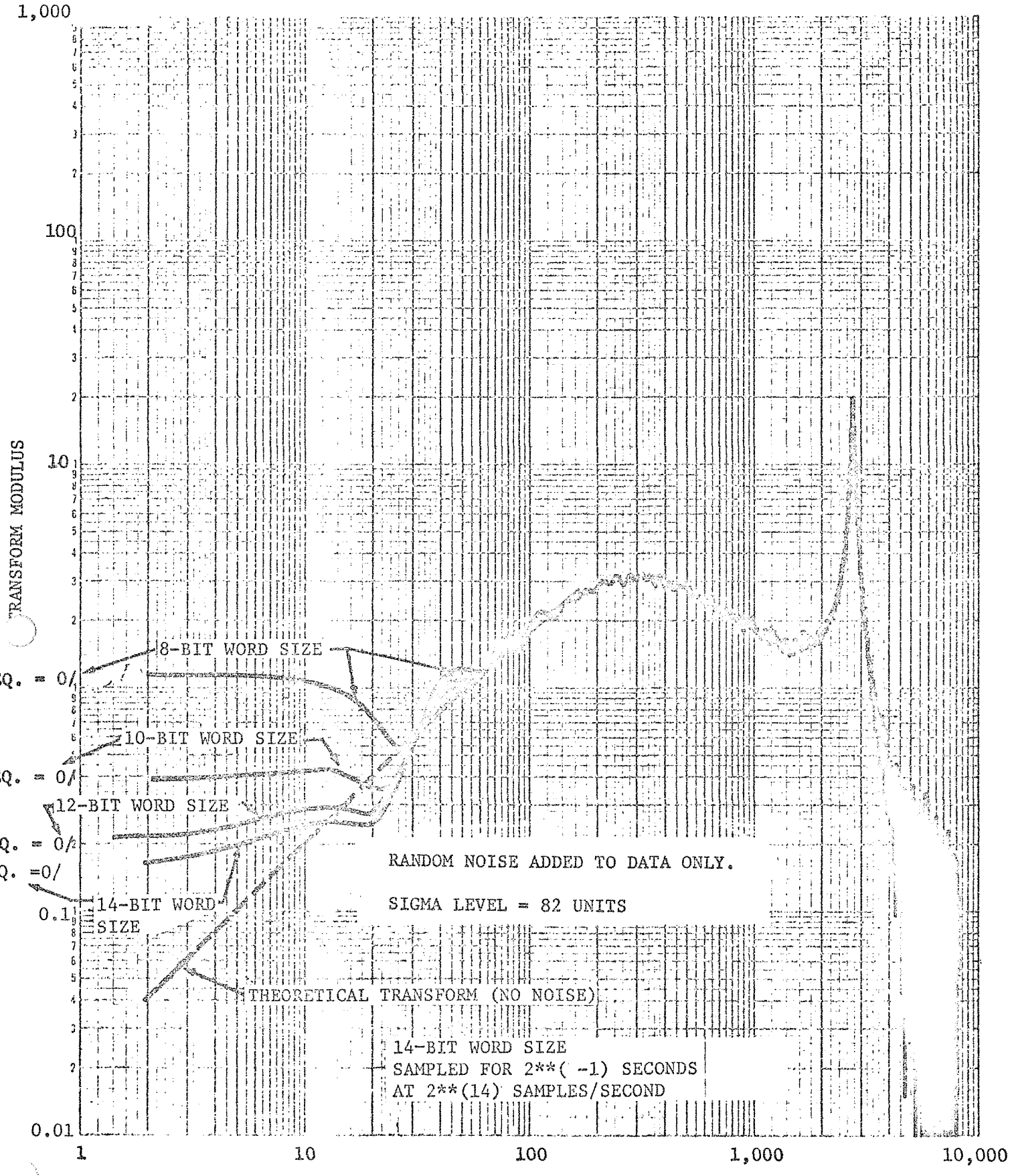



Figure 29: FOURIER TRANSFORMS OF SHAKER IMPULSE RESPONSE WITH NOISE ADDED, WITH AND WITHOUT UNBIAS ROUTINE

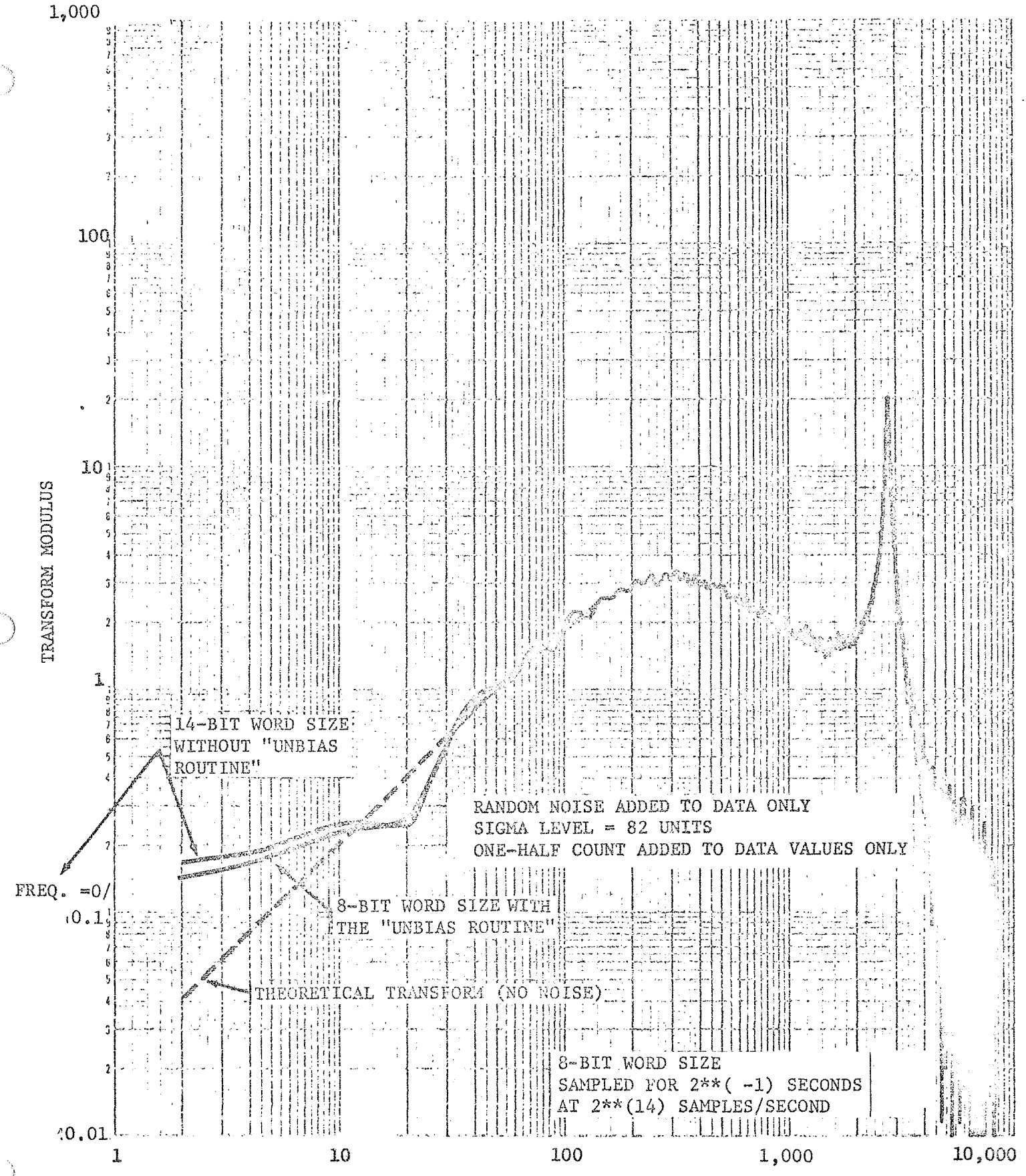



Figure 30: FOURIER TRANSFORMS OF SHAKE IMPULSE RESPONSE WITH VARIOUS WORD SIZE, WITH NOISE ADDED

Experimental Investigation with a Transient Waveform Prototype Control System

An on-line prototype control system, corresponding to the "Transient Waveform Control Logic Diagram" (Figure 3) was developed and evaluated in the Environmental Test Laboratory of the Aerospace Group, The Boeing Company, Seattle, Washington. The primary elements of the control system are contained in a digital "Dynamic Data Analysis System Data Processing" (Figure 31) schematic and pictured in Figures 32A and 32B.

This data system provides data processing support for vibration, acoustic, and shock test operations and is geared to provide a large-volume production analysis capability for random and transient data.

The analysis capabilities include:

1) Power spectral density;

2) Cross power spectral density;

3) Amplitude probability density;

4) Amplitude probability distribution;

5) Auto correlation;

6) Cross correlation;

7) Shock spectrum;

8) Fourier spectrum;

9) Transfer functions.

Communication between the vibration test laboratory and the computer was accomplished with a remote computer test station (Figures 33A and 33B). The computer is controlled by the vibration test system operator using six thumbwheel switch positions on the remote station. The Transient Waveform "Control System Signal Definition and Flow Diagram" are defined by Figure 34. The software "Inter-Overlay Operational Logic Versus Remote Test Station Switch Position" is shown on Figure 35.

The vibration test control console operator exercises complete control over the transient environment in the following manner:

1) The operator establishes that the required transient waveform is realizable on the equipment. This implies that the required deflection, velocity, and acceleration will not exceed test equipment limitations.

2) The operator enters a digital description of the required waveform into the computer via card reader at switch Position 1. This data is nominally scaled to slightly less than 2.00 volts maximum.[7]

[7] The Dynamic Data Analysis System has a 2.0 volt maximum limit at the A/D converter and at the D/A converter.

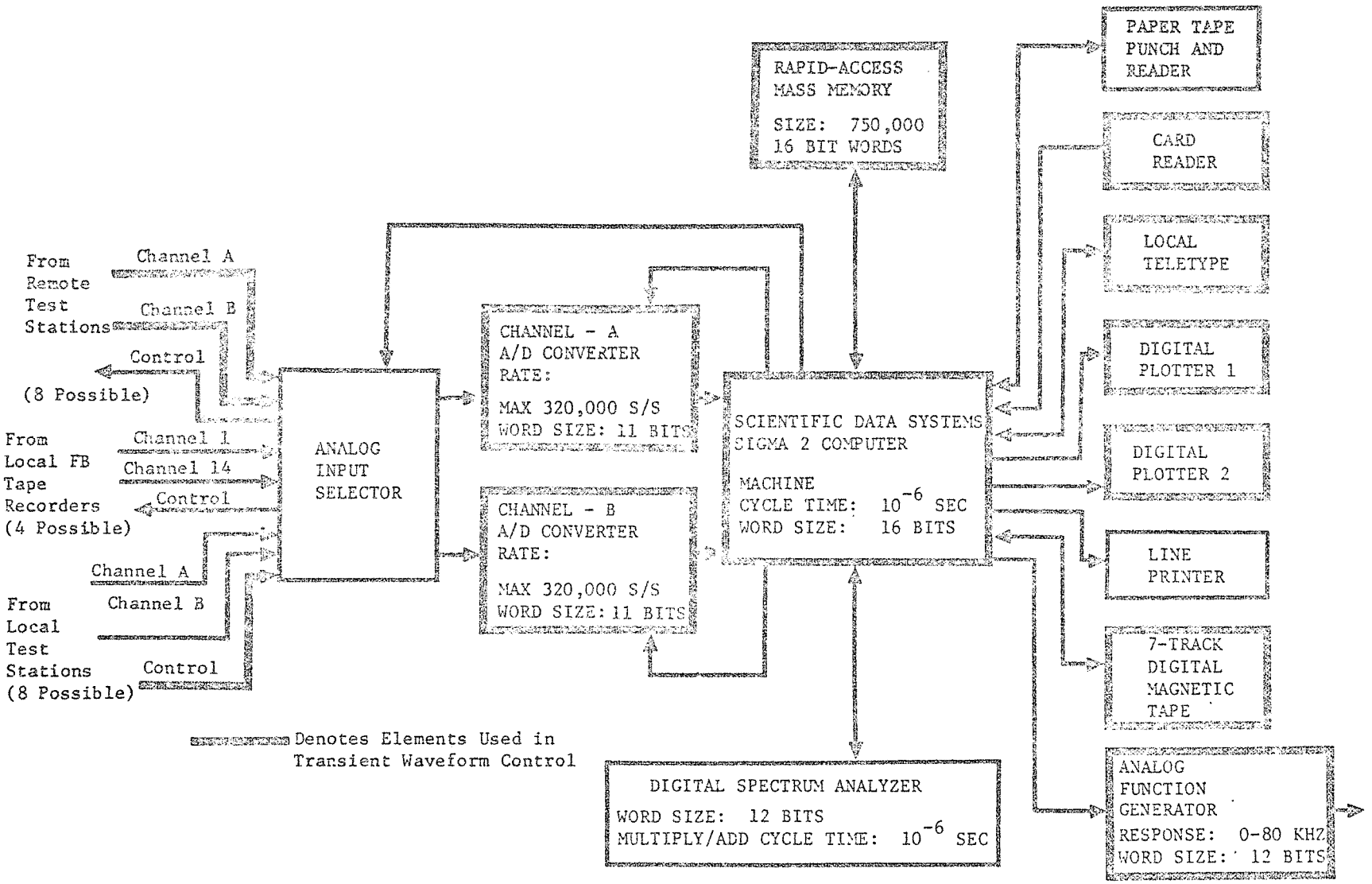



Figure 31: DYNAMIC DATA ANALYSIS SYSTEM DATA PROCESSING



Figure 32A: SIGMA II COMPUTER
RAPID ACCESS MASS MEMORY
HI-SPEED TAPE PUNCH
CARD READER
HI-SPEED LINE PRINTER

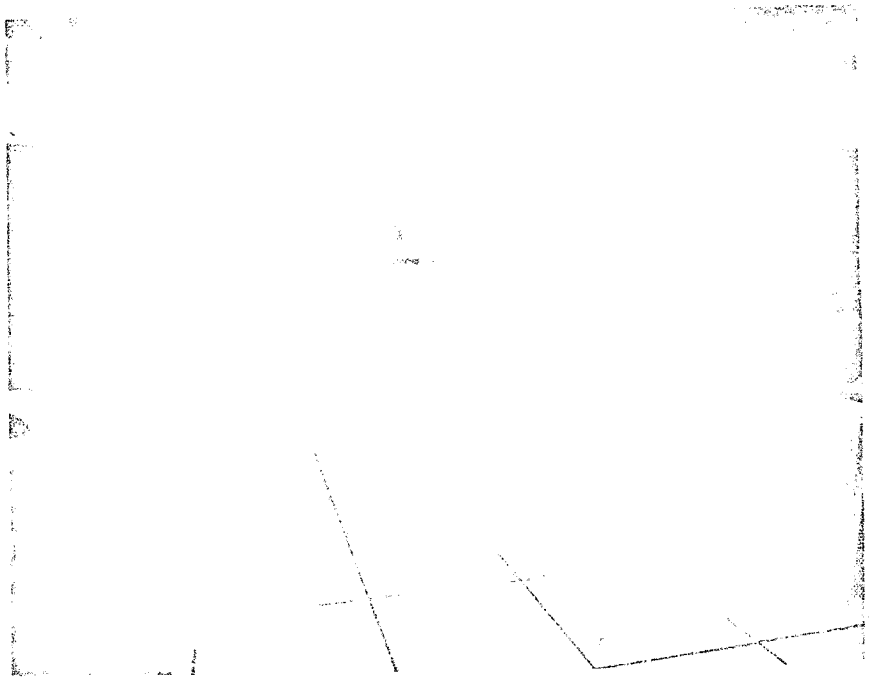


Figure 32B: DIGITAL MAGNETIC TAPE
DIGITAL SPECTRUM ANALYZER
ANALOG FUNCTION GENERATOR
LOCAL TELETYPE, DIGITAL PLOTTER

Figure 32: DYNAMIC DATA ANALYSIS SYSTEM

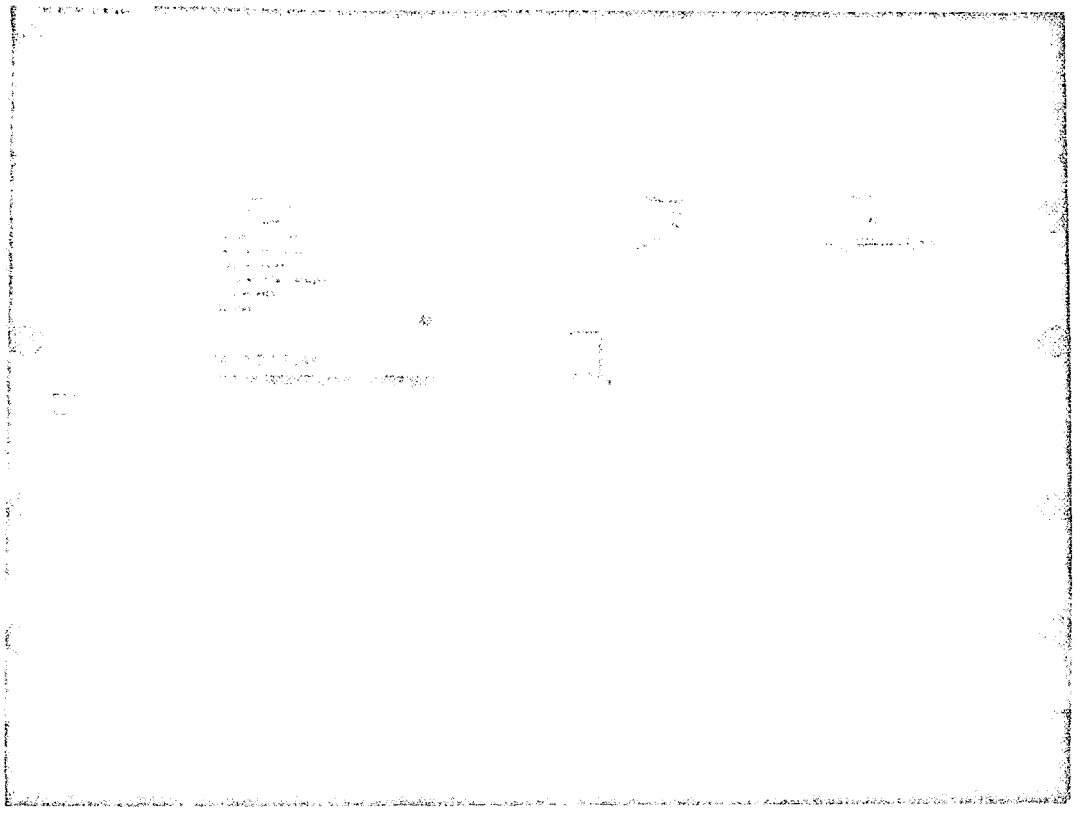


Figure 33A: TEST STATION FUNCTIONAL LAYOUT

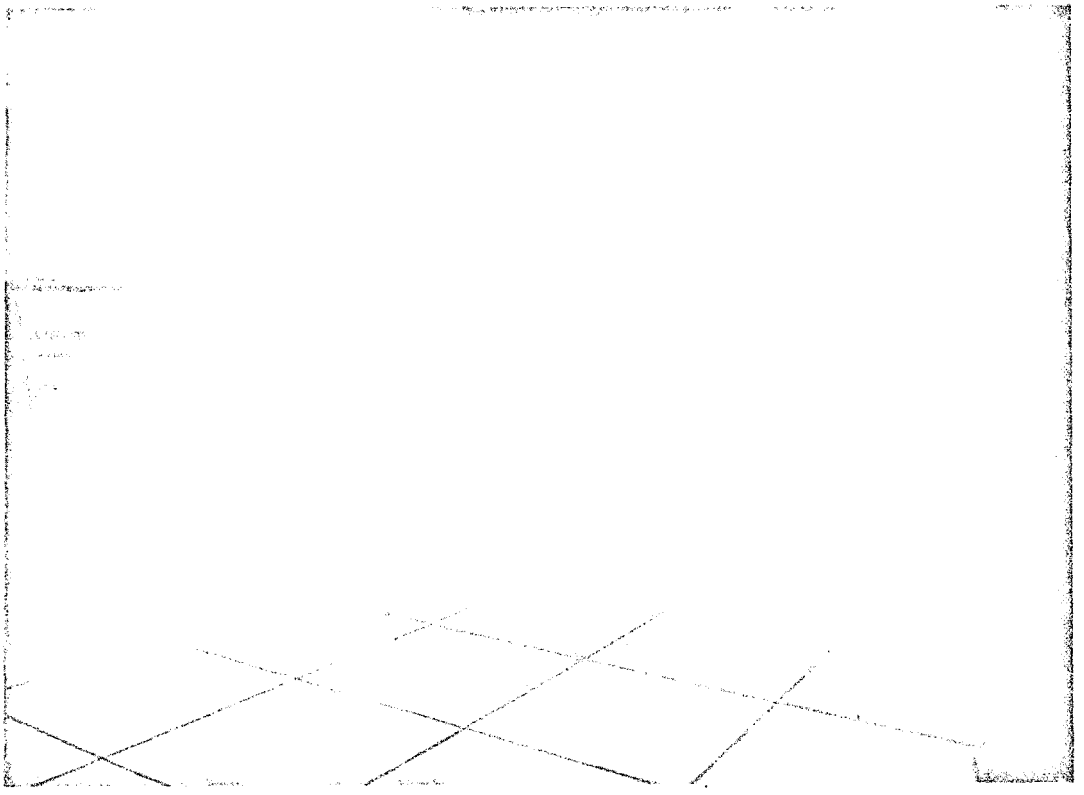
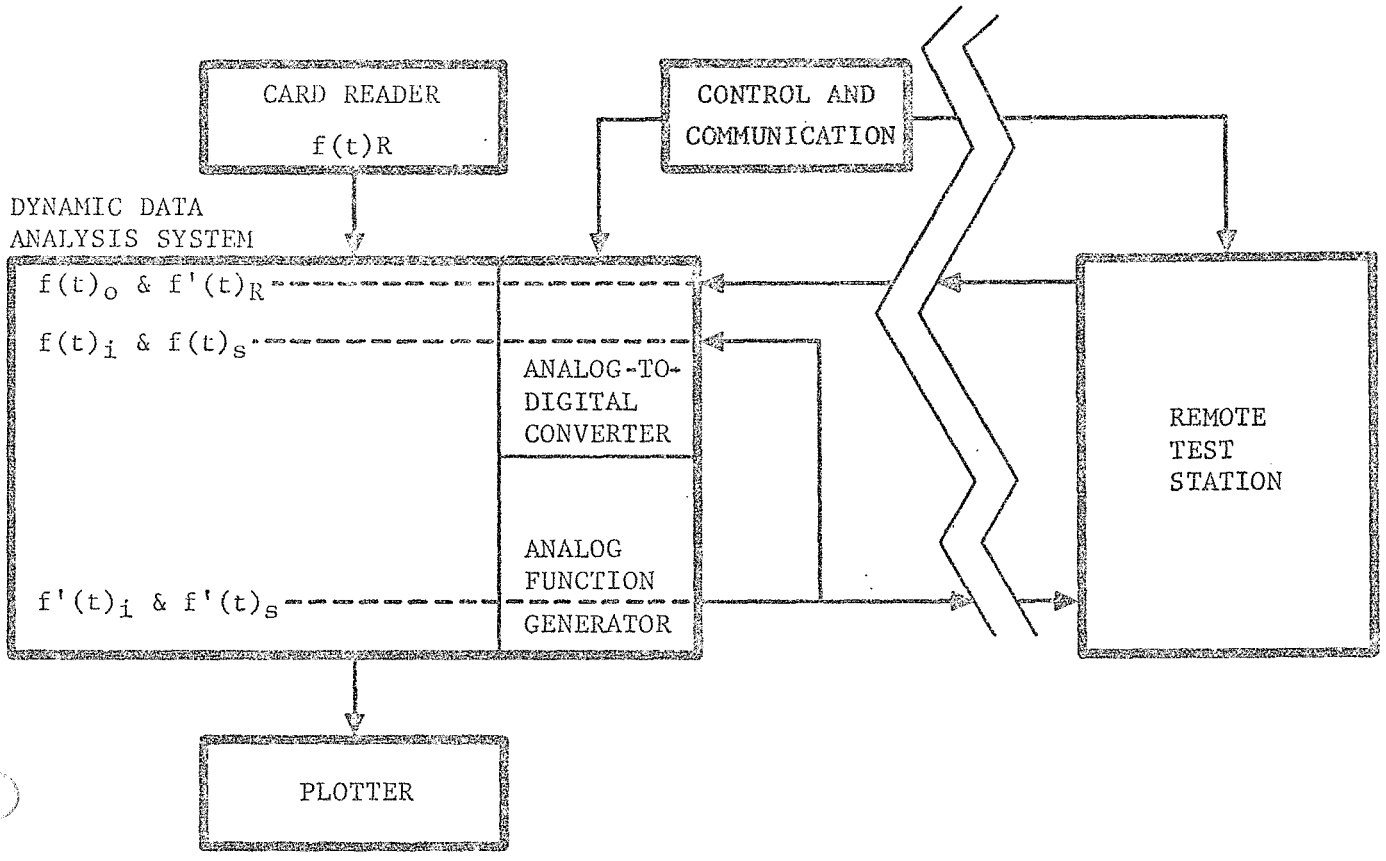


Figure 33B: TEST STATION LOCATION AT VIBRATION CONTROL CONSOLE

Figure 33: COMPUTER INTERFACE TEST STATION
IN VIBRATION TEST LABORATORY




SIGNAL DEFINITION

$f'(t)_i$ = Calibration pulse (computer internal description, digital form) [6]

$f(t)_i$ = Calibration pulse as seen by the external world

$f(t)_o$ = Response to calibration pulse

$f'(t)_s$ = Synthesized signal (computer internal description, digital form)

$f(t)_s$ = Synthesized signal as seen by the external world

$f'(t)_R$ = Response to synthesized signal (control accelerometer)

$f(t)_R$ = Required response function from card reader

[6] $f(t)_i$ or $f(t)_s$ is produced by passing $f'(t)_i$ or $f'(t)_s$ through a Digital-to-Analog Converter and Lo-Pass Filter.

Figure 34: CONTROL SYSTEM SIGNAL DEFINITION AND FLOW DIAGRAM

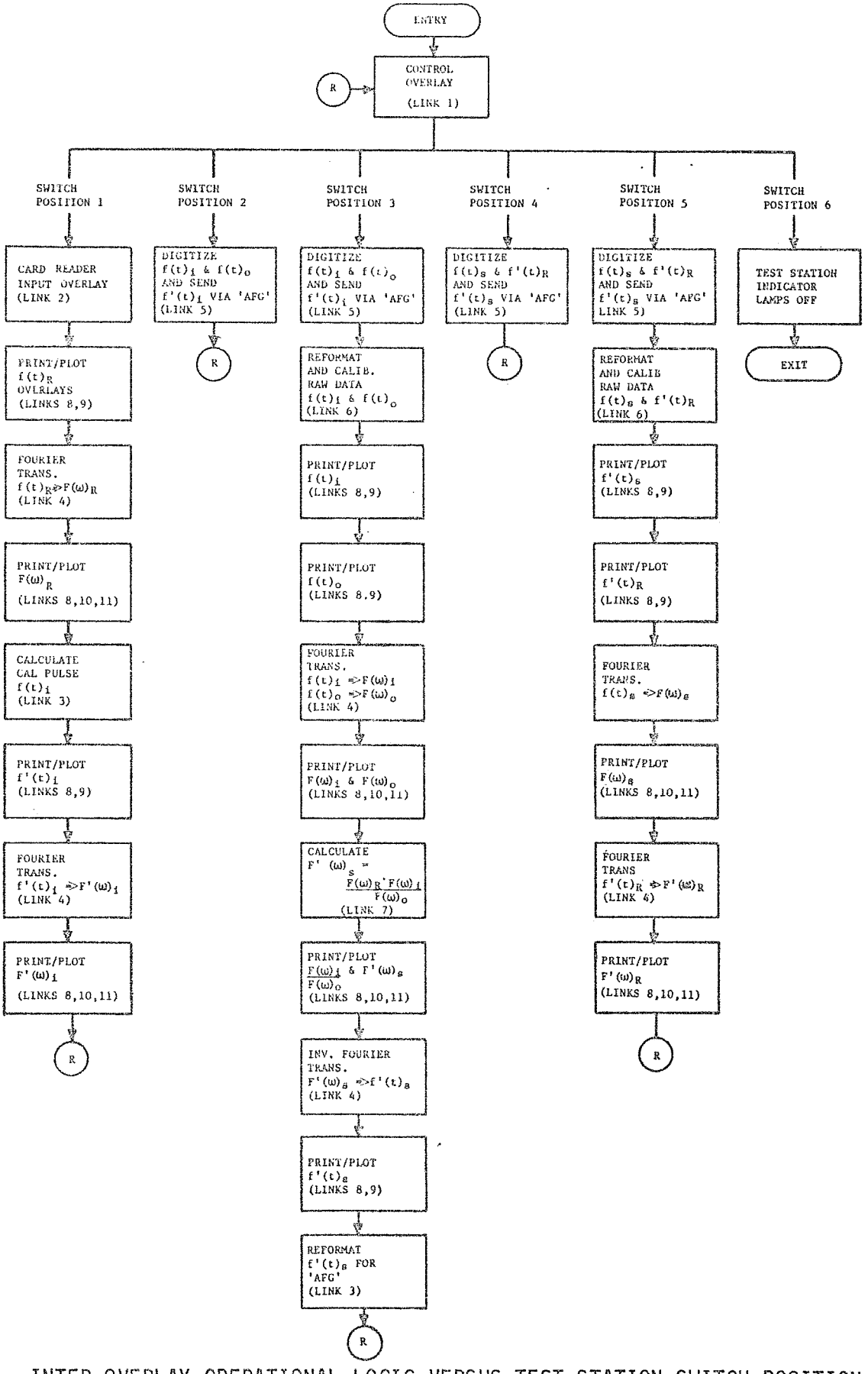



Figure 35: INTER-OVERLAY OPERATIONAL LOGIC VERSUS TEST STATION SWITCH POSITION

3) The operator advances to switch Position 2, activates the test system, and establishes the vibration test console master gain setting for the calibration pulse control accelerometer response. This setting is obtained by viewing the peak response. The operator presses the ENTER button on the remote station, permitting the calibration pulse to be transmitted to the control console as an input signal. The correct nominal level is normally attained by the second iteration of console gain adjustment.

4) The operator advances the remote station control to Position 3, with the test system active, and actuates the ENTER button. In this position, the calibration pulse excites the system and the computer, via A/D converters, interrogates the calibration and response time histories and from them develops the system transfer function. The computer then goes on to compute the synthesized signal. It then returns control to the operator via a waiting light on the remote test station.

5) The operator advances the control to Position 4. This position enables the operator to look at the synthesized voltage time history to evaluate its probability of synthesizing the correct waveform (i.e., is it clipped in transmission, does it contain an initial or final step function that will violate the intent of the calculation?). For example, see Figures 47 and 57.

6) The operator advances the remote test station control to Position 5 for the actual test. The test system is active at the previously established master gain setting and the ENTER button is activated. The synthesized signal is transmitted to the control console to produce the required waveform at the response location. The response waveform is monitored by the computer and subsequently analyzed and plotted in the time domain and frequency domain.

7) The operator options to advance to Position 6 to exit the program (testing complete), or to return to Position 1 or 2 for further testing.

The prototype control system characteristics during the evaluation were:

1) Analog to digital converter word size equal to 10 bit plus sign;

2) Sampling rate of 20,000 samples/second (i.e., 4-data points for the highest frequency of interest);

3) Antialiasing filters in front of the A/D converters (6-pole Butterworth, low-pass (5 kHz)).

The waveforms selected for this experiment were derived from the TAT/Agena-D launch vehicle (OGO-D spacecraft)[7][8] and were considered typical of staging transients eligible for simulation on laboratory test apparatus.

[8]TAT is Thrust Augmented Thor/Agena-D Launch Vehicle and OGO-D is Orbiting Geophysical Observatory

The prototype control system included many print and plot options that were used during the development of the digital program. A complete set (15 plots) are included for one transient simulation PL 20 at T + 234.5, Agena + x vibration, which was a vibratory response to shroud ejection. The second transient to be simulated was PL 30 at T + 234.5, Agena + x acceleration. The experiment was conducted on a Ling 249 (30,000 force pound) vibrator driven by a Ling PP 120/150 kva amplifier. The test specimen was a 450 pound plate.

A statistical analysis of the synthesized OGO-D flight data[7] that had a time domain error variance of less than 13% is given in Appendix III.

The experimental data, derived from the digital control system plot options, are:

1) A time history plot of the test system calibration pulse (Figure 36);

2) The Fourier transform modulus of the calibration pulse (Figure 37);

3) The phase spectrum of the calibration pulse (Figure 38);

4) The time history of the test system control accelerometer response to the calibration pulse (Figure 39);

5) The Fourier transform modulus of the control accelerometer calibration response (Figure 40). (Note that this response approximates the modulus of the transfer function, $H(\omega)$, of the system. The vibration console operator would view this plot as the "open loop" response of his system.);

6) The phase spectrum of the test system calibration response (Figure 41);

7) The frequency domain plot of the test system inverse transfer function modulus (Figure 42);

8) The frequency domain plot of the test system inverse transfer function phase spectrum (Figure 43);

9) A time history plot of the required waveform to be controlled at the test specimen (Figure 44);

10) The Fourier transform modulus of the required waveform (Figure 45);

11) The phase spectrum of the required waveform (Figure 46);

Note that during the operation of the control system (Figures 36, 37, 38, 44, 45, and 46) plots are available to the test console operator in switch Position 1 before establishing the calibration level in switch Position 2.

12) A time history of the synthesized input voltage to the test system (Figure 47);

13) A time history plot of the synthesized transient waveform (Figure 48);

14) The Fourier transform modulus of the synthesized transient waveform (Figure 49);

15) The phase spectrum of the synthesized transient waveform (Figure 50).

The fidelity of the synthesis can be judged by comparing:

1) Time domain (Figure 44 with Figure 48);

2) Fourier transform modulus (Figure 45 with Figure 49);

3) Phase spectrum (Figure 46 with Figure 50).

As previously noted, this data contains an error in the low frequency domain caused by quantizing error. This data is the result of the initial attempt at transient waveform control. The data from a second experiment, incorporating some of the techniques developed in this study; (i.e., reduction of test system noise, optimized data transmission) are presented in Figures 1-B and III-1.

To verify the operational characteristics of the control system, the master gain control at the test console was adjusted for a 33-1/3% increase in the amplitude of the required waveform. Using the same time history illustrated in Figure 47, the synthesized transient waveform is completely defined by Figures 51, 52, and 53. This data is included to provide an empirical insight into the adverse effects of test system nonlinearities.

The synthesized waveform in Figure 48 has characteristic peaks of +27.5 g's and -26.5 g's. With the 33-1/3% increase in the master gain setting, the corresponding peaks increase to 37 g's and -35 g's for respective increases of 34-1/2% and 32%. This data shows that the system is very nearly linear (see Page 114, "Nonlinearities").

Figures 54 through 60 relate the results of applying waveform control to a transient with known d.c. content. The Fourier transform modulus, $F'(\omega)_R$ (Figure 59), of the synthesized transient waveform, $f'(t)_R$ (Figure 58), did not match the Fourier transform modulus, $F(\omega)_R$ (Figure 55), of the required transient waveform, $f(t)_R$ (Figure 54), because the synthesized input voltage, $f(t)_S$ (Figure 57), did not start (first data point) at or near zero. Consequently, a large step function was inherent in the synthesized input voltage, $f(t)_S$. The systems' response, $f'(t)_R$, to the synthesized input, $f(t)_S$, with superimposed step function, was a superposition of the required transient waveform, $f(t)_R$, and the system step function response. This is clearly identified by observing the high frequency spectra, above 500 Hz, in Figures 40 and 59. Note the similarity of form. This is due to the system "ringing." Figure 55 represents the required transform. Therefore, Figure 59 represents the superposition of Figures 40 and 55. This illustrates the importance of ensuring that large discontinuities at $t_o$ do not occur. With the step function removed, an improved waveform control is illustrated in Appendix III.

This prototype transient waveform control system, used on an electromagnetic test system, is currently in use for the successful conduct of shock test requirements per MIL STD 810B specification. An example of this type of waveform control is shown in Figure 2.

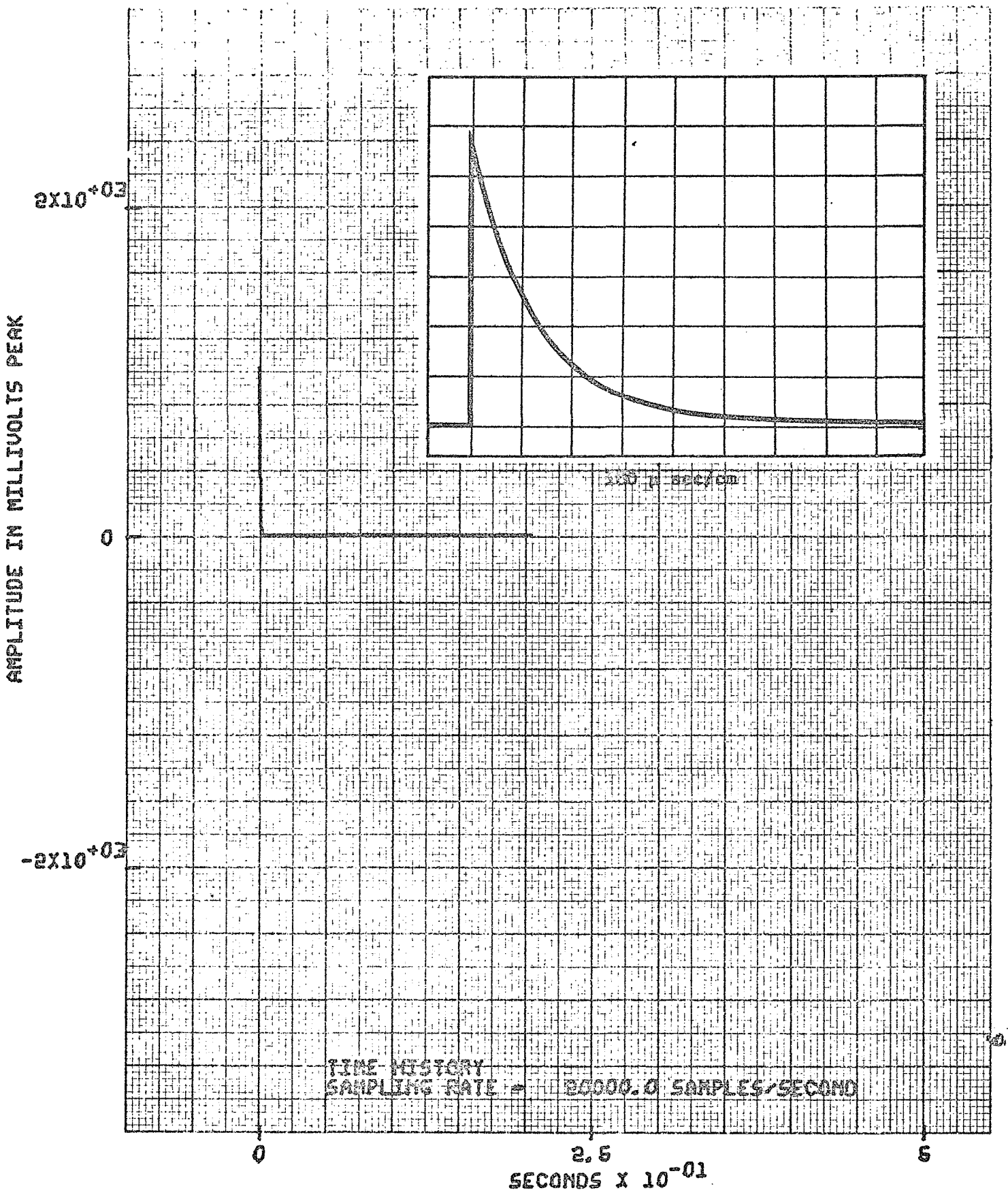



Figure 36: TEST SYSTEM CALIBRATION PULSE, $f(t)_1$

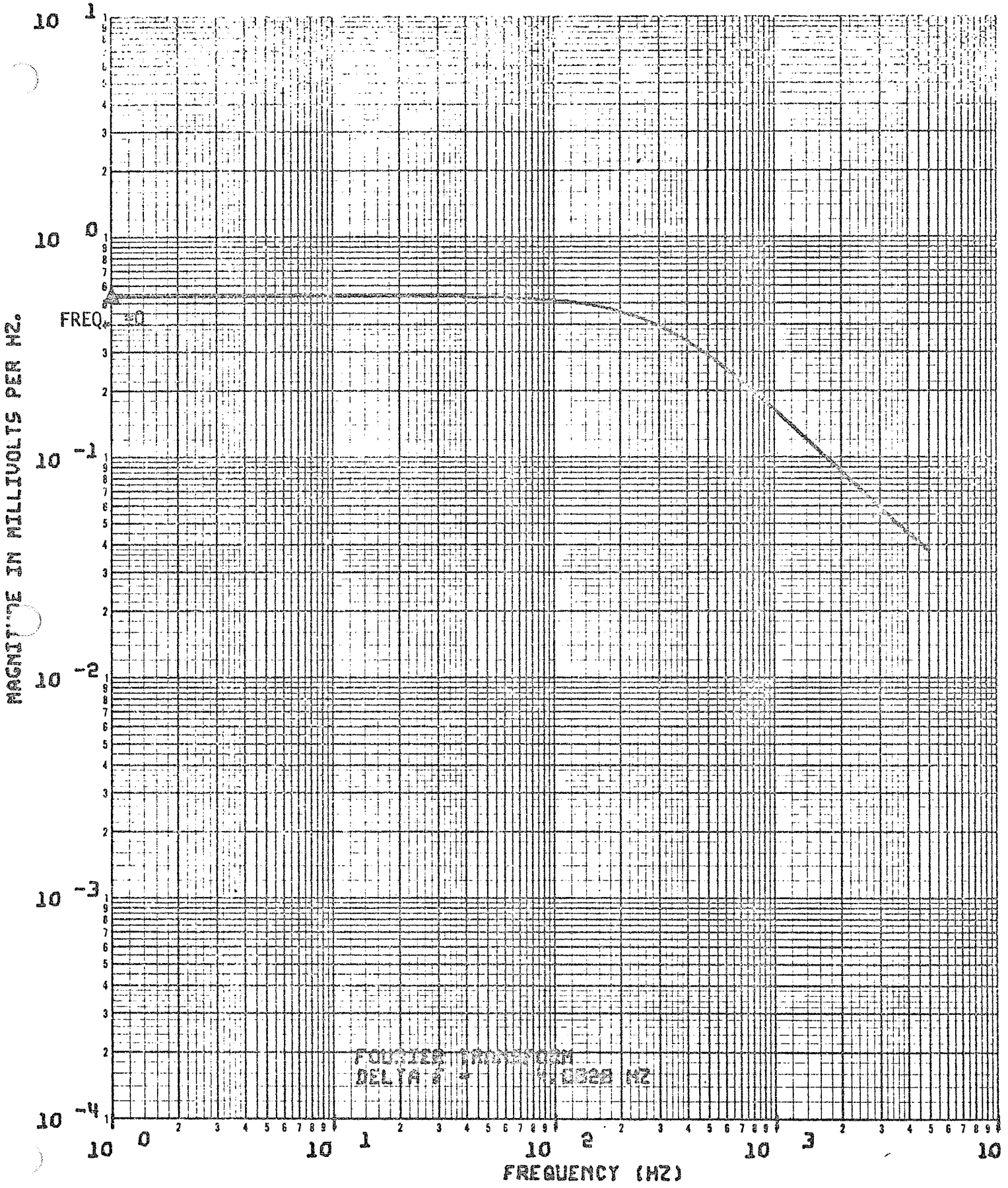



Figure 37: CALIBRATION PULSE, FOURIER TRANSFORM MODULUS, $f(\omega)_i$

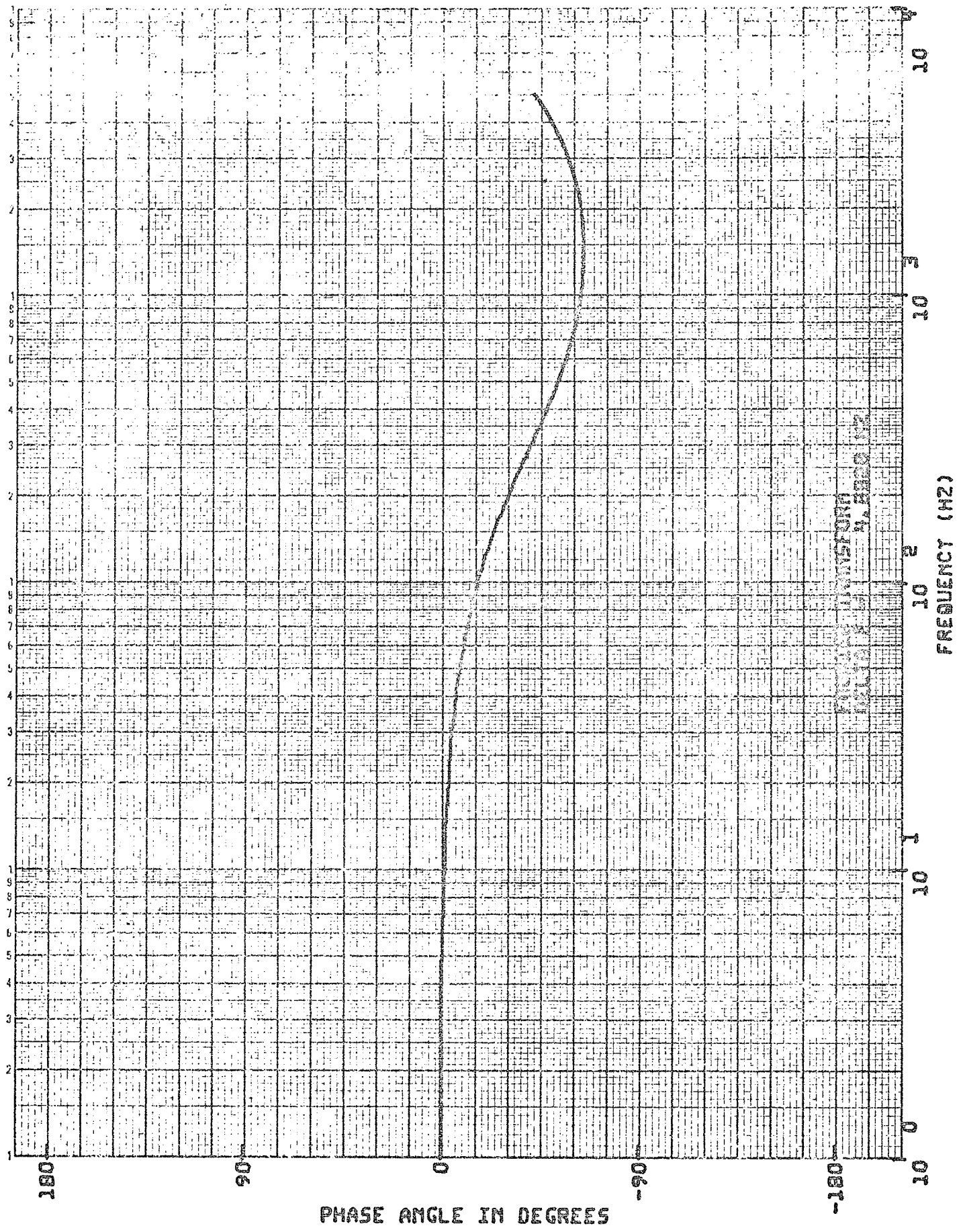



Figure 38: CALIBRATION PULSE, FOURIER TRANSFORM PHASE SPECTRUM, $F(\omega)_i$

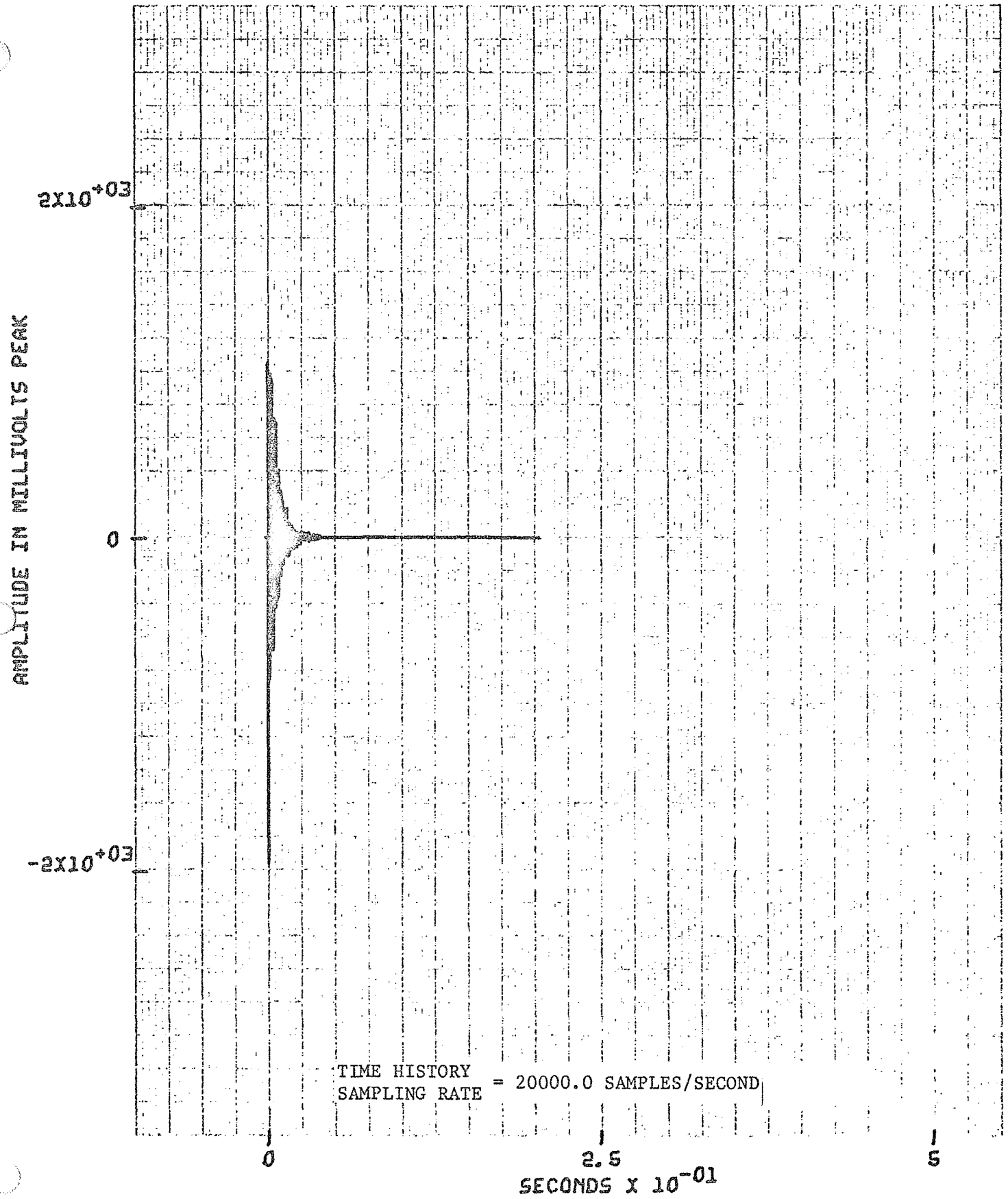



Figure 39: TRANSIENT CALIBRATION OUTPUT, $f(t)_o$

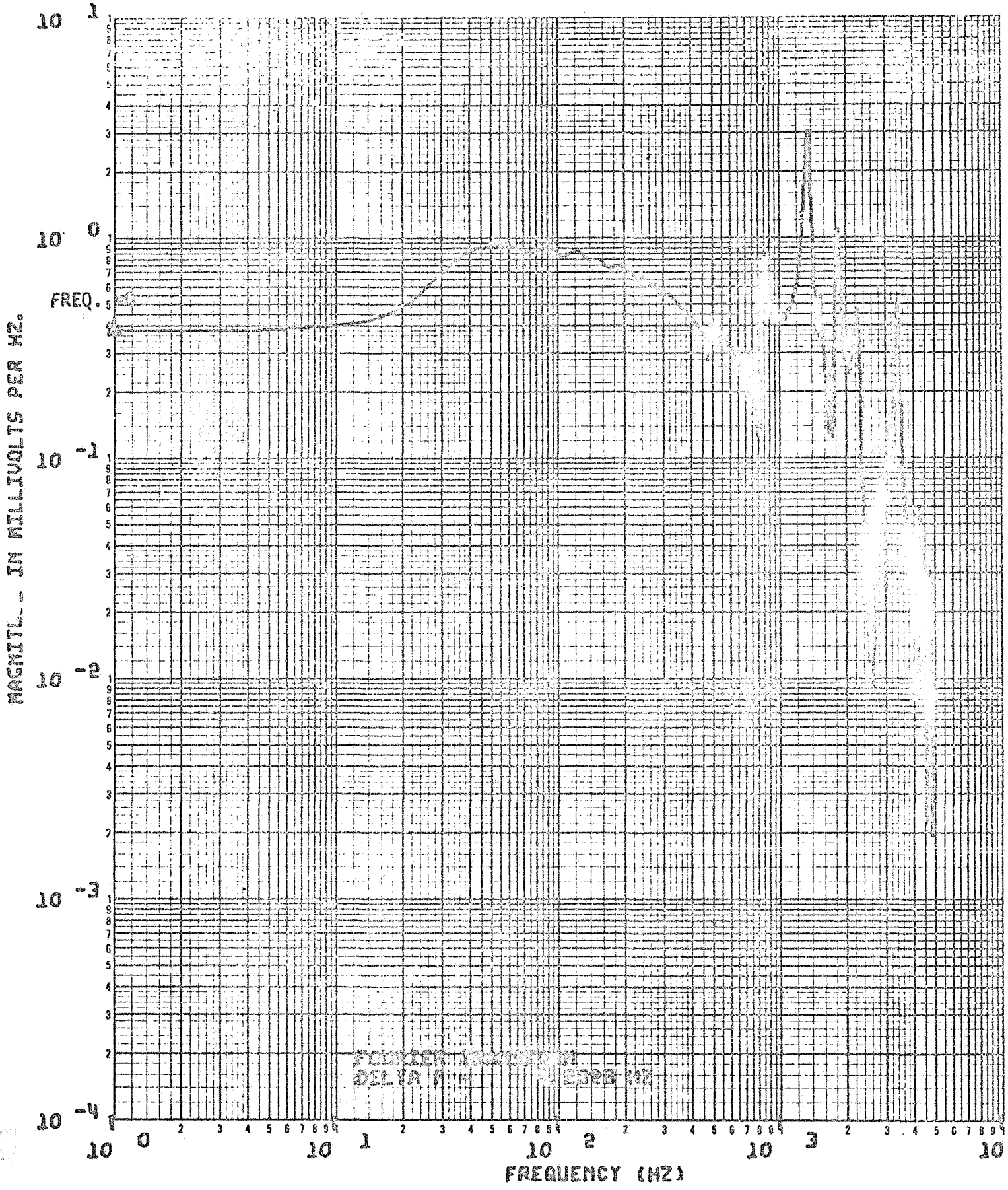



Figure 40: TRANSIENT CALIBRATION OUTPUT, FOURIER TRANSFORM MODULUS, $f(\omega)_o$

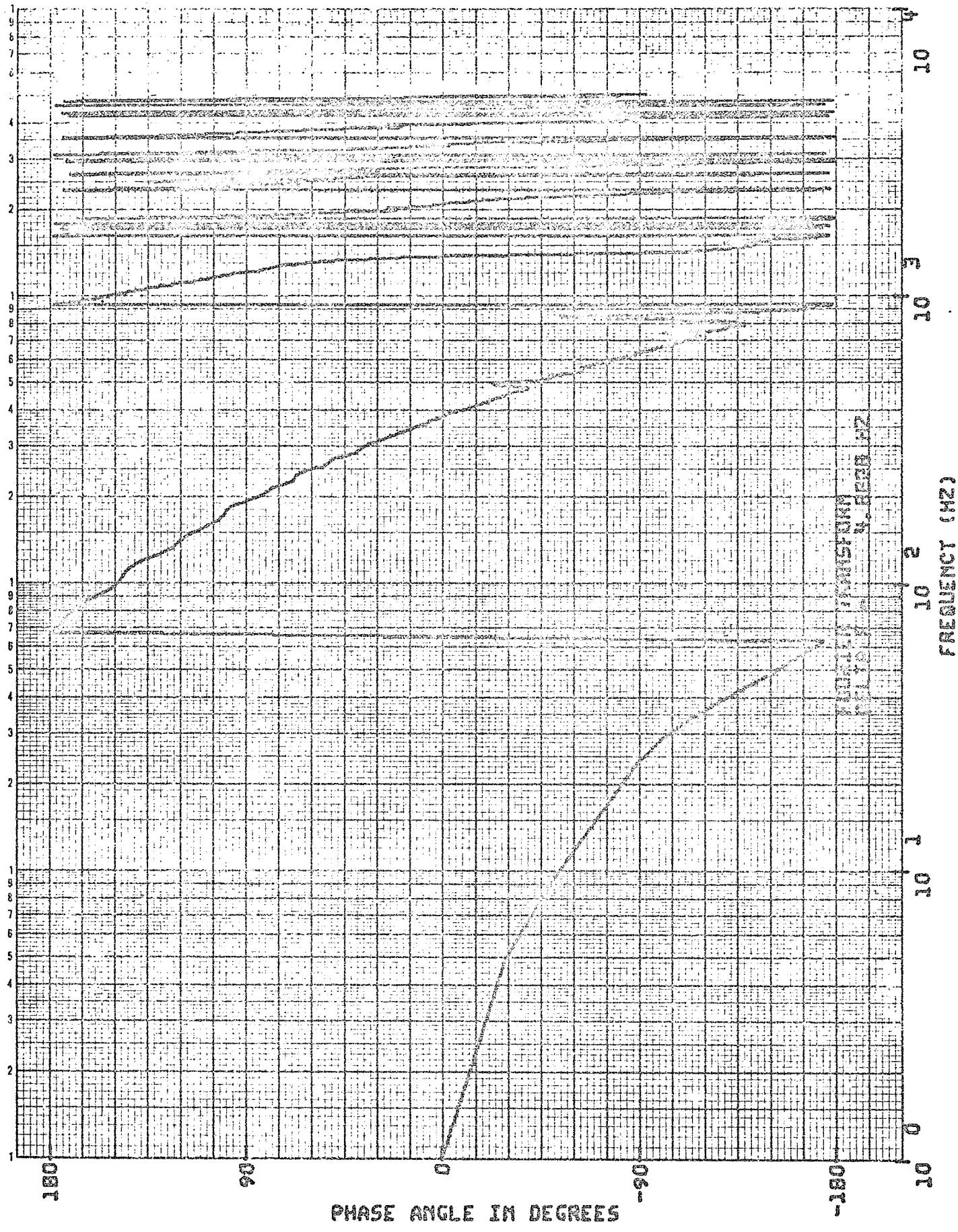



Figure 41: TRANSIENT CALIBRATION OUTPUT, FOURIER TRANSFORM PHASE SPECTRUM, $F(\omega)_o$

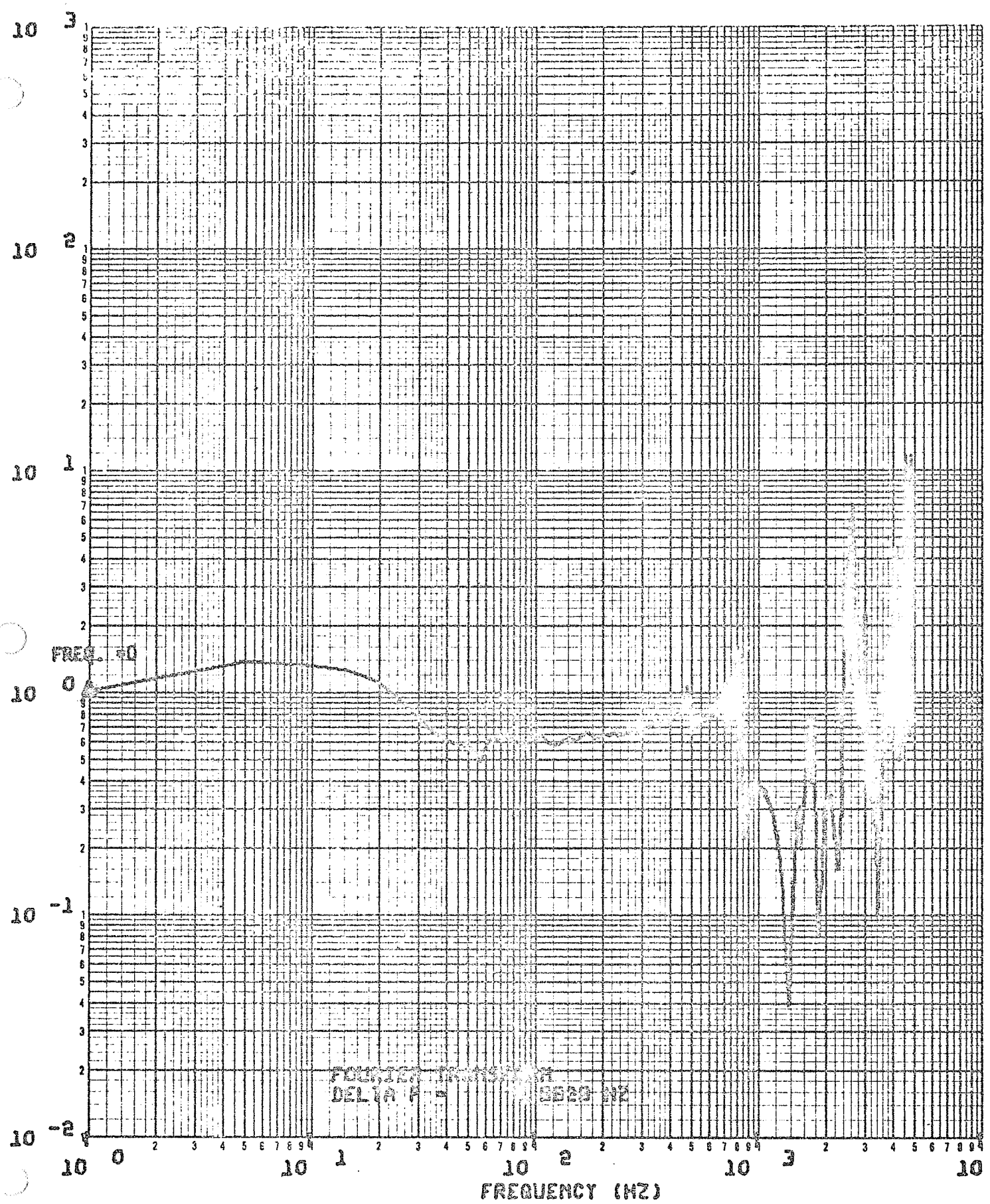



Figure 42: INVERSE TRANSFER FUNCTION MODULUS, $1/H(\omega) = F(\omega)i/F(\omega)o$

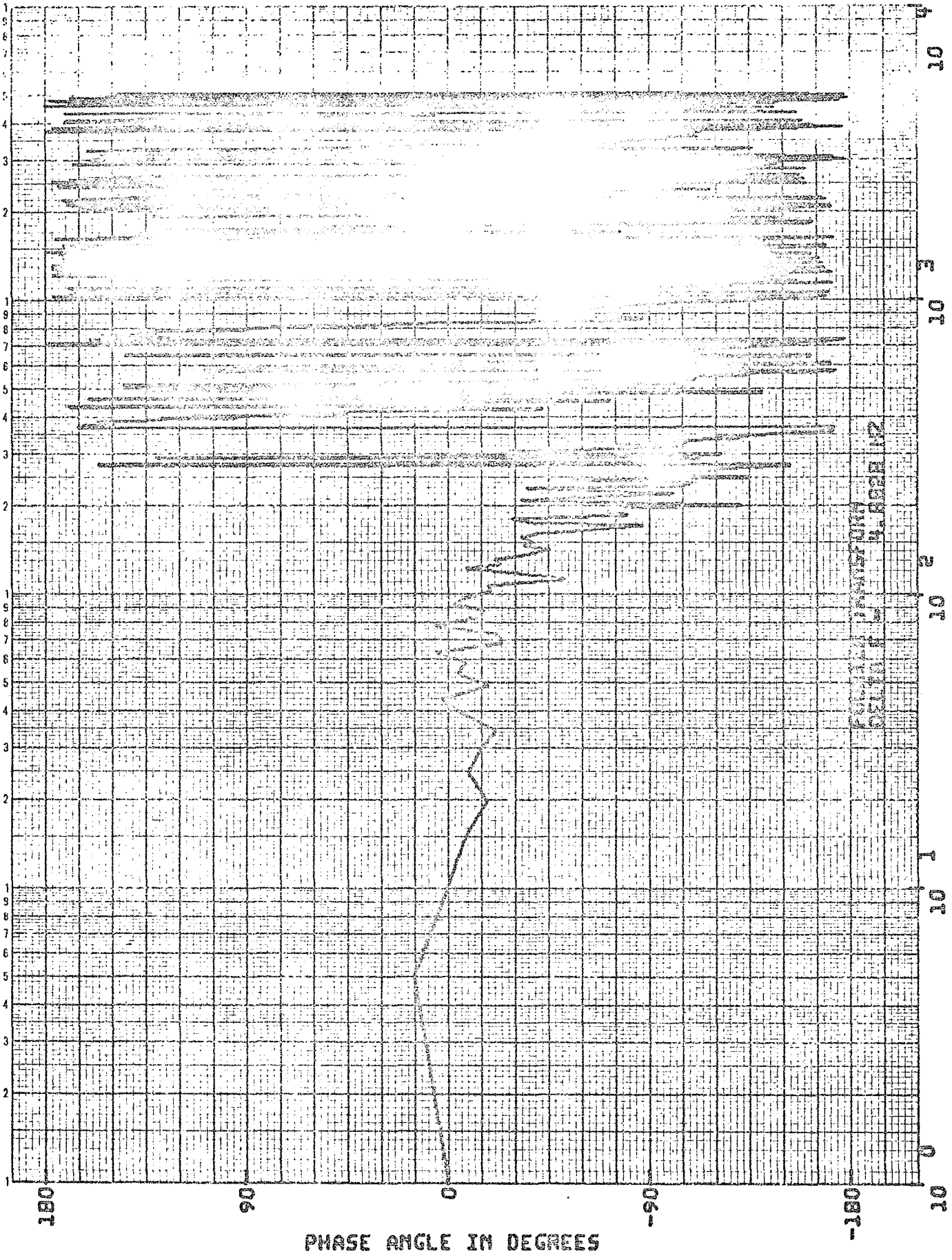



Figure 43: INVERSE TRANSFER FUNCTION PHASE SPECTRUM, $1/H(\omega) = F(\omega) 1/F(\omega)$.

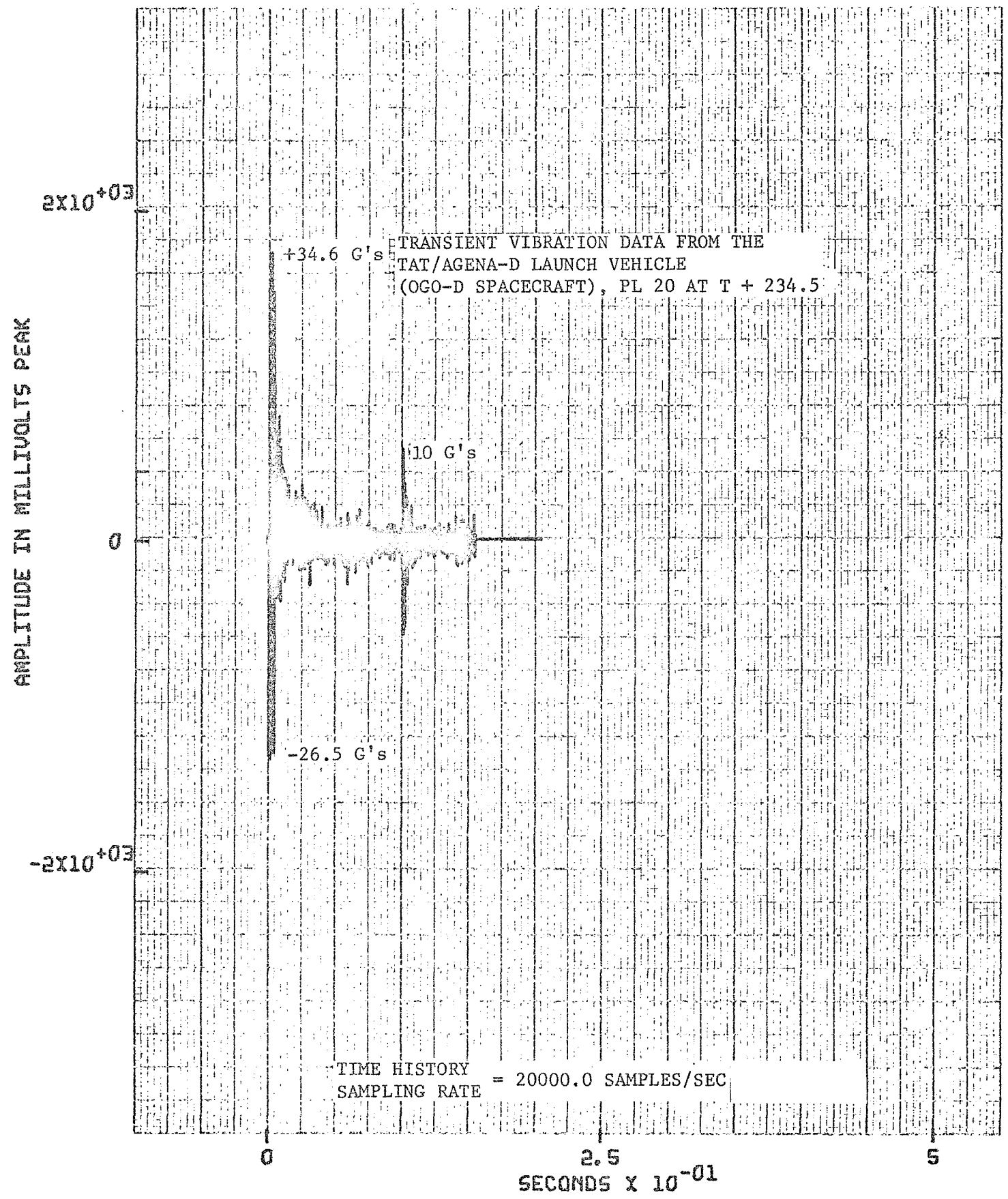



Figure 44: REQUIRED TRANSIENT WAVEFORM, $f(t)_R$

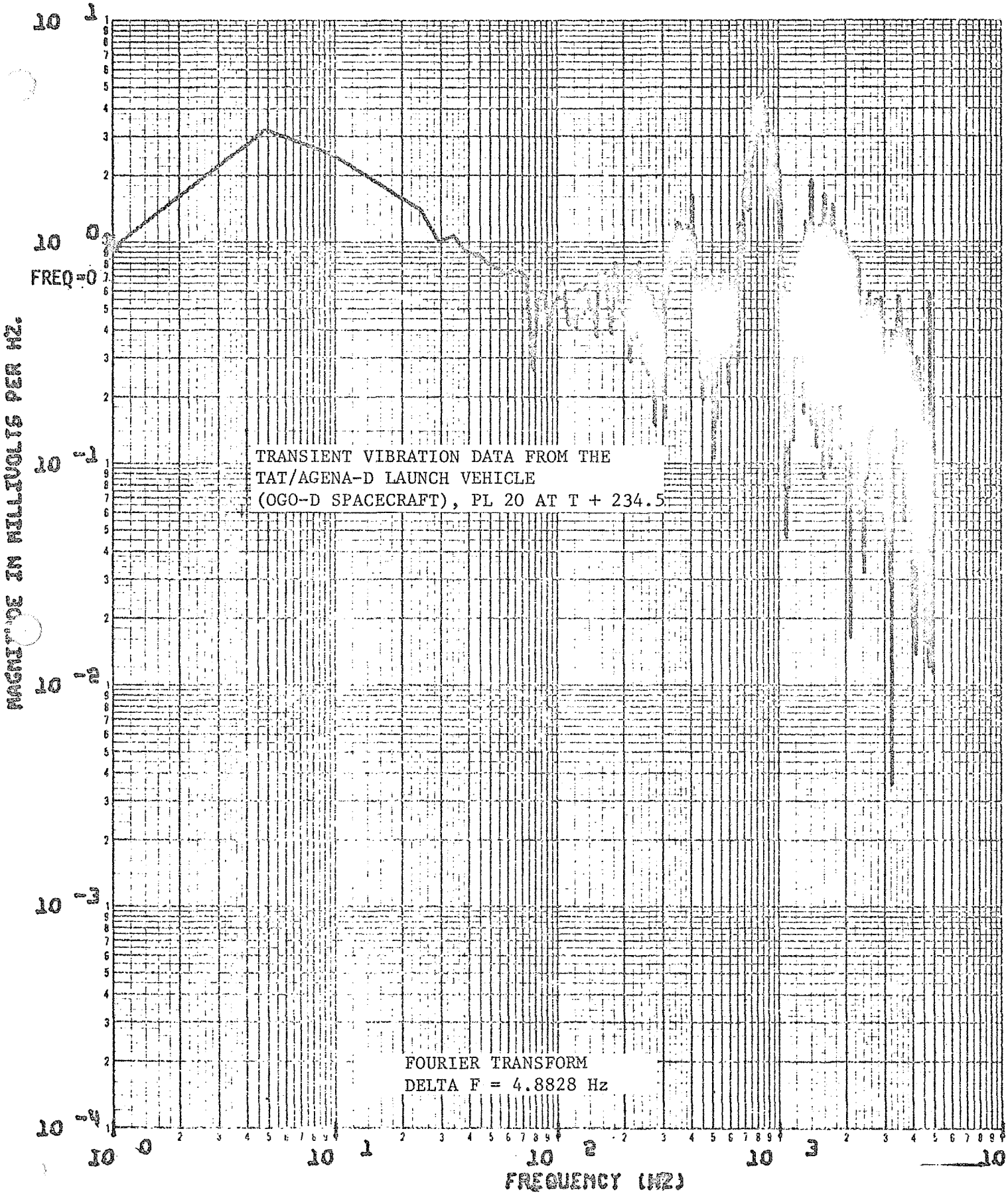



Figure 45: REQUIRED TRANSIENT WAVEFORM, FOURIER TRANSFORM MODULUS, $F(\omega)_R$

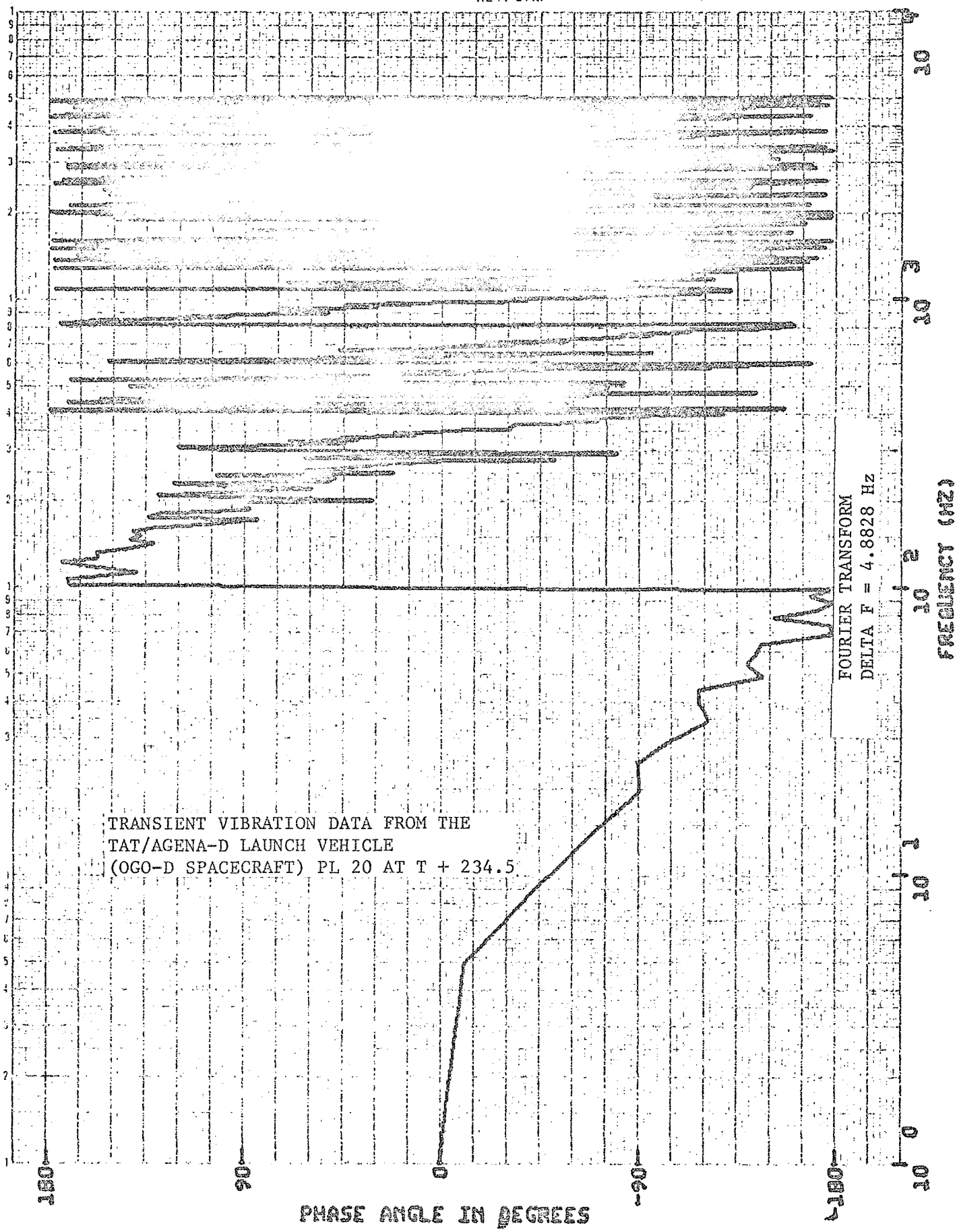



Figure 46: REQUIRED TRANSIENT WAVEFORM, FOURIER TRANSFORM PHASE SPECTRUM, $F(\omega)_R$

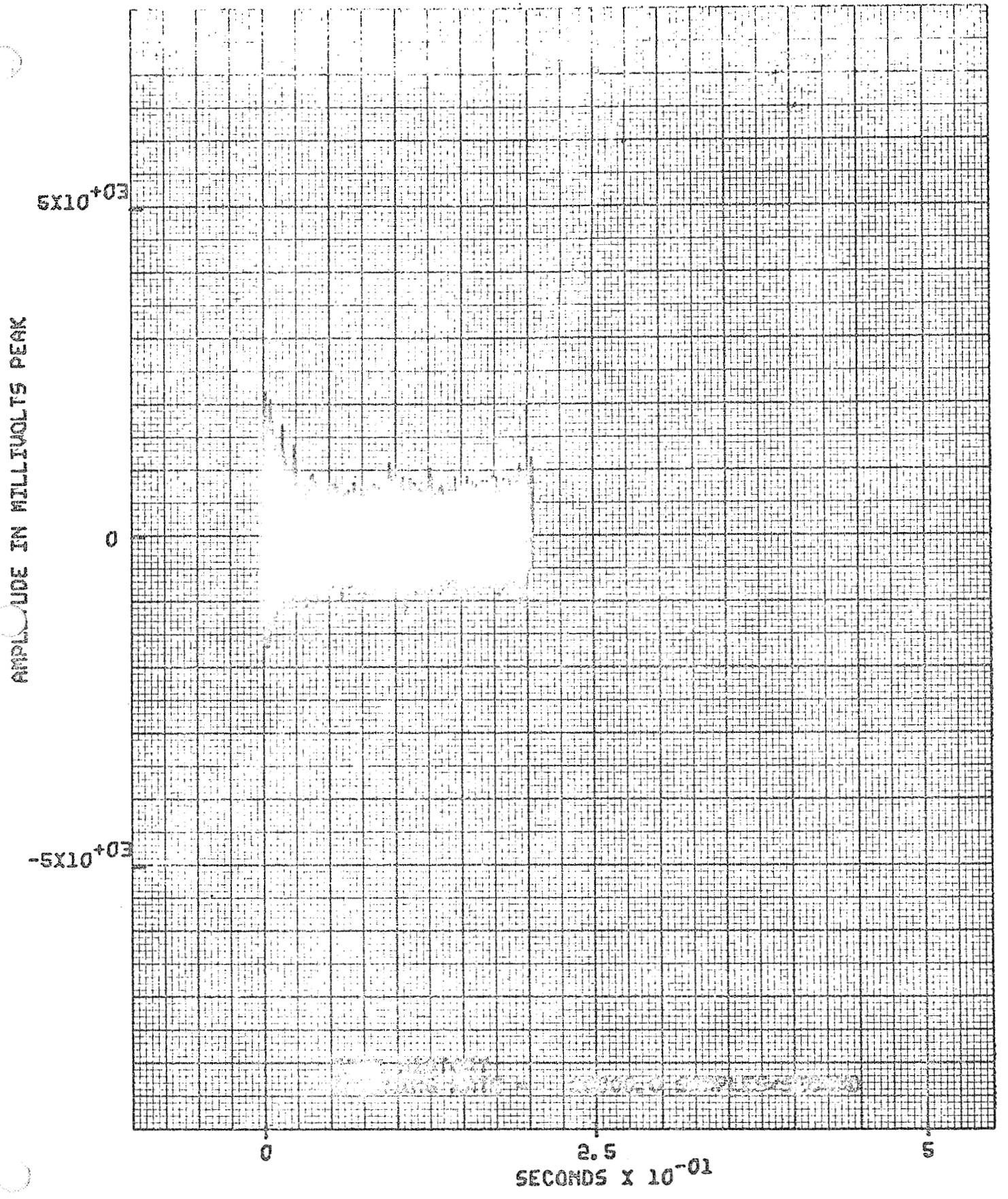



Figure 47: SYNTHESIZED INPUT VOLTAGE, $f(t)_S$

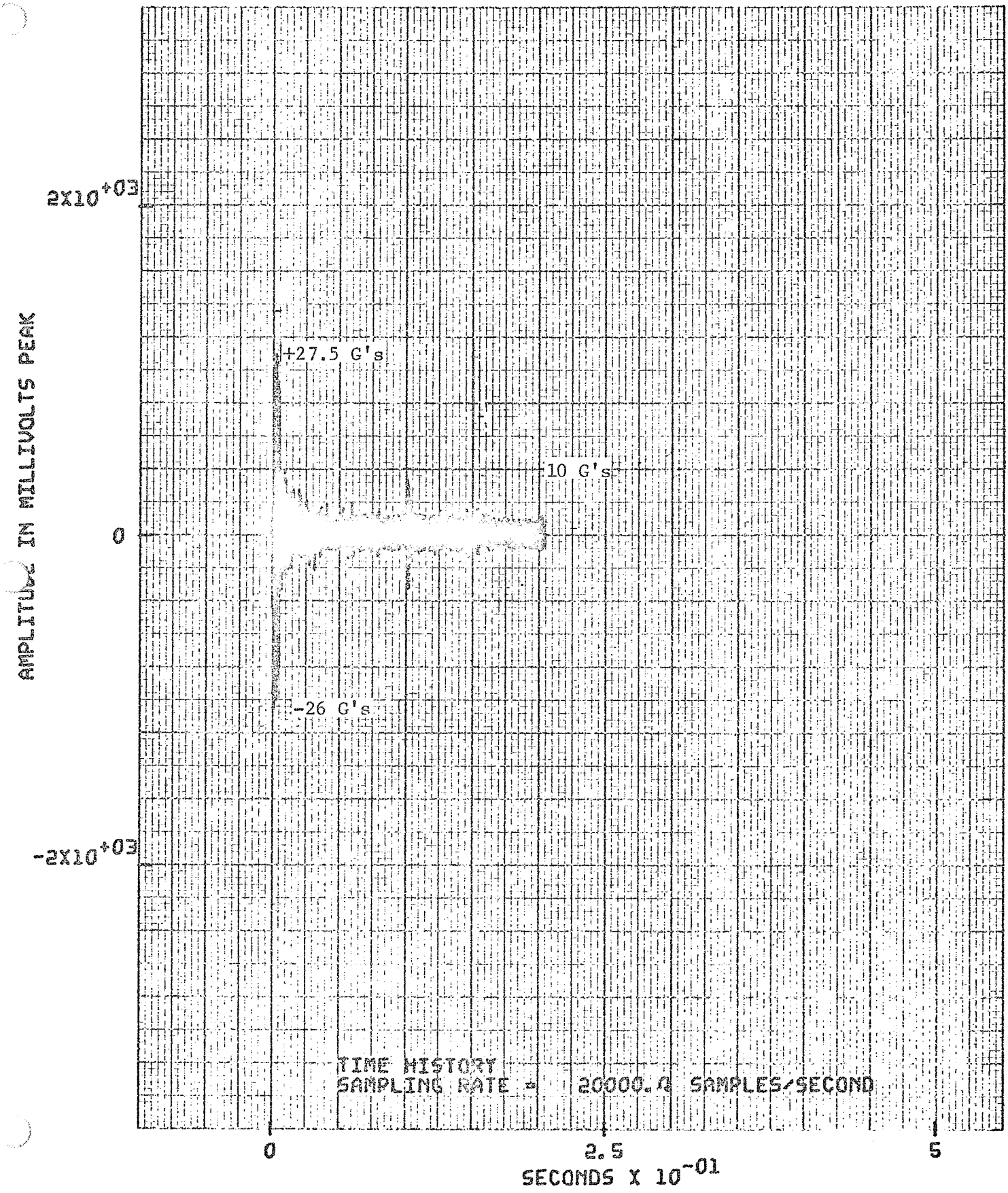



Figure 48: SYNTHESIZED TRANSIENT WAVEFORM, $f'(t)_R$

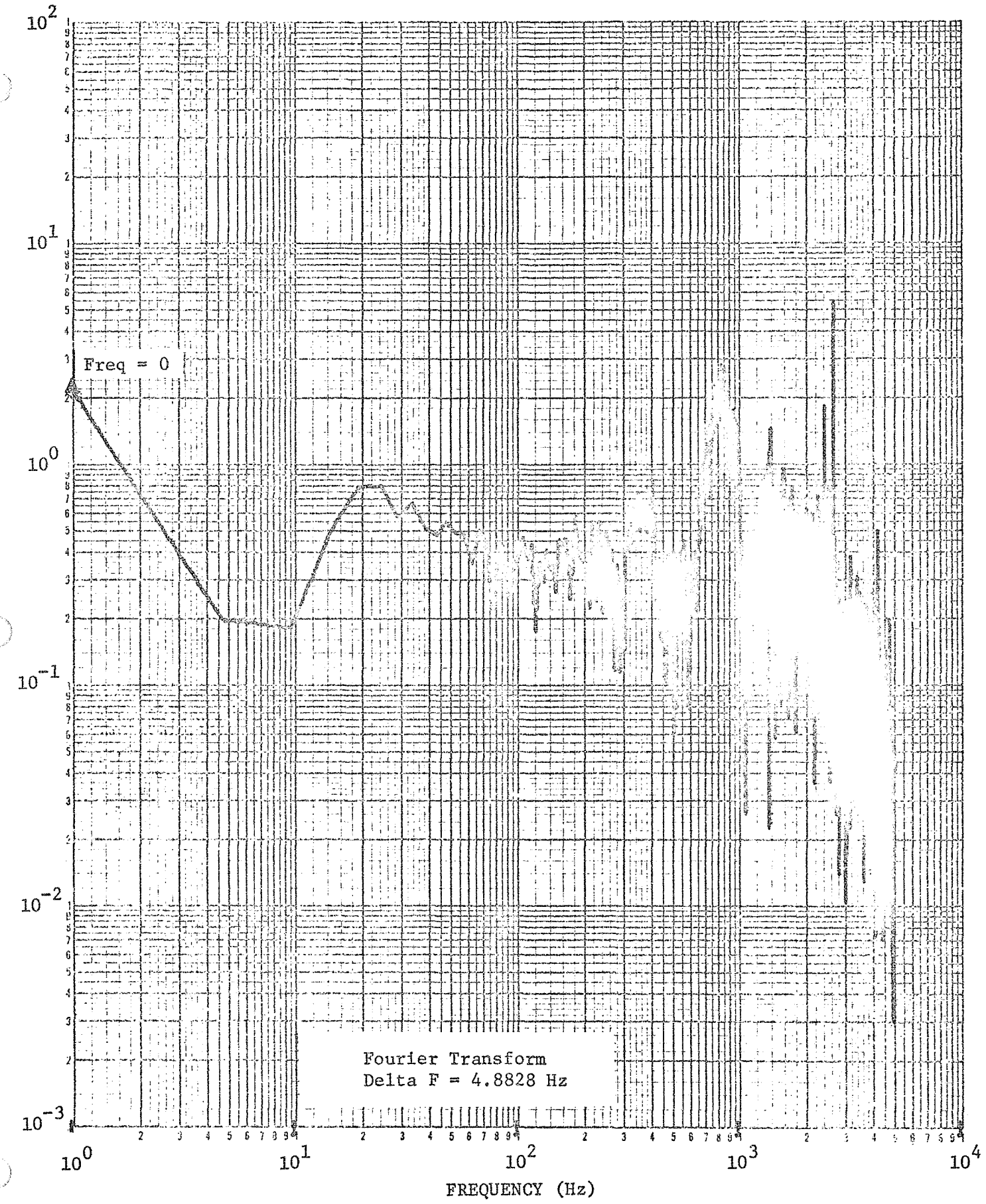



Figure 49: SYNTHESIZED TRANSIENT WAVEFORM, FOURIER TRANSFORM MODULES, $F'(\omega)_R$

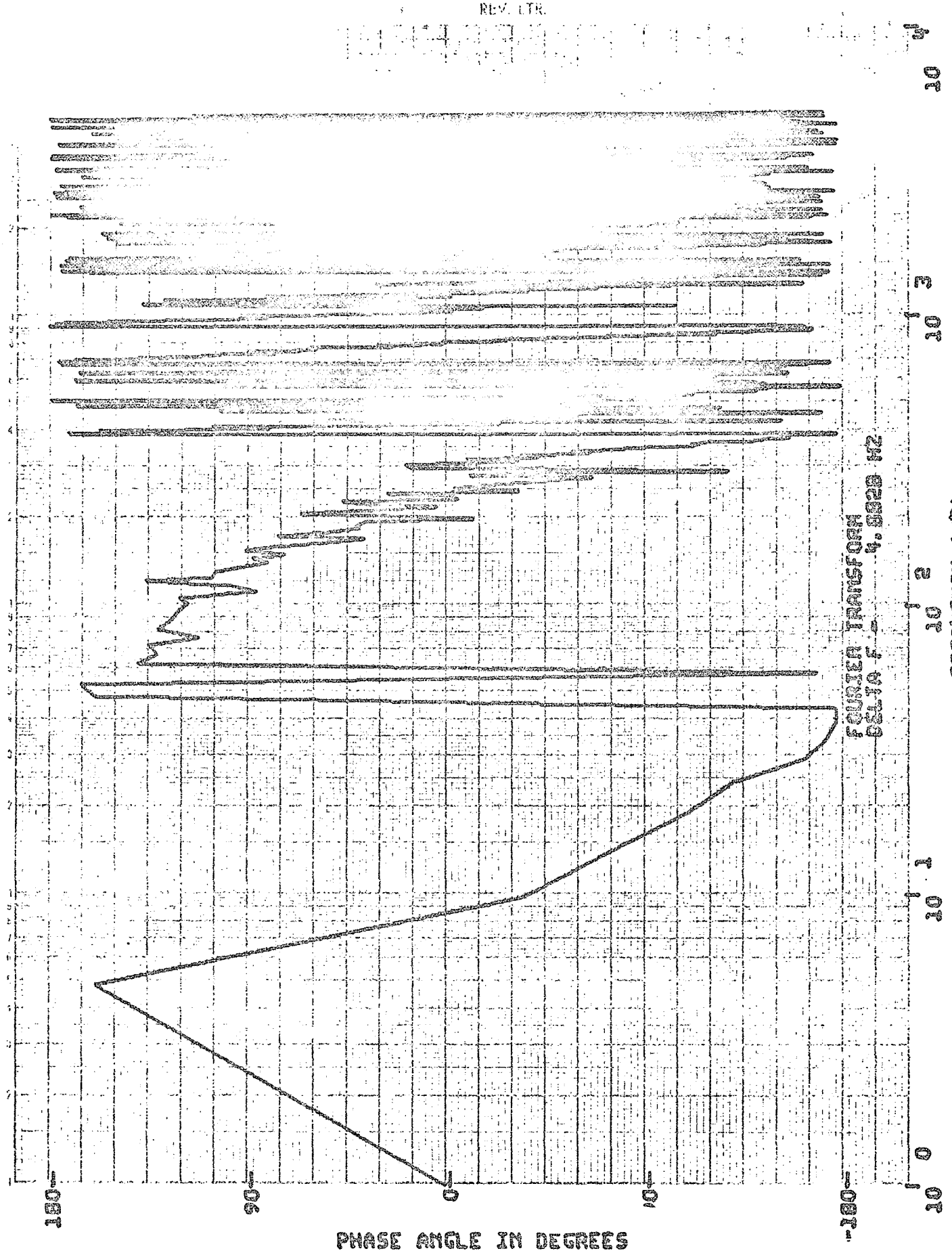



Figure 50: SYNTHESIZED TRANSIENT WAVEFORM, FOURIER TRANSFORM PHASE SPECTRUM, $F'(\omega)_R$

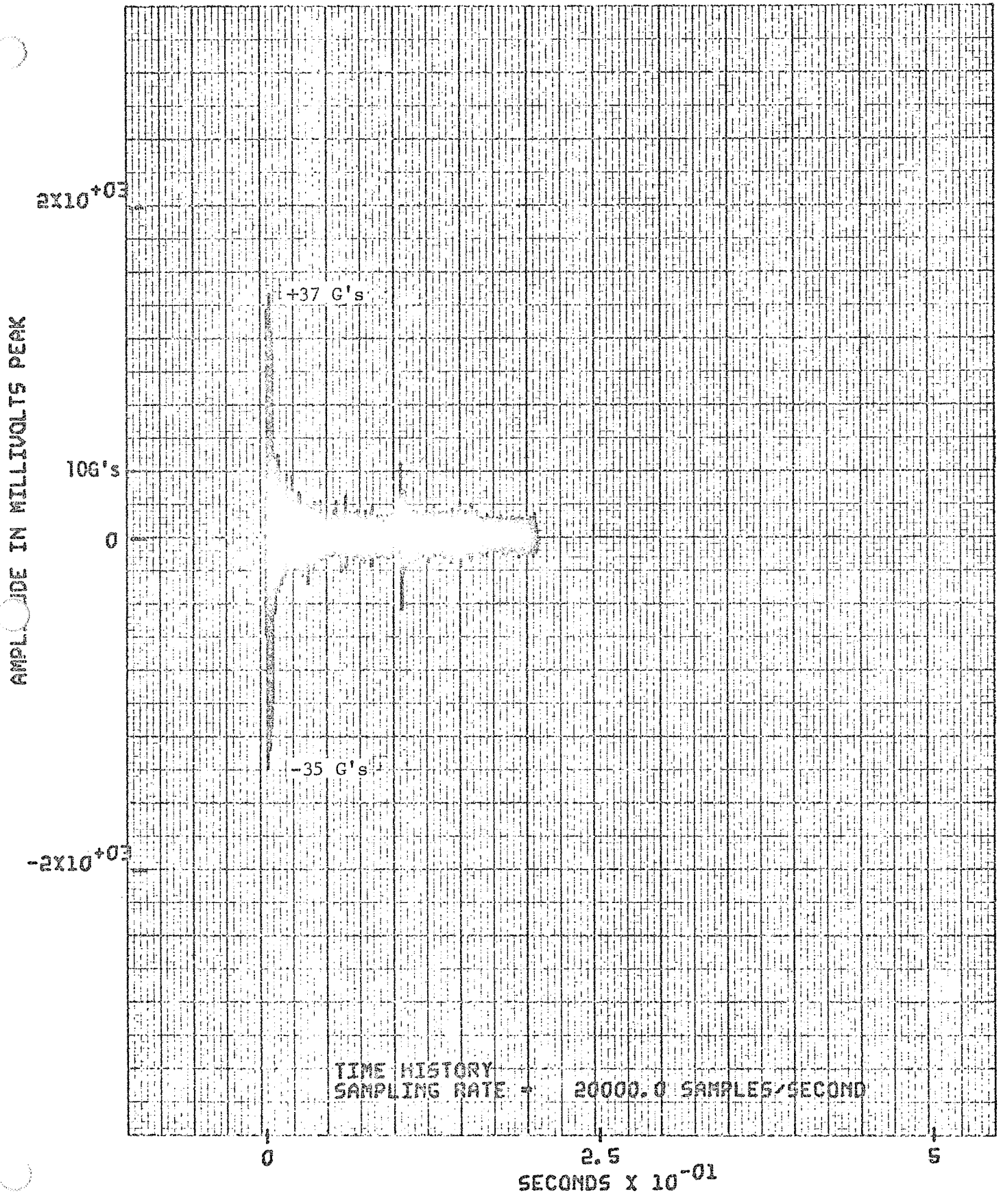



Figure 51: SYNTHESIZED TRANSIENT WAVEFORM, $f'(t)_R$

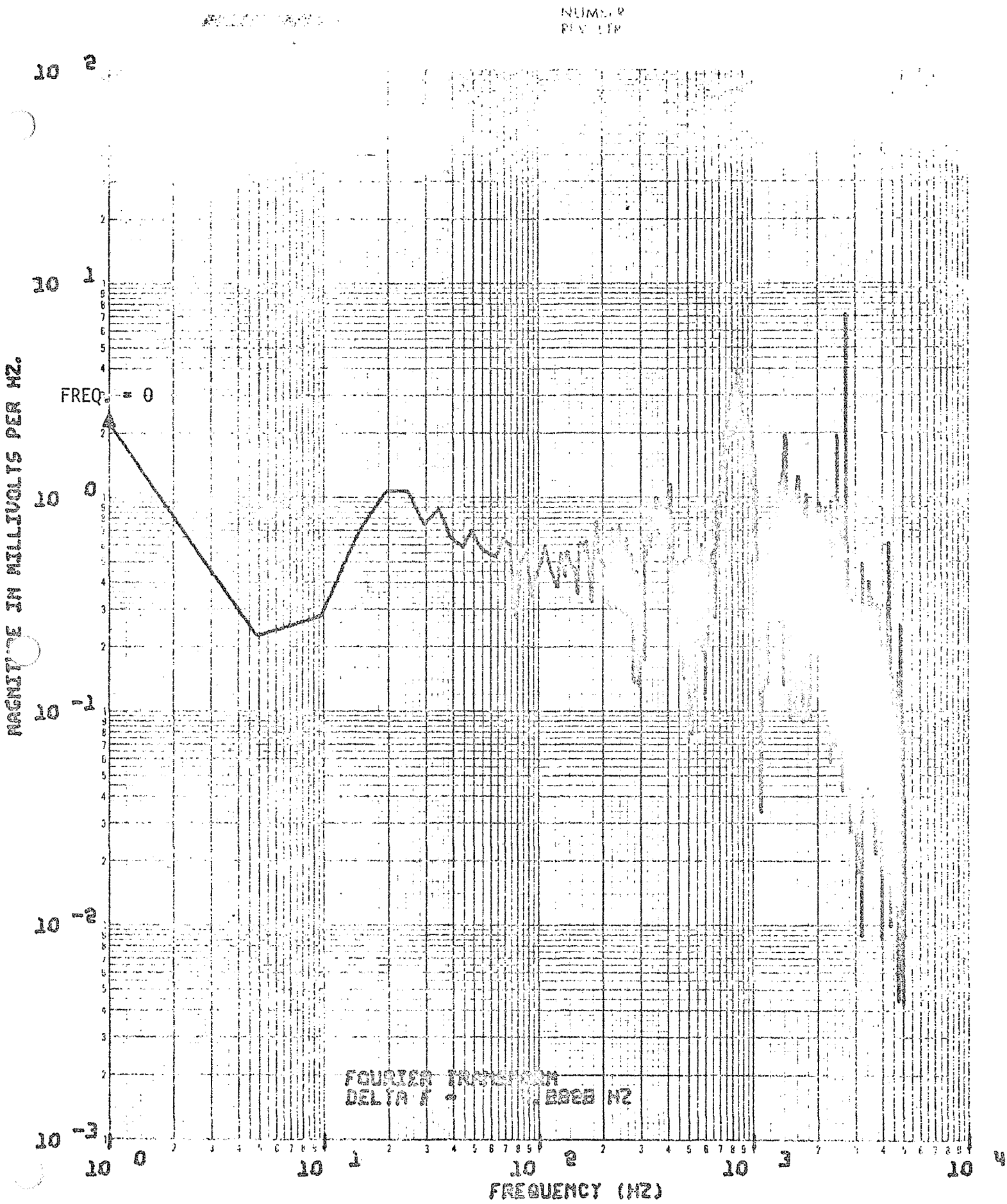



Figure 52: SYNTHESIZED TRANSIENT WAVEFORM, FOURIER TRANSFORM MODULUS, $F'(\omega)_R$

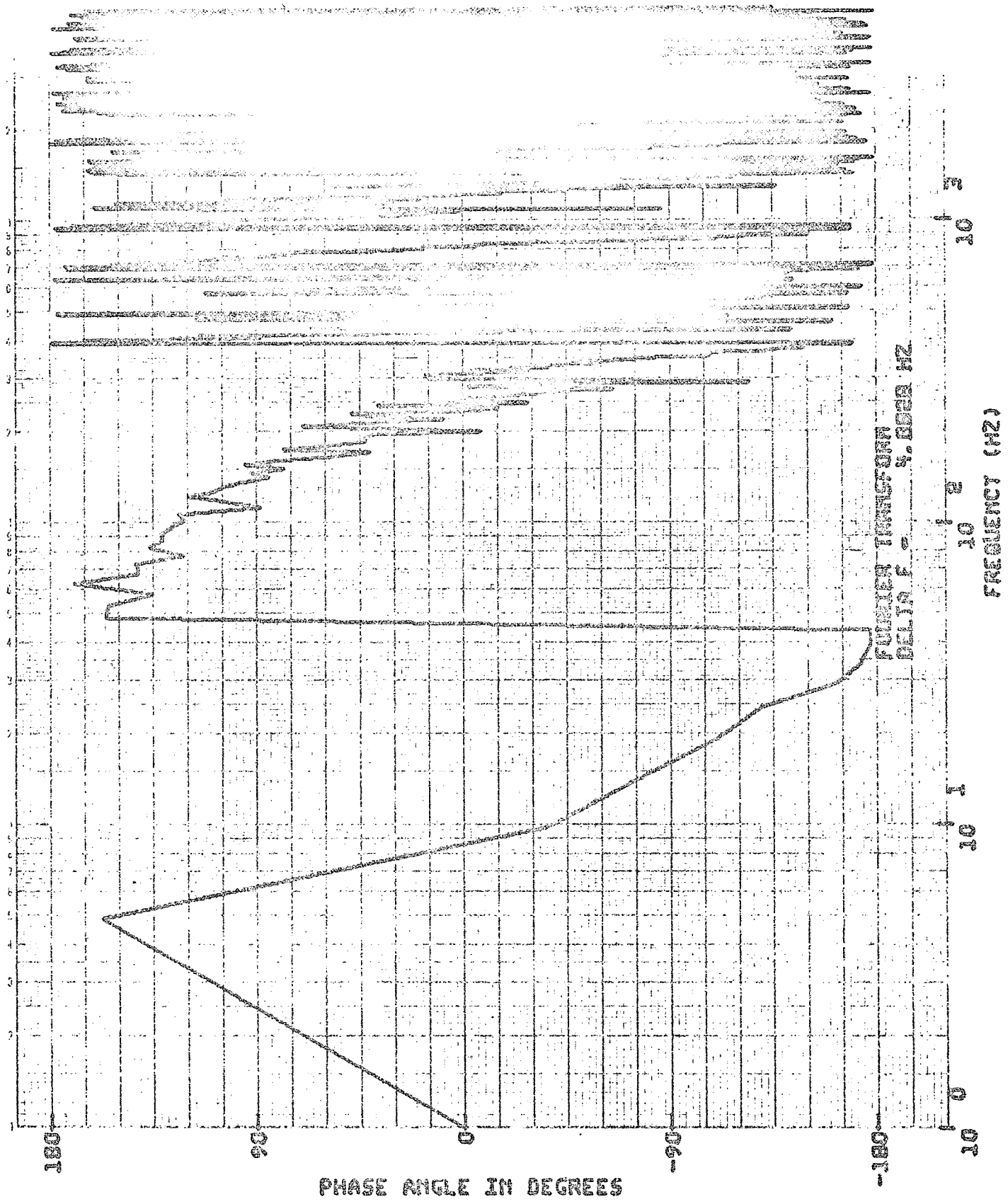



Figure 53: SYNTHESIZED TRANSIENT WAVEFORM, FOURIER TRANSFORM PHASE SPECTRUM, $F'(\omega)_R$

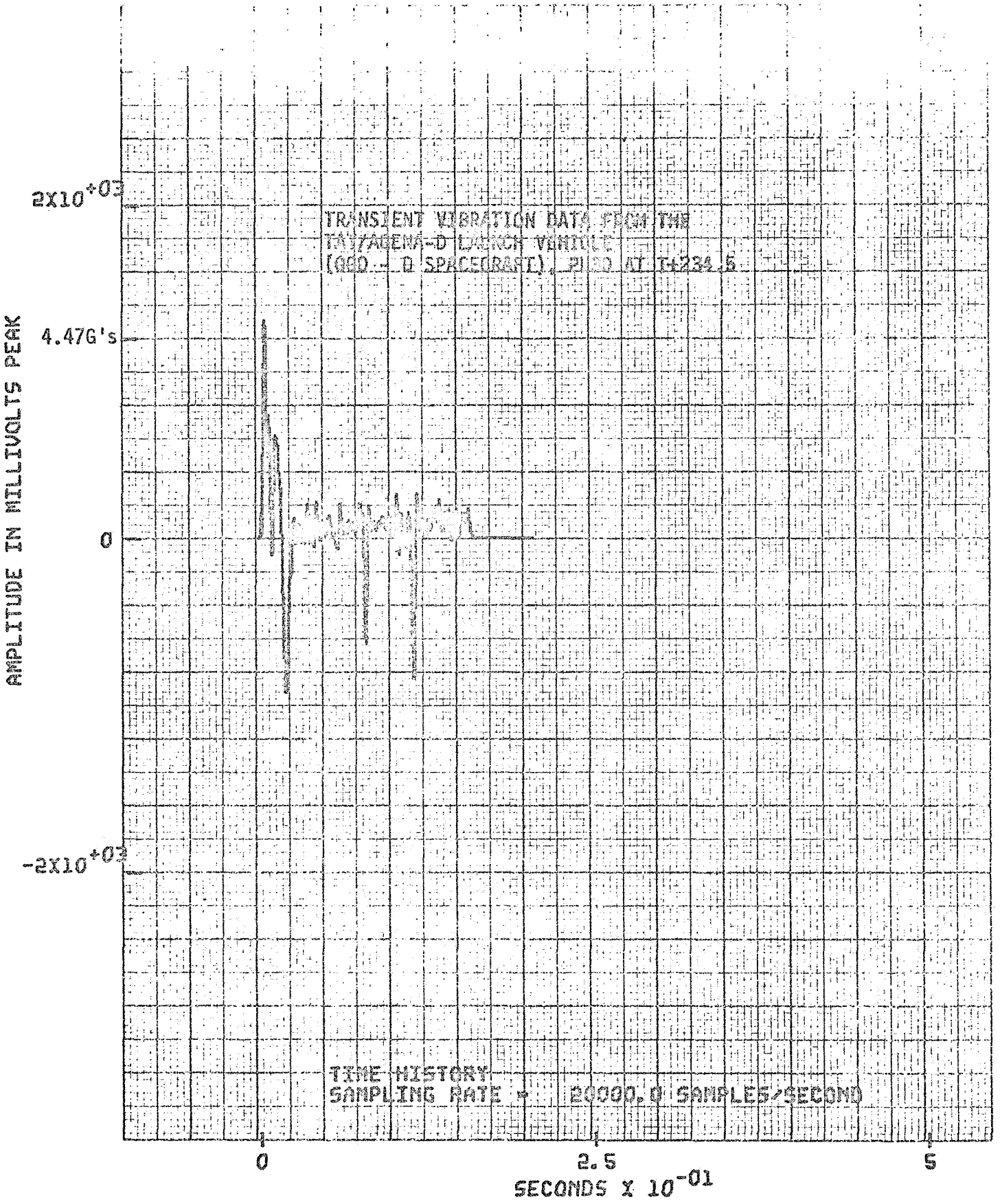



Figure 54: REQUIRED TRANSIENT WAVEFORM, $f(t)_R$

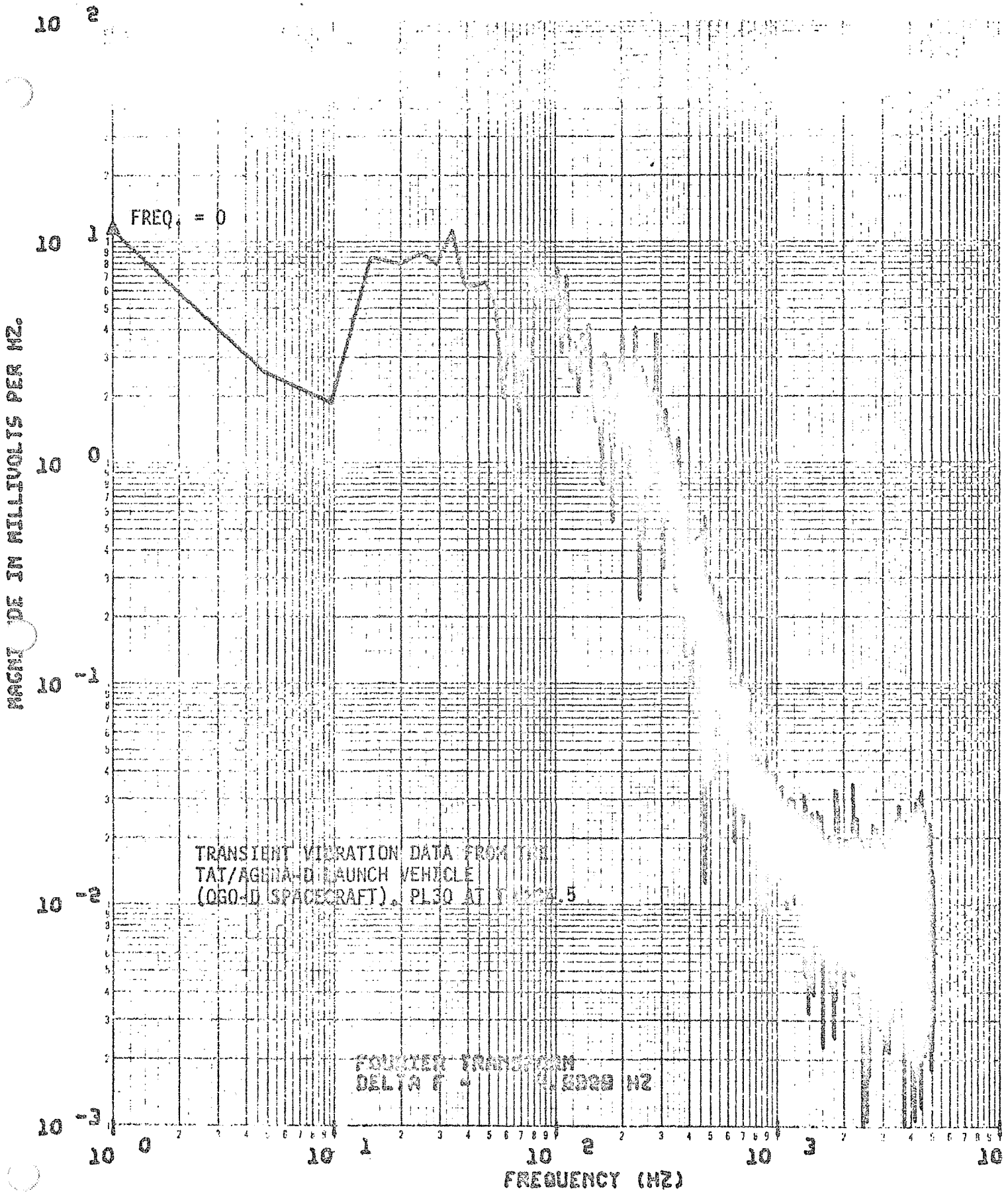



Figure 55: REQUIRED TRANSIENT WAVEFORM, FOURIER TRANSFORM MODULUS, $F(\omega)_R$

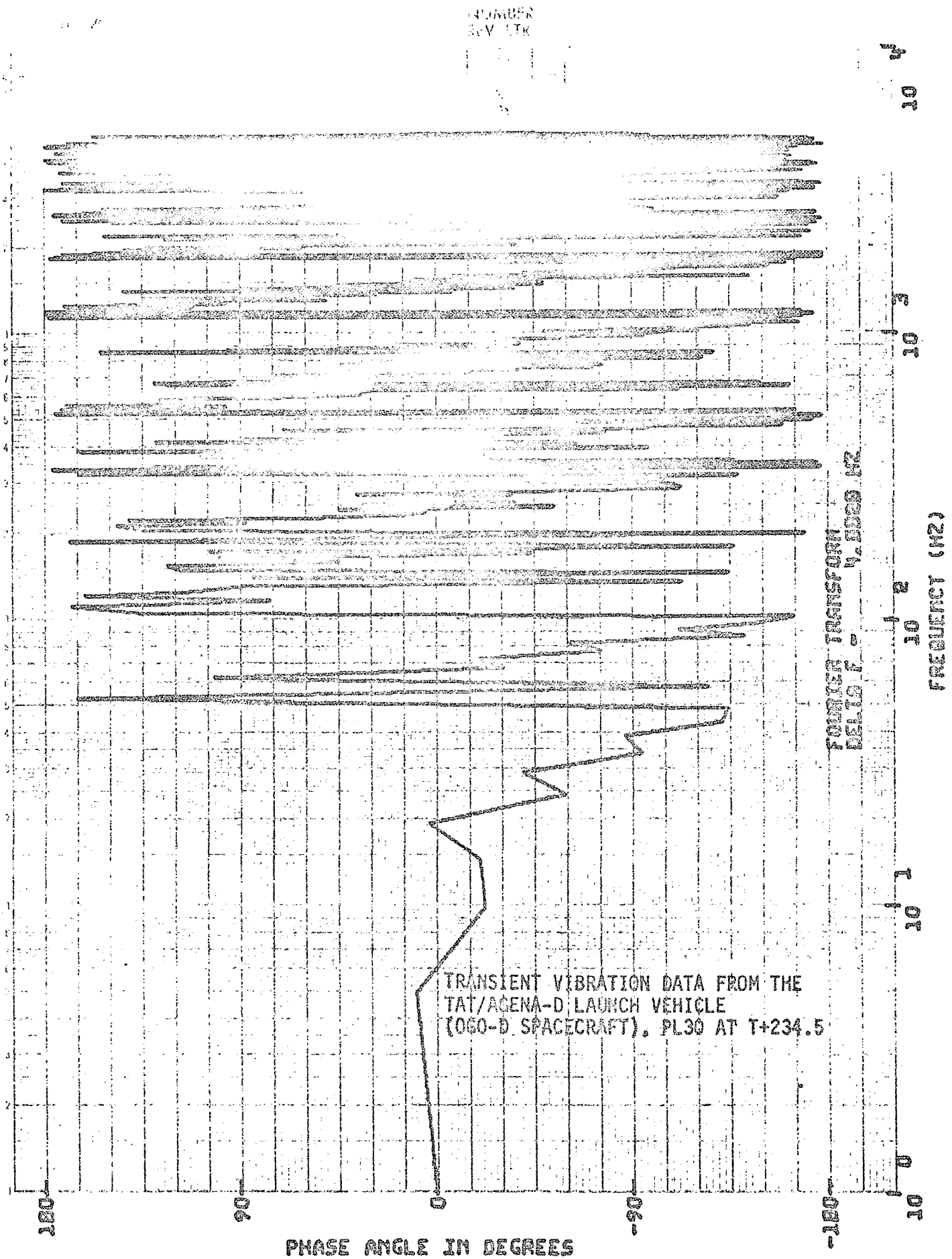



Figure 56: REQUIRED TRANSIENT WAVEFORM, FOURIER TRANSFORM PHASE SPECTRUM, $F(\omega)_R$

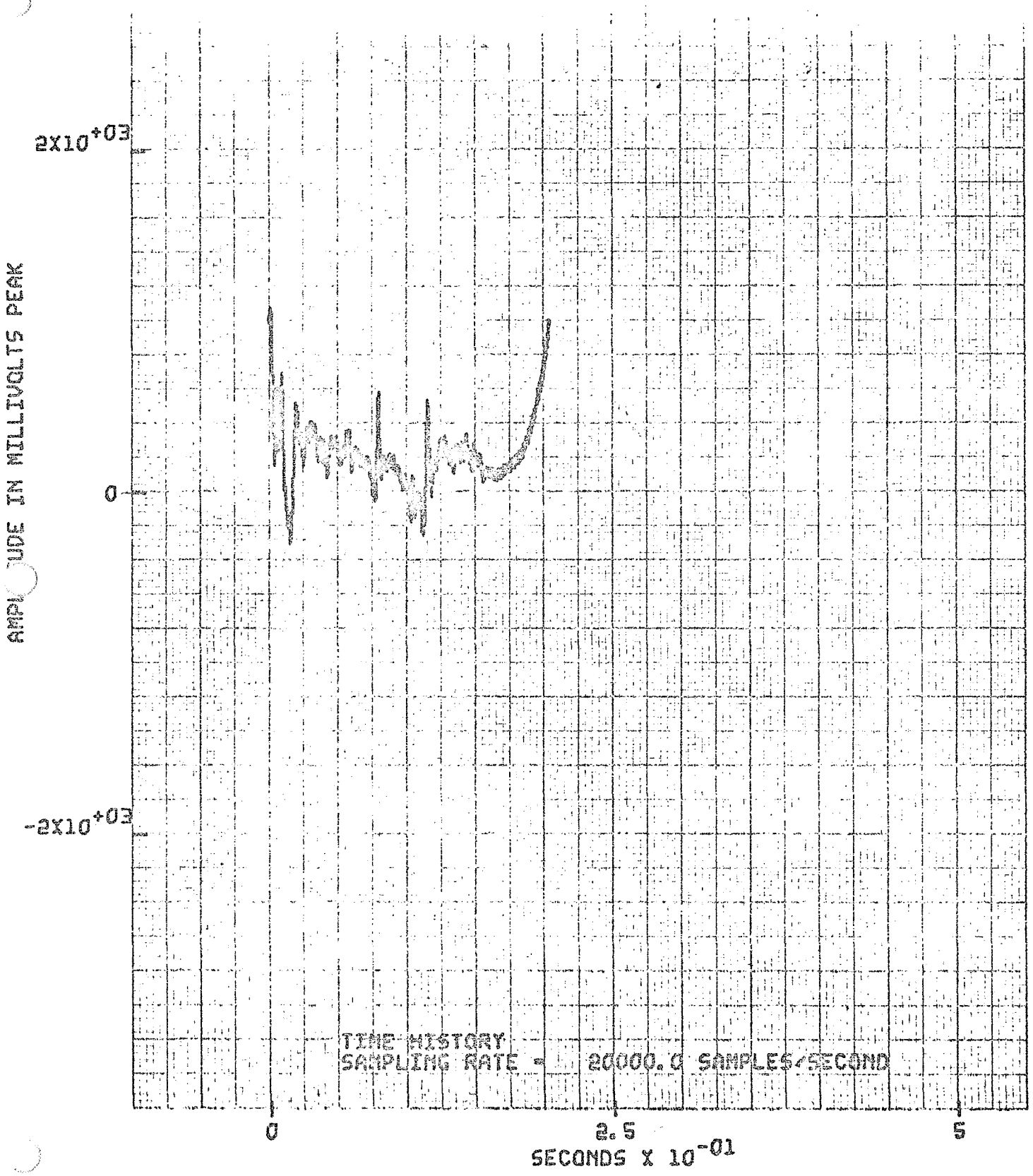



Figure 57: SYNTHESIZED INPUT VOLTAGE, $f(t)_S$

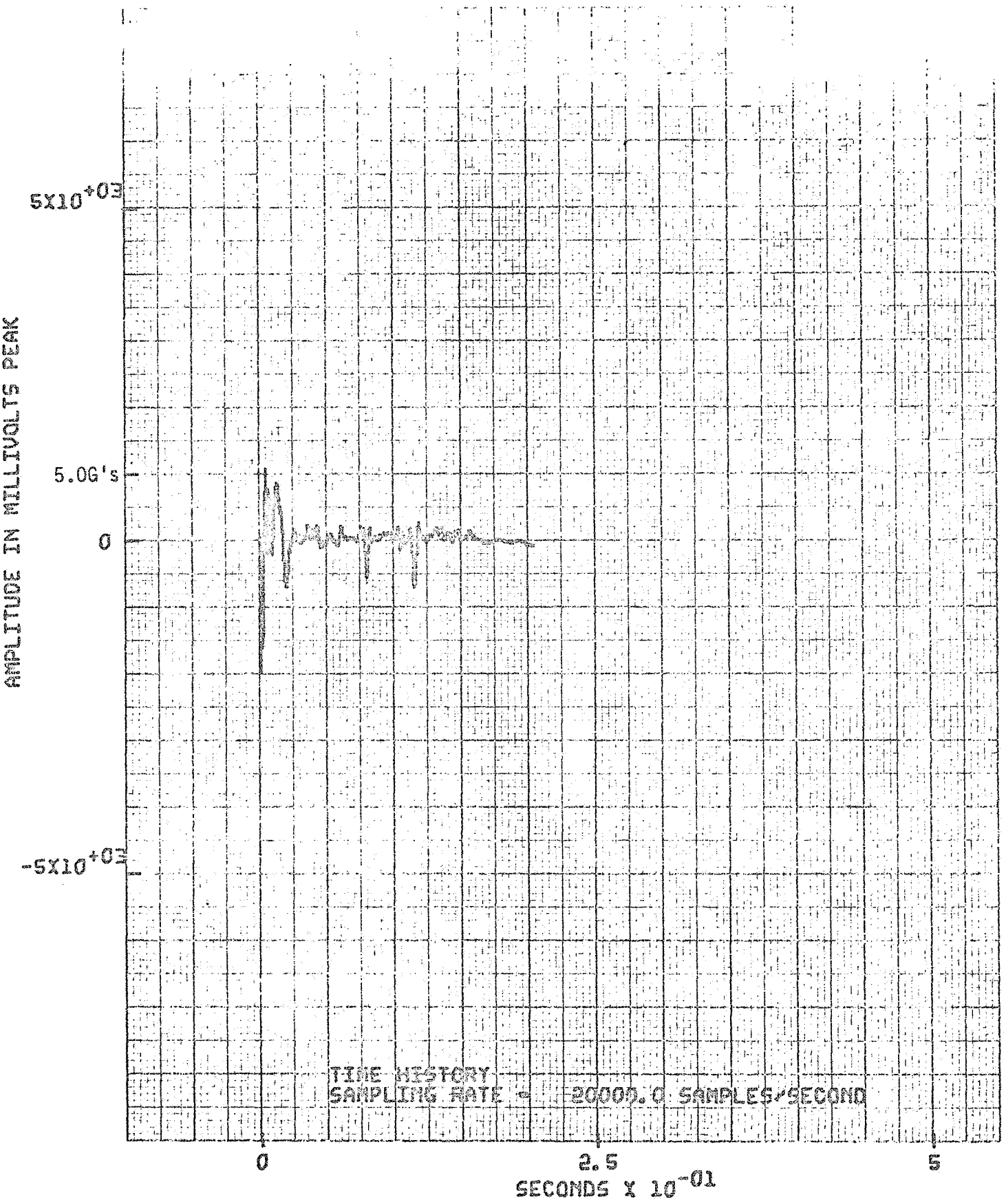



Figure 58: SYNTHESIZED TRANSIENT WAVEFORM, $f'(t)_R$

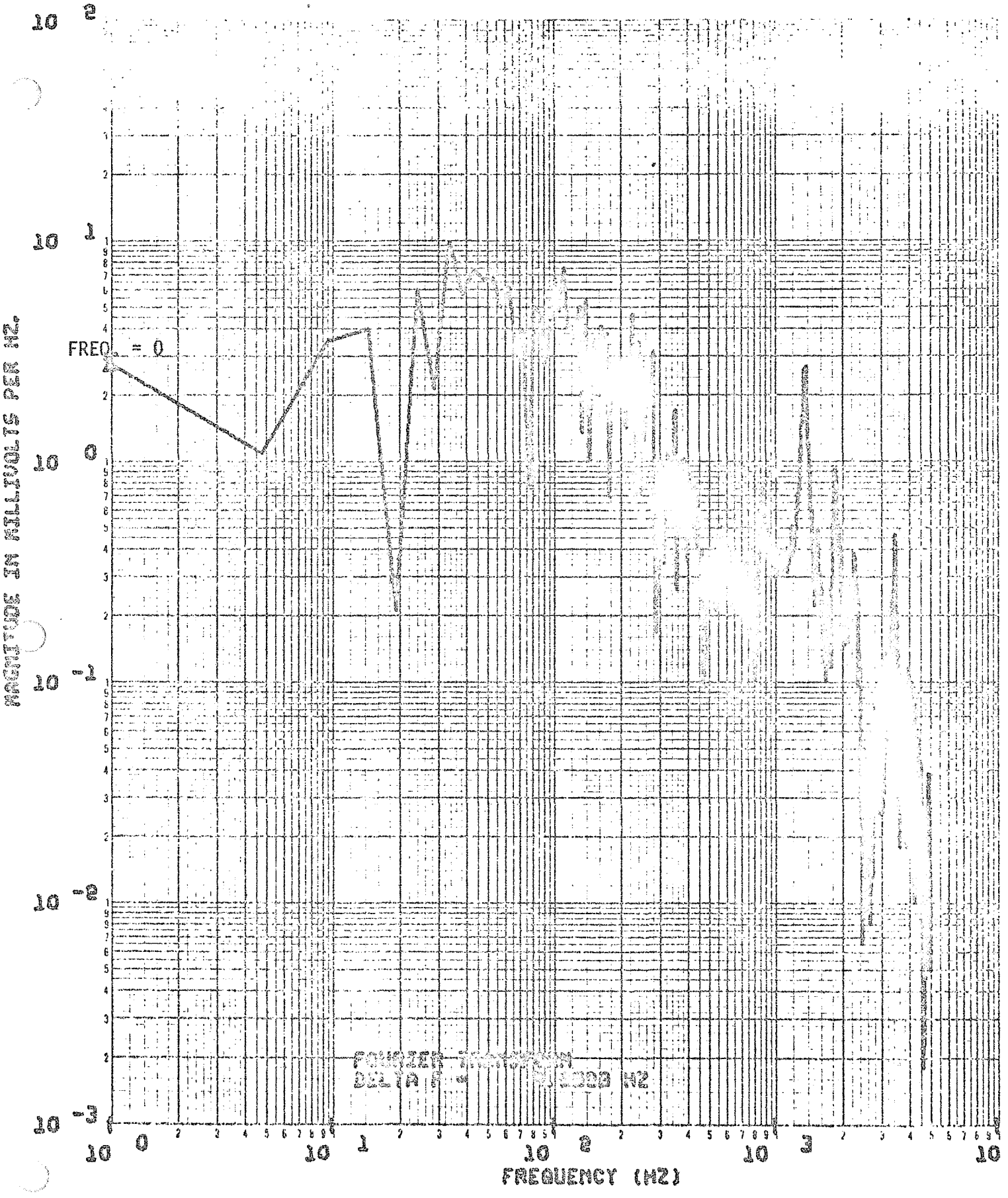



Figure 59: SYNTHESIZED TRANSIENT WAVEFORM, FOURIER TRANSFORM MODULUS, $F'(\omega)_R$

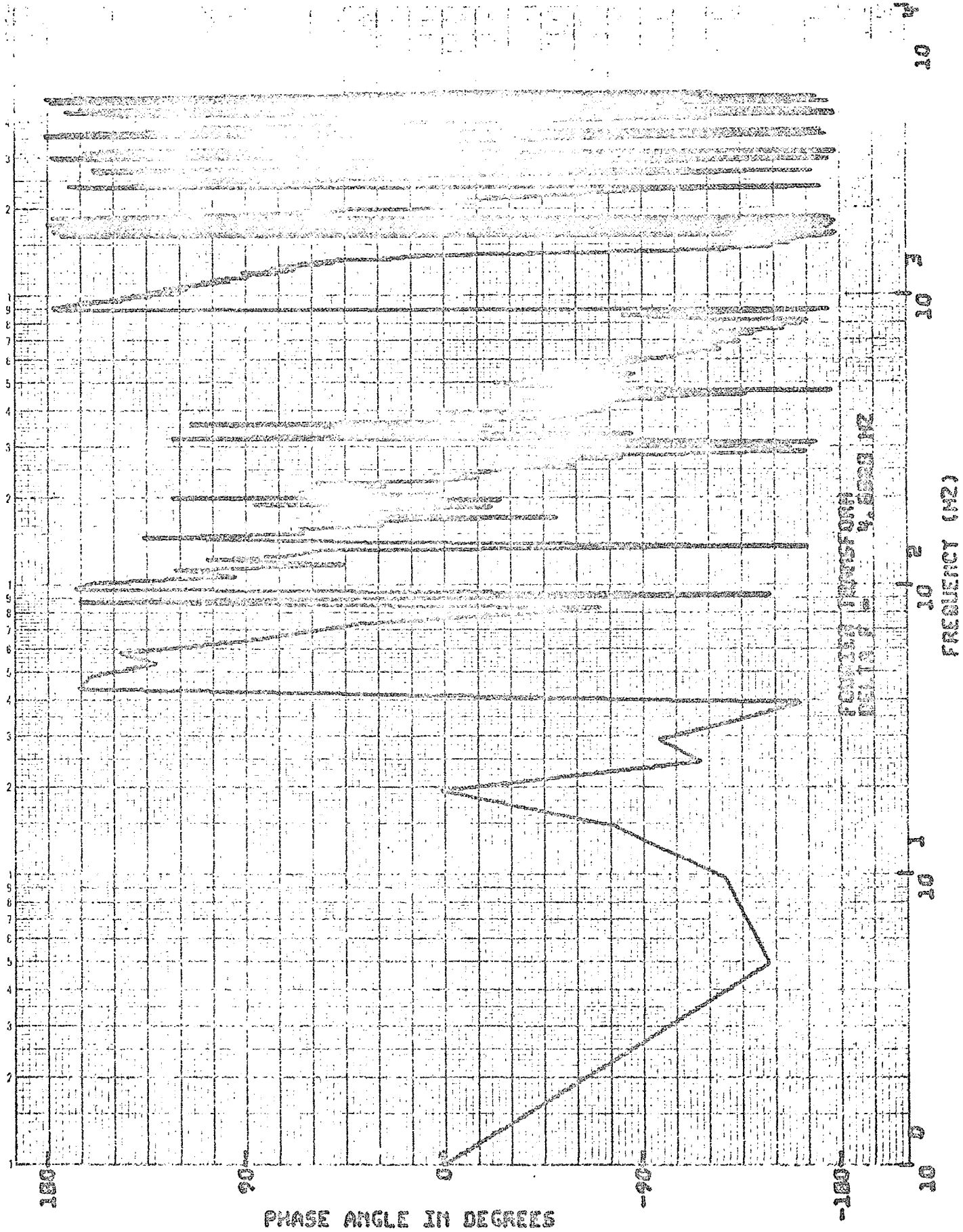



Figure 60: SYNTHESIZED TRANSIENT WAVEFORM, FOURIER TRANSFORM PHASE SPECTRUM, $F'(\omega)_R$

## Control System Empirical Error Study

The objective of the error study is to provide a model of the control system for estimating the bound on reproducibility of the required transient waveform on typical laboratory test apparatus. Identification, isolation, and evaluation of error sources are semiempirical. Initial efforts to obtain the proper framework for the expected error bound are developed in Appendix I, "Error Analysis of a Transient Waveform Control System." Its basic assumption, that the background noise could be represented by a stationary stochastic process, is in error as demonstrated with practical experience experimenting with the prototype control system.

Optimization of this type of control system demands explicit attention to every source of potential noise in both the test system and the media of data processing. Background material for this study is derived from the specialized knowledge of signal theory practiced by the communication engineer[1][2][4][8].

The major error sources; considering test equipment, measurement, and data processing techniques are:

1) Vibration test system noise;

2) Test system nonlinearity;

3) Data aliasing;

4) Data Truncation;

5) Data interpolation;

6) Data quantization.

These error sources are discussed as follows, together with empirical results, directing the structure of an applicable error model.

1) Vibration test system error. This error is caused by a time-variant response of the system, due to noise. The characteristics of typical test system noise was measured and estimated by Fourier transforming a 400 msec sample (2.5 Hz resolution). Baseline data for this experiment were derived from swept-sine excitation of a vibration test system. The response of the system is shown in Figure 61. This noise, equivalent to 0.1 G rms, measured at the control accelerometer, and its spectral representation are shown in Figures 62 and 63. The characteristics cannot be represented by a stochastic process; the energy in the time domain is predominately 60 Hz and harmonics. The error source is readily tested by sequentially impulsing the vibration test system at various power levels and evaluating the difference in the noise-error term. The Fourier transforms of the impulse response, Figures 65, 67, and 69, demonstrate that as the acceleration amplitude is increased, the noise error contributes a smaller percentage of the total energy. Corresponding time histories of system response are shown in Figures 64, 66, and 68. Improving signal-to-noise ratio will improve the accuracy and resolution of the synthesized waveform, $f'(t)_R$.

The acceleration noise floor, measured by the control accelerometer, is a measure of the resolution error in the synthesized waveform, $f'(t)_R$. If the noise is considered as a signal and nonrandom, an expected error-bound can be defined. The error attributable to the vibration test system noise is equal to the peak-to-peak value of the system noise. In this case (Figure 62), $\pm 0.25$ g peak, wherein, the best resolution obtainable will be $\pm 0.25$ g peak. The resolution may be better than this if the error terms (i.e., considering noise as a signal and examining the spectral distribution of this signal (Figure 63) are not critical in defining the test system transfer function, $H(\omega)$.

The time-invariant response of the vibration system will not contribute to an error term. Any invariant response is calculated as part of the test system transfer function, $H(\omega)$.

2) Test system nonlinearities. This error source is the subject of a separate study element. Transient waveform control has been demonstrated on electromagnetic test equipment that is characterized by mild nonlinearities similar to G.S.F.C. test systems. The errors in the Fourier transform of a nonlinear time function occurs at a relatively low amplitude and at frequencies greater than 4 kHz.

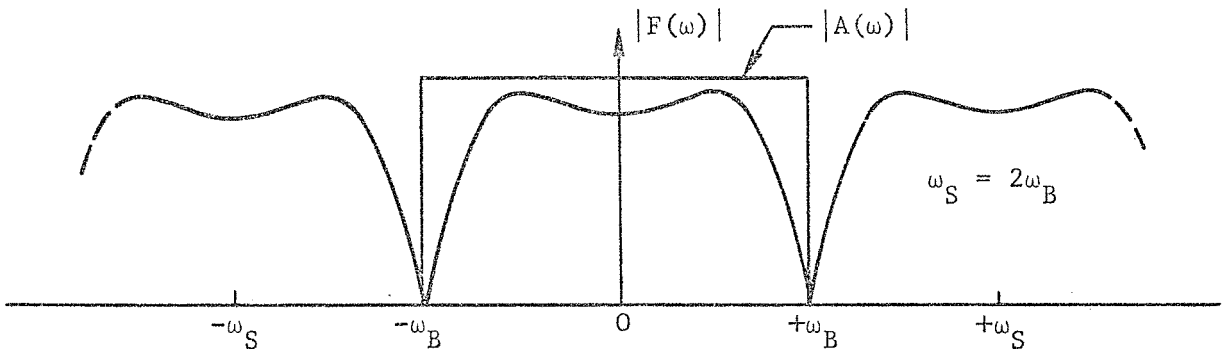
3) Aliasing error. The error term resulting from folding of all frequency content above one-half the sampling frequency of the discrete Fourier transform into lower frequencies[8].

In this analysis, a signal, $f(t)$, is bandlimited such that

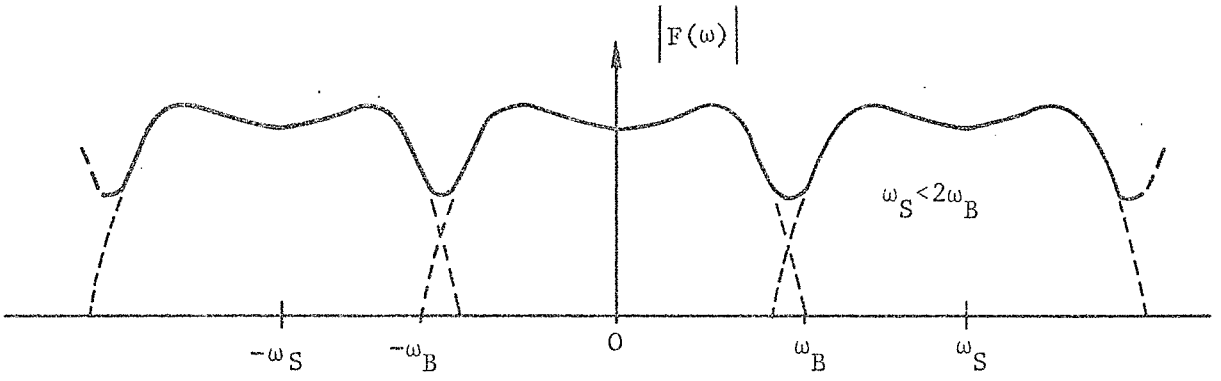
$$F(\omega) = \int_{-\infty}^{\infty} f(t)e^{-j\omega t}dt \qquad \text{for } |\omega| < \omega_B, \tag{24}$$

$$F(\omega) = 0 \qquad \text{for } |\omega| > \omega_B.$$

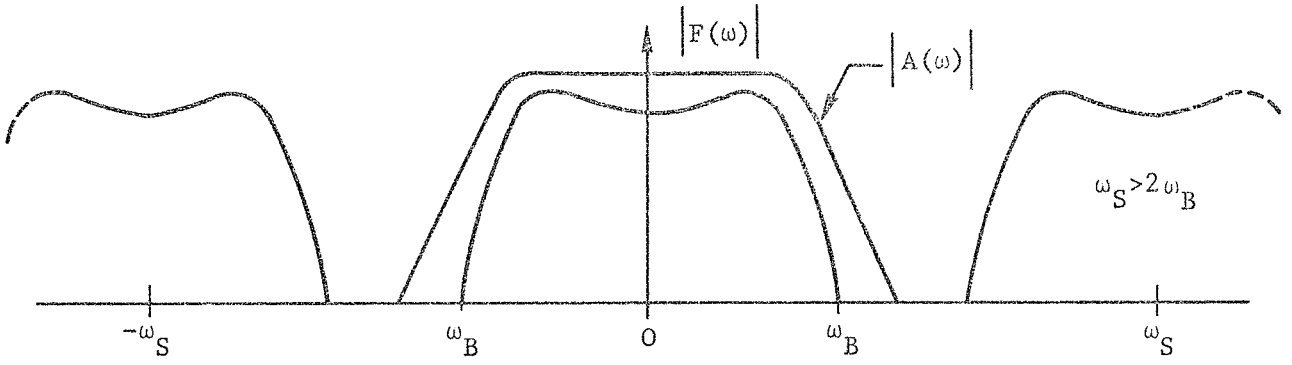
If this signal is sampled at a rate twice the bandlimit frequency, $\omega_B$, a spectrum, $F(\omega)$, is generated as shown. Note the generation of periodic components centered about the sampling frequency, $\pm\omega_s$. These components must be removed by lowpass filtering. The filter characteristic is $A(\omega)$. For $\omega_s = 2\omega_B$ the required filter is not physically realizeable.



If the sampling frequency, $\omega_s$, is less than twice the bandwidth, $\omega_B$, an overlap in spectra occurs in the higher frequencies as shown.




Sampling frequencies for the Transient Waveform Control System should be at least four times the bandlimit, $\omega_B$. The maximum sampling speed is limited by the number of data points the computer is capable of storing and manipulating at any one time. The bandlimit, 5 kHz, will dictate a sampling frequency of at least 20 kHz. By increasing the sampling frequency, the abrupt-cutoff filter bandpass characteristic, A(ω), can be relaxed as shown.




Applying this logic, a square pulse was analyzed. This can be considered a worst case, on basis of rise time input to the Transient Waveform Control System. Figure 70 shows the time history of this pulse, and Figure 71 shows the modulus of the Fourier transform of this pulse. The unaliased Fourier transform of a square pulse will decay at a slope of -1. The deviation from -1 slope, shown in the transform of Figure 71, is a measure of aliasing error.

The Transient Waveform Control System upper bandlimit is specified at 5 kHz. The transient calibration input, $f(t)_i$, and the transient calibration output, $f(t)_o$, were sampled at 20 kHz samples per second. With the sampling theory outlined above, a 6-pole Butterworth filter was chosen to reduce the energy content of the Fourier spectrum by 36 db at 10 kHz. The filtered square pulse is shown in Figure 72 and the Fourier spectrum in Figure 73.

The high sampling rate and low-pass filter have reduced the aliasing error to an unmeasurable level. The low-pass filter has also reduced the energy by 3 db at 5 kHz. This energy loss will not affect the definition of the transfer function, $H(\omega)$, if identical low-pass filters are used to filter the transient calibration input, $f(t)_i$, and the transient calibration output, $f(t)_o$. The transfer function is the ratio of the Fourier transform of $f(t)_o$ and the Fourier transform of $f(t)_i$. The low-pass filter characteristics cancel when this ratio is computed. With proper signal processing techniques, the aliasing error will not contribute to the error model.

The sampling rate for a 5 kHz bandwidth should be at least 20 kHz. The low-pass-antialiasing filter should have a corner frequency at 5 kHz and an attenuation slope of at least 36 db per octave. This will reduce the aliasing term to 1.66% of it's unfiltered value.

4) Truncation error. The operation of transient waveform control requires that the transient input calibration signal, $f(t)_i$; the transient output calibration, $f(t)_o$; and the required response function, $f(t)_R$; must each be described by an equal number of data points, N. The sampling interval, $\Delta t$, and the sample record length must also be equal for all pulses. Obviously, this will not occur naturally and some adjustment must be made. For example, $f(t)_i$ will essentially go to zero in 5 msec, $f(t)_o$, will go to zero within approximately 20 to 60 msec, and $f(t)_R$ may endure for 200 msec. If $f(t)_o$ is recorded for the full 200 msec, about 140 to 180 msec (70% to 90%) will be residual system noise and will seriously affect the computation of the system transfer function, $H(\omega)$. The solution to this problem is to incorporate into the computer software a truncation parameter, $\tau$, for the input calibration signal, $f(t)_i$, and for the output calibration response, $f(t)_o$. This truncation parameter is defined as that point in time after which all record data is to be replaced by zeros until the required sample record length, T, is achieved. Since the input calibration signal, $f(t)_i$, is generally fixed, so is it's truncation parameter. The system output response function, $f(t)_o$, is not fixed and as such, it's truncation parameter must be variable. $\tau$ must be determined by observing $f(t)_o$ and estimating its proper value. The estimate is determined by observing the envelope of the response decay and deciding where $f(t)_o$ approaches zero and only residual noise continues.

In practice, only $\tau$ for $f(t)_o$ must be estimated; however, if $\tau$ is too short, $f(t)_o$ will be truncated, its Fourier transform will be in error, and the resulting system transfer function will be in error. Conversely, if $\tau$ is too long, too much noise energy will be analyzed, and the system transfer function will become noisy.

Another result of too long a truncation length is wrap around error[2]. The required waveform, $f(t)_R$, is convolved with the inverse of the system

impulse response function, $1/h(t)$[9]. This cyclic convolution may generate significant wrap around error if the required waveform, $f(t)_R$, is quite long in time relative to the time duration of the impulse response function, $h(t)$. Wrap around error can be eliminated by ensuring that enough zero amplitude data points are added, such that their number exceeds the number of data points in the required waveform, $f(t)_R$.

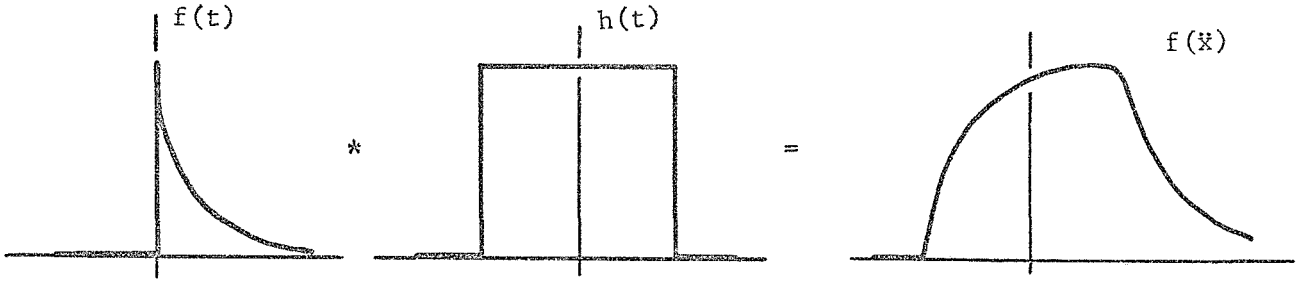
Convolution(4) describes the action of a physical system as it takes a weighted average of some physical quantity about a small range of some variable. Thus, the integral

$$f(X)_o = \int_{-\infty}^{\infty} f(X-t)h(t)\,dt \qquad (25)$$

describes the process for continuous data. The input function is $f(t)$ and $h(t)$ is the impulse response function. The function $f(X)_o$ is the system response to the input $f(t)$.

For a graphic example of convolution, consider the input function, $f(t)$, to be a stepped exponential decay function. Convolve this input function with an impulse response function $h(t)$, arbitrarily a rectangle function. Let * symbolically denote convolution. Then,

$$f(X)_o = f(t)_i * h(t)$$




Note that in Equation 25, the input function is reversed before the multiplication and integration take place.

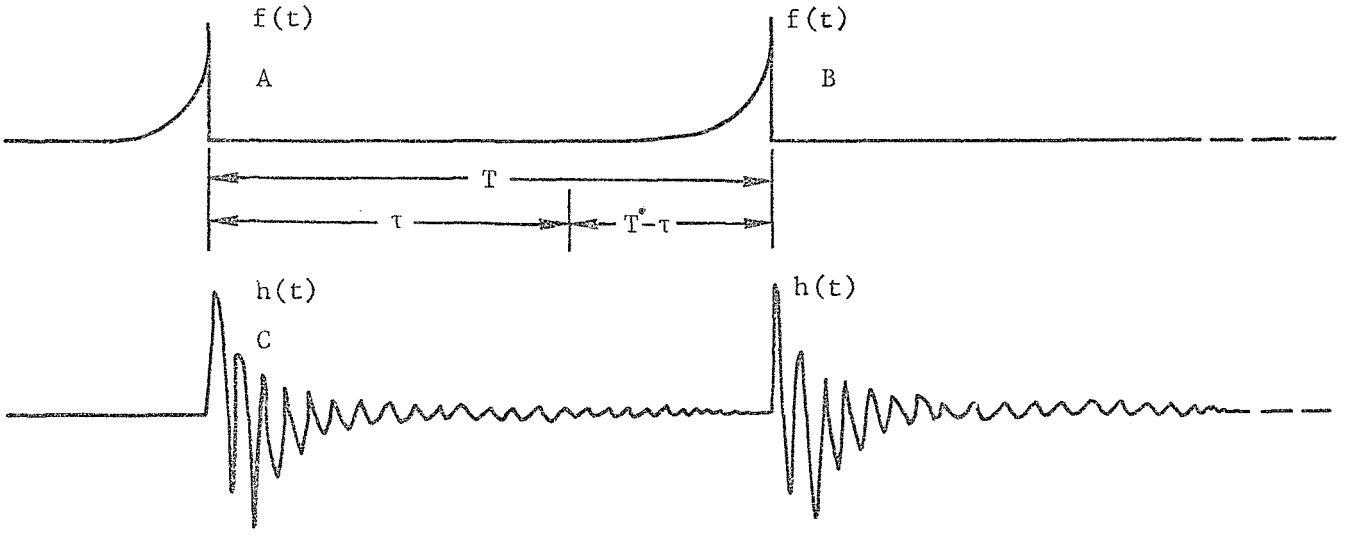
The convolution process for discrete data is periodic in time and is called cyclic convolution. Cyclic convolution(2) can be described by the summation

---

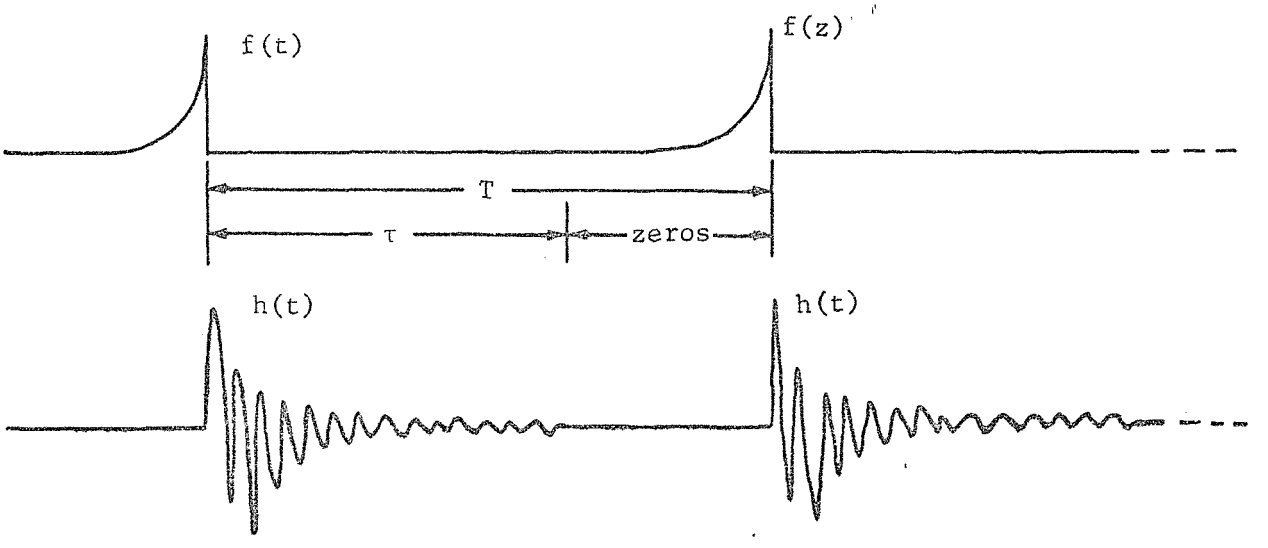
[9] The Fourier transform of the system impulse response, $h(t)$, is equal to the system transfer function, $H(\omega)$. Therefore, as the transient calibration input, $f(t)_i \rightarrow \delta(t)$, an impulse function(4), the transient calibration output, $f(t)_o \rightarrow h(t)$, the system impulse response.

$$f(X\Delta t) = \Delta t \sum_{n=-N}^{n=N} f(X\Delta t - n\Delta t)h(X\Delta t). \qquad (26)$$

Cyclic convolution can be understood by referring to the following diagram.




Ideally, pulse A is convolved with pulse C, but note that as A is convolved with C, pulse B is overlapping the end of pulse C and is simultaneously convolved with pulse C. This overlap, or wrap around, can be avoided by truncating the sequences to some length, $\tau$, less than T and adding n zeros, such that $\tau$+n zeros = T, as shown below.



The effect of varying values of the truncation parameter, $\tau$, was empirically tested by sequentially inputting a calibration pulse to the vibration system and calculating the system transfer function, $H(\omega)$.

The calibration output, $f(t)_o$ (Figure 74), was truncated to 350 data points (17.5 msec) out of a total of 4,096 data points (187.3 msec). Note the poor definition of the transient calibration output, $f(t)_o$ (Figure 75) below 100 Hz. Thus, the truncation time, $\tau$, is too short.

The truncation time was then increased to 800 data points (40 msec) out of 4,096 data points (187.3 msec). Again, truncation error is evident and the definition of the calibration output, $f(t)_o$, is poor (Figures 76 and 77).

Figures 78 and 79 represent a further improvement. The truncation time, $\tau$, is 2,048 data points (102.4 msec). The definition of the calibration output, $f(t)_o$, is adequate, except for aberrations below 40 Hz which are attributable to quantization error, and enough zero amplitude data points have been added to accommodate a 100 msec required waveform, $f(t)_R$, without wrap around error.

The final test in this sequence was to let $\tau$ equal the total data length (no truncation). The results are shown in Figures 80 and 81. An undesirable increase in the d.c. term and in the noise (60 Hz and harmonics) term is evident. In conclusion, the transient calibration pulses, $f(t)$, if much shorter in time duration than the response, $(f(t)_o)$, will not generate significant wrap around error. In addition, the test system noise contributes a much larger error term in defining the transfer function, $H(\omega)$, than does the wrap around effect.

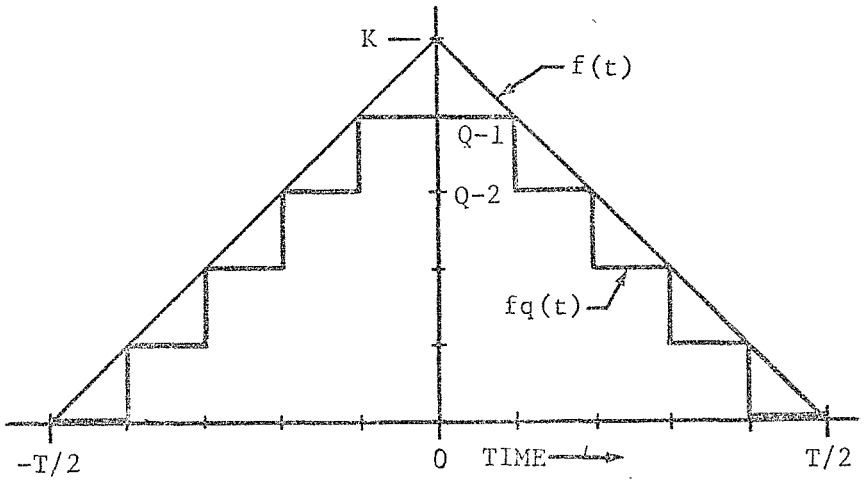
5) Interpolation error. The synthesized signal, $f'(t)_s$, calculated by the Transient Waveform Control System is converted to an analog signal before it can be used by the vibration system. A digital-to-analog converter produces voltage steps of constant amplitude between sampling points. The input signal, $f(t)_s$, is a step-function interpolant of the ideal continuous signal. This type of conversion can induce:

   a) Rapidly varying transients (i.e., those which contain high frequency) that can be distorted by the step-function interpolant (this interpolation error is proportional to the slope of the required waveform);

   b) Discontinuities in the step-function, that produce high frequency noise in the vibration test system.

   The method of minimizing these error sources is to low-pass filter the step function interpolant[7] directly after the digital-to-analog conversion process. Experimentation with the prototype control system determined this source of error to be secondary.

6) Quantization error. This type of error is the result of the nonlinear process of converting continuous analog data into data points at discrete quantized levels. As an example, consider a symmetrical-triangular function in time, $f(t)$, as illustrated as follows.




If this function, f(t), were quantized by means of a chopping routine into Q quantized levels from zero to K, the function fq(t) results (fq(t) is shown as a continuous function to eliminate sampling rate errors (i.e., the sampling interval approaches zero). The Fourier transform of f(t) is

$$F(\omega) = \frac{KT}{2}\left[\frac{\text{SIN}\frac{\omega T}{2}}{\frac{\omega T}{2}}\right]^2 , \tag{27}$$

and the Fourier transform of fq(t) is

$$Fq(\omega) = \frac{KT}{Q}\sum_{n=1}^{Q-1}\left(1 - \frac{n}{Q}\right)\left[\frac{\text{SIN}\frac{\omega T}{2}\left(1 - \frac{n}{Q}\right)}{\frac{\omega T}{2}\left(1 - \frac{n}{Q}\right)}\right]. \tag{28}$$

Where K = peak amplitude of triangular function;

T = pulse duration;

Q = number of quantization levels from zero to K;

$\omega$ = radian frequency;

n = an integer.

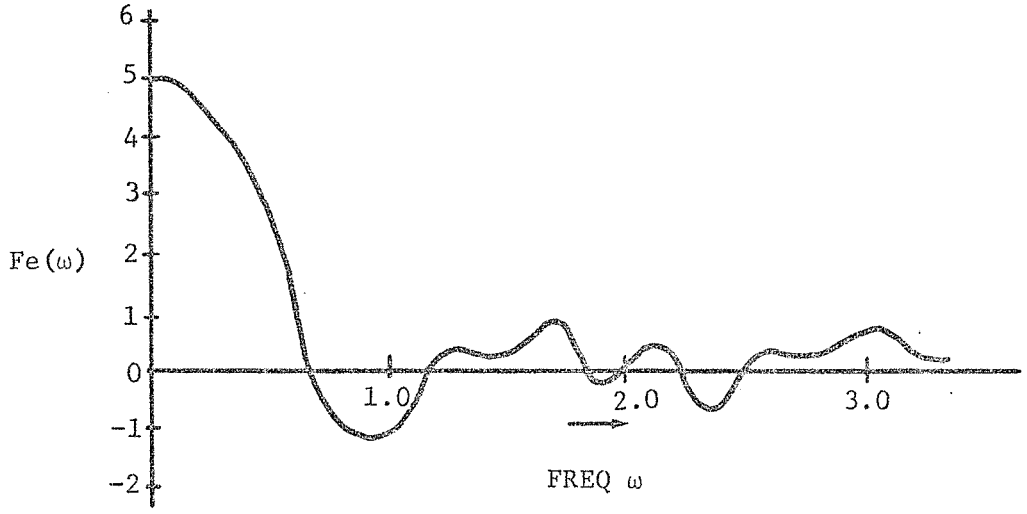
Therefore, the generalized error in the frequency domain due to quantizing a symmetrical triangular pulse, f(t), into a quantized function, fq(t), is

$$Fe(\omega) = KT\left\{\frac{1}{2}\left[\frac{\text{SIN}\frac{\omega T}{2}}{\frac{\omega T}{2}}\right]^2 - \frac{1}{Q}\sum_{n=1}^{Q-1}\left(1 - \frac{n}{Q}\right)\left[\frac{\text{SIN}\frac{\omega T}{2}\left(1 - \frac{n}{Q}\right)}{\frac{\omega T}{2}\left(1 - \frac{n}{Q}\right)}\right]\right\} \tag{29}$$

for the situation where,

$$K = 5,\ Q = 5,\ T = 10$$

the error function is as illustrated as follows:




The preceding graph illustrates large aberrations in the low frequency domain; therefore, it generally agrees with the results in the "Fourier Integral Transform Error Study" Section of this report.

This error source was also studied in detail and the results are reported in the "Fourier Integral Transform Error Study" Section. That study indicated the need for large word size conversions (i.e., 14 bits plus sign). Further, it demonstrated the need for an unbiasing routine to reduce the low frequency errors generated in the Fourier transforms of quantized data, due to the bias imposed by the quantization method.

Error model.-The empirical error model incorporates six sources of error (Figure 82). The model identifies and locates each error in the signal flow paths of the control system, and is further developed in Appendix I.

Bound on reproducibility.-Any error source defined previously can contribute an error term, such that the required waveform cannot be reproduced. Special data processing techniques previously outlined will reduce quantization error, aliasing error, truncation error, and interpolation error to a negligible level. Nonlinearity error for electromagnetic vibration systems of NASA Goddard is small and considered not serious (see "Nonlinearity" Section).

The major source of error, the vibration ystem response error, is due to system noise. The system noise floor will establish the upper-bound on the reproducibility of the required signal.

A statistical description of the bound on expected performance characteristics of the proposed system is presented in Appendix III. The OGO-D flight data,[7] subject of experimental investigation in this transient waveform control feasibility study, exhibited a time-domain variance of less than 13%.

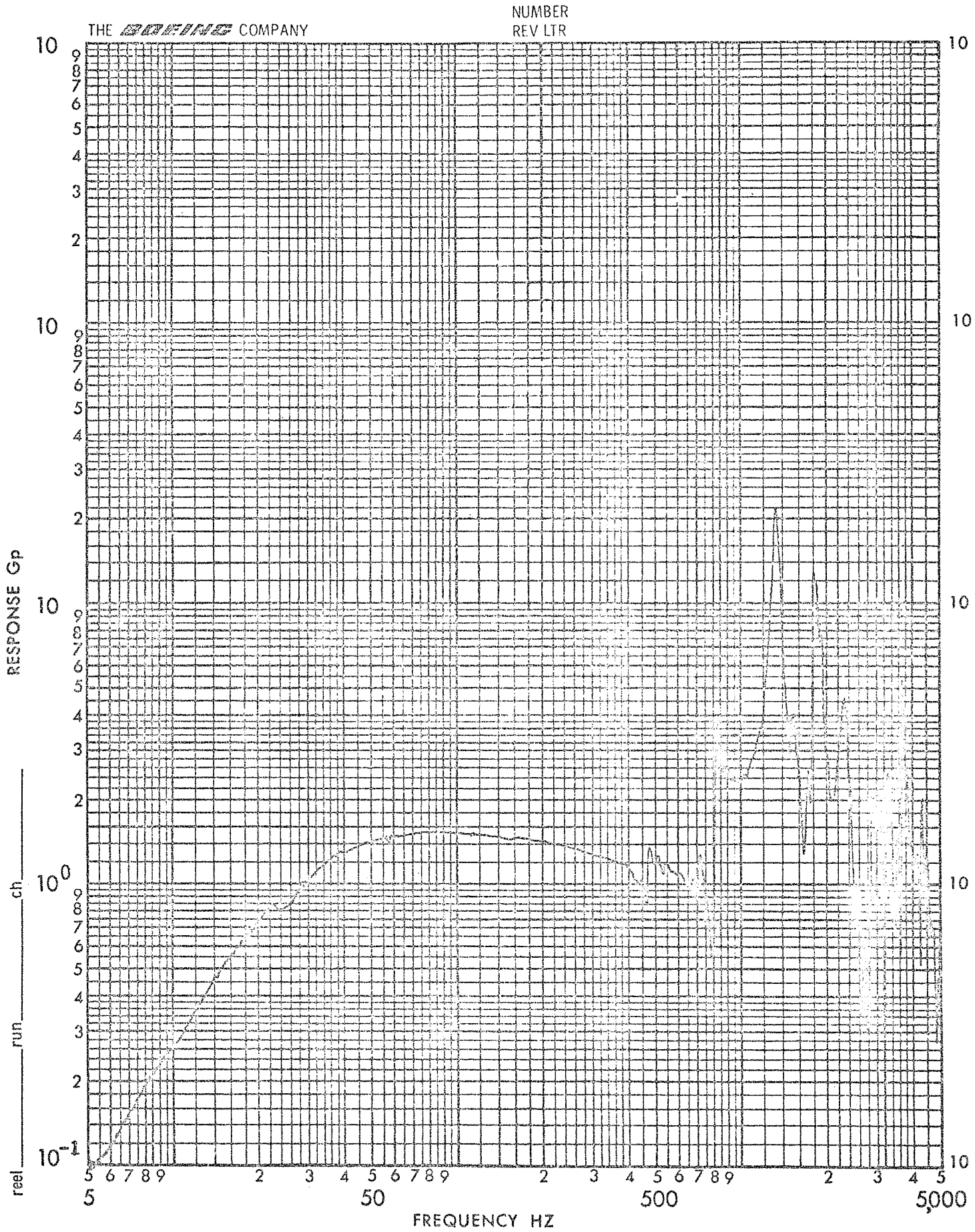



Figure 61: BASELINE IMPULSE RESPONSE FUNCTION DERIVED FROM SINE SWEEP

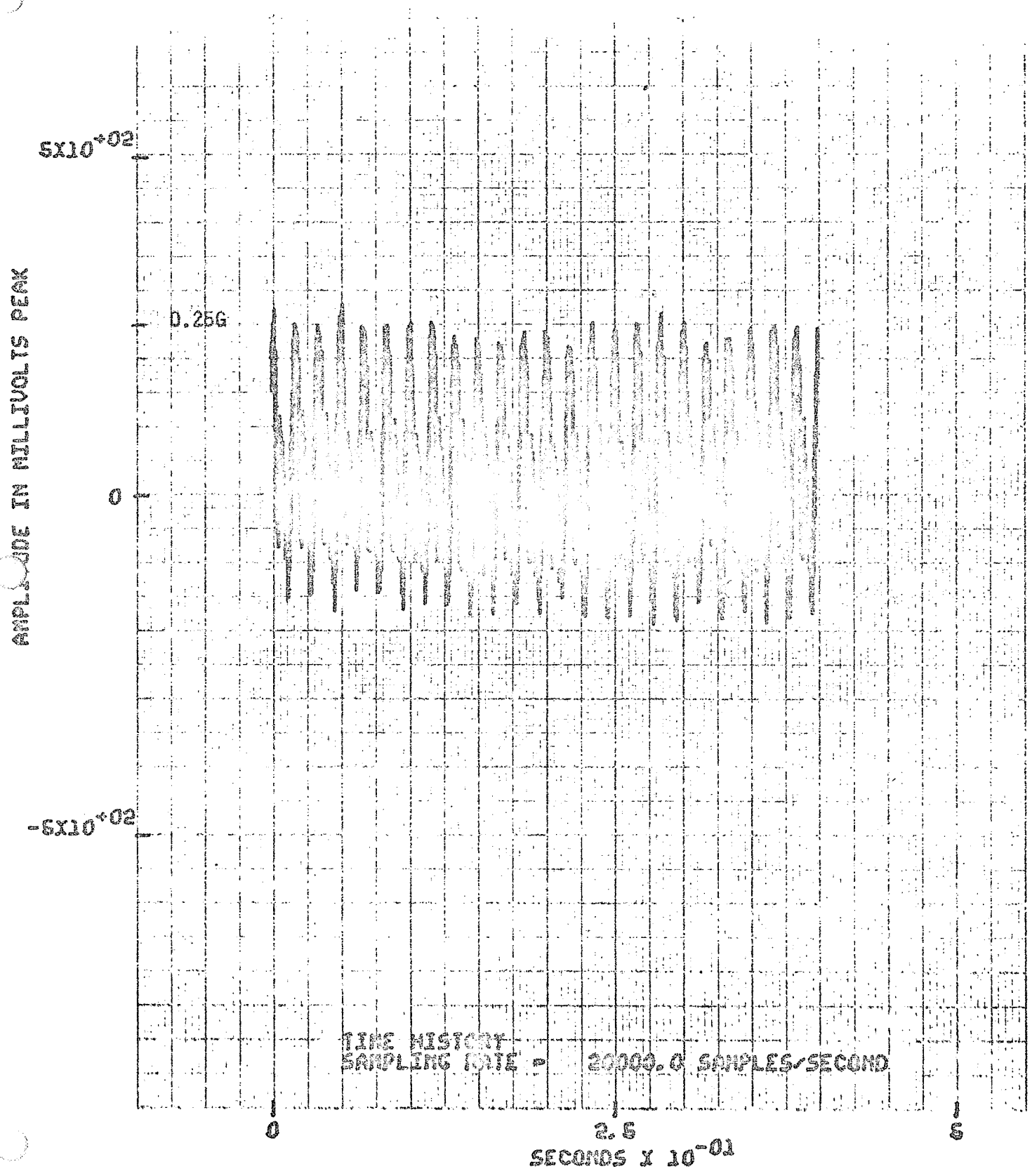



Figure 62: VIBRATION CONTROL SYSTEM BACKGROUND NOISE

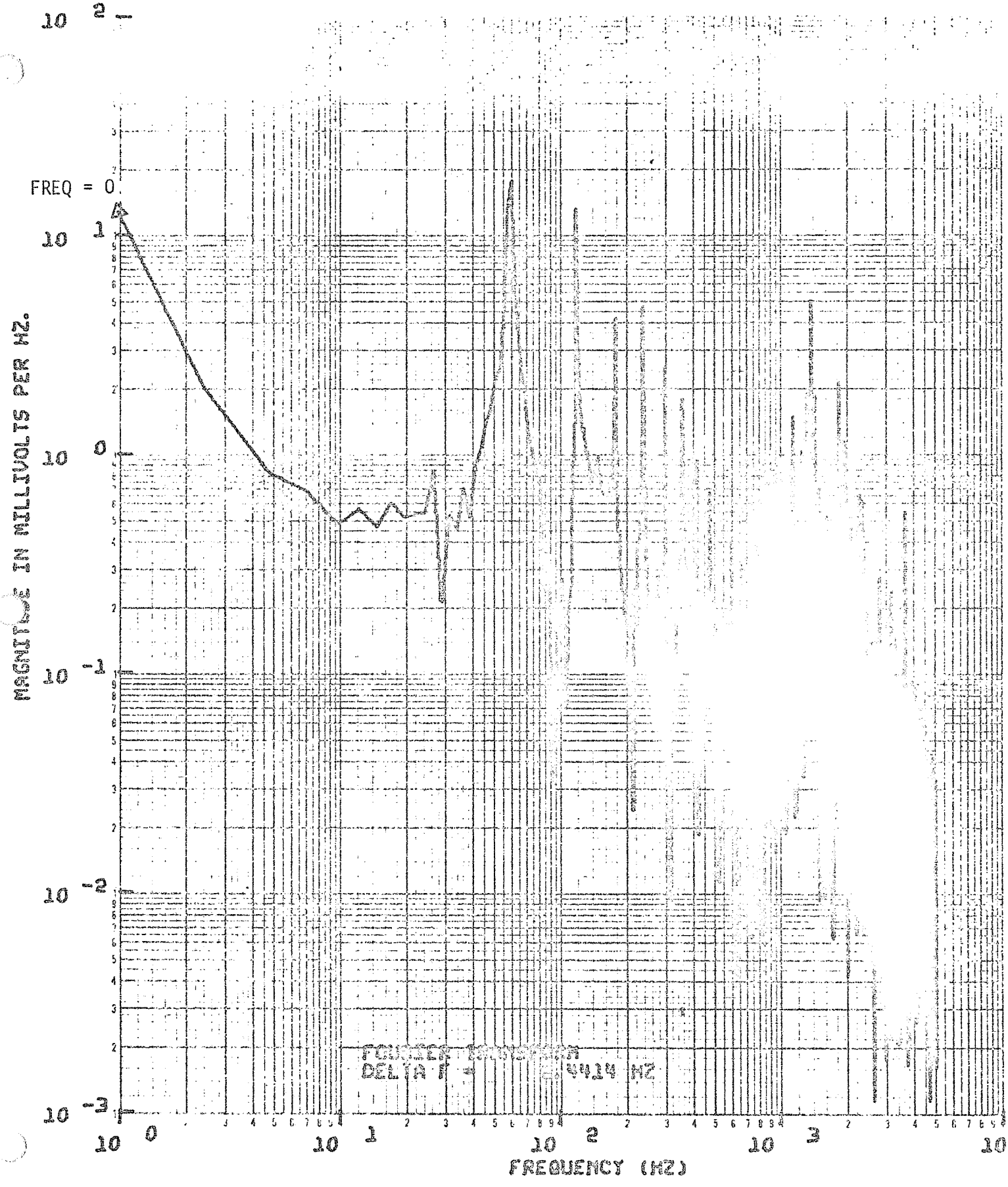



Figure 63: FOURIER TRANSFORM MODULUS OF VIBRATION CONTROL SYSTEM NOISE

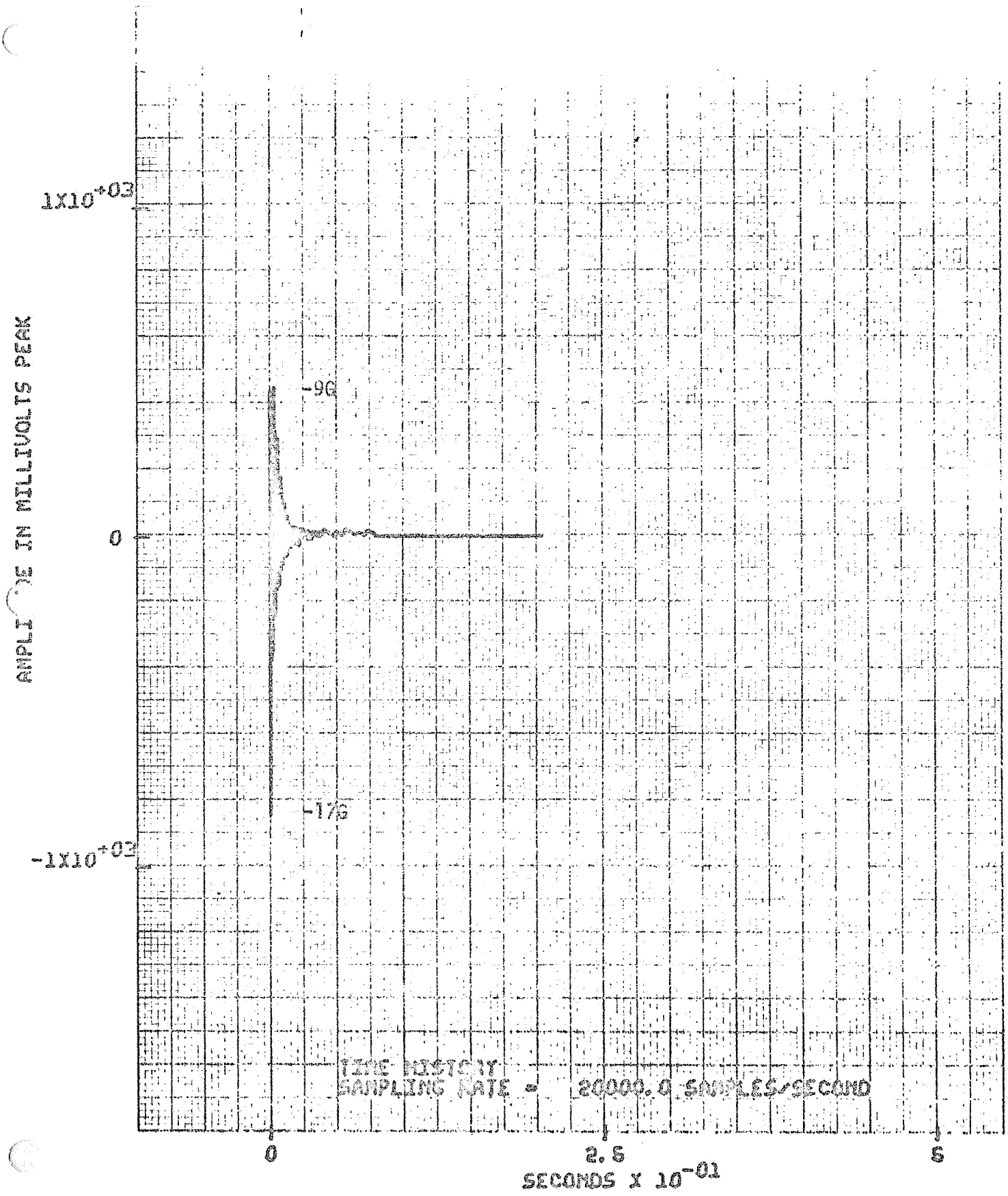



Figure 64: TIME HISTORY OF TRANSIENT CALIBRATION OUTPUT f(t)o 9G POSITIVE PEAK

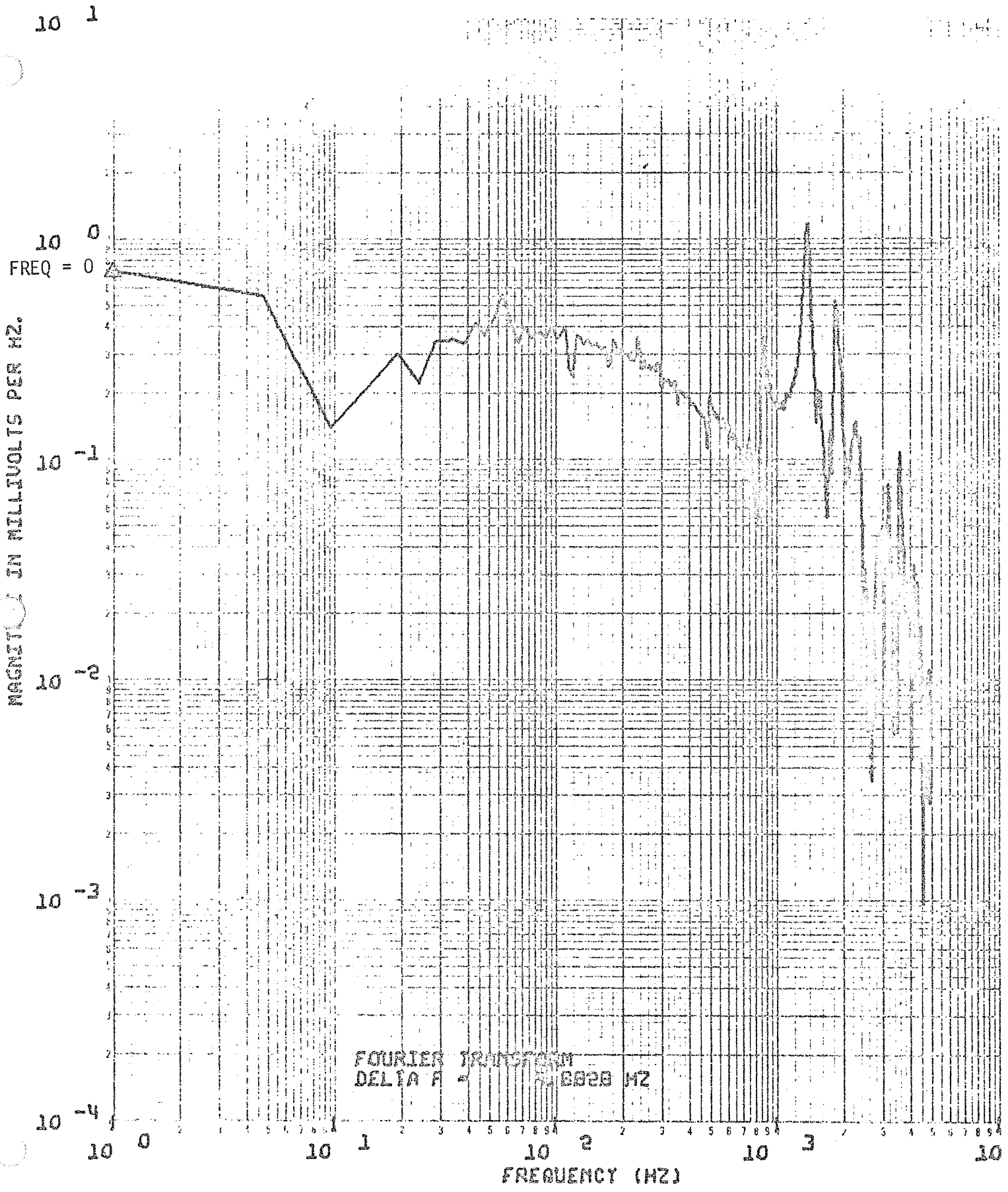



Figure 65: FOURIER MODULUS OF TRANSIENT CALIBRATION OUTPUT f(t)o 9G POSITIVE PEAK

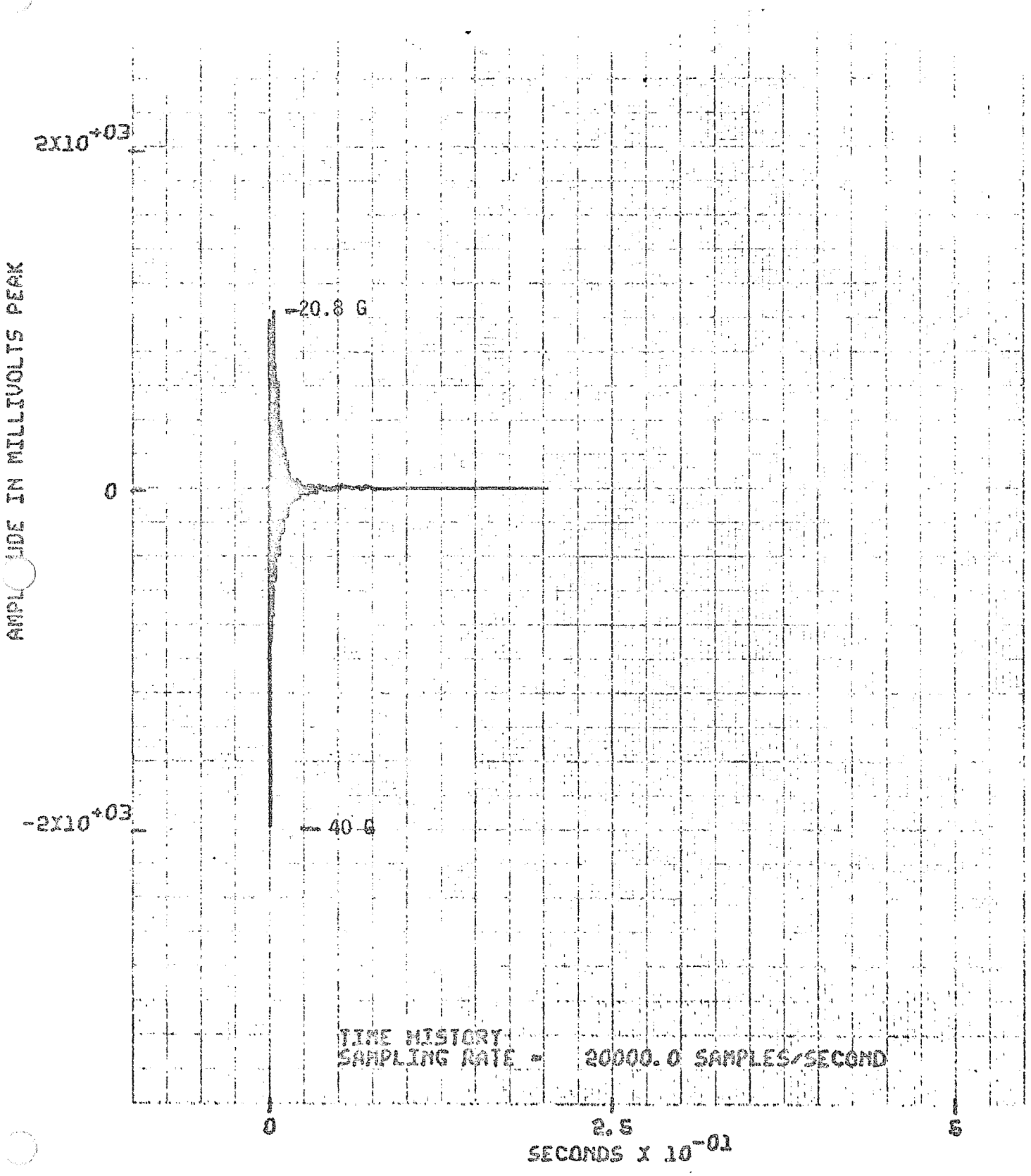



Figure 66: TIME HISTORY OF TRANSIENT CALIBRATION OUTPUT f(t)o 20.8G POSITIVE PEAK

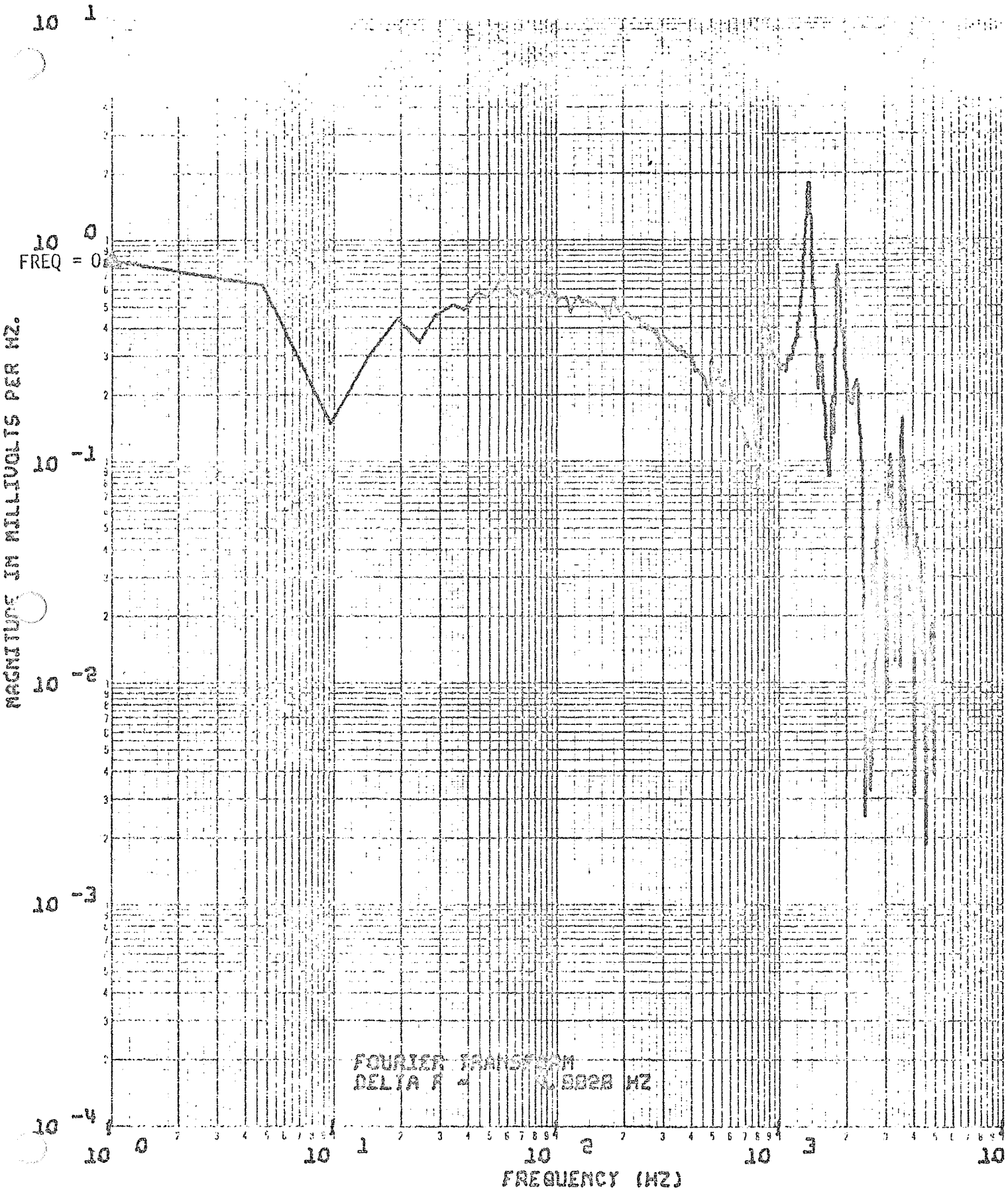



Figure 67: FOURIER MODULUS OF TRANSIENT CALIBRATION OUTPUT f(t)o 20.8G POSITIVE PEAK

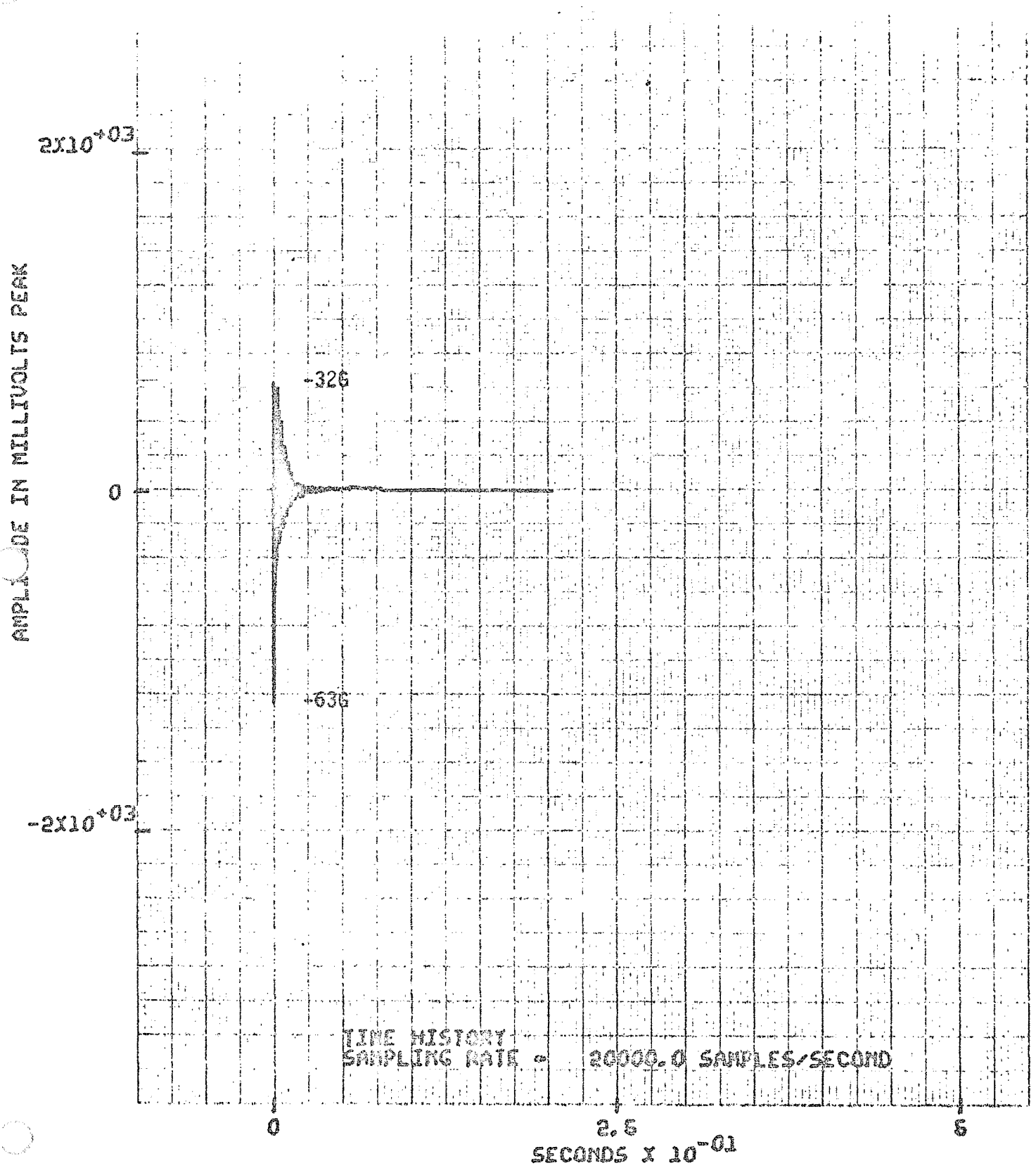



Figure 68: TIME HISTORY OF TRANSIENT CALIBRATION OUTPUT f(t)o 32G POSITIVE PEAK

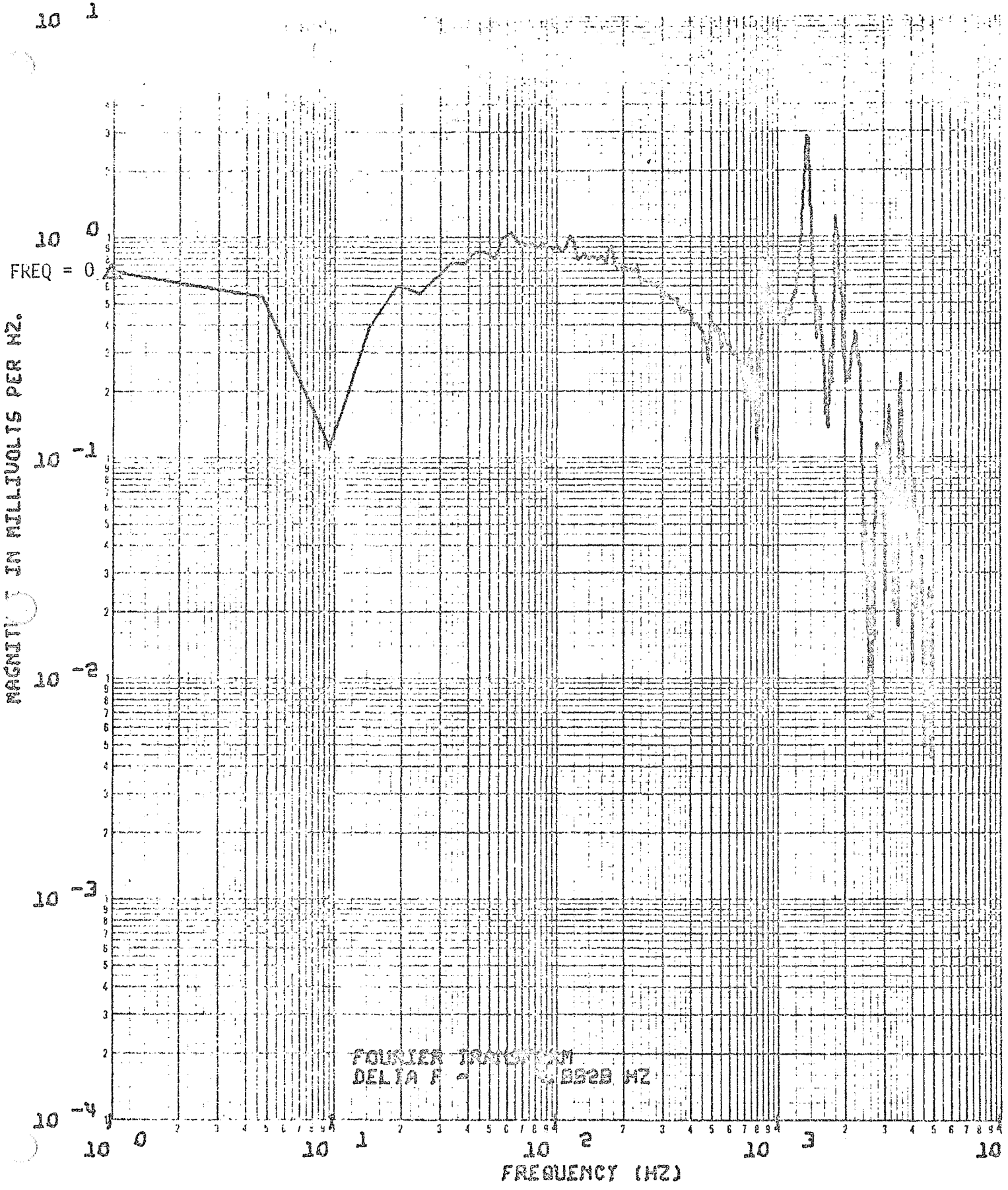



Figure 69: FOURIER MODULUS OF TRANSIENT CALIBRATION OUTPUT f(t)b 32G PEAK

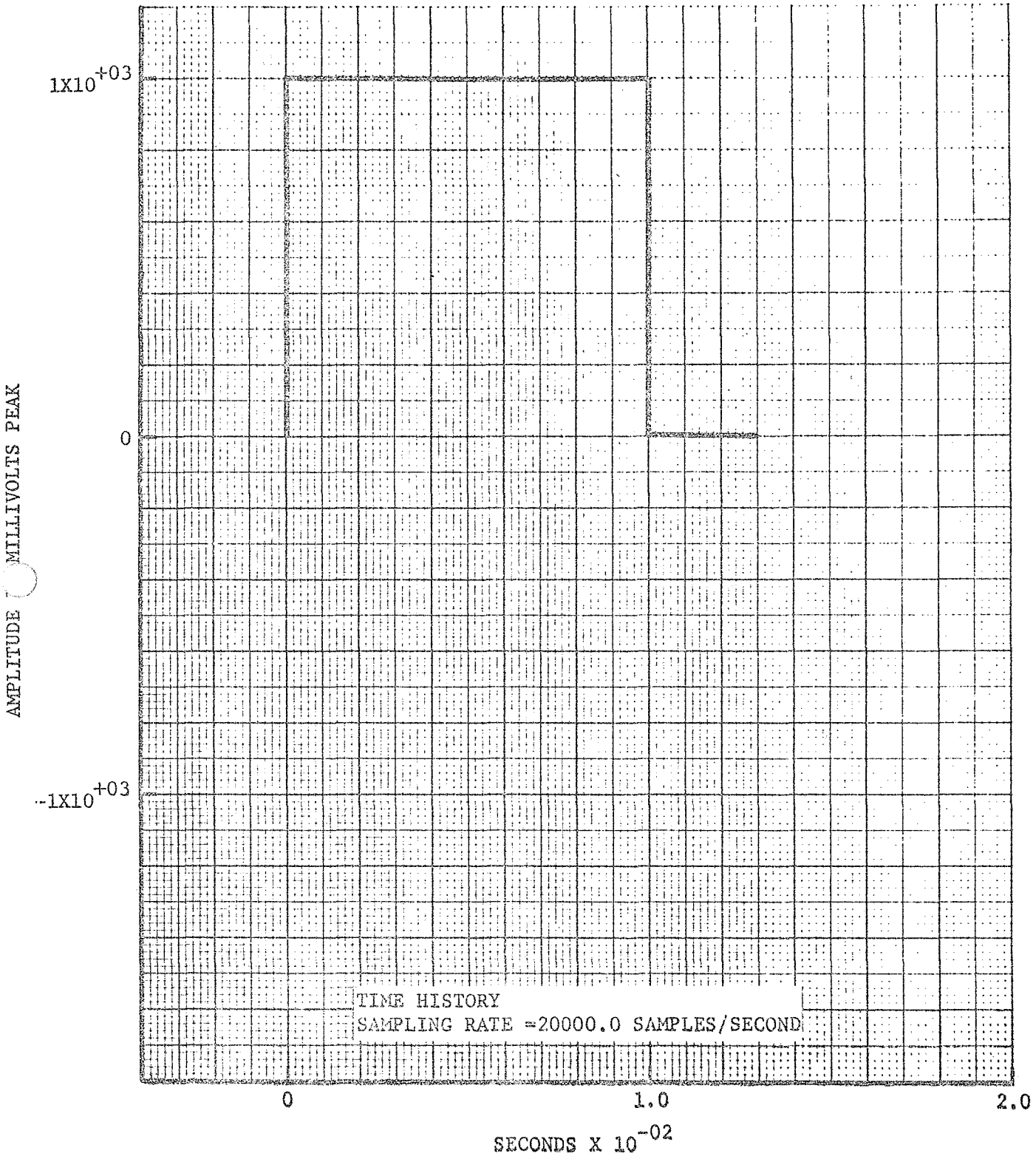



Figure 70: UNFILTERED SQUARE WAVE TIME HISTORY

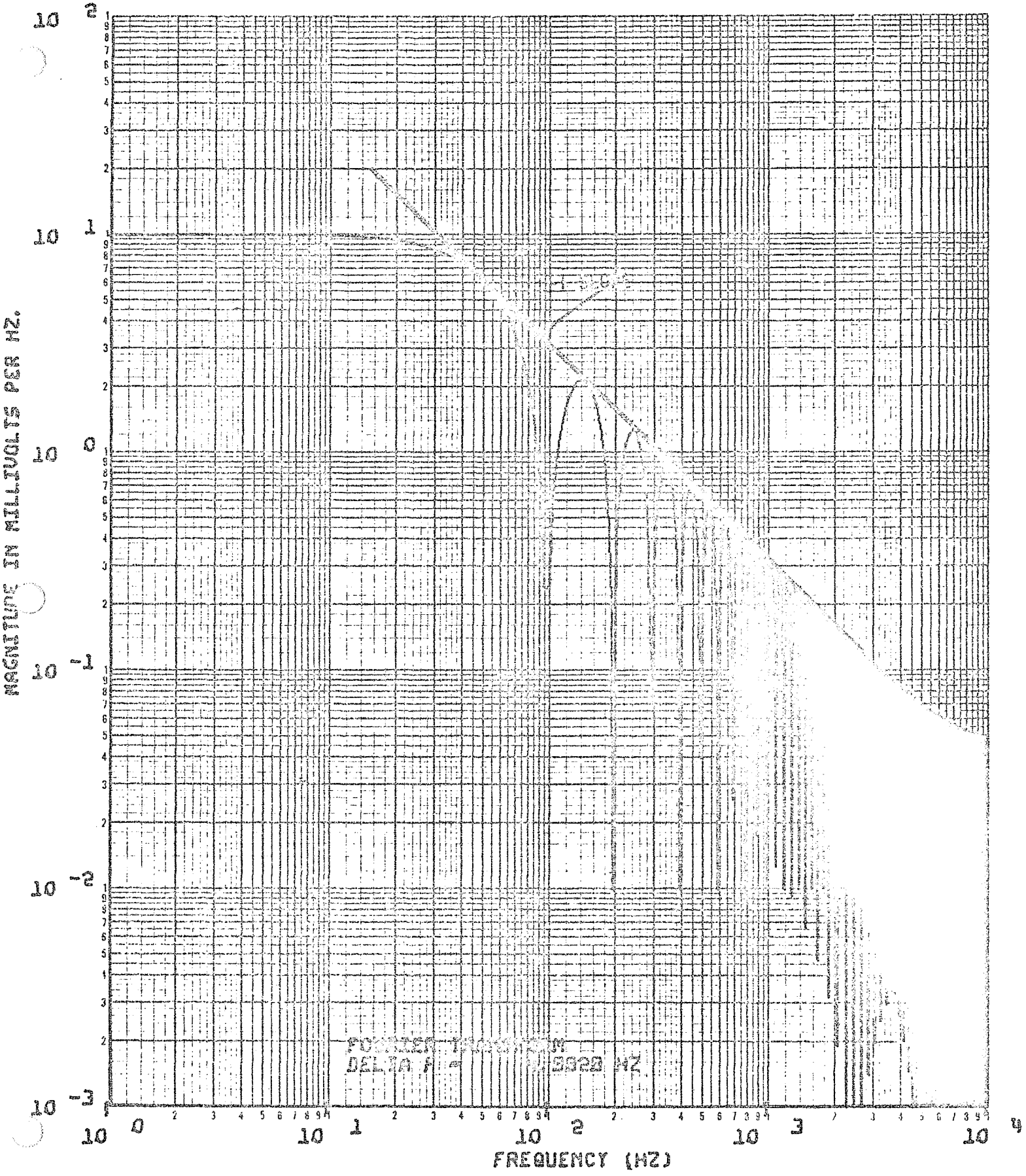



Figure 71: FOURIER MODULUS OF UNFILTERED SQUARE WAVE WITH ALIASING

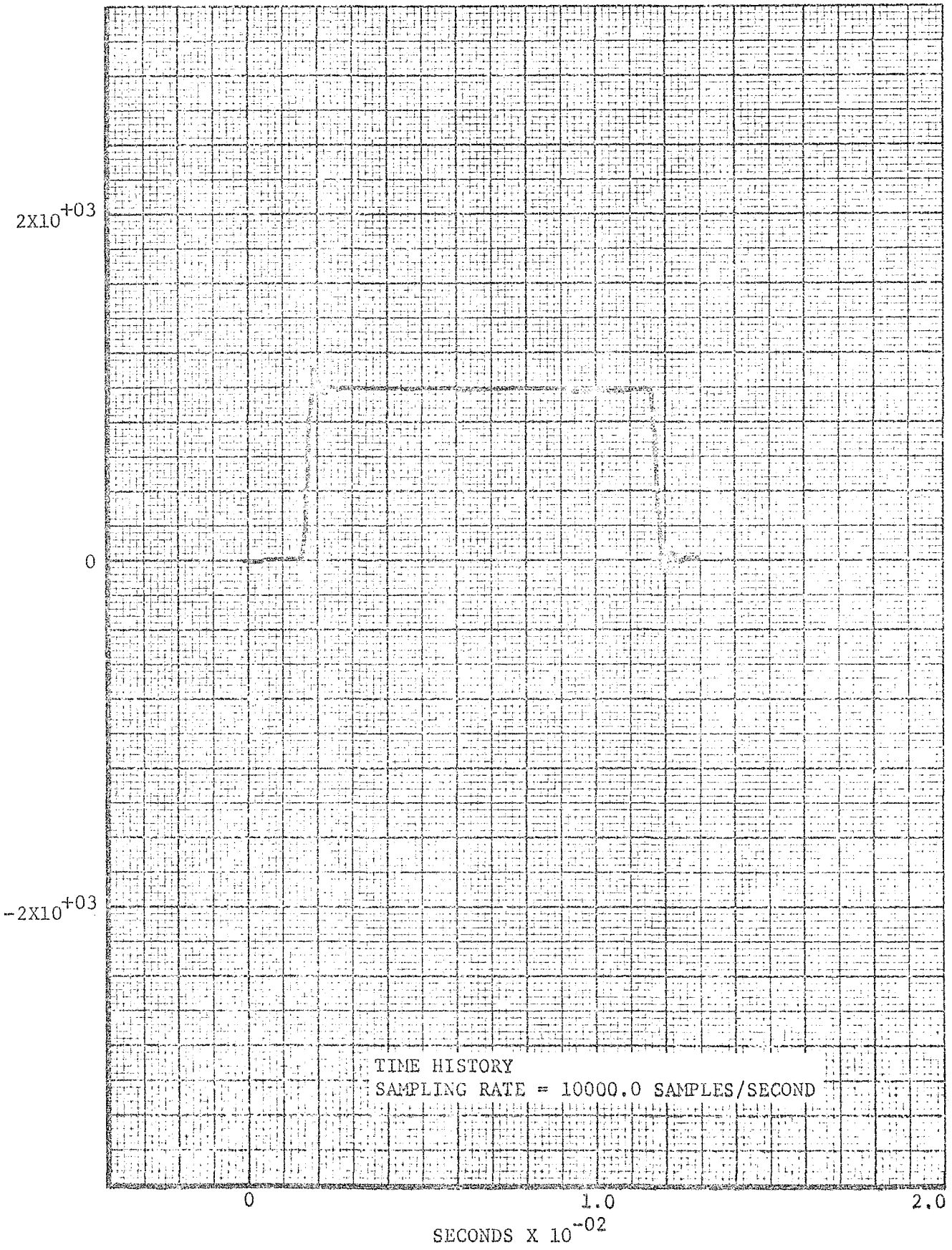



Figure 72: FILTERED SQUARE WAVE TIME HISTORY

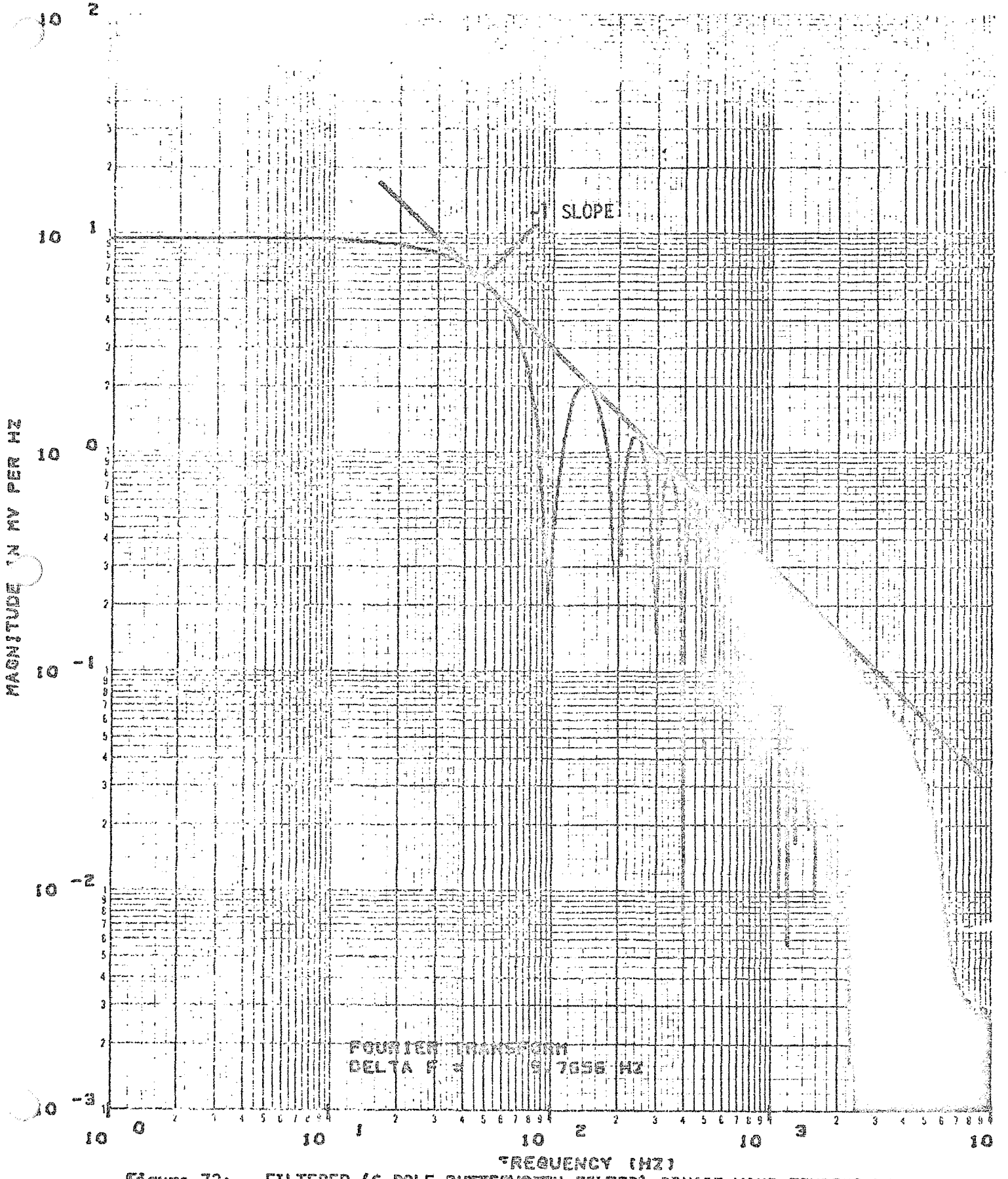



Figure 73: FILTERED (6-POLE BUTTERWORTH FILTER) SQUARE WAVE FOURIER SPECTRUM

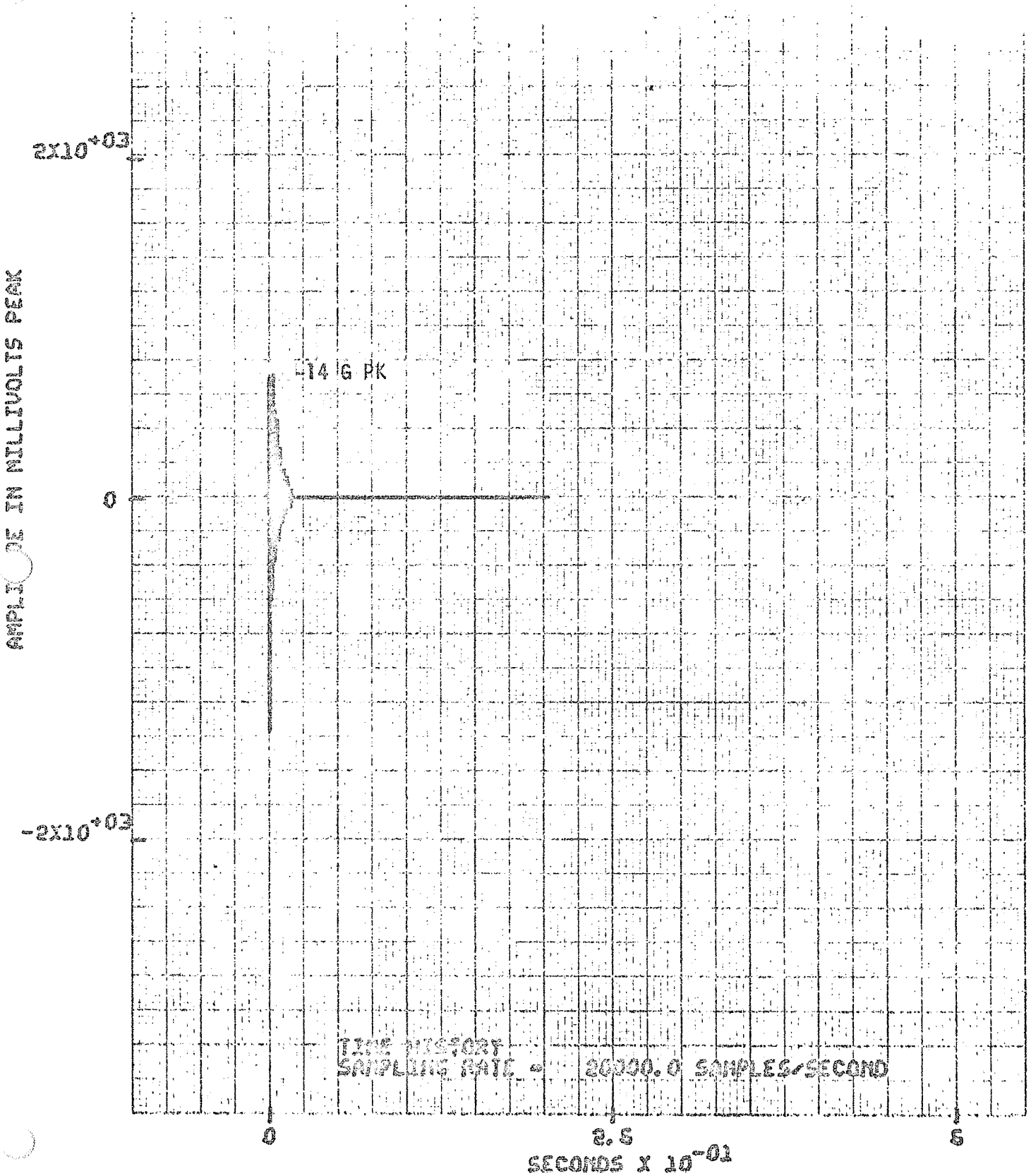



Figure 74: TRANSIENT CALIBRATION OUTPUT f(t)o TRUNCATED $\tau$=350 DATA POINTS, 3,746 ZERO DATA POINTS

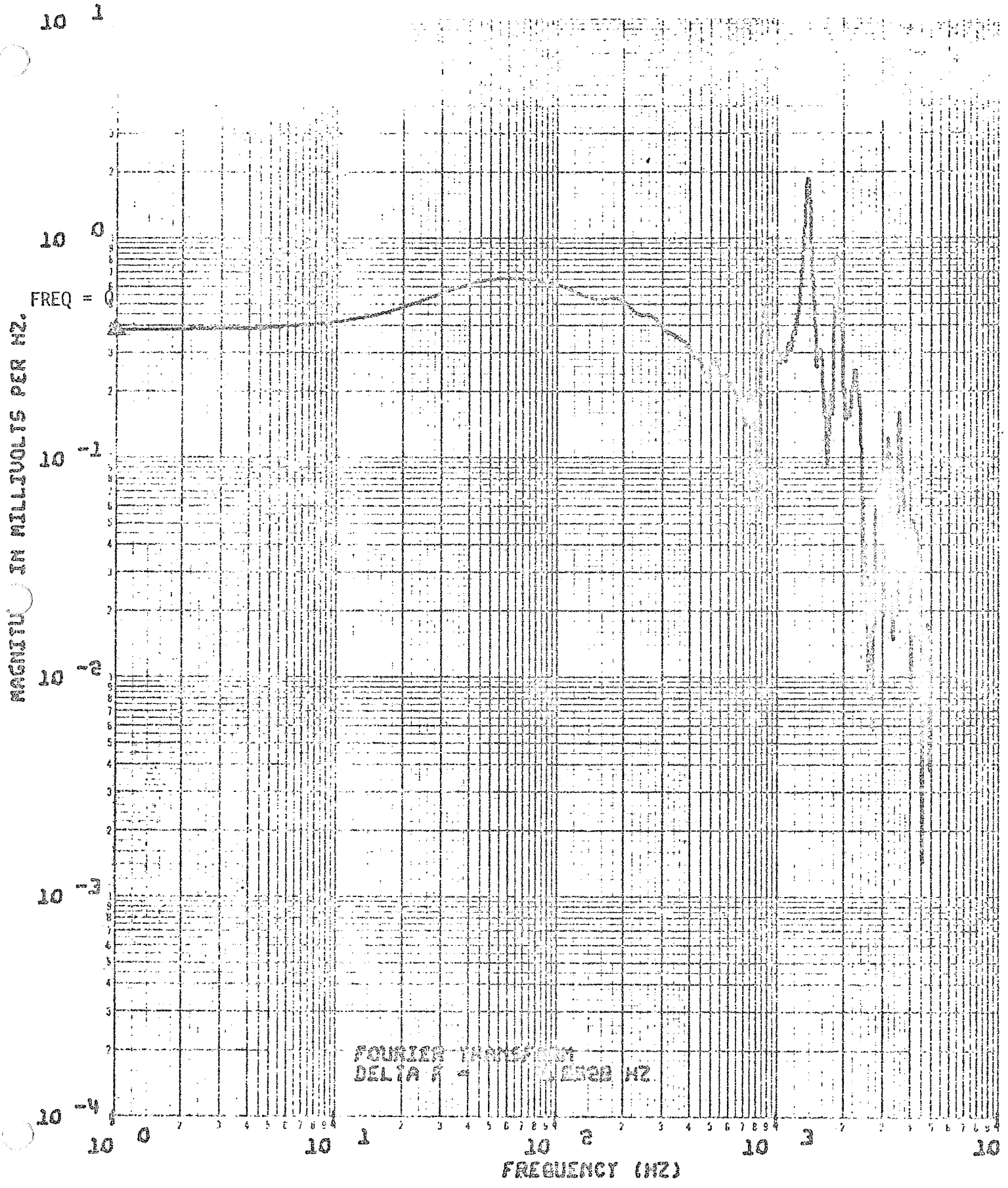



Figure 75: TRANSIENT CALIBRATION OUTPUT f(t)o TRUNCATED $\tau$ = 350 DATA POINTS

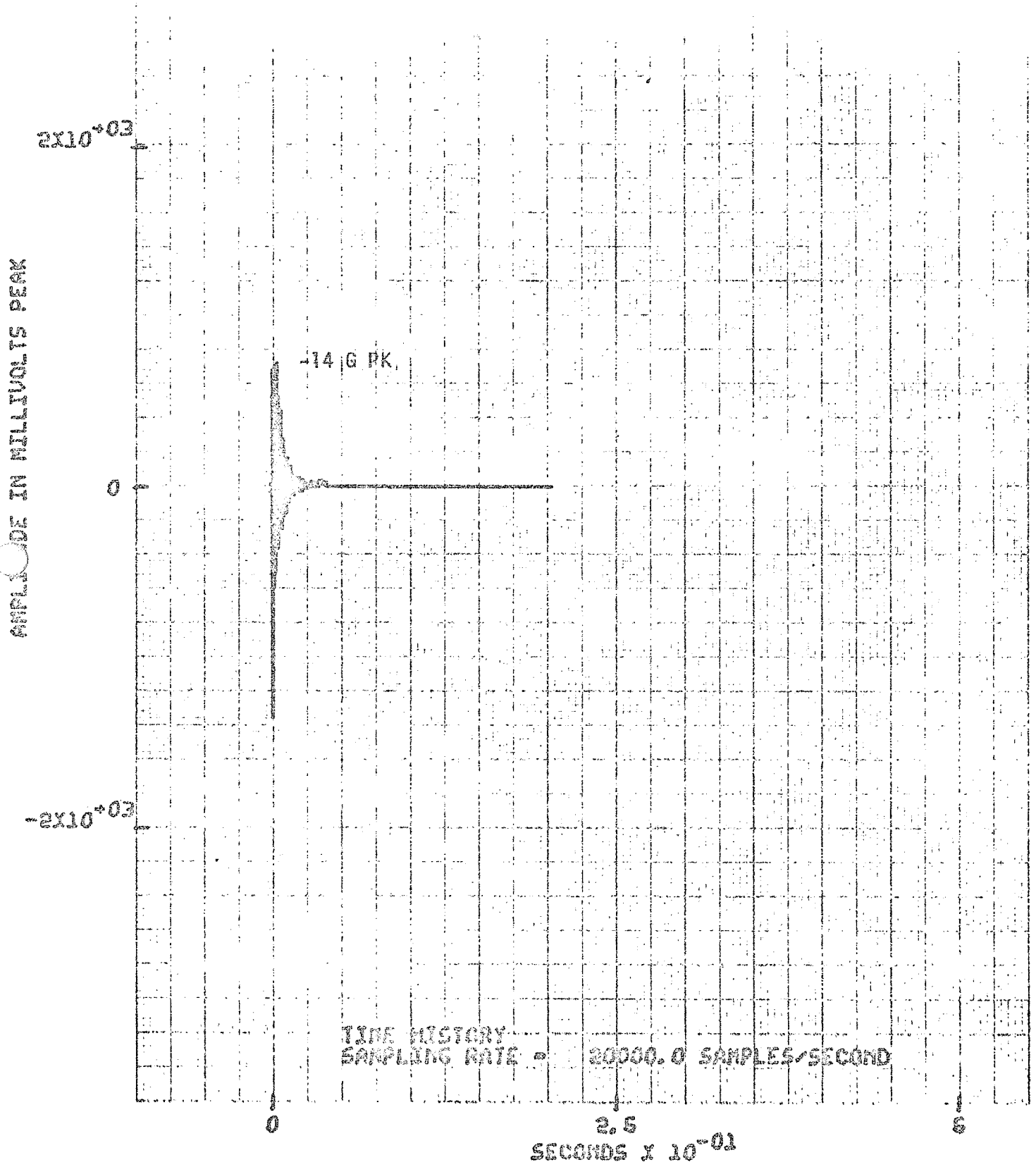



Figure 76: TRANSIENT CALIBRATION OUTPUT f(t)o TRUNCATED $\tau$ = 800 DATA POINTS, 3296 ZERO DATA POINTS

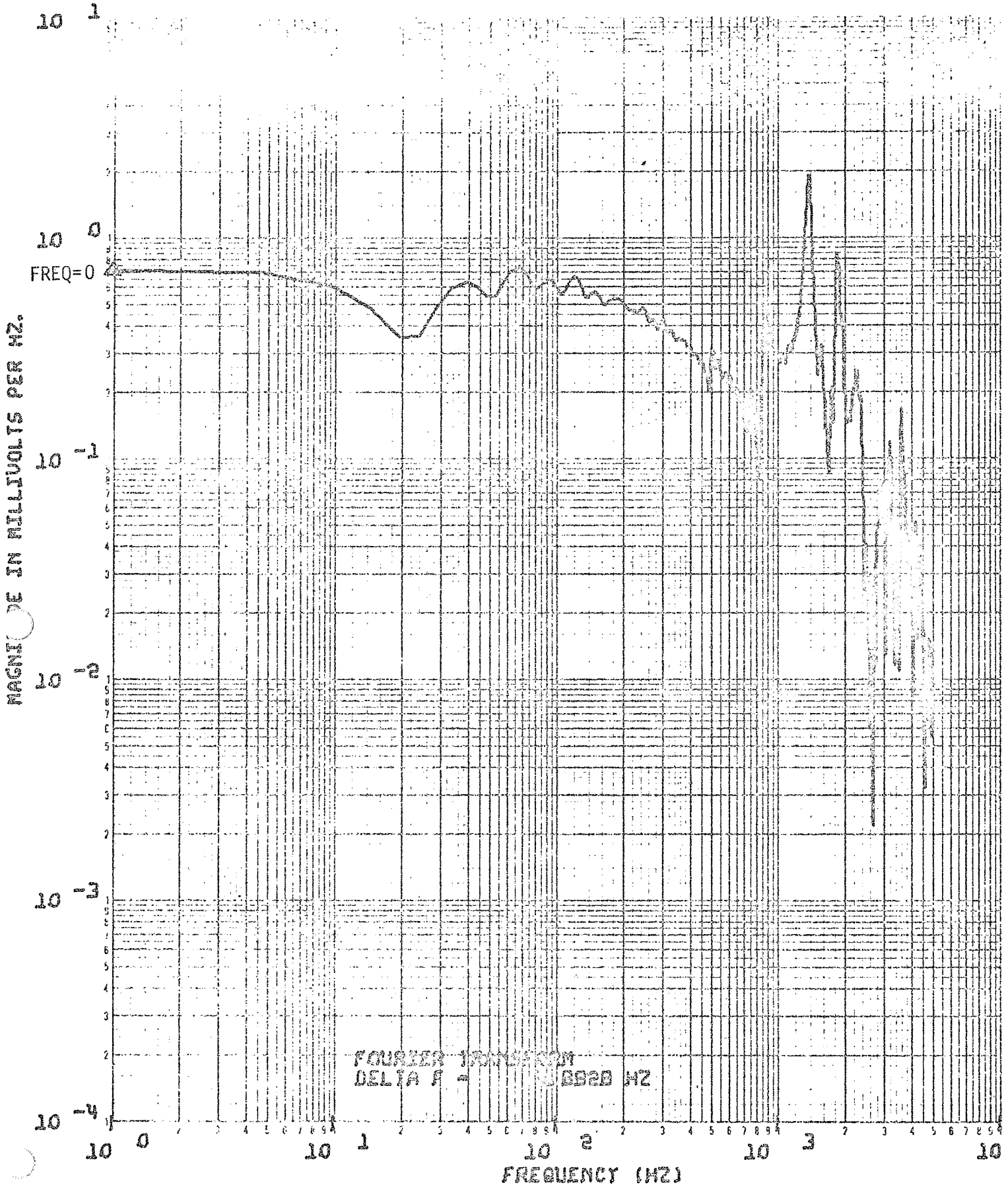



FIGURE 77: TRANSIENT CALIBRATION OUTPUT f(t)o TRUNCATED T=800 DATA POINTS

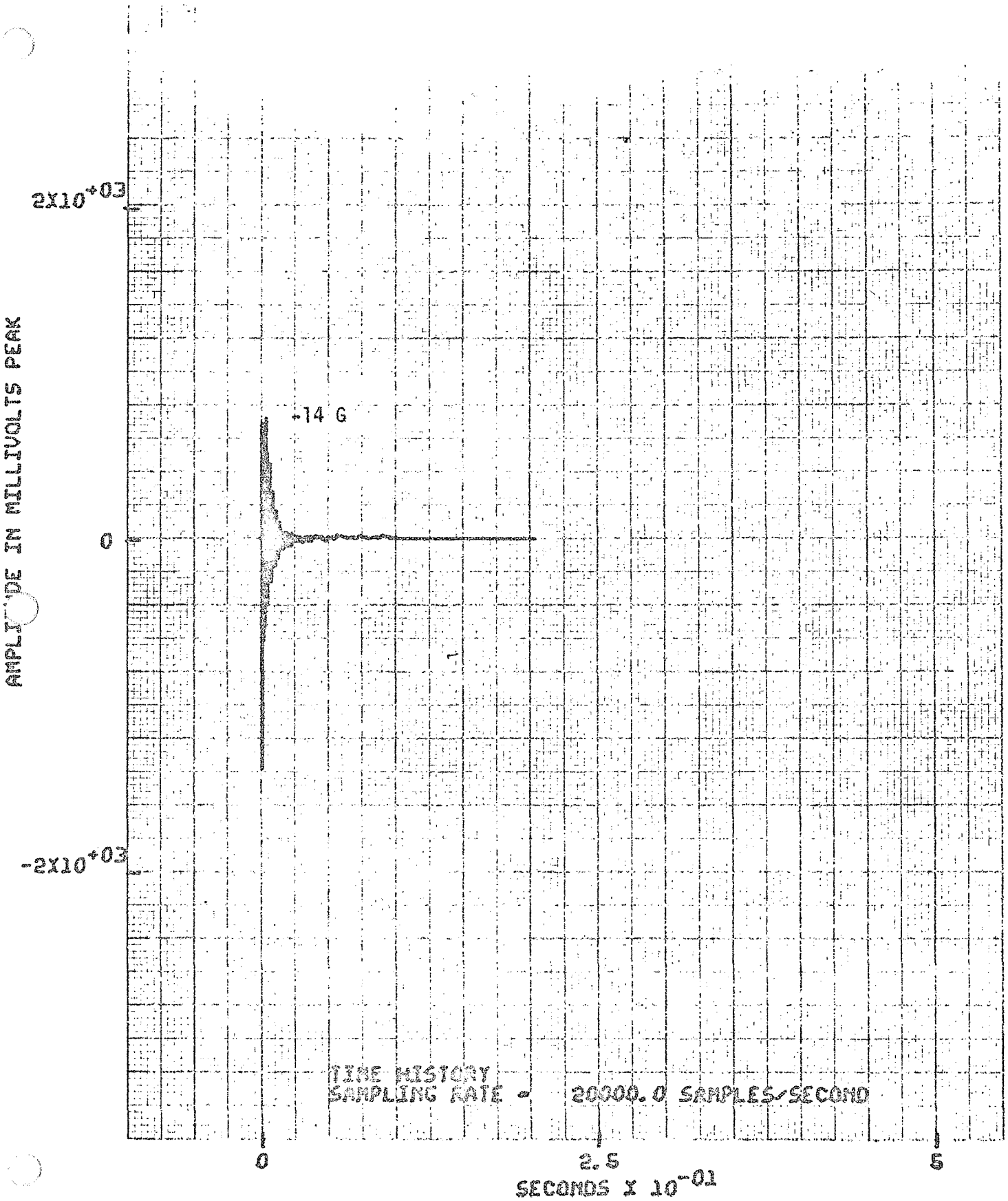



Figure 78: TRANSIENT CALIBRATION OUTPUT f(t)o TRUNCATED T = 2048 DATA POINTS, 2048 ZERO DATA POINTS

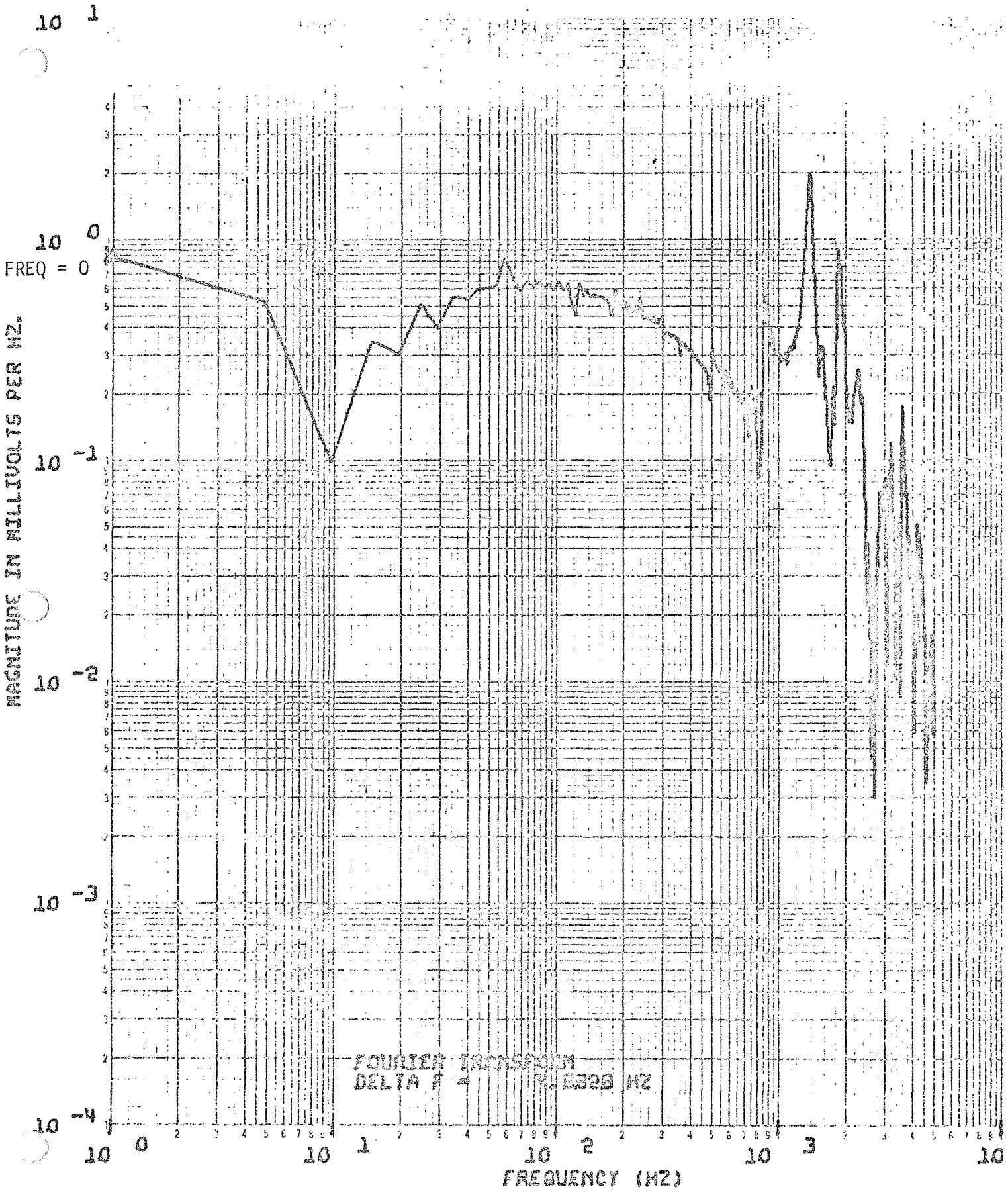



Figure 79: TRANSIENT CALIBRATION OUTPUT f(t)o TRUNCATED $\tau$ = 2,048 DATA POINTS

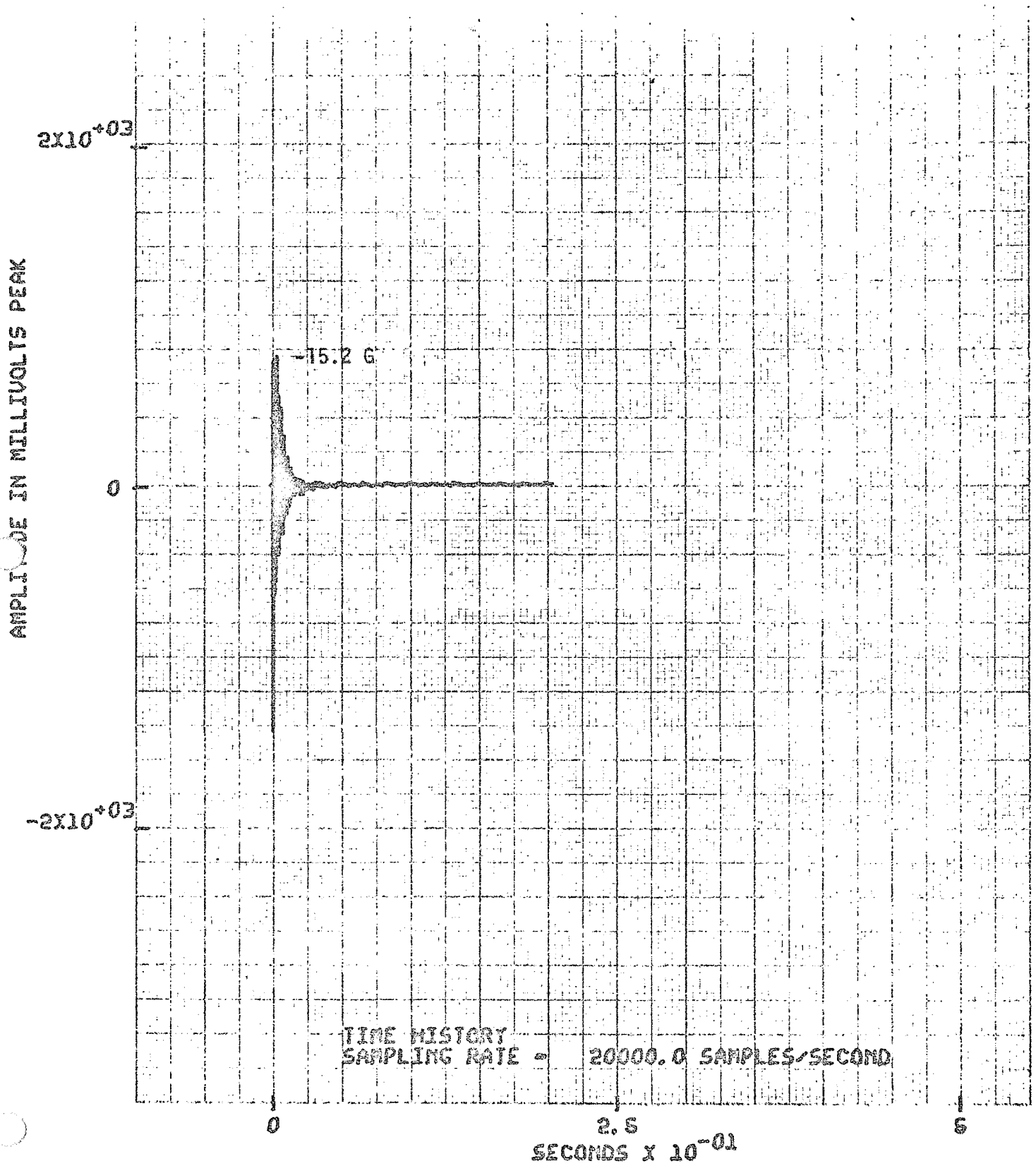



Figure 80: TRANSIENT CALIBRATION OUTPUT f(t)o TRUNCATED $\tau$ = 4,096 DATA POINTS, NO ZERO DATA POINTS

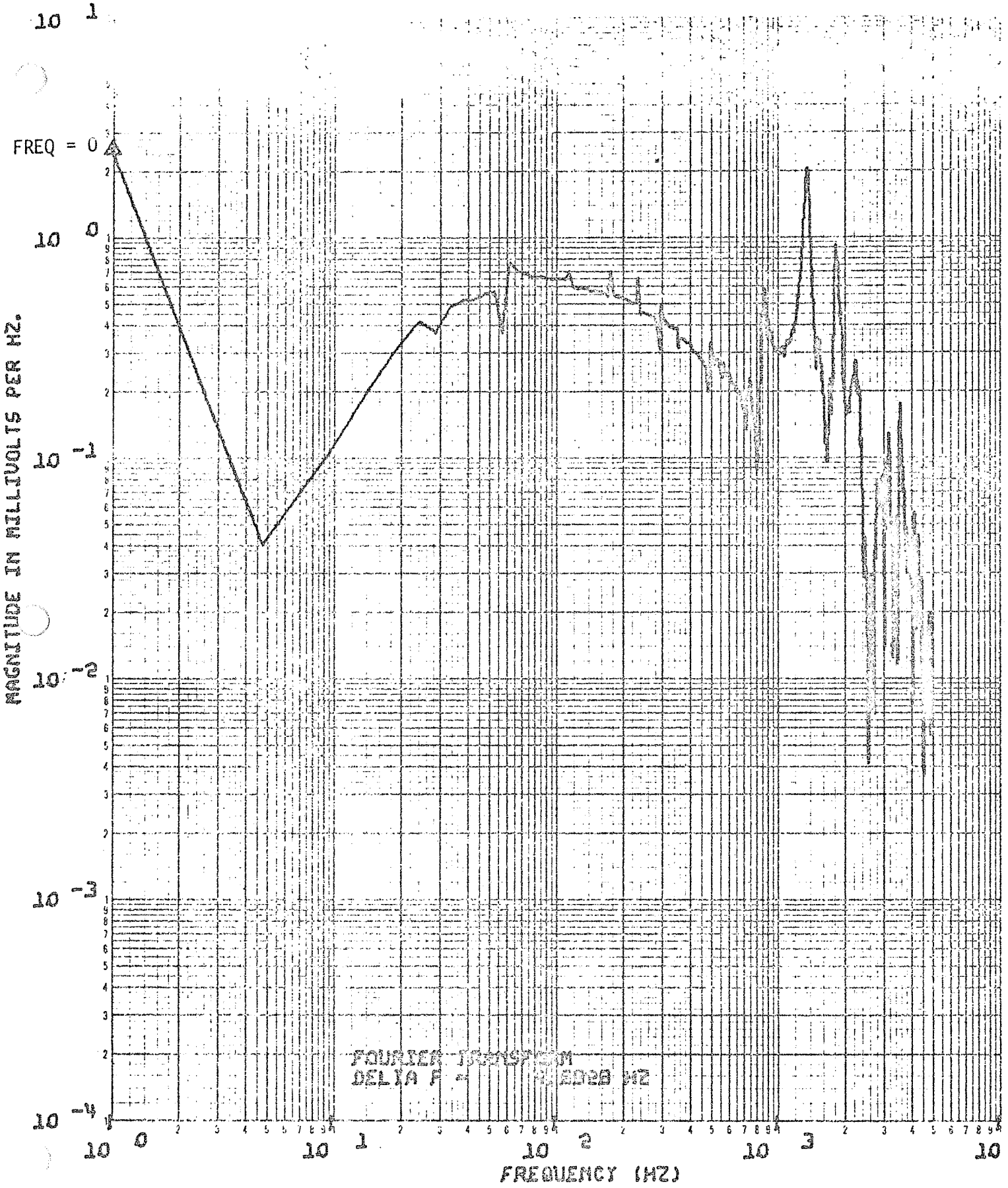



Figure 81 TRANSIENT CALIBRATION OUTPUT f(t)o TRUNCATED T = 4,096 DATA POINTS

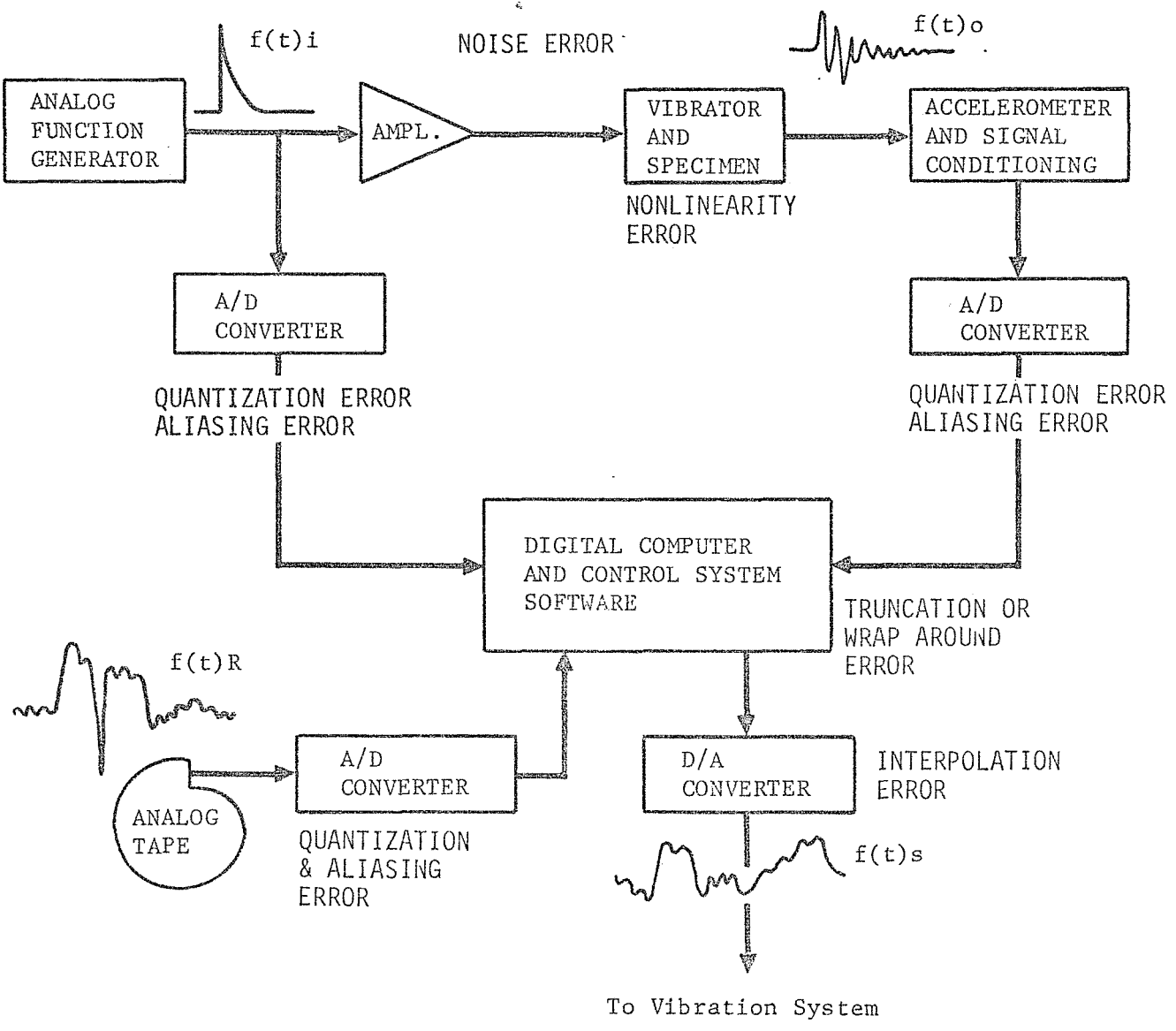



Figure 82: ERROR MODEL OF CONTROL SYSTEM

## Equipment Limitations

The use of an electrodynamic vibrator for transient waveform control [9] [10] [11] is subject to limitations imposed by: (1) the mechanical configuration of the shaker; (2) the capability of the driving power amplifier; and (3) the nature of the transient waveform to be synthesized.

To avoid damaging the armature of the shaker, the velocity at the end of the total transient acceleration must be zero. Because of this requirement, it may be necessary to add an acceleration transient of the opposite polarity to that of the original pulse. An application of this requirement (Figure 2) shows a rectangular shaped deceleration transient (within the specification tolerance) added to meet this requirement.

The total displacement of the armature must be within the displacement limitation of the vibrator. The peak acceleration of the transient waveform must not exceed the acceleration limit of the vibrator armature. The experimentation with the prototype control system operated within these conditions. It is feasible that either electrical or mechanical biasing of the armature be used to alter the vibrator's stated deflection limitations. Another possibility is to design the required transient waveform with a very-long acceleration pulse of low magnitude before the required transient waveform, $f(t)_R$, to mechanically bias the armature. The actual armature deflection available can always be related to specimen/fixture weight and the specified spring rate of the armature flexures.

The limitations imposed by the power amplifier are as follows.

1) The design of the high voltage power supply determines the maximum time duration available for the transient waveform.

2) The frequency response of the amplifier determines the vibrator's ability to reproduce complex high frequency content waveforms.

3) The force capability is limited by the current capability of the amplifier.

4) The final output tube plate voltage swing limits armature velocity.

5) The transformer coupling characteristics limit the low frequency capability (illustrations of low-frequency limitations are contained in Appendix II).

There is a general reluctance of equipment manufacturers to specify the transient capability of their vibration test systems.

The transient rating problem relates to the specific test system and its load. Recognizing the load (i.e., vibrator armature, fixture, and specimen) cannot be considered as purely resistive since both resonances and antiresonances influence the power requirement. Future procurement specifications for laboratory equipment, dedicated to transient testing, should be subject to the following considerations.

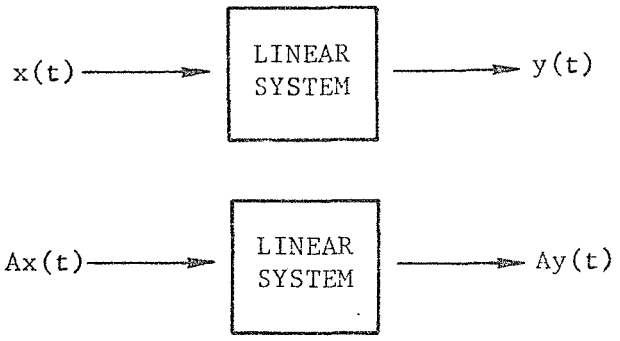
1) The design of the power amplifier must be capable of driving the final output tube plate load to maximum current or maximum voltage under vibrator load conditions without grid clipping or saturation of the preamplification stages.

2) The design of the amplifier/vibrator coupling transformers must accomodate a specified low frequency criteria.

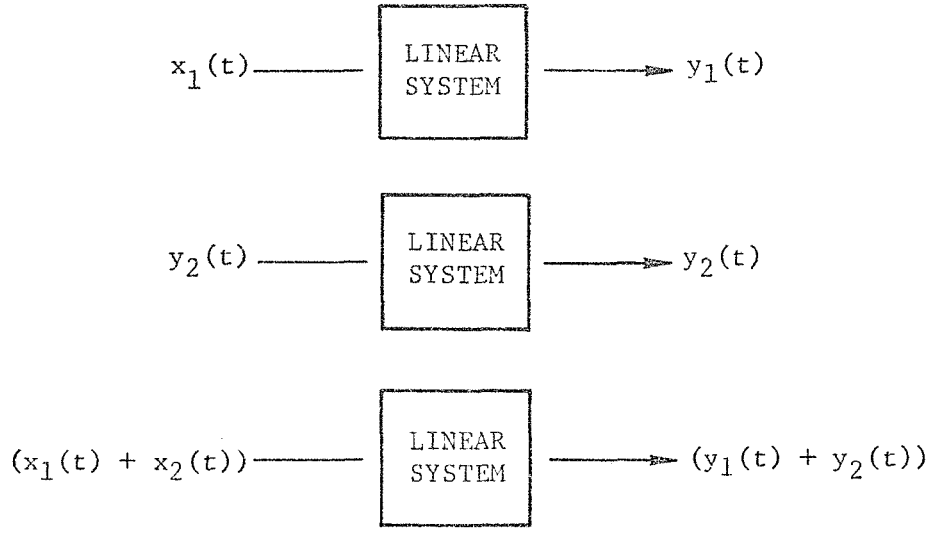
One ancillary step in the laboratory synthesis of any waveform is obtaining knowledge of its acceleration, velocity, and deflection characteristics if they are not specified. The capability defined in the conceptual design, as a result of this study, could readily integrate the required waveform, $f(t)_R$, to provide these parameters.

## Nonlinearities

Background.-The concept of transient waveform control, as defined in this report, is based on the theory of linear systems. A linear system is defined by the following two properties: the first property is proportional response. Thus, if an input signal, x(t), results in an output signal, y(t), when applied to a system, then multiplication of the input signal by a constant "A" results in a proportionate change in output.




The second property is superposition. Thus, if two separate input signals $x_1(t)$ and $x_2(t)$, are first applied to the system separately and result in separate outputs, $y_1(t)$ and $y_2(t)$, then, if the two inputs are summed, $(x_1(t) + x_2(t))$, and applied to the system, the output will be the sum of the separate outputs.




Further, if a pure sign wave is applied to the input of a linear system, then a pure sine wave will appear at the output. Any distortion in the output wave is an indication of system nonlinearity. In the real world of engineering, systems only approximate the quality of linearity and that introduces the following question. "Are the existing vibration test systems located in Environmental Testing Laboratories sufficiently linear to make transient waveform control feasible?" To answer that question, the following procedure was followed.

Procedure.-As a part of the equipment familiarization section of this study, NASA Goddard supplied certain raw data on the performance characteristics of their electromagnetic and hydraulic shakers. This data was reduced to define the linearity of the shaker systems. The nonlinearity of the L.P.S. (hydraulic) shaker was defined[10] as the magnitude difference between the output motion and an expected sine wave output motion. This was developed from the 8 Hz sine dwell data. The acceleration waveform was double-integrated to provide velocity and displacement waveforms, and therefore similar nonlinearity data. The nonlinearity of the electromagnetic shakers [11] was defined by plotting the normalized magnitudes of the respective input and output sine waves at 50 Hz and up to 20 g rms acceleration against each other. A linear system would yield a straight line, at a slope of 1.0, from this data. Since Boeing has successfully performed transient waveform control on its Ling 249/Ling PP-120/150 shaker-amplifier combination, its linearity was similarly defined for comparison. Distortion measurements were also made on NASA Goddard equipment and in Appendix II compared to Boeing's Ling 249/Ling PP-120/150 system.

Since the Transient Waveform Control System technique relies upon the computation of an accurate system transfer function, the effect of nonlinearities on the transfer function definition was studied. This was done by modifying[12] a known pulse by the defined system nonlinearities; then computing the Fourier transform of the modified data; and then comparing that transform with the theoretical transform of the known pulse.

Figures 83, 85, and 87 represent the acceleration, velocity, and displacement nonlinearity functions of the L.P.S. hydraulic shaker. The modified step-decay pulse used in the Fourier transform error study (Figure 11) was modified by each of these nonlinearities and then Fourier transformed. Figures 84, 86, and 88 show the resulting transforms. A visual comparison of the transform (Figure 84) with the theoretical transform (Figure 12) shows the vast errors generated by these nonlinearities.

Based upon the above cursory study, it is concluded that transient waveform control is not feasible on the L.P.S. hydraulic shaker in its present condition.

Figures 89, 91, and 93 represent the acceleration nonlinearity functions of the MB C210/MB 5140 system (Figure 89); MB C125/MB 996A system (Figure 91) at NASA Goddard; and the Ling 249/Ling PP120/150 system (Figure 93) at Boeing.

---

[10] This procedure was used since the distortion was so large that a conventional technique, harmonic analysis, did not seem reasonable.

[11] MB C210/MB 5140 and MB C125/MB 996A. Only these were analyzed since distortion data indicated similarity with the other systems.

[12] Digital word size, sampling rate, and sampled record length were sufficiently large so as not to introduce significant errors.

The shaker impulse response pulse used in the Fourier transform error study (Figure 20) was modified by each of the above nonlinear functions and then Fourier transformed. Figures 90, 92, and 94 show the resulting transforms. A visual comparison of the transform with the theoretical transform (Figure 21) indicates error generation in the high frequency domain (freq >4kHz). The two NASA Goddard systems exhibited more nonlinear error generation than did the Boeing system. However, since the errors only occur above 4kHz and at relatively low amplitude, their overall effect is not serious. Recognizing the fact that Boeing has successfully performed transient waveform control on its Ling 249/Ling PP120/150 system (Figures 2 and 3), and since the nonlinearities of the NASA Goddard systems have a similar effect, it is concluded that the NASA Goddard electromagnetic systems have adequate linearity to successfully perform transient waveform control.

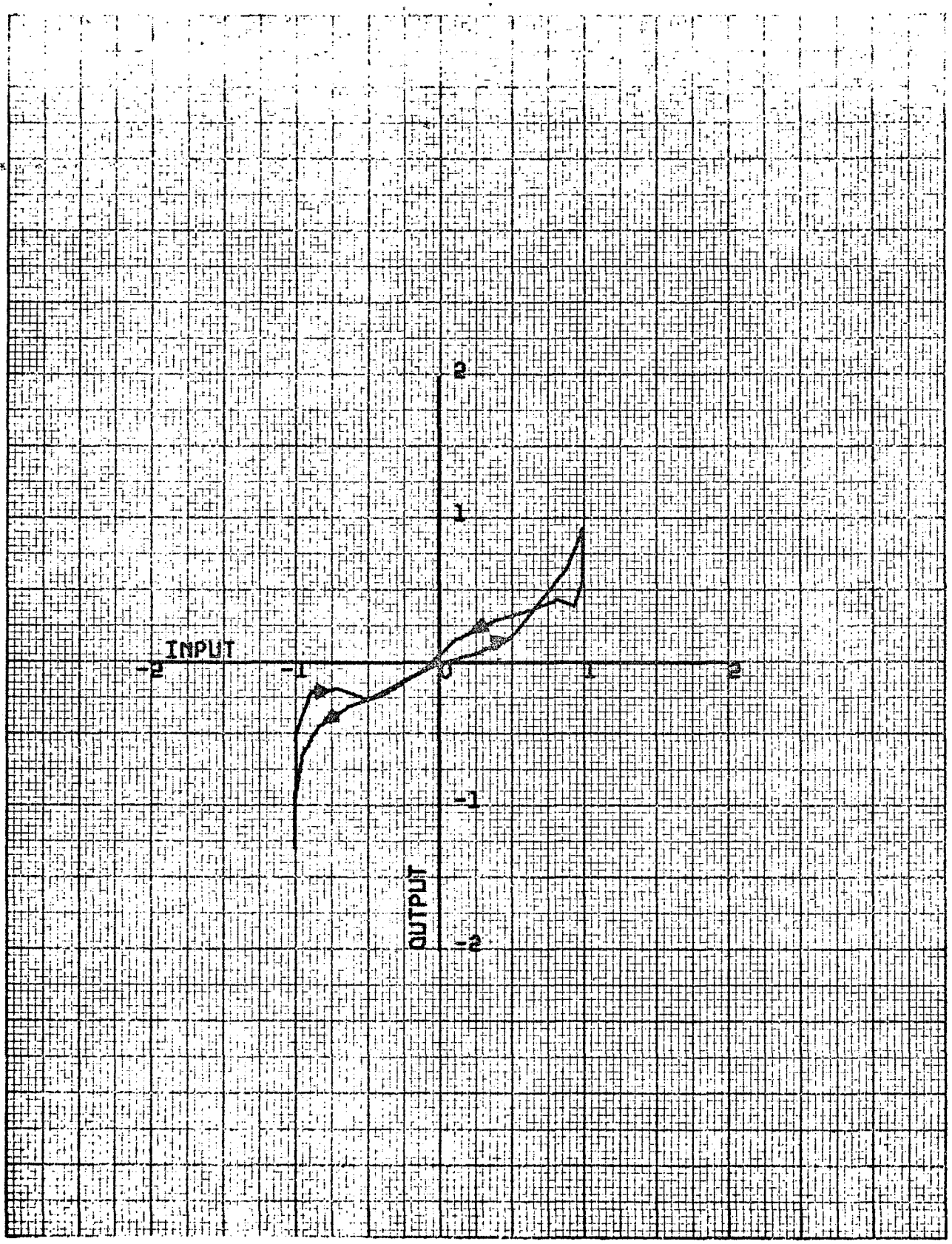



Figure 83: ACCELERATION NONLINEARITY FUNCTION OF THE G.S.F.C.-L.P.S. HYDRAULIC VIBRATOR

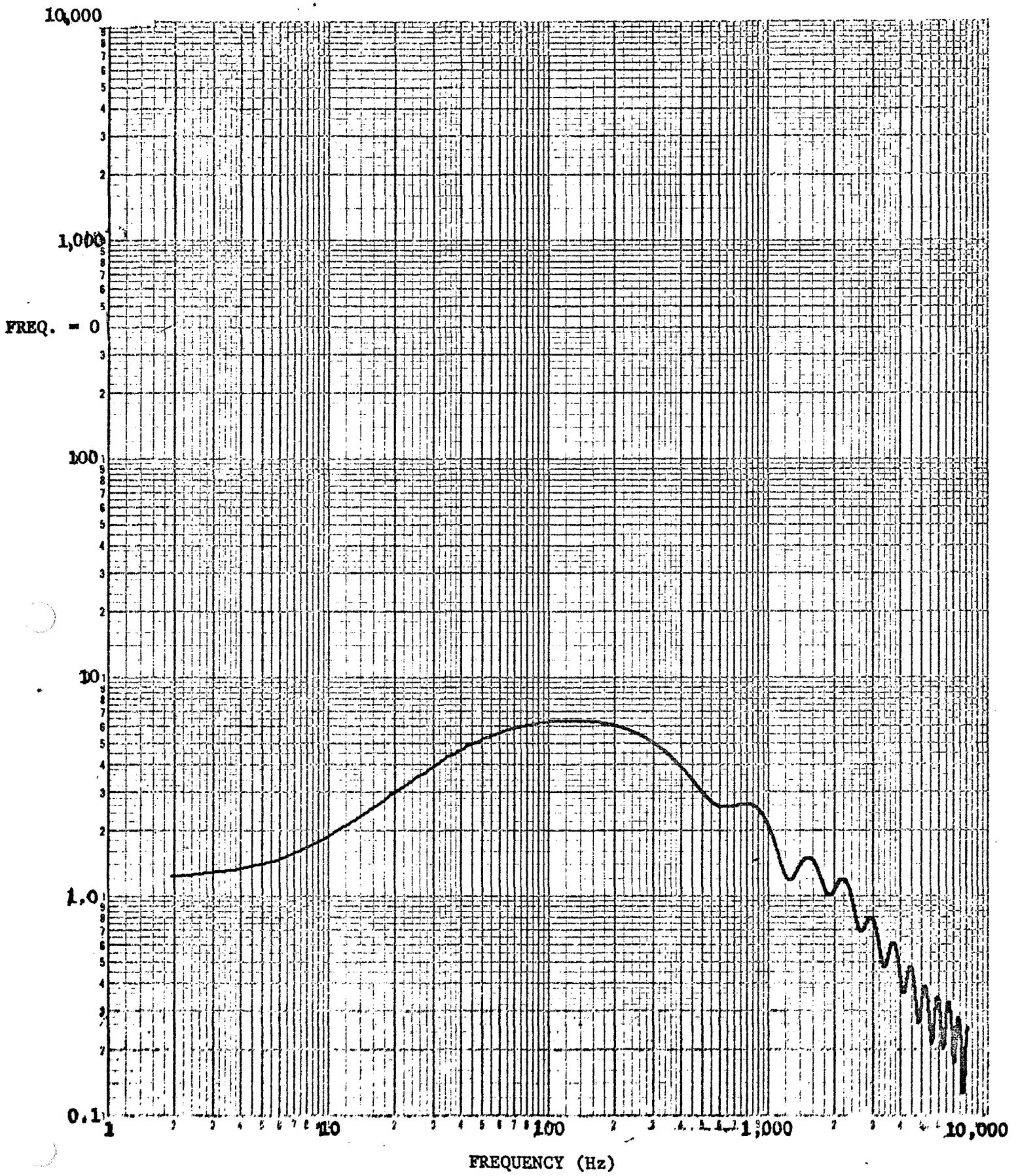



Figure 84: FOURIER TRANSFORM OF THE MODIFIED STEP-DELAY PULSE, MODIFIED BY THE G.S.F.C.-L.P.S. ACCELERATION NONLINEARITY FUNCTION

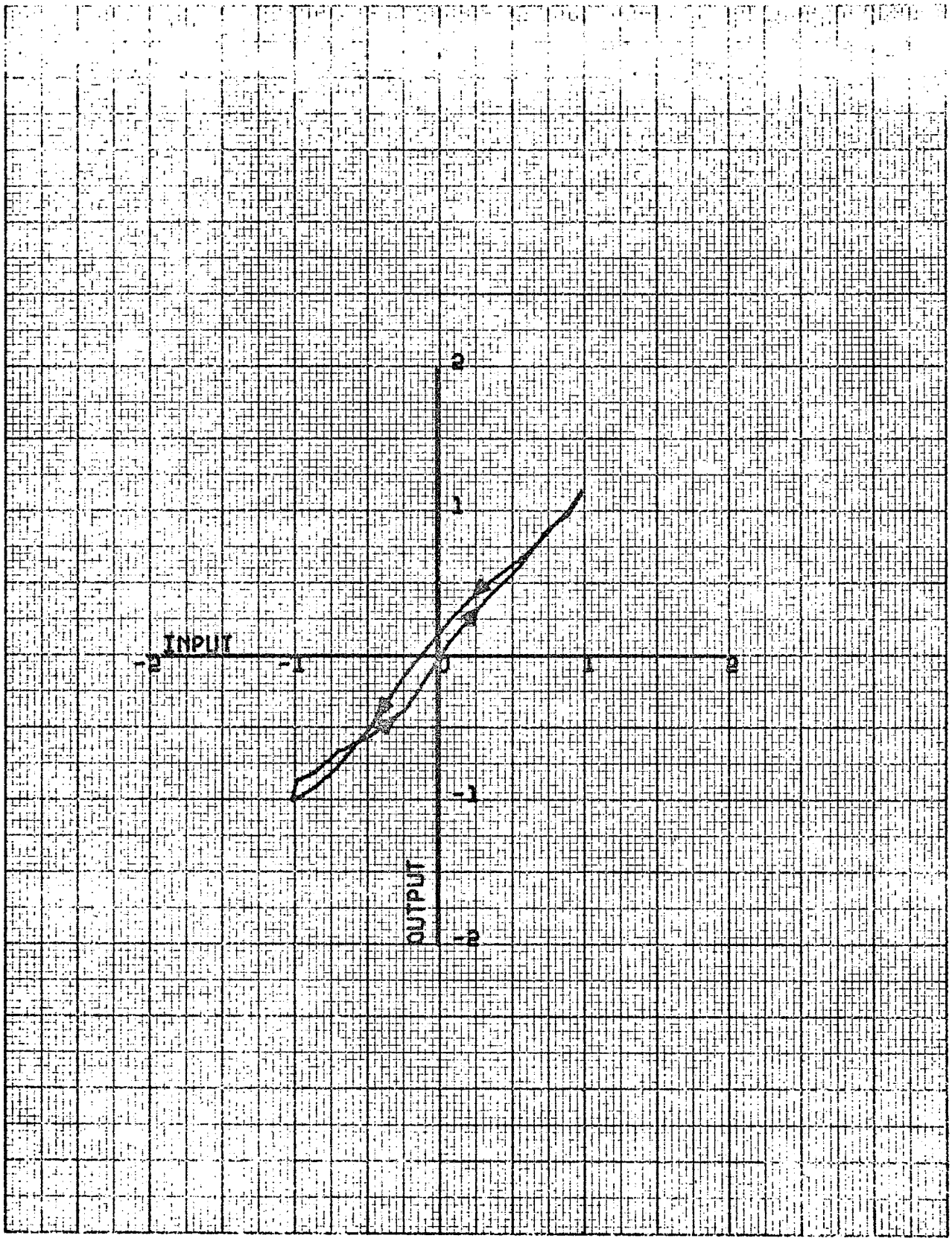



Figure 85: VELOCITY NONLINEARITY FUNCTION OF THE G.S.F.C.-L.P.S. HYDRAULIC VIBRATOR

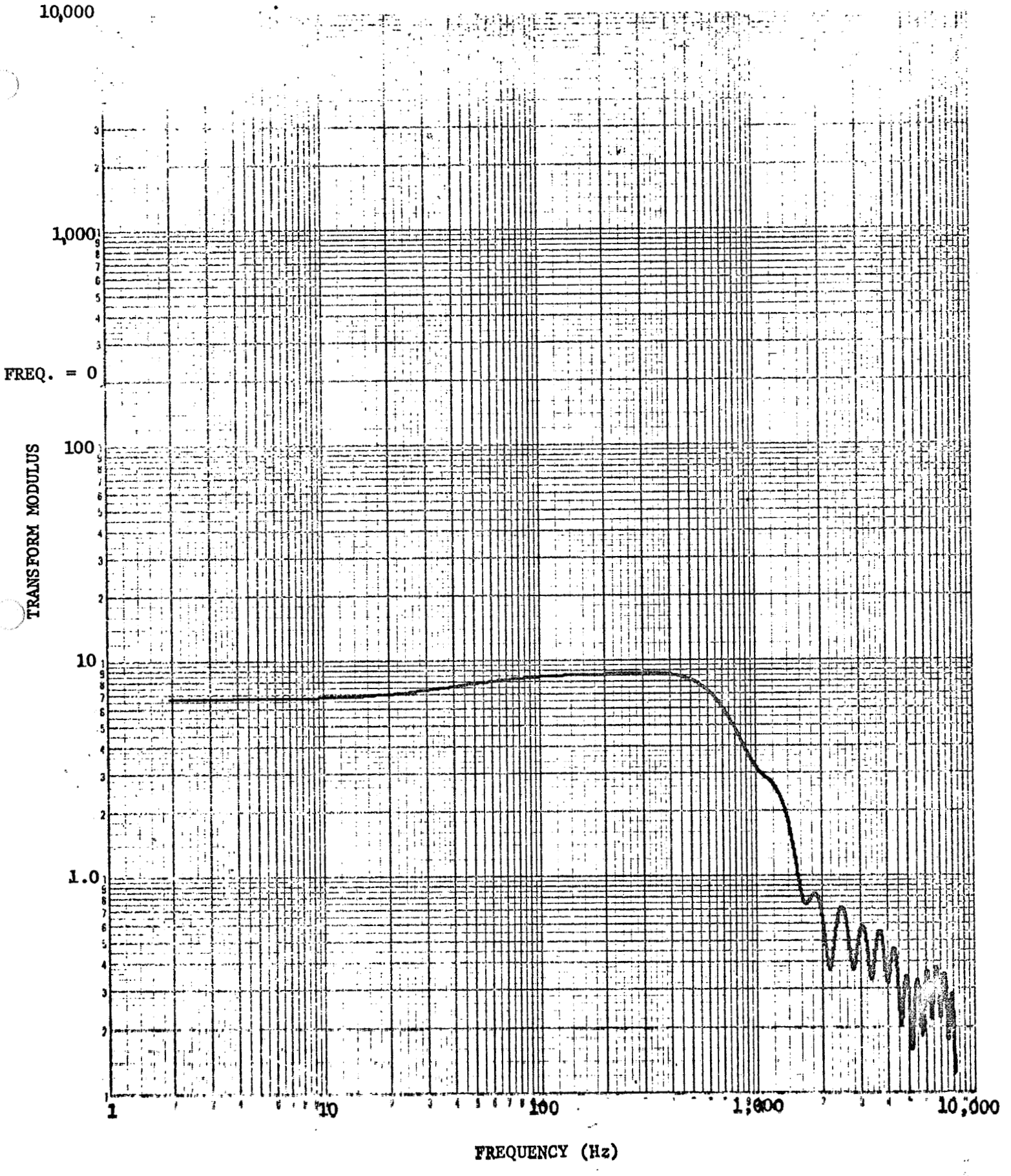



Figure 86: FOURIER TRANSFORM OF THE MODIFIED STEP-DELAY PULSE, MODIFIED BY THE G.S.F.C.-L.P.S. VELOCITY NONLINEARITY FUNCTION

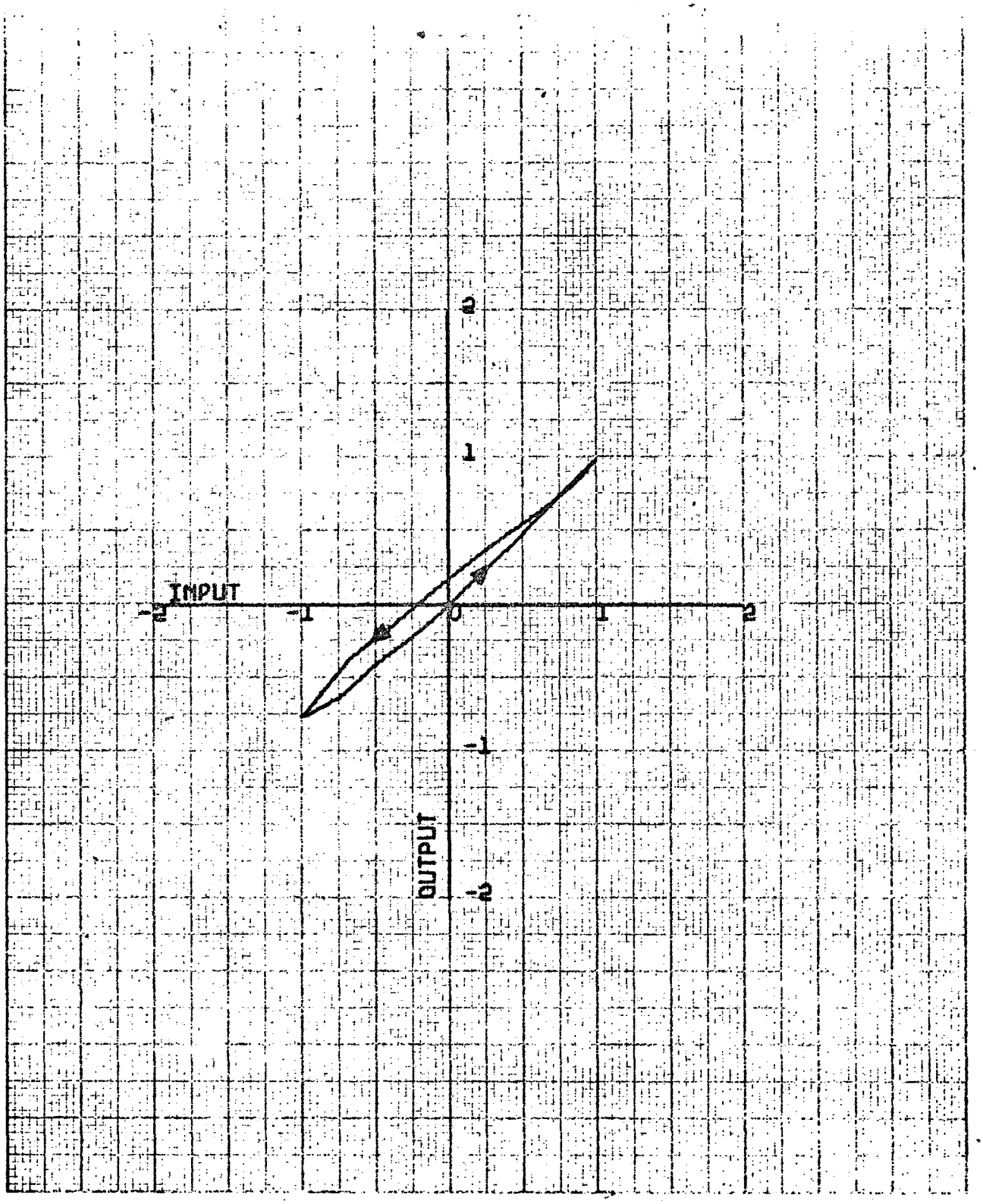



Figure 87: DISPLACEMENT NONLINEARITY FUNCTION OF THE G.S.F.C.-L.P.S. HYDRAULIC VIBRATOR

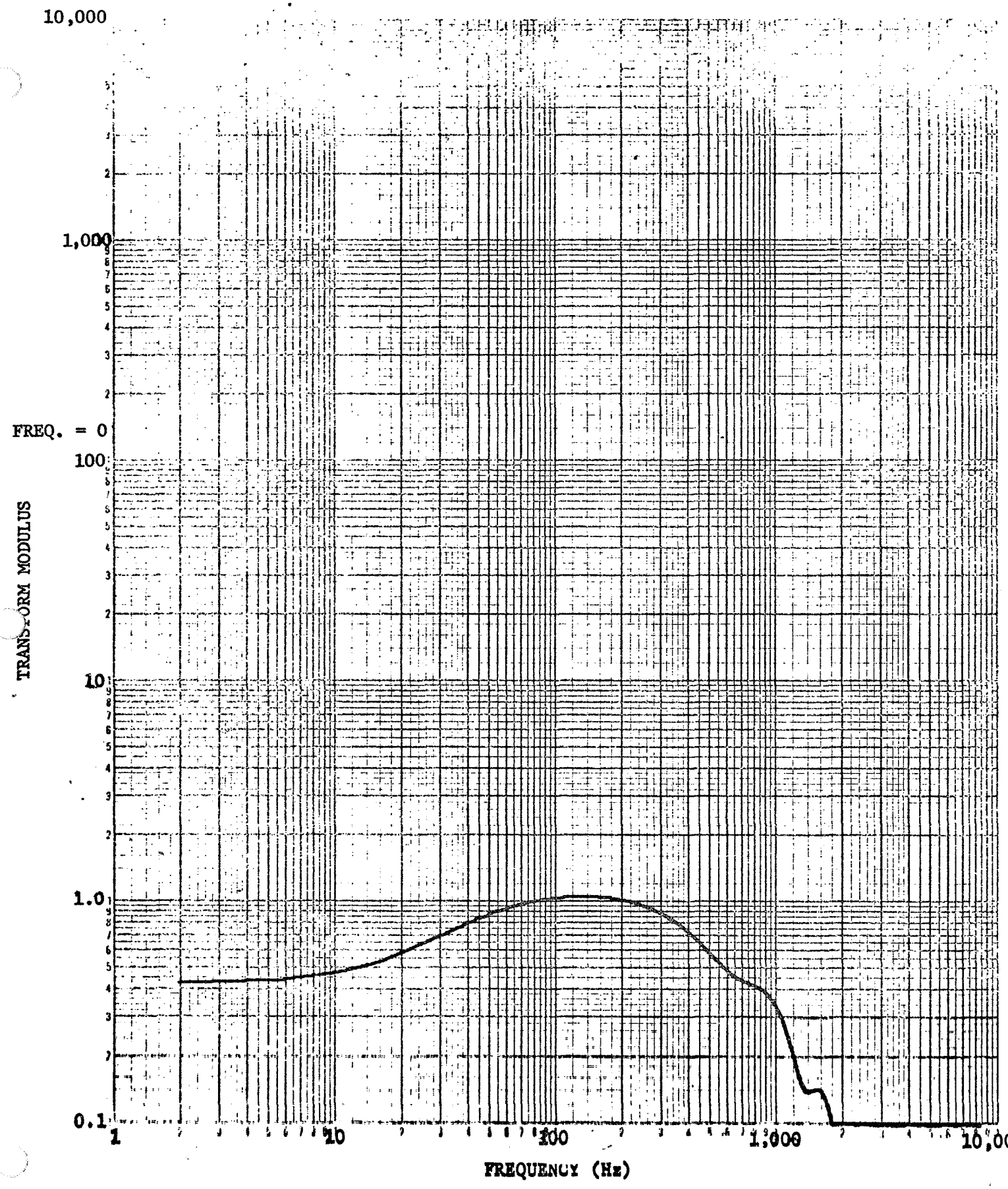



Figure 88: FOURIER TRANSFORM OF THE MODIFIED STEP-DELAY PULSE, MODIFIED BY THE G.S.F.C.-L.P.S. DISPLACEMENT NONLINEARITY FUNCTION

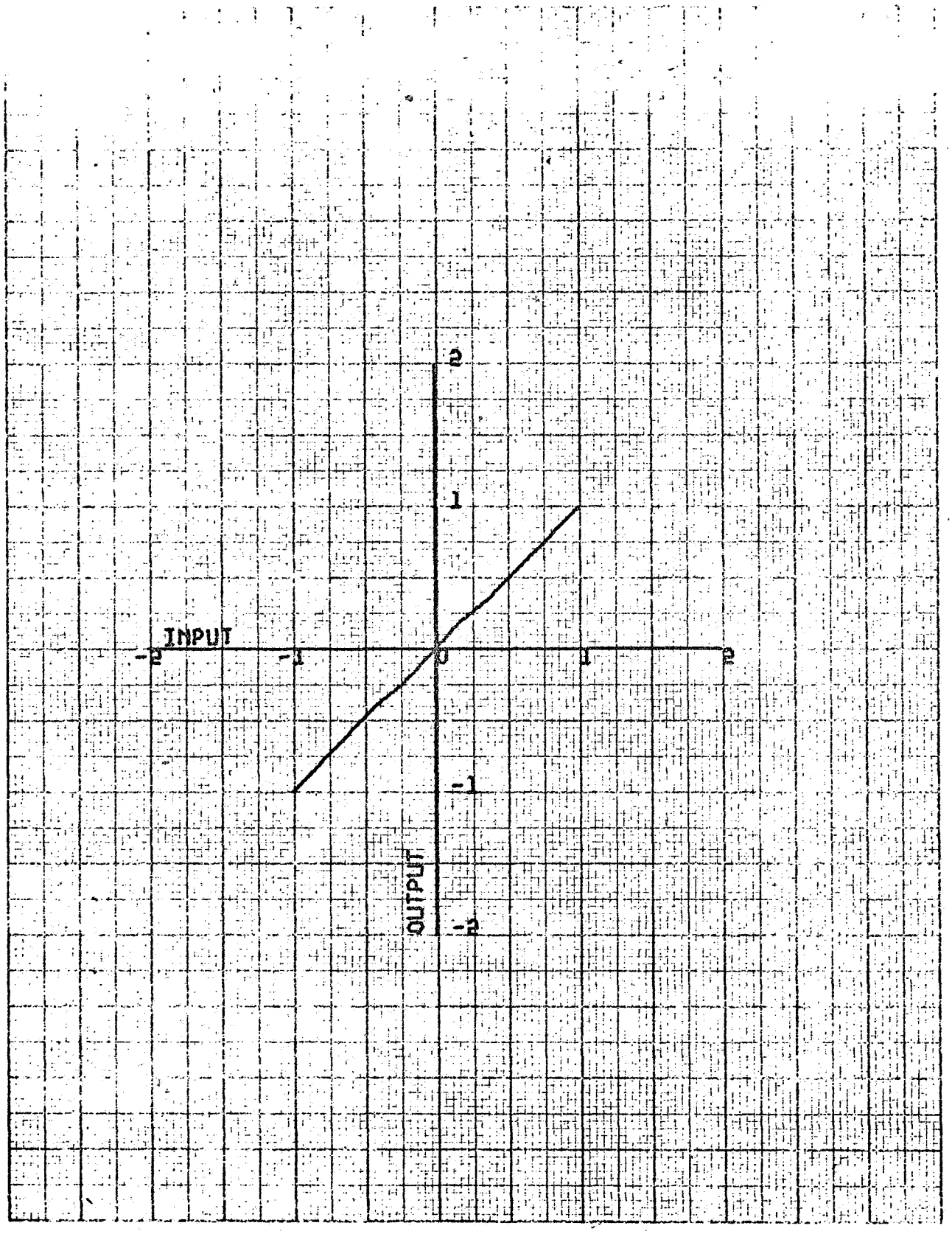



Figure 89: ACCELERATION NONLINEARITY FUNCTION OF THE MBC210/MB5140 SYSTEM (G.S.F.C.)

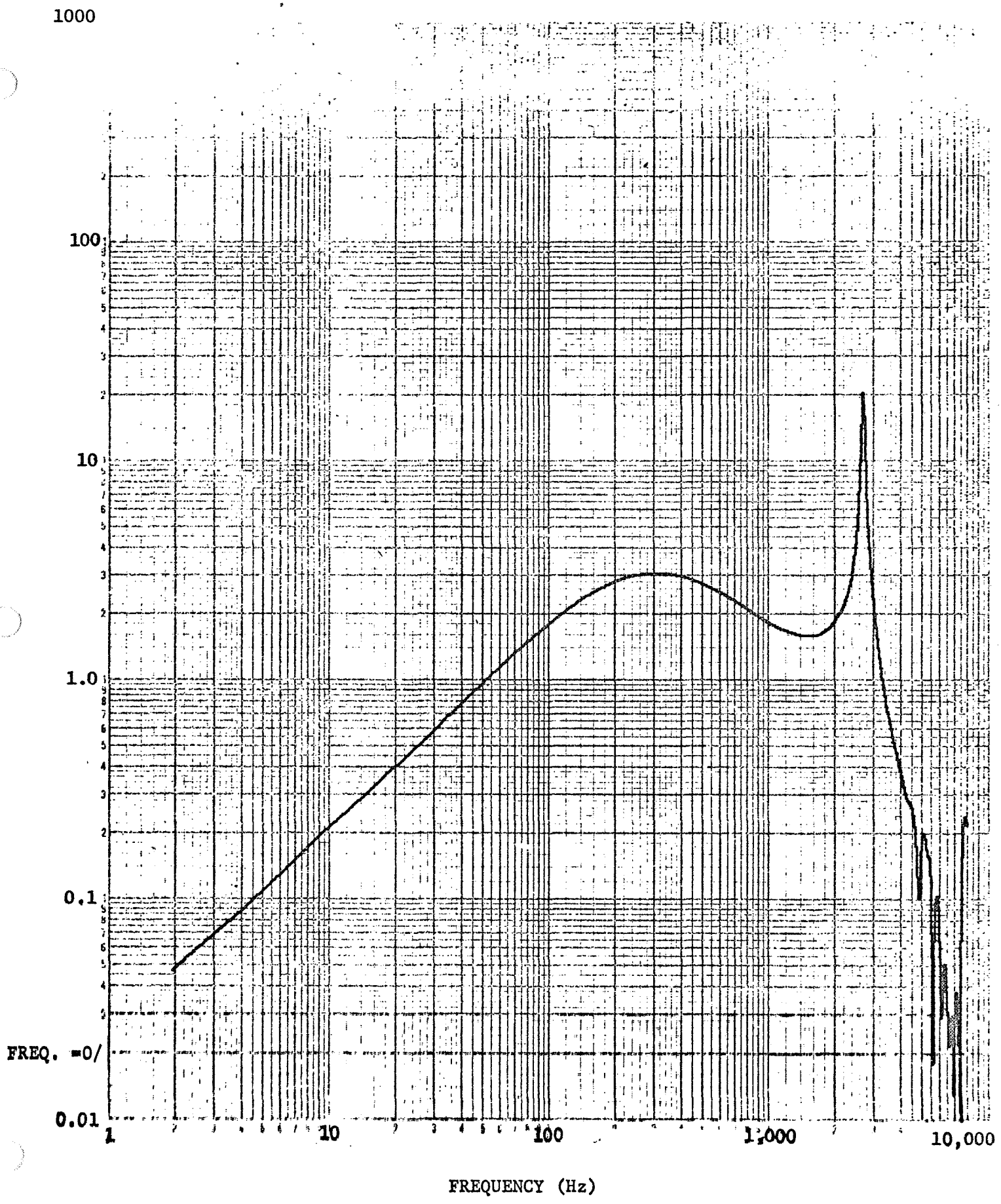



Figure 90: FOURIER TRANSFORM OF THE SHAKER IMPULSE RESPONSE MODIFIED BY THE ACCFLERATION NONLINEARITY FUNCTION OF THE MBC210/MB5140 SYSTEM

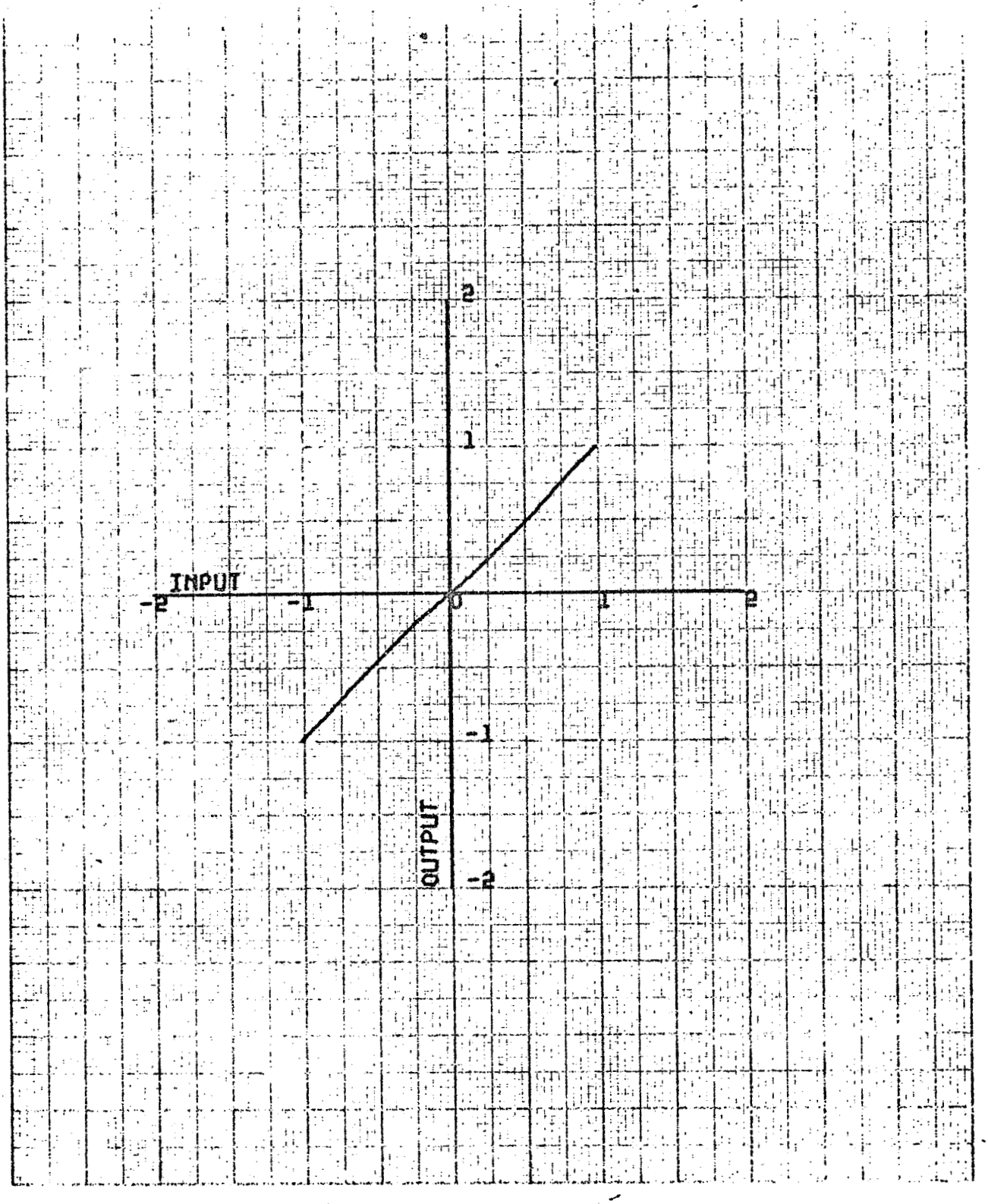



Figure 91: ACCELERATION NONLINEARITY FUNCTION OF THE MBC125/MB996A SYSTEM

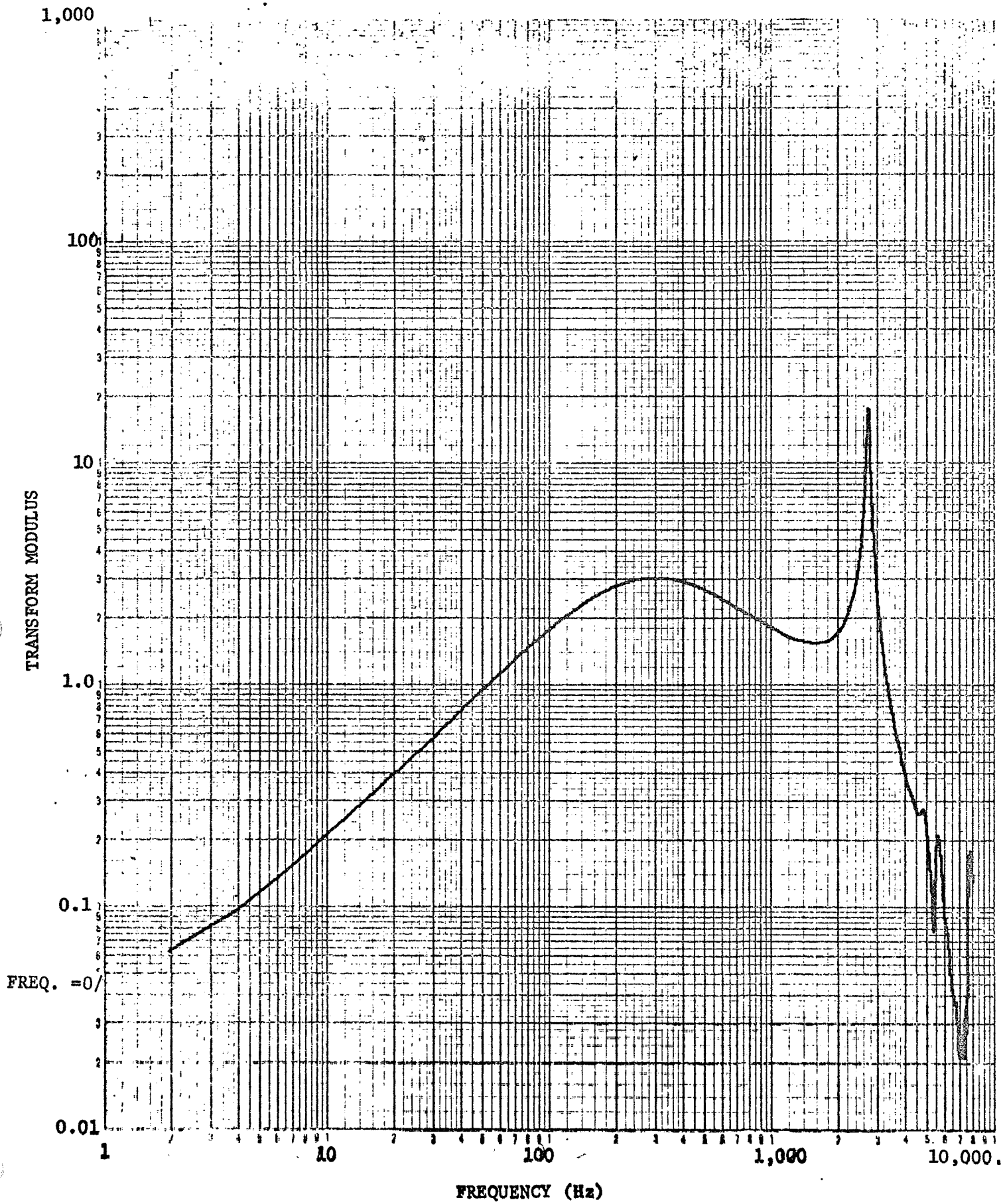



Figure 92: FOURIER TRANSFORM OF THE SHAKER IMPULSE RESPONSE MODIFIED BY THE ACCELERATION NONLINEARITY FUNCTION OF THE MBC125/MB996A SYSTEM

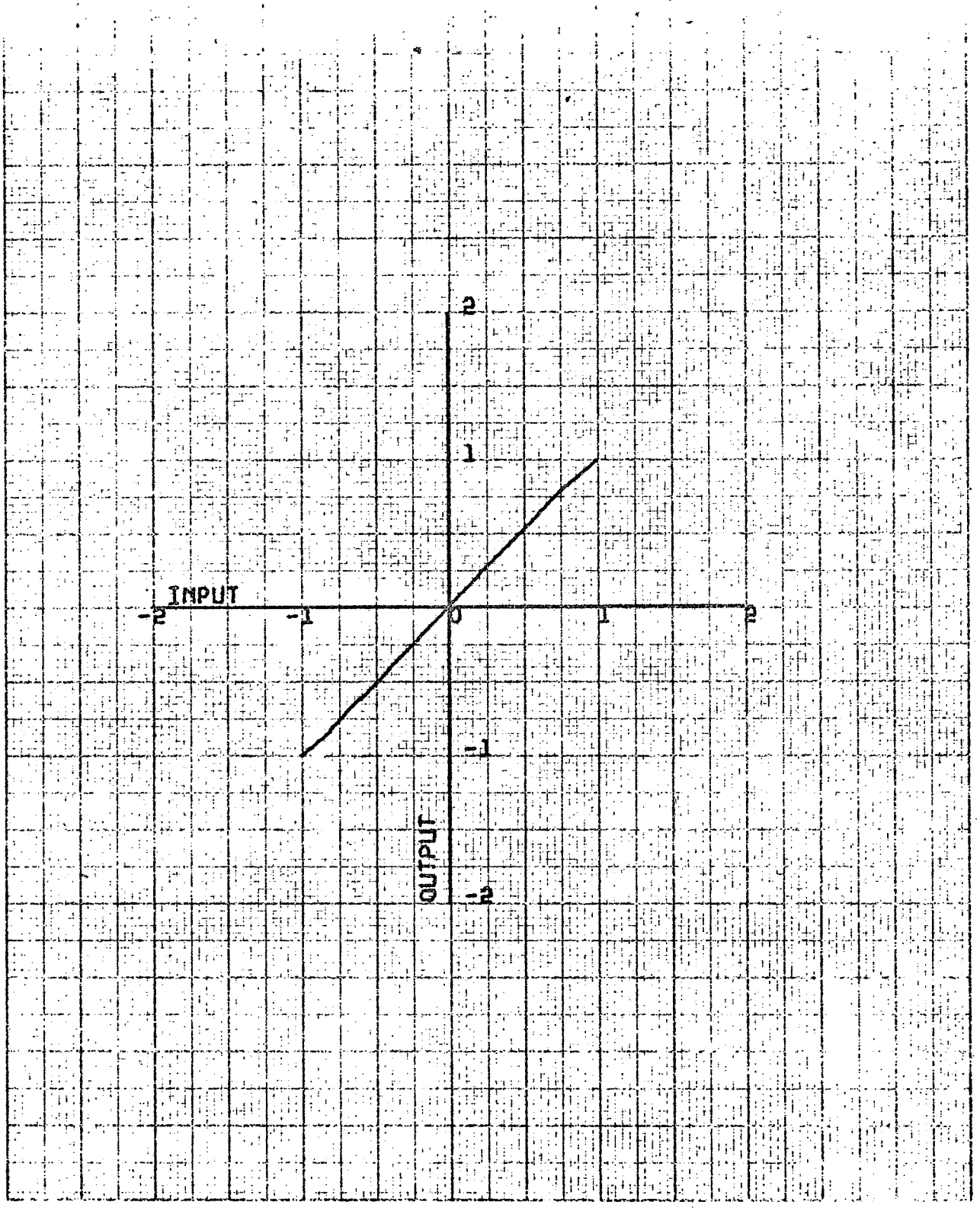



Figure 93: ACCELERATION NONLINEARITY FUNCTION OF THE BOEING-LING 249/LING PP-120/150 SYSTEM

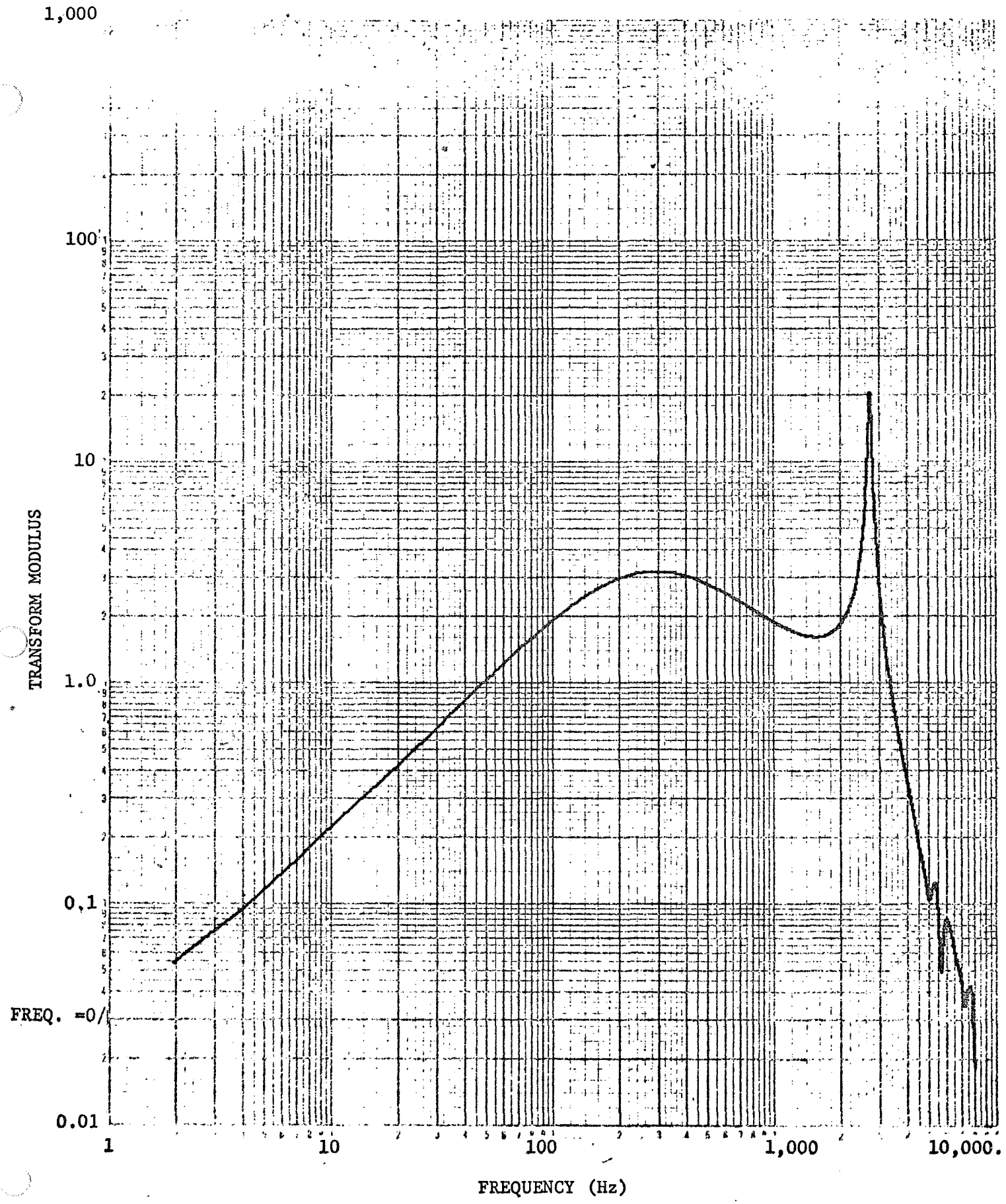



Figure 94: FOURIER TRANSFORM OF THE SHAKER IMPULSE RESPONSE MODIFIED BY THE ACCELERATION NONLINEARITY OF THE BOEING-LING 249/LING PP-120/150 SYSTEM

## Conceptual Design of Control System

A Transient Waveform Control System, in conformance to Figure 95, is proposed as a result of this study. Both signal flow and identification and inter-overlay operational logic comply with Figures 34 and 35. Individual components and their minimum requirements for the control system are as follows:

1) The digital computer. The digital computer should include: (1) the computer central processing unit; (2) the computer core memory; (3) the computer input/output (I/O) system; and (4) the priority interrupt system. It should be well integrated with the other system components to produce an operating system with high overall efficiency and flexibility.

The digital computer should be of advanced design with a memory cycle time of approximately 1 microsecond and a simultaneous multiple channel input/output and compute capability.

The computer's instruction set should include a hardware multiply and divide. The machine should have at least one general purpose index register. A 16-bit word size machine may be included provided the assembler will permit 100% parametric programming without regard to multiple instruction memory addressing.

The computer system should include 16,384 words of core memory (8,196 words of internal memory where the CPU has priority and 8,190 words of external memory where I/O transfers have priority).

The computer core memory should include a parity bit. All memory operations should include the checking of memory parity; the detection of an error shall cause the occurrence of the parity error interrupt.

The computer should have I/O capability such as: (1) computer I/O channels; (2) a word parallel I/O system; and (3) direct access I/O channels.

Six I/O channels should be included in the computer. One channel should couple the rapid access mass memory; the second the line printer; and the third the console teleprinter. The card reader and high speed paper tape punch and reader should share the fourth channel, while five and six would be ADC channels. Each channel should be independent, and it should be possible to operate all six channels at the same time. Each channel should be automatic in operation. Once an I/O operation has been initiated by the computer, the I/O channel should perform the block transfer. The channel should provide status and completion signals to the computer via interrupts.

The computer I/O channels should be standard devices with the digital computer. The peripheral devices, coupled through the computer I/O system, should be completely compatible with the computer manufacturer's standard software.

Each direct I/O channel should be independent and it should be possible to operate all channels at the same time. Each channel should be automatic in operation and be functionally equivalent to the previously described computer I/O channels. The direct I/O system should access all 8,196 words of external memory and when the computer is not addressing the external memory bank, no cycle stealing should occur.

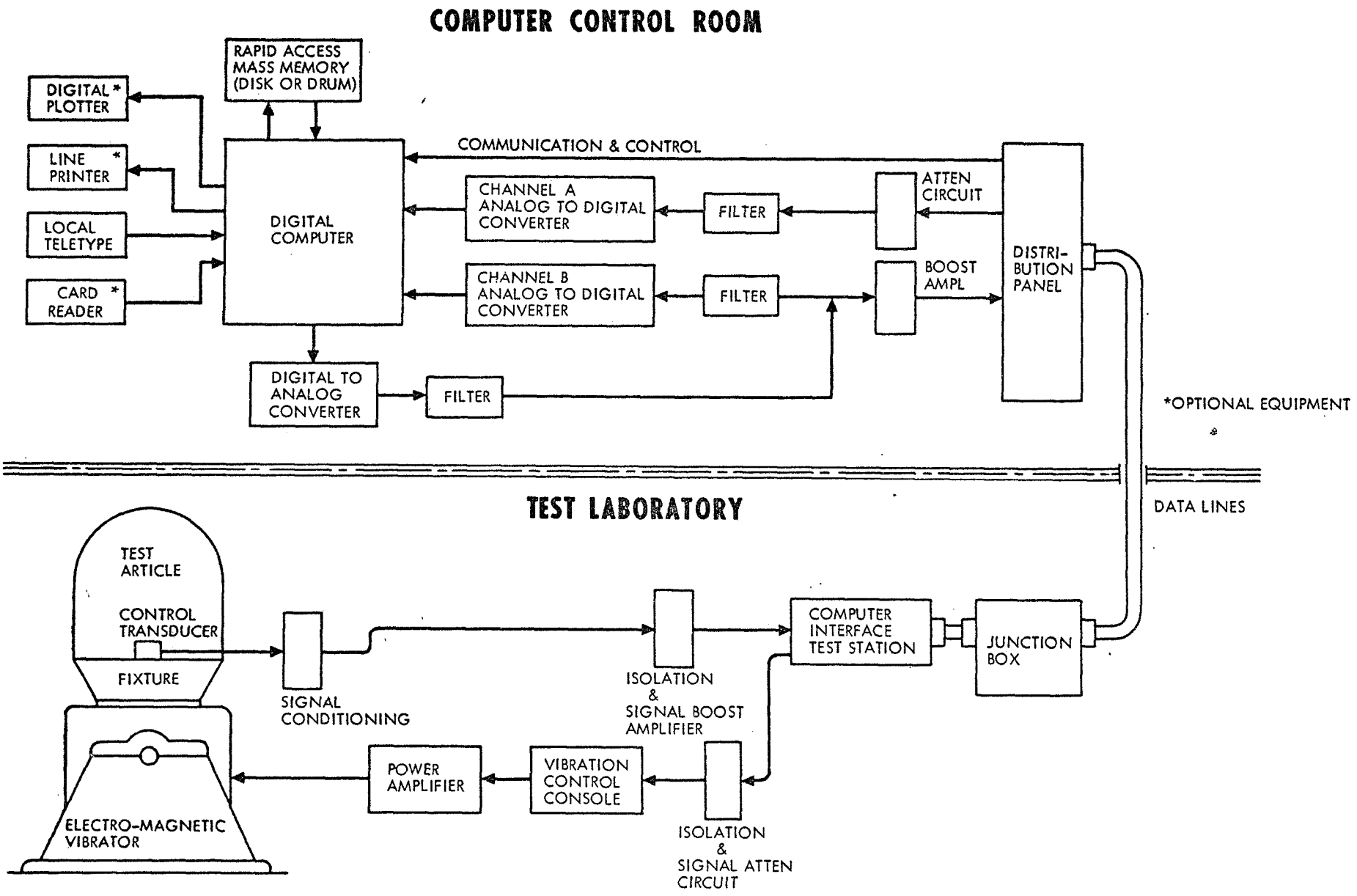



Figure 95: CONCEPTUAL DESIGN - TRANSIENT WAVE FORM CONTROL SYSTEM

The word parallel I/O output system should be used for transfers of one word or less under program control. The word parallel system should initialize other I/O operations, communicate with the remote teletypes, drive the remote and local digital plotters, communicate with and drive the digital to analog converters, and be used to decode multipurpose interrupts.

2) Rapid Access Mass Memory. A rapid access mass memory should be coupled to the computer to provide bulk storage for data and programs. The mass memory should provide a minimum storage capability of 500,000 computer words with an average access time of 17.5 milliseconds. The block transfer rate should be no less than 100,000 16-bit words/seconds. Contents of the mass memory should not be destroyed by power failure. Blocks of storage should be protected from inadvertent destruction by manual write-project switches.

3) Analog-to-Digital Converter. Two channels of analog-to-digital conversion writing a 14-bit word and sampling at 20,000 samples per second.

4) Digital-to-Analog Converter. One channel of digital-to-analog conversion reading a 14-bit word at 20,000 samples per second.

5) Digital Plotter. A digital plotter compatible with the digital computer.

6) Line Printer. A line printer compatible with the digital computer.

7) Teletype. A local teletype compatible with the digital computer.

8) Card Reader. A card reader compatible with the digital computer.

9) Low-Pass Filter. Three identical low-pass filters---5,000 Hz 6-pole Butterworth.

10) Data Lines and Signal Conditioning Equipment. Data lines and signal conditioning equipment are included as elements in this conceptual design. These elements, by definition, are included in the test system transfer function. Since the total system error is a direct function of system noise, data lines and signal conditioning equipment must be of high quality, properly grounded, and shielded.

The following criteria are applicable to the data transmission network. Data distribution lines should be Belden 8769, or equivalent (i.e., twisted shielded pair, capacitance between conductors less than 0.004 microfarad per 100 ft, wire size 22 gauge). These lines should be run through shielded troughs and conduits. The computer is normally a single-ended device and is kept isolated from the vibration test laboratory by instrumentation-quality, differential amplifiers with line driving capability. To optimize signal-to-noise ratio, the line signal level is nominally 10 volts. The predominant noise in this type of installation is a function of the common-mode rejection capability of the amplifiers.

11) Computer Interface Test Station. The computer interface test station functions as a laboratory communication and control link with the computer. The detail design is contingent upon computer control room hardware selection and software options elected from the conceptual design.

## Cost Estimate of Proposed System

The following estimate is prepared as a capital item budgetary estimate and does not consider the various elements of implementation, such as detail design, planning specifications, system responsibility, installation, system checkout and acceptance testing, transportation, and taxes. The system software is a conservative estimate based on out-of-house procurement.

| | |
|---|---|
| Digital Computer | $35,000 |
| 16,000 word core | 30,000 |
| Rapid Access Mass Memory | 35,000 |
| Analog-to-Digital Converter (2 channels) | 7,000 |
| Digital-to-Analog Converter (1 channel) | 2,000 |
| Low-Pass Filters (3 required) | 3,000 |
| Teletype (Local) | 5,000 |
| Interface Logic (Analog) | 5,000 |
| Software 8 months at $4,000/month | 32,000 |
| Data Lines | 2,000 |
| Isolation/Line Driving Amplifiers | 3,200 |
| Computer Interface Test Station | 500 |
| | $159,700 |
| Options: | |
| Digital Plotter | $ 6,000 |
| Line Printer | 16,000 |
| Card Reader | 8,000 |
| Interface Logic | 10,000 |
| | $ 40,000 |
| TOTAL | $199,700 |

## CONCLUSIONS AND RECOMMENDATIONS

This study resulted in the following conclusions and recommendations:

1) A transient waveform control system was successfully developed for on-line use in an environmental laboratory. Operating on a 4,096 data-point description of the required waveform, the cycle time from test system calibration to the controlled waveform was 16 minutes, including a digital plot of the synthesized input voltage.

   Because most of the 16 minutes was devoted to producing the digital plot, which is used by the test equipment operator to determine the suitability of the waveform, an obvious reduction in cycle time can be achieved through the use of an oscilloscope with memory for displaying the waveform. Additional improvements can be made by improving the efficiency of the software used in the program (through the use of machine language instead of Fortran, for example). A cycle time of 2 minutes or less can be achieved.

   Although a further reduction of cycle time might be attained through the substitution of a hard-wired computational process for the software routine, the expense of such a change is prohibitive considering the relatively small amount of improvement that would result.

2) Experimental results using the prototype control system demonstrated controllability with a time domain variance of less than 13%. A 10-bit-word size was used in this system. The specified analog-to-digital/digital-to-analog converter word size of 14 bits, and its attendant improvement in defining the test system transfer function, will reduce this percentage.

3) Special data processing procedures were defined, evaluated, and tested. They include:

   a) Antialiasing filters;

   b) Sampling rate criteria;

   c) Sampling length criteria;

   d) Digital word size;

   e) Digital data unbiasing (i.e., the unbias routine redistributes the quantized data to a uniform distribution between quantization levels).

4) A requirement was established for increased signal resolution on vibration test systems. An order-of-magnitude decrease in ambient noise is a direct result of that requirement. This requirement can be realized by tighter specifications to equipment manufacturers, increased directed maintenance on test apparatus, and changes in test equipment consigned to a transient testing mission. Recommended equipment changes directed at the reduction of system noise include:

   a) Driving the exciter field with pure d.c.;

b) Substitution of amplifier tubes having a minimum cathode to filament leakage;

c) Powering all vacuum tube filaments with d.c.;

d) Specifying and maintaining the regulation on power supplies,

e) Using delta wound power transformers with tertiary windings to reduce the effects of line transients.

A technique change to decrease the ambient test system noise consists of (1) decreasing the vibrator field current, thereby driving more armature current for less field current; or (2) selecting the output transformer voltage taps so that the maximum voltage is just sufficient to drive the exciter to the required level.

5) The electrohydraulic equipment surveyed at GSFC is not amenable to transient waveform control. Both system noise level and linearity characteristics are incompatible with control system requirements.

6) The fidelity measurement for laboratory transient waveform synthesis requires time history, Fourier transform modulus, and phase spectrum representations. An error variance figure should be investigated as a technique for specifying test fidelity.

7) Detailed knowledge of the required transient is fundamental to correct control. This requires that:

a) The transient is within the capability of the vibration equipment;

b) The digital description of the transient is within the capability of the computational equipment (i.e., storage requirements for long-duration, high-frequency transients).

8) The digital computer and local teletype requirements defined in the conceptual design can be satisfied with existing GSFC components located in a specialized data analysis and display system. The Time/Data 100 System includes a Varian 6201 computer and local teletype. The necessary computer options required for transient waveform control are:

a) Hardware multiply and divide;

b) External memory (8,192 words) with minor engineering modifications;

c) Buffered input-output channels for the analog-to-digital converters and rapid access mass memory.

Additional Recommendations---The following recommendations are the result of this study.

1) This study related the fidelity of the laboratory synthesized waveform to the characteristic noise floor of the vibration test system. The possibility exists for the removal of the 60-Hz noise component if the timing of the synthesized waveform were coincident with the 60-Hz phase relationship at the time the calibration pulse was initiated to describe the test

system transfer function. Future work on the control system should be done to develop a method of accomplishing this synchronization and evaluating the results.

2) Transient test techniques should be developed as a practical technology. The potential cost savings of accomplishing laboratory shock-test requirements on an electromagnetic vibrator, coupled with the use of digital techniques to analyze and present data, will make on-line digital transient test capability attractive to many segments of the testing industry. The distribution of transient energy in the frequency domain to produce a unique specimen response can be a viable reality. The ability to rapidly compute and present the structural transfer function of a specimen (i.e., the frequency domain ratio of the response at one point on a structure to another) will provide an index of the number of degrees of freedom and the participation of each in a laboratory test situation. Data analysis techniques, operating on the Fourier transform phase spectrum, can readily calculate damping matrix coefficient elements. The damping ratio for a modal response observed on the Fourier transform modulus can be computed from the Fourier transform phase spectrum.

$$\delta = \frac{1}{f_R} \left[ \frac{f_1 - f_2}{\cot \theta_2 - \cot \theta_1} \right]. \qquad (29)$$

3) Apply transient test techniques to establish component and subsystem dynamic environments from system testing. Transfer function logic, coupled with transform operations, would produce information relating varying component descriptions to the parent structure as well as the parent structure to the component without subjecting the test specimen to the damage potential of swept sine excitation (i.e., a destructive resonance or cumulative fatigue damage).

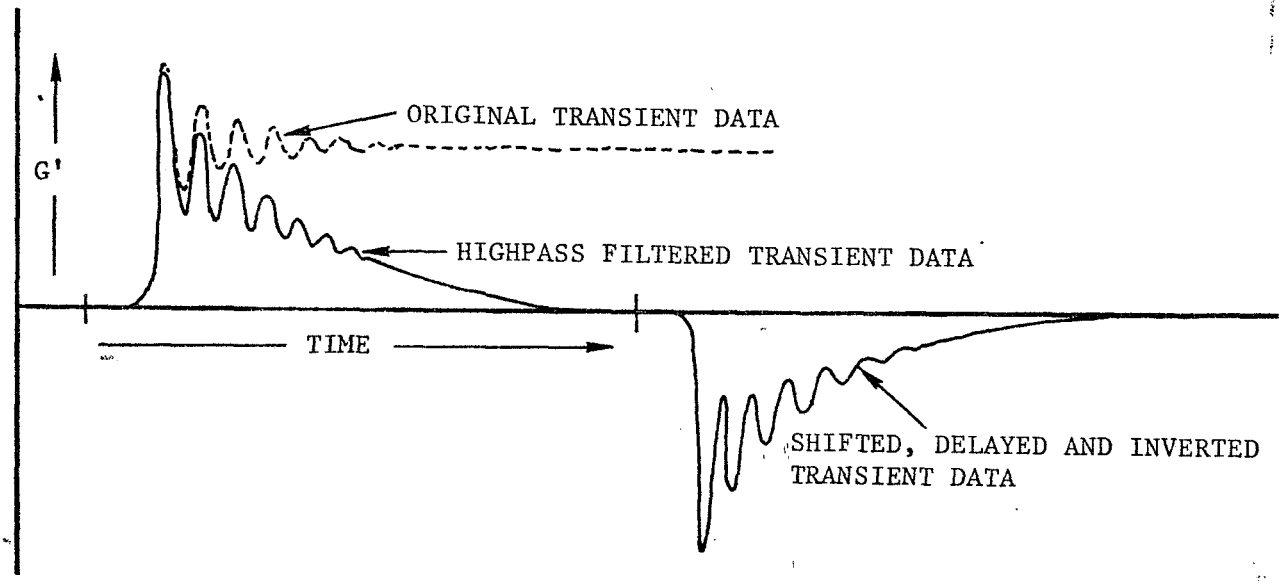
4) Unless a test can be related to probability of failure in service, it is almost impossible to demonstrate that it is a rational test. With the advent of control techniques that lend realism to transient forcing functions, the damage potential theories on documented structural configurations should be related to vibration equivalence. Applying known techniques with fatigue sensors, parametric relationships relating damage potential to structural vibration response should be established.

Experience with the S/N Fatigue Life Gage under random conditions indicates that it will be capable of determining the constant-amplitude sinusoidal equivalent input required to cause the same fatigue damage as a complex wave in some structural materials over a fairly wide range of conditions. The S/N Fatigue Life Gage is a small, bondable resistance sensor, similar in appearance to a foil strain gage. When bonded to certain structural materials, such as 2024 or 7075 aluminum, the gage generates a permanent resistance change as a function of the fatigue experience at its point of attachment. Properties and limitations of the gage are described in References 13 and 14.

Empirical relationships derived from rms stress level, peak probability density distribution, and zero crossing rate should also be explored as possible failure prediction techniques capable of removing the ambiguity that the test specification writer now faces in structuring his requirements.

The prospect of recoverable space hardware and extended life concepts will emphasize the need for knowledge of fatigue damage accumulation, both in service and during life testing. Transient waveform control should be used as a test requirement to produce a realistic force/motion environment for life testing.

5) Further study and experimentation should be done to define simulation requirements for those transients rich in d.c. or low-frequency content (i.e., booster ignition or cutoff). For example, in the case of booster ignition, the vehicle response will contain a transient response superimposed upon steady-state response. The question is, is it necessary to fully simulate the steady-state portion of the response? If not, how fast might one allow the steady-state environment to "bleed" off? Other techniques[12] would allow the simulation of a pseudo d.c. response by shifting, inverting, and delaying data (see figure below).




Certainly, this area of simulation is lacking in definition and workable technology. It is recommended that the theory and practice of this technology be developed.

# REFERENCES


1. Cooley, J. W., Tukey, J. W., "An Algorithm for the Machine Calculation of Complex Fourier Series," Math. of Comp., Vol. 19, No. 90, pp 297-301 (1965)

2. Cooley, J. W., Lewis, A. W., and Welch, P. D., "The Fast Fourier Transform Algorithm and Its Applications," IBM Research Report RC 1743, February 9, 1967

3. Brenner, N. M., "Three Fortran Programs that Perform the Cooley-Tukey Fourier Transform," M.I.T. Lincoln Laboratory Technical Note 1967-2 (AD 657019), 28 July 1967

4. Bracewell, Ron, The Fourier Transform and Its Applications, McGraw Hill, 1965

5. Chapman, C. P., "Derivation of the Mathematical Transfer Function of an Electrodynamic Vibration Exciter," NASA Contract NAS 7-100

6. Ratz, A. G., "Statistical Effects in Automatic Random Equalizers," IEEE Transactions on Instrumentation and Measurement, Vol. IM-16, No. 4, December 1967

7. Munson, A. N., Jr., "Flight Shock and Vibration Data from the TAT/AGENA-D Launch Vehicle (OGO-D Spacecraft)," Report No. 681-10 Test and Evaluation Division - Goddard Space Flight Center, Greenbelt, Maryland, May 13, 1968

8. Papoulis, A., "Error Analysis in Sampling Theory," Proceedings of the IEEE, Vol. 54, No. 7, July 1966

9. Miller, R. W., "Shaping Shock Acceleration Waveforms for Optimum Electro-Dynamic Shaker Performance," LTV Ling Electronics Division, Anaheim, California

10. Angus, Richard N., "Reality of Vibration System Random Noise Ratings in Light of Shaped Spectrum Requirements," 1964 Institute of Environmental Sciences Proceedings

11. Young, F. W., "Shock Testing with Vibration Systems," Radiation Incorporated, Melbourne, Florida

12. Favour, John D., Stewart, Ralph, "Primary Calibration of Pressure Transducers to 10,000 Hz," Proceedings of the 15th National Aerospace Instrumentation Symposium, Instrument Society of America (in Press)

13. Harting, D. R., "Remote Sensing of Random Fatigue Damage With the -S/N- Fatigue Life Gage," Society for Experimental Stress Analysis, 21 Bridge Square, Westport, Connecticut

14. -S/N- Fatigue Life Gage Applications Manual, Second Edition, Micro-Measurements, 38905 Chase Road, Romulus, Michigan

# APPENDIX I

## ERROR ANALYSIS OF A TRANSIENT WAVEFORM CONTROL SYSTEM

TABLE OF CONTENTS

[0] Introduction

[1] Description of Transient Waveform Control System

[2] Error Sources in the Control System
1. Vibrator response errors.
2. Quantization errors.
3. Aliasing errors.
4. Truncation errors.
5. Interpolation errors.

[3] Modification of the Data Processing System
1. Prefiltering signals.
2. Removing trends.
3. Calibrating the simulation error.

[4] Error Analysis
1. Introduction to error analysis.
2. Clarification of problem.
3. Error sources.
4. Notation and preliminaries.
5. Error due to data processing and noise.
6. Practical error bounds.
7. Example of computing error bounds.

## PREFACE

Appendix I presents a detailed theoretical error study and mathematical model. Although its basic assumption of "white" wideband stationary noise was invalidated by laboratory experience on the prototype control system, the analysis and modeling is considered accurate and valuable, within the limitations of the assumptions. The nomenclature is explained within the Appendix.

### [0] Introduction

This memorandum analyzes known error sources produced by the transient waveform control system for simulating acceleration records on spacecraft modules. Its purpose is twofold: (1) to suggest areas in which filtering and special data processing techniques may be employed to reduce errors or economize computations, and, (2) to provide a model for estimating the resultant effect of all error sources in simulating known acceleration histories. This effort is subdivided into four subsections. Section [1] contains a brief description of the transient waveform control system as an analog-digital data processing system. In Section [2] the known error sources are identified and procedures for testing their effect on system performance are outlined. Section [3] describes some recommended digital and analog modifications of the basic data processing system of Section [1]. In Section [4] a mathematical model of the system is derived. Using this model a bound is obtained on the total simulation error due to the accumulative effect of the various error sources. This bound is given as a function of a number of source parameters. Detailed techniques for estimating the parameters are derived. These techniques are then illustrated by an example using data from an actual flight.

## [1] The Transient Waveform Control System

The purpose of the transient waveform control system is to simulate acceleration histories for testing the ability of spacecraft modules to endure critical phases of flight. The module to be tested is mounted on a vibrator, which is electrically controlled, to simulate recorded acceleration histories. The vibrator system is assumed to be a time invariant linear system, i.e. the vibrator response to an arbitrary input signal is determined by the response to an impulsive input. This property of time invariant linear systems is employed in the transient waveform control system to simulate acceleration transients. The control system consists of the following basic operations:

1. A modeled impulsive signal $y(t)$ is input into the vibrator and the response $z(t)$ is observed.

2. The Fourier transforms of $y(t)$ and $z(t)$ are computed and then ratioed to estimate the vibrator frequency response. If $\mathcal{F}y(\omega)$ and $\mathcal{F}z(\omega)$ denote the theoretical Fourier transforms of $y(t)$ and $z(t)$ respectively, then the vibrator frequency response $\varphi(\omega)$ is given by $\varphi(\omega) = \mathcal{F}z(\omega)/\mathcal{F}y(\omega)$.

3. The required acceleration record $x(t)$ is sampled and its Fourier transform $\mathcal{F}x(\omega)$ is computed.

4. If $\mathcal{F}f(\omega)$ denotes the Fourier transform of the required input $f(t)$ then we have $\varphi(\omega) = \mathcal{F}x(\omega)/\mathcal{F}f(\omega)$. Consequently $\mathcal{F}f(\omega)$ is computed from the formula.

[1.1] $$\mathcal{F}f(\omega) = \mathcal{F}x(\omega)/\varphi(\omega) = \mathcal{F}x(\omega) \cdot \mathcal{F}y(\omega)/\mathcal{F}z(\omega) .$$

5. $\mathcal{F}f(\omega)$ is inverse Fourier transformed and the signal $f(t)$ is reproduced as an input voltage to the vibrator.

6. The vibrator response is observed and compared with the required acceleration waveform $x(t)$.

The operational control system only approximates the simulation described above due to limitations in the data processing equipment and non-linearities in the vibrator response such as internally generated noise. In particular, the data processing for Steps 1 through 6 is implemented in the following manner: Steps 1 and 3 are accomplished by quantizing and sampling the analog time histories $y(t)$, $z(t)$, and $x(t)$. The discrete Fourier transforms in Steps 2-4 are computed digitally from the respective discrete quantized data. The discrete transform corresponding to $\mathcal{F}f(\omega)$ is inversed digitally for Step 5 producing a sampled input signal. Then a time series of rectangular voltage pulses proportional to the sampled input is generated for the required control input to the vibrator. The vibrator response is digitized and the time domain and frequency domain information plotted.

[2] Error Sources in the Control System

It is important to realize at the outset that we are here primarily concerned with errors which are generated in the data processing system defining the input control. The total system performance is limited by distortions in the vibrator response in addition to the errors generated in the data processing system. Errors in the vibrator or shaker are assumed to have two primary sources: (1) non-linearities arising from the inability of the vibrator to reproduce arbitrary acceleration records, and (2) internally generated noise or background noise. It is presumed that the first type of distortion can be reduced to a negligible level by restricting the frequency content and amplitude levels of the acceleration waveforms to be reproduced. In this case the background noise level is a natural bound on the reproducibility of the required waveforms. In other words, a control which minimizes the system simulation error would yield acceleration records differing from known transients by residuals having the characteristics of the background noise.

The major error sources in defining the input control occur in the following data processing operations:

1) Recording the vibrator response $z(t)$,
2) Digitizing and sampling the input $y(t)$, the output $z(t)$ and the required transient $x(t)$,
3) Truncating the analog records of $y(t)$ and $z(t)$,
4) Producing voltage transients which interpolate the discrete control input obtained digitally.

There is strong evidence that the roundoff errors in computing the discrete Fourier transform and inverse transform are of negligible size compared to the errors introduced above. Consequently, we ignore these errors in the analysis below. The errors introduced in data processing thus fall into five categories: 1. vibrator response errors, 2. quantization errors, 3. aliasing errors, 4. truncation errors, and 5. interpolation errors. Assuming reasonable care is taken in the measurement and data processing technique we may expect some of these errors to have secondary effects compared with other errors. These assumptions are discussed below together with methods for testing the error model assumptions.

1. Vibrator Response Errors: The data processing system of the previous section is based on modeling the vibrator system as a time invariant, linear system. It is presumed that distortions due to non-time-invariance of the vibrator response are primarily generated by the background noise. This assumption is easily tested by comparing response records when a given transient is input sequentially to the vibrator. It is clear that the response records should differ by a noiselike residual.

It is assumed, moreover, that the frequency content and amplitude levels of the input transients are restricted so that non-linearities in the vibrator response are primarily due to background noise. This assumption may be tested by inputing a control transient at different power levels and with various changes of time scale. The background noise is assumed to be a stationary stochastic process. Thus characteristics of the noise can be estimated by Fourier transforming a sufficiently long time record of the noise background, hanning, and computing the modified periodogram or power spectra.

2. Quantization Errors: The quantizing errors in digitizing the analog tapes are assumed to behave like a sequence of independently distributed random variables uniformly distributed over the interval $\left[0, 2^{-n}\right]$ where n is the bit size of the quantizer. This model is based on the assumption that the digitized values vary by several bits or quantizing boxes in successive samples. For emperical data where additive noise causes spurious local errors in otherwise smooth trends this is generally true. On the other hand the input $y(t)$ may have regions with slowly varying trends which introduce local correlations in the quantizing errors. Low frequency errors in the discrete transform, however, are believed to be primarily due to the bias resulting from rounding down, or chopping, in the analog to digital conversion. These assumptions may be tested by varying the bit size and mode of rounding when digitizing an analytically defined input. Discrete transforms of the quantization error record may then be compared with the power spectra of the error model described above.

3. Aliasing Errors: In the sampling process we replace a continuous analog record by a discrete set of data. The aliasing error in the time history is the difference between the analog record and a trignometric function which interpolates the discrete data. This error has the effect of symmetrically folding all frequency content above the cutoff frequency of the discrete transform back into lower frequencies. The error can be reduced to a negligible level by filtering the signals $y(t)$, $z(t)$ and the record of $x(t)$ in order to attenuate high frequency content. Then the primary source of high frequency error is quantization error and noise in the analog records, i.e. the effect of aliasing error is secondary to that of sampling noise. These assumptions may be tested by comparing discrete transforms at various sample rates and by employing filters with

varying bandwidths before digitizing.

4. Truncation errors: The discrete transform is a periodic transform which replaces a signal of length T with a T periodic signal. Consequently, the data processing program in effect replaces an input signal of length T by a T periodic signal and replaces the truncated vibrator response by a T periodic response. However, the periodic vibrator response to a T periodic input differs from the truncated response to an input of duration T due to wrap around effects caused by the response lag in the system. These truncation errors can be reduced to a negligible level relative to other errors by observing the response until the signal falls below the noise level or quantization level. For then the sampled difference between the periodic response and the truncated response will be a residual with the behavior of the sampling noise. It is seen that the effect of truncation errors can be emperically tested by comparing the response records obtained when a given transient is input sequentially to the vibrator.

5. Interpolation errors: The control transient which corresponds to the sampled input obtained from the data processing program is a trignometric interpolation of the sampled input data. The digital to analog converter, however, produces voltage pulses with roughly constant amplitude between sampling points. Thus the actual input control is a step function interpolant of the sampled input data. This type of input control can produce relatively large errors in the vibrator response due to the following characteristics: (1) the interpolation error is roughly proportional to the slope of the desired input control so that rapidly varying or impulsive transients could be grossly distorted by the step function interpolant, and (2) discontinuities or jumps in the input step function contain high frequency content which could produce rippling in the vibrator response. The effect of these errors can be tested by comparing the response of smooth analytic inputs with the vibrator response to the corresponding step function interpolants.

## [3] Modification of the Data Processing System

This section analyzes some modifications of the basic data processing technique of section [1] which are recommended to improve system simulation or evaluation of simulation errors. Some of the modifications may prove to have little effect on overall system accuracy. In any case emperical tests should be employed to verify the necessity for data modification and to evaluate the effect of these techniques.

1. Prefilter signals before digitizing.
   The transients $y(t)$, $z(t)$ and the analog record $x(t)$ should be filtered to attenuate high frequency content before digitizing. There are several reasons for this requirement. The primary reason for filtering these signals before digitizing is to reduce aliasing errors in the respective transforms. In addition, random background noise may be the dominant source of high frequency content in the transients $y(t)$ and $z(t)$. Filtering these transients will thus reduce the noise power in the sampled records. Finally, the vibrator system may not respond properly to input transients with an excessive concentration of high frequency content. Consequently the acceleration history $x(t)$ should be filtered so that the input control $f(t)$ will have suitably limited frequency content. Precaution must be taken, however, so that the filtered signals are not radically altered by the transmission characteristics of the respective filters. This may be accomplished by dividing the transform of the filtered signals by the frequency response of the respective filter, or by employing low pass filters which have linear phase responses over the frequency range of interest. (The linear phase response in the latter case corresponds to a simple time lag in the filter response.) In either case aliasing errors can be reduced to a negligible level without altering the signal content over the frequency band of interest.

2. Remove trends in input transients.
   The vibrator system cannot respond linearly to signals with low frequency content, i.e. slowly varying voltage bias, since the vibrator is physically constrained to have zero average acceleration.

Consequently low frequency content in the input transients $y(t)$ and $f(t)$ should be reduced to an appropriately small level. The transient $y(t)$ can be preselected so that low frequency bias is negligible. However, low frequency content in the input control $f(t)$ may be a significant factor due to several possible sources. The most obvious potential source is low frequency bias or trends in the required acceleration history $x(t)$. Since the vibrator system cannot simulate these low frequency trends properly it is recommended that they be removed from the acceleration record $x(t)$ prior to computation of the transform. It is probably sufficient to modify the sampled data $x(t_i)$ $i = 0, \ldots, N-1$ by removing the linear curve of least regression $\bar{x}(t)$ which satisfies

$$\sum_{i=0}^{N-1} \left[x(t_i) - \bar{x}(t_i)\right] = 0, \text{ and } \sum_{i=0}^{N-1} i \left[x(t_i) - \bar{x}(t_i)\right] = 0 .$$

The discrete transform of the modified data is then suitably attenuated at low frequencies. Another possible source of low frequency trends in the transient $f(t)$ is quantization bias when digitizing the signals $x(t)$, $y(t)$ and $z(t)$. This source of bias can be corrected either by programming a rounding procedure in the digitizing process or by choosing the bit size of the quantizer sufficiently small. With the above data modifications low frequency bias in the control transient $f(t)$ should be reduced to a negligible level.

3. Calibrate the simulation error.

In order to evaluate the accuracy of the waveform control system, it is necessary to compare the required transient $x(t)$ with the simulated signal $\tilde{x}(t)$. In principle it suffices to digitize the output $\tilde{x}(t)$, normalize the magnitude by a suitable scaling factor and compute the sampled error $\epsilon_i = x(t_i) - \tilde{x}(t_i)$ . In practice the transient $\tilde{x}(t)$ is sampled at times $t_i'$ which differ from the sampling times $t_i$ by a constant lag. Consequently it is necessary to calibrate the sampled signal $\tilde{x}(t_i')$ with the digitized transient $x(t_i)$ prior to error computations. This section describes a numerical technique for calibrating these signals.

The calibration scheme is based on estimating the time lag $z = t_j - t'_j$ by minimizing the mean square error

$$(3.1) \quad E(z) = \sum_j \left| x(t_j) - \tilde{x}(t'_j + z) \right|^2 .$$

Assuming z is small we have

$$\sum_j \left| \tilde{x}(t_j + z) \right|^2 \cong \sum_j \left| \tilde{x}(t_j) \right|^2 .$$

In this case we obtain

$$(3.2) \quad E(z) \cong \sum_j \left| x(t_j) \right|^2 + \sum_j \left| \tilde{x}(t'_j) \right|^2 - 2 \sum_j x(t_j)\, \tilde{x}(t'_j + z).$$

It follows that $E(z)$ is minimized if the cross correlation $C(z) = \sum_j x(t_j)\, \tilde{x}(t'_j + z)$ is maximized. The proposed calibration scheme maximizes $C(z)$ in a two stage search and then interpolates the sampled values $\tilde{x}(t'_j)$ to estimate $\tilde{x}(t_j) = \tilde{x}(t'_j + z)$ .

Let $x_j$ denote the values of $x(t)$ at the sampling times $t_j = t_o + j\Delta$ $j = 0, 1, \ldots, N-1$. It is assumed that $\tilde{x}(t)$ is sampled at times $t'_j = t'_o + j\Delta$ $j = -m, m+1, \ldots 0, 1, \ldots N+m-1$ where $t'_o$ is an estimate of the time $t_o$ and m is chosen large enough so that $|t_o - t'_o| < m\Delta$ . Let $\tilde{x}_j$ denote the sampled values of $\tilde{x}(t)$ at $t'_j$ and let z denote the lag time $z = t_o - t'_o = t_j - t'_j$ . Suppose r is the integer for which

$$(3.3) \quad C_r = \max \left\{ C_k : k = -m, -m+1, \ldots 0, 1 \ldots m \right\} ,$$

$$\text{where } C_k = \sum_{j=0}^{N-1} x(t_j)\, \tilde{x}(t'_{j+k}) = \sum_{j=0}^{N-1} x_j \tilde{x}_{j+k} .$$

If $C_{r-1} > C_{r+1}$ and $C(t)$ is sufficiently smooth then $(r-1)\Delta \le z \le r\Delta$ since the cross correlation $C(t)$ is maximized between $C_{r-1} = C((r-1)\Delta)$ and $C_r = C(r\Delta)$. In order to estimate z more accurately it is necessary to interpolate $C(t)$ for $(r-1)\Delta \le t \le r\Delta$. (The case $C_{r-1} < C_{r+1}$ may be treated similarly. Hence corresponding estimation formulas for this case are produced below but not explicitly derived.)

Let $t = (r-1)\Delta + \epsilon\Delta$ where $0 \le \epsilon \le 1$. Then $C(t)$ is given by

$$(3.4)\quad C((r-1)\Delta + \epsilon\Delta) = \sum_{j=0}^{N-1} x(t_j)\, \tilde{x}(t'_j + (r-1)\Delta + \epsilon\Delta) = \sum_{j=0}^{N-1} x_j \tilde{x}(t'_{j+r-1} + \epsilon\Delta)$$

The values $\tilde{x}(t'_{j+r-1} + \epsilon\Delta)$ $0 \le \epsilon \le 1$ may be obtained by interpolation from the values $\tilde{x}_{j+r-2}$, $\tilde{x}_{j+r-1}$, $\tilde{x}_{j+r}$, $\tilde{x}_{j+r+1}$. A suitable interpolation formula is

$$(3.5)\quad \tilde{x}(t'_{j+r-1} + \epsilon\Delta) \doteq a_1(\epsilon)\, \tilde{x}_{j+r-2} + a_2(\epsilon)\, \tilde{x}_{j+r-1} + a_3(\epsilon)\, \tilde{x}_{j+r} + a_4(\epsilon)\, \tilde{x}_{j+r+1} ,$$

where
$$a_1(\epsilon) = \frac{\epsilon}{2}(1-\epsilon)^2$$
$$a_2(\epsilon) = \frac{\epsilon^2}{2}(1-\epsilon) + 3(1-\epsilon)^2 - 2(1-\epsilon)^3$$
$$a_3(\epsilon) = -\frac{\epsilon}{2}(1-\epsilon)^2 + 3\epsilon^2 - 2\epsilon^3$$
$$a_4(\epsilon) = -\frac{\epsilon^2}{2}(1-\epsilon) .$$

The above interpolation consists of piecewise cubic polynomials which are fitted together at the "joints" $t'_j$ by the conditions $\tilde{x}(t'_j) = \tilde{x}_j$ and $\frac{d}{dt}\tilde{x}(t'_j) = (\tilde{x}_{j+1} - \tilde{x}_{j-1})/2\Delta$.)

Substituting (3.5) into (3.4) we obtain

$$(3.6)\quad C((r-1)\Delta + \epsilon\Delta) \doteq a_1(\epsilon)\, C_{r-2} + a_2(\epsilon)\, C_{r-1} + a_3(\epsilon) C_r + a_4(\epsilon)\, C_{r+1} .$$

It is clear that $C(t)$ may be maximized for $(r-1)\Delta \le t \le r\Delta$ by differentiating (3.6) with respect to $\epsilon$. Thus $z = (r-1)\Delta + \bar{\epsilon}\Delta$, where $\bar{\epsilon}$ satisfies

$$(3.7)\quad 0 = a'_1(\bar{\epsilon})\, C_{r-2} + a'_2(\bar{\epsilon})\, C_{r-1} + a'_3(\bar{\epsilon}) C_r + a'_4(\bar{\epsilon})\, C_{r+1} .$$

Equation (3.7) can be reduced to the form

$$(3.8)\quad 0 = 3\alpha_1 \bar{\epsilon}^2 + 2\alpha_2 \bar{\epsilon} + (C_r - C_{r-2}) \text{ , where}$$

$$\alpha_1 = -C_{r-2} + 3C_{r-1} - 3C_r + C_{r+1}$$

$$\alpha_2 = 2C_{r-2} - 5C_{r-1} + 4C_r - C_{r+1} \quad .$$

Equation (3.8) may be solved recursively or by employing the quadratic formula

$$(3.9)\quad \bar{\epsilon} = -\frac{\alpha_2}{3\alpha_1} \pm \left( \left( \frac{\alpha_2}{3\alpha_1} \right)^2 - \frac{(C_r - C_{r-2})}{3\alpha_1} \right)^{1/2} ,$$

provided $\alpha_1$ is sufficiently large.

If $\bar{\epsilon}$ is the solution to (3.7) then the values of $\tilde{x}(t)$ at $t_j = t'_j + z = t_{j+r-1} + \bar{\epsilon}\Delta$ are obtained from equation (3.5):

$$(3.10)\quad \tilde{x}(t_j) \doteq \tilde{x}(t_{j+r-1} + \bar{\epsilon}\Delta)$$

$$\doteq \alpha_1(\bar{\epsilon})\, \tilde{x}_{j+r-2} + \alpha_2(\bar{\epsilon})\, \tilde{x}_{j+r-1} + \alpha_3(\bar{\epsilon})\, \tilde{x}_{j+r}$$

$$+ \alpha_4(\bar{\epsilon})\, \tilde{x}_{j+r+1} \qquad j=0, 1, \ldots, N-1 .$$

If $C_{r+1} > C_{r-1}$ then we have $r\Delta \le z \le (r+1)\Delta$ . In this case we obtain

$$(3.11)\quad \tilde{x}(t_j) \doteq \tilde{x}(t_{j+r} + \bar{\epsilon}\Delta) \qquad j=0, 1, \ldots, N-1.$$

$$\doteq \alpha_1(\bar{\epsilon})\, \tilde{x}_{j+r-1} + \alpha_2(\bar{\epsilon})\, \tilde{x}_{j+r} + \alpha_3(\bar{\epsilon})\tilde{x}_{j+r+1} + \alpha_4(\bar{\epsilon})\, \tilde{x}_{j+r+2} ,$$

where $0 \le \bar{\epsilon} \le 1$ satisfies a quadratic equation similar to (3.8):

$$(3.12)\quad 0 = 3\sigma_1 \bar{\epsilon}^2 + 2\sigma_2 \bar{\epsilon} + (C_{r+1} - C_{r-1}) \quad ,$$

with $\sigma_1 = -C_{r-1} + 3C_r - 3C_{r+1} + C_{r+2}$

$$\sigma_2 = -2C_{r-1} + 5C_r - 4C_{r+1} + C_{r+2} \quad .$$

Consequently, the sampled values $\tilde{x}_j$ may be calibrated with the sampled values $x_j$ in three steps:

(1) The cross correlations $C_k$ are computed and the integer r which maximizes $C_k$ is found.

(2) The lag time $\tau$ is computed. If $C_{r-1} > C_{r+1}$ then $\tau \doteq (r-1)\Delta + \bar{\epsilon}\Delta$ where $\bar{\epsilon}$ satisfies (3.8). If $C_{r-1} < C_{r+1}$ then $\tau \doteq r\Delta + \bar{\epsilon}\Delta$ where $\bar{\epsilon}$ satisfies (3.12).

(3) The values of $\tilde{x}(t_j)$ are computed from (3.10) if $C_{r-1} > C_{r+1}$ and from (3.11) if $C_{r-1} < C_{r+1}$.

## 4.1 Introduction to Error Analysis

In this section we obtain a bound on the output error of the total system. In doing so we disregard second order errors, that is, if the error to signal ratio is of magnitude $\epsilon + \epsilon^2$ then we assume $\epsilon$ to be a good estimate of this error. We also make the assumption that the various quantizing errors can be treated as a sequence of independent random variables.

In Subsection 4.2 we define what we will consider the optimal output for the system. This gives us a standard by which to measure possible output errors. Subsection 4.3 separates the error sources into two categories which will be treated separately. Subsection 4.4 gathers together the various notations used throughout the paper. In 4.5 we are concerned primarily with data processing errors. We step by step follow the propagation of the individual error sources through the system. We obtain a bound on the output error in terms of these individual error sources. Then in Subsection 4.6 we suggest possible methods of bounding the error sources (and hence the output error of the total system). These methods are illustrated by an example which uses an actual OGO tape and tapes of the input-output used in determining the systems' transfer function. Subsection 4.7 is concerned with the error which originates in the digital to analog signal converter.

## 4.2. CLARIFICATION OF PROBLEM

The function $x(t)$ recorded on the OGO tape is of the form $x(t) = x_o(t) + N(t)$ where $x_o(t)$ is the signal we want to produce on the shaker and $N(t)$ can be considered noise. There is no way of extracting $x_o(t)$ from $x(t)$ unless we know $N(t)$ exactly. Assuming we only have statistical information on $N(t)$ then the best we can hope to do is to get some sort of optimal estimate $\hat{x}_o(t)$ on $x_o(t)$. We assume this can be obtained by a linear, band limited filter $m(t)$.

i.e. $$\hat{x}_o(t) = \int_{-\infty}^{\infty} m(t-s)x(s)ds.$$

Since we can't be expected to output more information about $x_o(t)$ then actually exists on the OGO tape we will assume that our task is to reproduce the band limited function $\hat{x}_o(t)$ on the shaker. Hence in the error analysis the possible outputs will be compared with $\hat{x}_o(t)$ to obtain error bounds.

## 4.3. ERROR SOURCES

There are two major sources of error. The first is in the data processing involved in computing input function to the shaker. This actually consists of the various aliasing and quantizing errors. However, due to convenience, the electrical noise involved in determining the shaker's transfer function (preshaker amplifier and accelerometer noise) is included in this error source. The second error occurs when we attempt to input the computed control function to the shaker. This error is due to the physical mechanism involved in transforming a digitally defined function into an analog signal and to non-linearities inherent in the system.

For example suppose the ideal input to the shaker is $f(t) = \sum_{n=-\infty}^{\infty} f(t_n) \frac{\sin w_o(t-t_n)}{w_o(t-t_n)}$.

Due to data processing errors we will compute $f(t_n) + \epsilon(t_n)$ $n = 0, 1, \ldots, N-1$ ($\epsilon(t_n)$ denoting the data processing error). But due to the physical mechanisms involved we actually input to the shaker a smoothed version of

$$f(t) = \sum_{n=0}^{N-1} \left[f(t_n) + E(t_n)\right] \pi(t-t_n) + N(t)$$

where $$\pi(\tau) \triangleq \begin{cases} 1, & \tau \in (0, \Delta t] \\ 0, & \tau \notin (0, \Delta t] \end{cases}$$

and N(t) is amplifier noise.

Finally the shaker may not react to the input signal in a linear fashion as we hypothesized, thus introducing additional errors.

The data processing errors will be treated in section 4.4 - 4.6. The "physical mechanisms" error will then be treated in section 4.7 - 4.8.

## 4.4. NOTATION AND PRELIMINARIES

Let f(t) be a function defined on the real line. $\mathcal{F}f(\omega)$ and $\mathcal{F}^{-1}(t)$ will denote its Fourier transform and inverse Fourier transform respectively. We will sample f(t) at the points $t_n = n\Delta t$, n = 0, 1, ...N-1 and define $T = N\Delta t$, $\omega_j = \frac{1}{j\Delta t}$, j = 0, 1, ...N-1. $F_o$ will denote the fast Fourier transform (F F T) of $f(t_n)$

i.e. $$F_o f(\omega_j) \triangleq \frac{1}{N} \sum_{n=0}^{N-1} f(t_n)\, e^{\frac{-2\pi i n j}{N}}$$

$F_o^{-1}$ will denote the inverse F F T

(Due to the particular form of the F F T algorithm we will assume $N = 2^k$ for some $k > 0$).

It will prove useful to define Ff(ω) as follows:

$$Ff(\omega) \triangleq \begin{cases} \mathcal{F}f(\omega), & 0 < \omega \le \frac{1}{2\Delta t} \\ \mathcal{F}f(\omega - F), & \frac{1}{2\Delta t} < \omega \le \frac{1}{\Delta t} \\ \text{extended periodically for other values of } \omega \end{cases}$$

We will assume that all discretizing will be performed with a quantizing box of height $\Delta h$ and that the errors in measurements due to quantizing are independent random variables.

$x(t)$ will represent the time history on the OGO tape and $\tilde{x}(t_n) = x(t_n) + N_x(t_n)$ will represent the sampled version of $x(t)$, where $N_x(t_n)$ denotes the error due to quantizing and noise in measuring $x(t_n)$. In determining the transfer function $\varphi(\omega)$ of the system we will let $z(t)$ denote the actual output of the system corresponding to an input $y(t)$. $\tilde{z}(t_n) = z(t_n) + N_z(t_n)$, $\tilde{y}(t_n) = y(t_n) + N_y(t_n)$ will denote the measured output and input respectively. We assume $\tilde{z}$ and $\tilde{y}$ are adjusted measurements obtained by adding $\frac{h}{2}$ to the actual measurements and hence $E\,N(t_n) = 0$ ($E \triangleq$ expectation operator).

$\varphi$ will represent the transfer function of the system,

i.e. $\varphi(\omega) = \dfrac{\mathcal{F}z(\omega)}{\mathcal{F}y(\omega)}$, and $\tilde{\varphi}$ will represent the computed transfer function,

$$\tilde{\varphi}(\omega_j) \triangleq \frac{F_o\tilde{z}(\omega_j)}{F_o\tilde{y}(\omega_j)} \qquad j = 0, 1, \ldots N-1$$

$\epsilon_x(\omega_j)$, $\epsilon_y(\omega_j)$, $\epsilon_z(\omega_j)$ will represent the frequency domain aliasing of x, y and z respectively.

Precisely:

$$\epsilon_z(\omega_j) \triangleq \begin{cases} \sum_{k\neq 0} \mathcal{F}z\left(\omega_j + \frac{k}{\Delta t}\right) & 0 \leq j < \frac{N}{2} \\ \sum_{k\neq -1} \mathcal{F}z\left(\omega_j + \frac{k}{\Delta t}\right) & \frac{N}{2} \leq j < N-1 \end{cases}$$

$\delta_x(t_n)$, $\delta_y(t_n)$ and $\delta_z(t_n)$ will represent the time domain aliasing error.

i.e. $\delta_z(t_n) \triangleq -\sum_{k\neq 0} z(t_n + kT)$

We will use repeatedly the following lemma relating the continuous and discrete Fourier transform.

lemma 1 (pg. 36 IBM Report)[1]

If f(t) is a function having a continuous Fourier transform then:

$$T\left[F_o \sum_{k=-\infty}^{\infty} f(t_n + kT \cdot \right](\omega_j) = \sum_{k=-\infty}^{\infty} \mathcal{F}f(\omega_j + \frac{k}{\Delta t}) \quad j=0, 1, \ldots N-1$$

i.e. $TF_o f = Ff + \epsilon_f + TF_o \delta_f$

[1] Cooley, J.W., Lewis, P.A.W., Welch, P.O., "The Fast Fourier Transform Algorithm and It's Applications", IBM Research Report RC 1743, Feb. 1967

## 4.5. DATA PROCESSING ERRORS

In order to minimize aliasing errors in the frequency domain it turns out that we should electronically filter the OGO tape before sampling and thus assume $x(t) = \hat{x}_o(t)$ is the band limited signal to be output on the shaker. However, with a slight gain in generality, we will assume $x(t)$ is to be filtered digitally.

Assuming the transfer function of the filter, $M \triangleq \mathcal{F}m$, is known we proceed as follows in our attempt to output $\hat{x}_o(t)$. We sample $x(t)$, getting $\tilde{x}(t_n)$, $n = 0, 1, \ldots, N-1$ and try to input to shaker a trigonometric interpolation of

$$F_o^{-1} \frac{MF_o\tilde{x}}{\tilde{\varphi}}(t_n) \quad n = 0, 1, \ldots N-1$$

i.e. we try to input:

$$\hat{f}(t) = \sum_{n=0}^{N-1} \hat{f}(t_n) \frac{\sin \omega_o(t-t_n)}{\omega_o(t-t_n)}$$

where $\omega_o \triangleq \frac{\Pi}{\Delta t}$ and $\tilde{f}(t_n) \triangleq F_o^{-1} \left| \frac{MF_o\tilde{x}}{\tilde{\varphi}} \right| (t_n) \quad n = 0, 1, \ldots N-1$

Now $\hat{f}(t_n) = F_o^{-1} \left| \frac{1}{T} \frac{FX \cdot M}{\varphi} + E_1 \right| (t_n)$

where $E_1(\omega_j) \triangleq M \left| \frac{F_o\tilde{x}}{\tilde{\varphi}} - \frac{1}{T} \frac{FX}{\varphi} \right| (\omega_j).$ (1)

and it follows from lemma 1 that:

$$\hat{f}(t_n) = \mathcal{F}^{-1} \left(M \frac{\mathcal{F}x}{\varphi}\right)(t_n) + F_o^{-1} E_1 - \Delta_f \quad \text{, see figure 1}$$

Since the ideal input to the shaker is

$$f(t) = \sum_{n=-\infty}^{\infty} f(t_n) \frac{\sin \omega_o(t-t_n)}{\omega_o(t-t_n)} \qquad (2)$$

where $f(t_n) \triangleq \mathcal{F}^{-1}\left(M \frac{\mathcal{F}x}{\varphi}\right)$, the data processing error in the input will be:

$$E_2(t) \triangleq \sum_{n=0}^{N-1} (F_o^{-1}E_1 - \delta_f) \frac{\sin \omega_o(t-t_n)}{\omega_o(t-t_n)} - \left(\sum_{n=-\infty}^{-1} + \sum_{n=N}^{\infty}\right) f(t_n) \frac{\sin \omega_o(t-t_n)}{\omega_o(t-t_n)} \qquad (3)$$

i.e. $\hat{f}(t) = f(t) + E_2(t)$ where $E_2$ is defined above.

Hence the actual error E in the output, due to data processing will be:

$$E = \mathcal{F}^{-1}(\varphi \mathcal{F} E_2) \qquad (4)$$

Before we actually compute $E_1$ (and hence $E_2$) let us first attempt to get an easily computable expression for E(t). It follows from lemma 1 and the fact that $E_2(t)$ is band limited that:

$$FE_2 = TF_oE_2 - TF_o\,\delta_{E_2} = TF_o(F_o^{-1}E_1 - \delta_f) - TF_o\,\delta_{E_2}$$

at points $\omega_j$ $j=0, 1, \ldots, N-1$.

But from the definition of $\delta_{E_2}$ and (3) we have that $F_o\delta_f(\omega_j) = -F_o\delta_{E_2}(\omega_j)$ $j=0, 1, \ldots N$
Hence $FE_2 = TE_1$ at points $\omega_j$ and we have

$$FE(\omega_j) = \varphi(\omega_j)\, FE_2(\omega_j) = T\varphi(\omega_j)\, E_1(\omega_j)$$

$j=0, 1, \ldots N-1$. Using lemma 1 again and the fact that E must also be band limited we have:

$$F_oE(\omega_j) + F_o\delta_E(\omega_j) = \frac{FE(\omega_j)}{T} \qquad j=0, 1, \ldots N-1.$$

$$\text{or: } E(t_n) = F_o^{-1}\left(\frac{FE}{T} - F_o\delta_E\right)(t_n) = F_o^{-1}(\cdot E_1)(t_n) - \delta_E(t_n)\ .$$

Thus we may write the following expression for E(t) in terms of $E_1$:

$$E(t) = \sum_{n=0}^{N-1} F_o^{-1}(\varphi \cdot E_1)(t_n) \frac{\sin \omega_o(t-t_n)}{\omega_o(t-t_n)} \qquad (5)$$

$$- \sum_{n=0}^{N-1} \delta_E(t_n) \frac{\sin \omega_o(t-t_n)}{\omega_o(t-t_n)} + \left( \sum_{n=-\infty}^{-1} + \sum_{N}^{\infty} \right) E(t_n) \frac{\sin \omega_o(t-t_n)}{\omega_o(t-t_n)}$$

And since we are only interested in the error $E(t)$ for $t \in [0, T]$ we can disregard the last two terms on the right as being of second order.

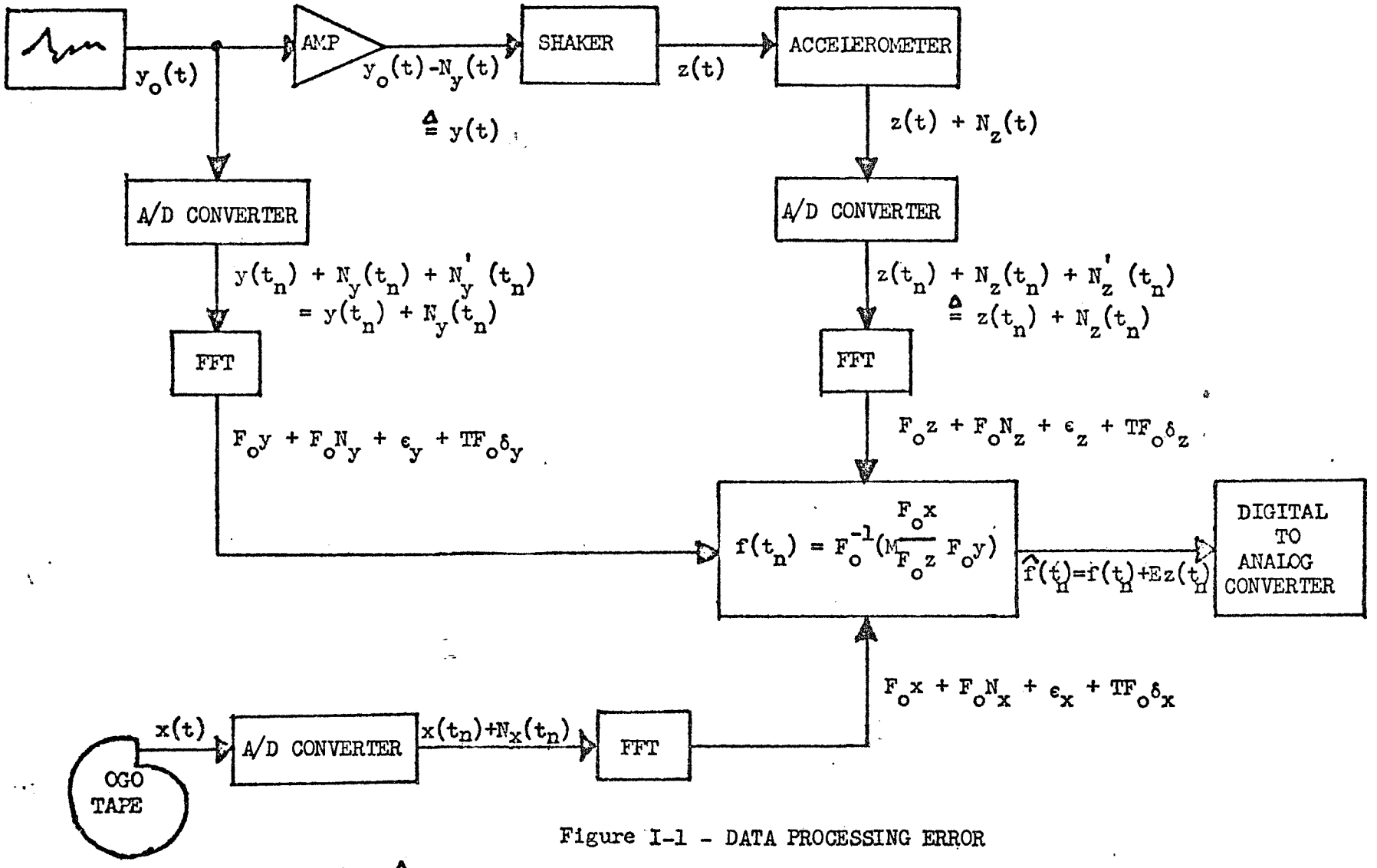



Figure I-1 - DATA PROCESSING ERROR

$Ez(t) \triangleq$ data processing error in input to shaker, it corresponds to an error in output of $E(t) = \mathcal{F}^{-1}(\varphi \cdot E_2)$ .

$Ez(t_n) = F_o^{-1} E_1 - \delta_f$ where $E_1$ is defined by (1) of subsection 4.5.

Computing $E_1$. Recall $E_1$ was defined to be $M\left(\frac{F_o\tilde{x}}{\tilde{\varphi}} - \frac{1}{T}\frac{Fx}{\varphi}\right)$. Now it follows from lemma 1 that : $TF_o\tilde{y}(\omega_j) = Fy(\omega_j) + \epsilon y(\omega_j) + TF_o\delta_y(\omega_j) + TF_oN_y(\omega_j)$

where $y(t)$ is the impulse input to the shaker and $\epsilon_y$, $\delta_y$, $N_y$ are defined in section 4.4. Similarly we have for the response $z(t)$ to $y(t)$:

$$TF_o\tilde{z}(\omega_j) = Fz(\omega_j) + \epsilon z(\omega_j) + TF_o\delta_z(\omega_j) + TF_oN_z(\omega_j)$$

Hence, the error in the computed transfer function $\tilde{\varphi} = \dfrac{F_o\tilde{z}}{F_o\tilde{y}}$ at points $\omega_j$, $j = 0, 1, \ldots, N-1$ is:

$$\left|\frac{F_o\tilde{z}}{F_o\tilde{y}} - \frac{Fz}{Fy}\right| = \left|\frac{Fz + \epsilon z + TF_o\delta_z + TF_oN_z}{Fy + \epsilon y + TF_o\delta_y + TF_oN_y} - \frac{Fz}{Fy}\right|$$

and disregarding second order terms we have:

$$= \frac{Fy(\epsilon_z + TF_o\delta_z + TF_oN_z) - Fz(\epsilon y + TF_o\delta_y + TF_oN_y)}{(Fy)^2}$$

$$= \frac{1}{Fy}\left[\epsilon_z + TF_o\delta_z - \varphi(\epsilon_y + TF_o\delta_y)\right] + \frac{T}{Fy}\left[F_oN_z - \varphi F_oN_y\right]$$

Let us temporarily denote the first term on the right as $E_1^A$ and the second as $E_1^Q$ then $\dfrac{F_o\tilde{x}}{\tilde{\varphi}} = \dfrac{Fx + \epsilon_x + TF_o\delta_x + TF_oN_x}{T(\varphi + E_1^A + E_1^Q)}$

Hence by the definition of $E_1$ we have:

$$\frac{E_1}{M} = \frac{F_o\tilde{x}}{\tilde{\varphi}} - \frac{1}{T}\frac{Fx}{\varphi} \simeq \frac{\varphi(\epsilon_x + TF_o\delta_x + TF_oN_x) - Fx(E_1^A + E_1^Q)}{T\varphi}$$

$$= \frac{1}{T\varphi}\left(TF_oN_x - \frac{FxE_1^Q}{\varphi}\right) + \frac{1}{T\varphi}\left(\epsilon_x + TF_o\delta_x - \frac{FxE_1^A}{\varphi}\right)$$

or from the definition of $E_1^Q$ and $E_1^A$

$$\frac{E_1}{M} = \frac{1}{\varphi}\left\{F_oN_x - \frac{1}{\varphi}\frac{Fx}{Fy}\left[F_oN_z - \varphi F_oN_y\right]\right\}$$

$$+\frac{1}{T\varphi}\left\{\epsilon_x + TF_o\delta_x - \frac{Fx}{\varphi Fy}\left[\epsilon_z + TF_o\delta_z - \varphi\left(\epsilon_y + TF_o\delta_y\right)\right]\right\}.$$

Since $\varphi = \frac{Fz}{Fy}$ for $\omega \in \left[0, \frac{1}{\Delta_t}\right]$ we have

$$\frac{E_1}{M} = \frac{1}{\varphi}\left\{F_oN_x - \frac{Fx}{Fz}\left(F_oN_z - \frac{FzF_oN_y}{Fy}\right)\right\}$$

$$+\frac{1}{T\varphi}\left\{\epsilon_x + TF_o\delta_x - \frac{Fx}{Fz}\left[\epsilon_z + TF_o\delta_z - \frac{Fz}{Fy}\left(\epsilon_y + TF_o\delta_y\right)\right]\right\}.$$

Thus:

$$E_1 = \frac{M}{\varphi}\left\{\left[F_oN_x - \frac{Fx}{Fz}F_oN_z + \frac{Fx}{Fy}F_oN_y\right] + \left(\frac{\epsilon_x}{T} + F_o\delta_x\right) + \frac{Fx}{Fy}\left(\frac{\epsilon_y}{T} + F_o\delta_y\right) - \frac{Fx}{Fz}\left(\frac{\epsilon_z}{T} + F_o\delta_z\right)\right. \quad (6)$$

completing the computation of $E_1$.

Estimating the output error E(t).

From the definition of E(t), (5), and the computed $E_1$, (6) we get:

$$F_oE(\omega_j) = M\left\{\left(F_oN_x + \frac{Fx}{Fy}F_oN_y - \frac{Fx}{Fz}F_oN_z\right)\right. \quad (7)$$

$$\left.+\left(\frac{\epsilon_x}{T} + F_o\delta_x\right) + \frac{Fx}{Fy}\left(\frac{\epsilon_y}{T} + F_o\delta_y\right) - \frac{Fx}{Fz}\left(\frac{\epsilon_z}{T} + F_o\delta_z\right)\right\}(t_n)$$

Now by Parseval's theorem we have:

$$\frac{1}{N}\sum_{n=0}^{N-1} E^2(t_n) = \sum_{j=0}^{N-1} |F_o E(w_j)|^2$$

Substituting (7) into this we will have a bound on the mean square error.

In order to get an absolute bound on the error in $E(t_n)$, n=0, 1, ...N-1, notice that from the definition of $F_o$ we have:

$$|E(t_n)| = \left|\sum_{j=0}^{N-1} F_o E(w_j)\, \ell^{\frac{2\pi i n j}{N}}\right| \quad \text{and it follows from (7) that}$$

$$|E(t_n)| \le \left|F_o^{-1} \cdot M\left(F_o N_x + \frac{Fx}{Fy} F_o N_y - \frac{Fx}{Fz} F_o N_z\right)\right| \qquad (8)$$

$$+ \sum_{j=0}^{N-1} \left| \sum_{\beta=x,y,z} \frac{MFx}{F\beta}\left(\frac{\epsilon_\beta}{T} + F_o \delta_\beta\right)\right|$$

Let us temporarily denote the two terms on the right by $E_r$ and $E_d$ respectively. $E_r(t_n)$ is the absolute value of a random varaible. We compute its mean and variance as follows:

For $\beta = x, y, z$ $N_\beta(t_n)$, n = 0, 1, ..., N-1 are assumed to be independent random variables with mean zero and variance $V_\beta = \frac{(\Delta h)^2}{12} + v_\beta$ where $\Delta h \triangleq$ size of quantizing box used when sampling $\beta$.
and $v_\beta \triangleq$ variance of the noise in the signal $\beta$.

Now since:

$$E\left[F_o N(w_n) \cdot \overline{F_o N(w_m)}\right] = E\,\frac{1}{N^2}\sum_{j=0}^{N-1}\sum_{k=0}^{N-1} N(w_j)N(w_k)\exp\left(\frac{-2\pi i j n}{N} + \frac{2\pi i k m}{N}\right)$$

$$= \frac{V}{N^2}\sum_{j=0}^{N-1}\exp\left(\frac{2\pi i (m-n) j}{N}\right) = \frac{V}{N}\,\delta_{n,m}$$

It follows that $\left\{ M\frac{Fx}{F\beta} F_o N_\beta(w_j) : j = 0, 1, \ldots N-1 \right\}$ are orthogonal random variables with mean zero and variance: $\left| M\frac{Fx}{F\beta}(w_j) \right|^2 \frac{V_\beta}{N}$

Similarly we can show that:

$$\left\{ F_o^{-1} \left(M\frac{Fx}{F\beta} F_o N_\beta\right)(t_n),\ n = 0, 1, \ldots N-1 \right\} \text{ are}$$

random variables with mean zero and variance $\frac{V_\beta}{N} \sum_{j=0}^{N-1} \left| M\frac{Fx}{F\beta}(w_j) \right|^2$ .

Thus we have for each $t_n$ that:

$$E_r(t_n) = \left| \sum_{\beta=x,y,z} E_Q\beta \right| \qquad \text{where:} \qquad (9)$$

$\left\{ E_Q\beta : \beta = x, y, z \right\}$ are independent random variables with mean zero and variance $\left\| M\frac{Fx}{F\beta} \right\|^2 V_\beta$ where the norm $\|\cdot\|$ is defined by:

$$\|f\| = \left( \frac{1}{N} \sum_{n=0}^{N-1} |f(t_n)|^2 \right)^{1/2}$$

Next we bound $E_d$, the second term in (8)

$$E_d = \sum_{j=0}^{N-1} \left| \sum_{\beta = x, y, z} \frac{MFX}{F\beta} \left( \frac{\epsilon_\beta}{T} + F_o\delta_\beta \right) \right|$$

$$\leq \sum_{\beta=x,y,z}^{N-1} \sum_{j=0}^{N-1} \left| \frac{MFX}{F\beta} \right| \left( \left| \frac{\epsilon_\beta}{T} \right| + \left| F_o\delta_\beta \right| \right)$$

And by the triangle inequality and Schwartz's inequality this gives:

$$E_d \leq \sum_{\beta=x,y,z} \left( \sum_{j=0}^{N-1} \left| \frac{MFX}{F\beta} \right|^2 \right)^{1/2} \left[ \left( \sum_{j=0}^{N-1} \left| \frac{\epsilon_\beta}{T} \right|^2 \right)^{1/2} + \left( \sum_{j=0}^{N-1} \left| F_o\delta_\beta \right|^2 \right)^{1/2} \right]$$

Now by Parseval's theorem*

$$\left( \sum_{j=0}^{N-1} \left| F_o\delta_\beta \right|^2 \right)^{1/2} = \left( \frac{1}{N} \sum_{n=0}^{N-1} \left| \delta_\beta(t_n) \right|^2 \right)^{1/2}$$

and hence:

$$E_d \leq \sum_{\beta=x,\ y,\ z} \left( \sum_{j=0}^{N-1} \left| \frac{MFX}{F\beta} \right|^2 \right)^{1/2} \left[ \left( \sum_{j=0}^{N-1} \left| \frac{\epsilon_\beta}{T} \right|^2 \right)^{1/2} + \left( \sum_{j=0}^{N-1} \left| F_o \delta_\beta \right|^2 \right)^{1/2} \right]$$

$$= \sum_{\beta=x,\ y,\ z} \left\| \frac{MFX}{F\beta} \right\| \left( \frac{N}{T} \left\| \epsilon_\beta \right\| + (N)^{1/2} \left\| \delta_\beta \right\| \right) \qquad (10)$$

Summarizing we have from (8), (9), and (10) that

$$\left| E(t_n) \right| \leq \left| \sum_{\beta=x,\ y,\ z} E^{Q}\beta \right| + \sum_{\beta=x,\ y,\ z} \left\| M \frac{FX}{F\beta} \right\| \left( \frac{N}{T} \left\| \epsilon_\beta + \sqrt{N} \left\| \delta_\beta \right\| \right) \right)$$

where $E_Q\beta$ is a random variable with mean zero and variance $\left\| M \frac{FX}{F\beta} \right\|^2 \left[ \frac{(\Delta h)^2}{12} + v_\beta \right]$

---

* I.B.M. Report page 11.

## 4.6 Practical Error Bounds

It follows from section 4.5 that the output error has the form:

$$E(t) = \sum_{n=0}^{N-1} E(t_n) \frac{\sin \omega_o(t-t_n)}{\omega_o(t-t_n)}$$

where $\omega_o = \frac{\pi}{\Delta t}$ and the $E(t_n)$ are bounded as follows:

$$|E(t_n)| \leq \sum_{\beta=x,y,z} \left\| M \frac{Fx}{F\beta} \right\| \left( \frac{N}{T} \left\| \epsilon_\beta \right\| + \sqrt{N} \left\| \delta_\beta \right\| \right) \qquad (9)$$

$$+ \left| \sum_{\beta=x,y,z} E_Q\beta \right|$$

Here the norm $\|\cdot\|$ is defined by:

$$\|f\| \triangleq \left( \frac{1}{N} \sum_{n=0}^{N-1} |f(t_n)|^2 \right)^{1/2}$$

and $E_Q\beta$ is a random variable with mean zero and variance

$$V_\beta = \left\| M \frac{Fx}{F\beta} \right\|^2 \left[ \frac{(\Delta h)^2}{12} + V_\beta \right] \qquad (10)$$

($V_\beta$ = variance of physical noise in $\beta$)

Bound on the error due to the noise alone.

From (9) we have:

$$|E(t_n)| \leq \left| \sum_{\beta = x,y,z} E_Q\beta \right|$$

where $E_Q\beta$, $\beta = x, y, z$, are independent random variables with mean zero and variance given by (10). Notice that in (10) $\Delta h$ is actually a function of $\beta$, that is for each $\beta$, $\beta = x, y, z$:

$$\Delta h = \frac{\text{scale factor for } \beta}{2^K}$$

where k = number of bits in digitizer. Hence from now on we will write $\Delta h = \Delta x, \Delta y, \Delta z$ when $\beta = x, y, z$ respectively.

Now by the definition of the problem $v_x = 0$ and thus:

$$V_x \leq \frac{(\Delta x)^2}{12}$$

$$V_y \leq \left\| M \frac{Fx}{Fy} \right\|^2 \left[ \frac{(\Delta y)^2}{12} + v_y \right]$$

where $v_y$ is the variance of the amplifier noise $N_y$.

$$V_z \leq \left\| M \frac{Fx}{Fz} \right\|^2 \left[ \frac{(\Delta z)^2}{12} + v_z \right]$$

where $v_z$ is the variance of the accelerometer noise $N_z$.

Determination of $v_z$

$v_z$ can be determined by an analysis of the power spectral density of $N_z(t)$ as follows:

For large N:

$$v_z \cong \frac{1}{N} \sum_{n=0}^{N-1} N_z^2(t_n) ,$$

By Parseval's theorem:

$$\frac{1}{N} \sum_{n=0}^{N-1} N^2(t_n) = \sum_{j=0}^{N-1} \left| F_o N(\omega_j) \right|^2$$

Hence

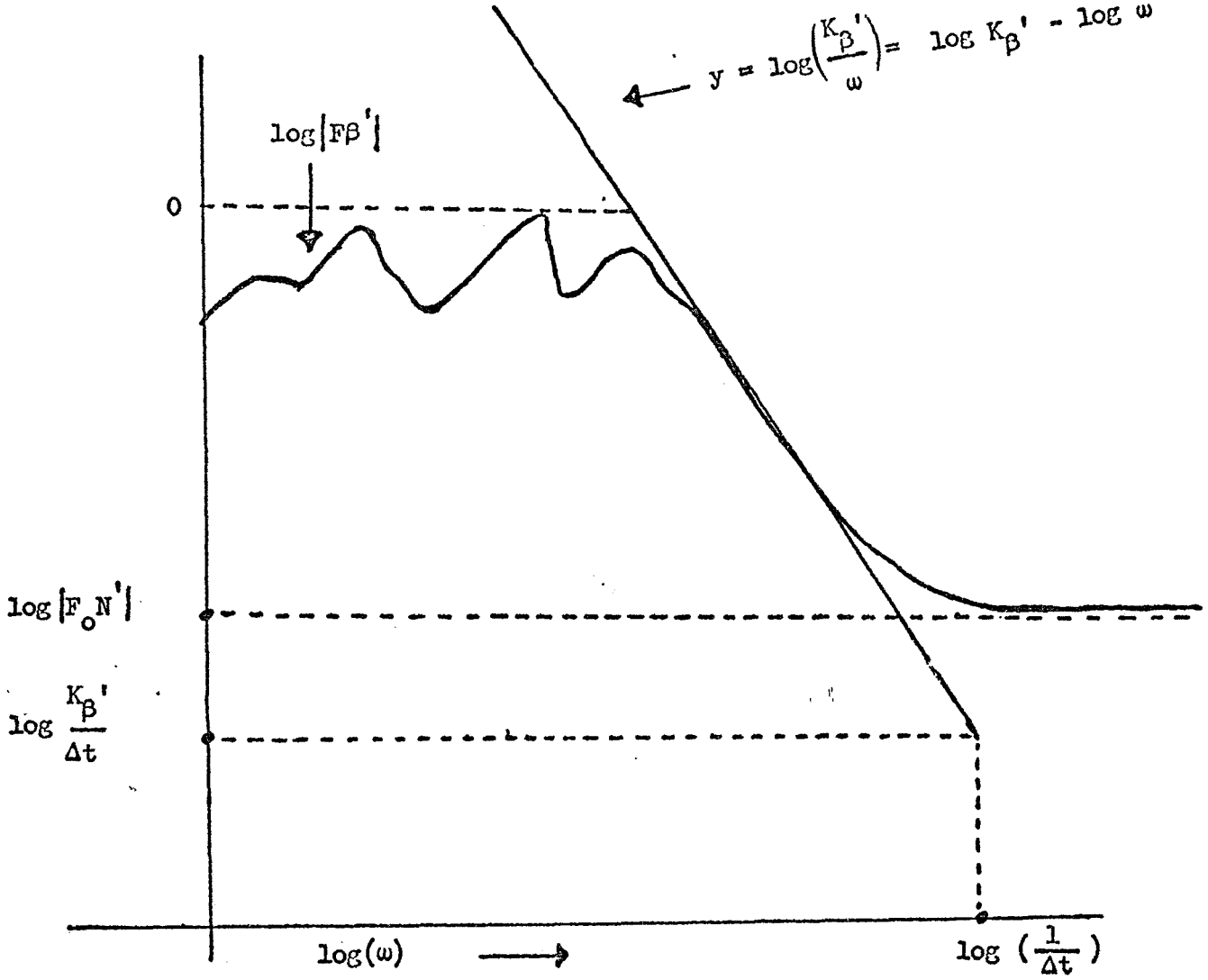
$$v_z \cong \sum_{j=0}^{N-1} \left| F_o N_z(\omega_j) \right|^2$$

Now since $N_z(t)$ is assumed to be white, $F_o N_z(\omega)$ is constant and hence:

$$v_z \cong N \left| F_o N_z(\omega) \right|^2$$

the constant $|F_o N_z(\omega)|^2$ can be determined by technique illustrated in Figure 2 from either the measured output $F_o\tilde{z}$ (computed when determining $\varphi$) or from the spectral density of $N_o(t)$. $N_o(t)$ is needed to determine $v_y$ and is defined in the following paragraphs. Notice that in Figure 2 the graph is of $z'(t)$, the normalized $z(t)$. Thus:

$$\log |F_o N_z| = \log |F_o N_z'| + \log \left| \max_j F_o N(\omega_j) \right|$$




Estimating $e_\beta$ and $v_\beta$ from log-log graph of $\beta$. Note here FB' is the normalized FB, i.e. $FB'(\omega) = \dfrac{FB(\omega)}{\max_j |FB(\omega_j)|}$

Figure I-2 - TYPICAL FOURIER TRANSFORM MODULUS

In our model we have treated the amplifier noise as an additive white noise which is introduced somewhere between digitizing the input signal $y_o(t)$ and the amplification of this signal. Then we treat the amplifier and shaker as a single unit, and calculate the transfer function of this unit. This is justified by the assumption that the amplifier has a constant gain k and hence a white amplifier noise N(t) can be considered to be the result of an equivalent $N_y(t) = \frac{N(t)}{k}$ introduced prior to amplification. However, since the signal is digitized prior to entering the amplifier, an analysis of the digitized signal $y_o(t)$ will not give any indication of the variance $v_y$. The following technique is suggested for the computation of $v_y$.

Determination of $v_y$

With amplifier on but with no input signal, record the F.F.T. (or P.S.D.) of output at shaker for as many data points as possible. We assume that the noise level is the same with or without an input signal to amplifier. The computed transform is:

$$F_o N_o = \varphi(\omega)\, F_o N_y(\omega) + F_o N_z(\omega)$$

where $\varphi(\omega)$ is the transfer function of the shaker. Since $N_y$ and $N_z$ are independent sequences with zero mean we have for N sufficiently large.

$$\sum_{j=0}^{N-1} \left|\varphi(\omega_j)\, F_o N_y(\omega_j) + F_o N_z(\omega_j)\right|^2$$

$$\cong \sum_{0}^{N-1} \left|\varphi(\omega_j)\, F_o N_y(\omega_j)\right|^2 + \sum_{j=0}^{N-1} \left|F_o N_z(\omega_j)\right|^2$$

$$\cong \sum_{j=0}^{N-1} \left|\varphi(\omega_j)\, F_o N_y(\omega_j)\right|^2 + v_z$$

Since $\varphi(\omega_j)$ and $F_o N(\omega_j)$ are independent we have that for large N:

$$\frac{1}{N} \sum_{0}^{N-1} \left|\varphi(\omega_j)\, F_o N_y(\omega_j)\right|^2 \cong \frac{1}{N} \sum_{0}^{N-1} \left|\varphi(\omega_j)\right|^2 \cdot \frac{1}{N} \sum_{0}^{N-1} \left|F_o N_y(\omega_j)\right|^2$$

$$= \frac{\|\varphi\|^2}{N}\, v_y$$

thus $\sum_{0}^{N-1} |F_o N_o(\omega_j)|^2 \cong \|\varphi\|^2 \; v_y + v_z$ or:

$$v_o = \|\varphi\|^2 \; v_y + v_z$$

where $v_o \triangleq$ variance of output noise $N_o$.

In (9) we consider the error in the shaker output due to computing the incorect input f(t). As was pointed out in the Subsection 4.3 there also exists possible errors resulting from the digital to analog conversion of f(t) and errors due to additional amplifier noise when we try to input f(t) to shaker. For completeness we will include in this subsection a bound on this additional amplifier noise.

It can be shown, by arguments similar to those in 4.6 that this error is bounded by a random variable N(t) with mean zero and variance:

$$V_N = \left\| M \frac{Fz}{Fy} \right\| \; v_y$$

where $v_y$ denotes the variance of the amplifier noise discussed in previous paragraphs.

Bound on error due to aliasing along.

From (9) we have:

$$|E(t_n)| \leq \sum_{\beta=x,y,z} \left\| M \frac{Fx}{F\beta} \right\| \left( \frac{N}{T} \|\epsilon_\beta\| + \sqrt{N} \, \|\delta_\beta\| \right) \qquad (11)$$

For computational reasons let's let $\beta'(t)$ represent the normalized $\beta(t)$, that is:

$$\beta'(t) \triangleq \frac{\beta(t)}{\max\limits_{j<\frac{N}{2}-1} |F \, \beta(\omega_j)|}$$

then (11) becomes:

$$\frac{|E(t_n)|}{\max\limits_{j=\frac{N}{2}-1} |Fx(\omega_j)|} \leq \sum_{\beta=x',y',z'} \left\| M \frac{Fx'}{F\beta} \right\| \left( \frac{N}{T} \|\epsilon_B\| + \sqrt{N} \, \|\delta_B\| \right)$$

We will now attempt to get bounds on $\|\epsilon_\beta\|$ and $\|\delta_\beta\|$ $\beta = x', y', z'$ in terms of physically measurable quantities.

a. $\epsilon_\beta$ (Aliasing in the frequency domain)

For all practical purposes we can assume*

$$\epsilon_\beta(\omega_j) = \begin{cases} \mathcal{F}\beta(\omega_j - \frac{1}{\Delta t}) + \mathcal{F}\beta(\omega_j + \frac{1}{\Delta t}) & , 0 \le j < \frac{N}{2} - 1 \\ \mathcal{F}\beta(\omega_j) + \mathcal{F}\beta(\omega_j - \frac{2}{\Delta t}) & , \frac{N}{2} - 1 \le j < N-1 \end{cases}$$

From the continuity properties of $\beta(t)$, $\beta = x, y, z$, we can assume that $\mathcal{F}\beta(\omega)$ has the form $\mathcal{F}\beta(\omega) = \frac{k_\beta}{\omega}$ for some $K_\beta > 0$** . So as a crude bound on $\epsilon_\beta$ we have

$$|\epsilon_\beta| \le \frac{K_\beta}{\Delta t} \quad \text{or} \quad \log |\epsilon_\beta| \le \log K_\beta - \log \frac{1}{\Delta t}$$

Thus $\log \|\epsilon_\beta\| \le \log\left(\frac{K_\beta}{\Delta t}\right)$ and the $\log\left(\frac{K_\beta}{\Delta t}\right)$ , $\beta = x', y', z'$ can be estimated from the log-log graph of x, y, z, see Figure 2.

# APPENDIX II - VIBRATION TEST SYSTEM DISTORTION MEASUREMENTS

One objective of the transient waveform feasibility familiarization study, using G.S.F.C. test equipment, was to measure low frequency harmonic distortion in typical vibration systems.

A test plan was submitted to G.S.F.C. defining the test procedure. Five G.S.F.C. systems were tested by G.S.F.C.; one Boeing system was tested by Boeing. The Boeing system harmonic distortion data can be considered baseline since the Transient Waveform Control System is operational on this amplifier/exciter combination.

Each amplifier/exciter system was driven with a sinusoidal signal at maximum allowable deflection. Both the amplifier input signal and armature acceleration response were recorded for 60 seconds. The recording speed was 7.5 inches per second. The driving frequencies were 2 Hz, 5 Hz, 10 Hz, 15 Hz, 20 Hz, 50 Hz, and 100 Hz. This was repeated at 20%, 40%, 60%, and 80% of maximum allowable deflection.

The data was analyzed by Boeing with a Hewlett Packard 331A distortion analyzer. The FM tapes were played back at 60 inches per second. This 8 to 1 speed increase translated 2 Hz information to 16 Hz that is within the 5 Hz lower rated limit of the distortion analyzer.

The percent of harmonic distortion was plotted versus frequency for each system. Figure II-1 shows the percent of harmonic distortion measurements of the Boeing L-249, PP-120/150 system used in the Transient Waveform Control System. Figures II-2 through II-6 show percent of harmonic distortion of the G.S.F.C. vibration equipment. This test equipment characteristic is a direct index of the expected controlled waveform fidelity.

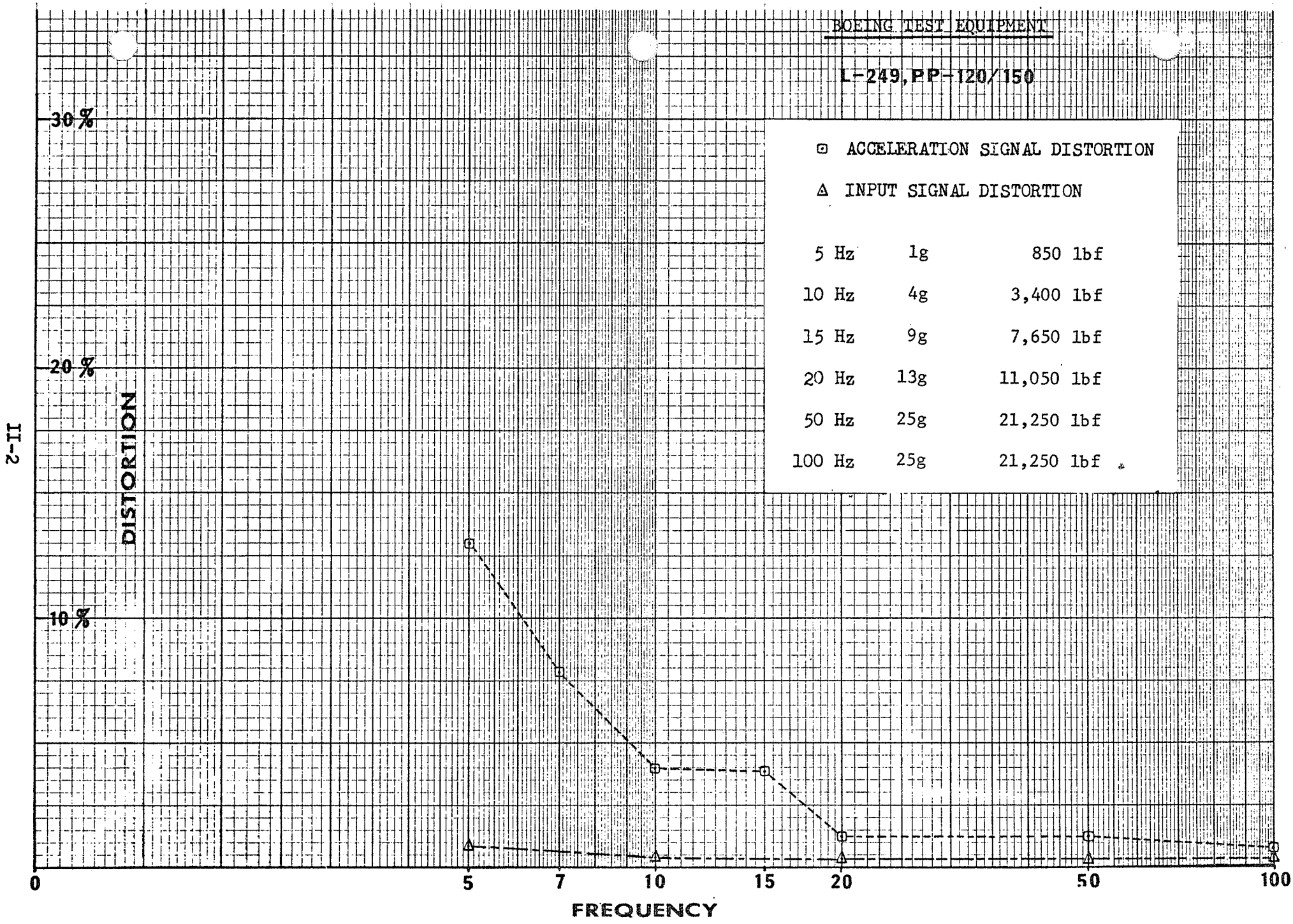



Figure II-1: VIBRATION SYSTEM DISTORTION

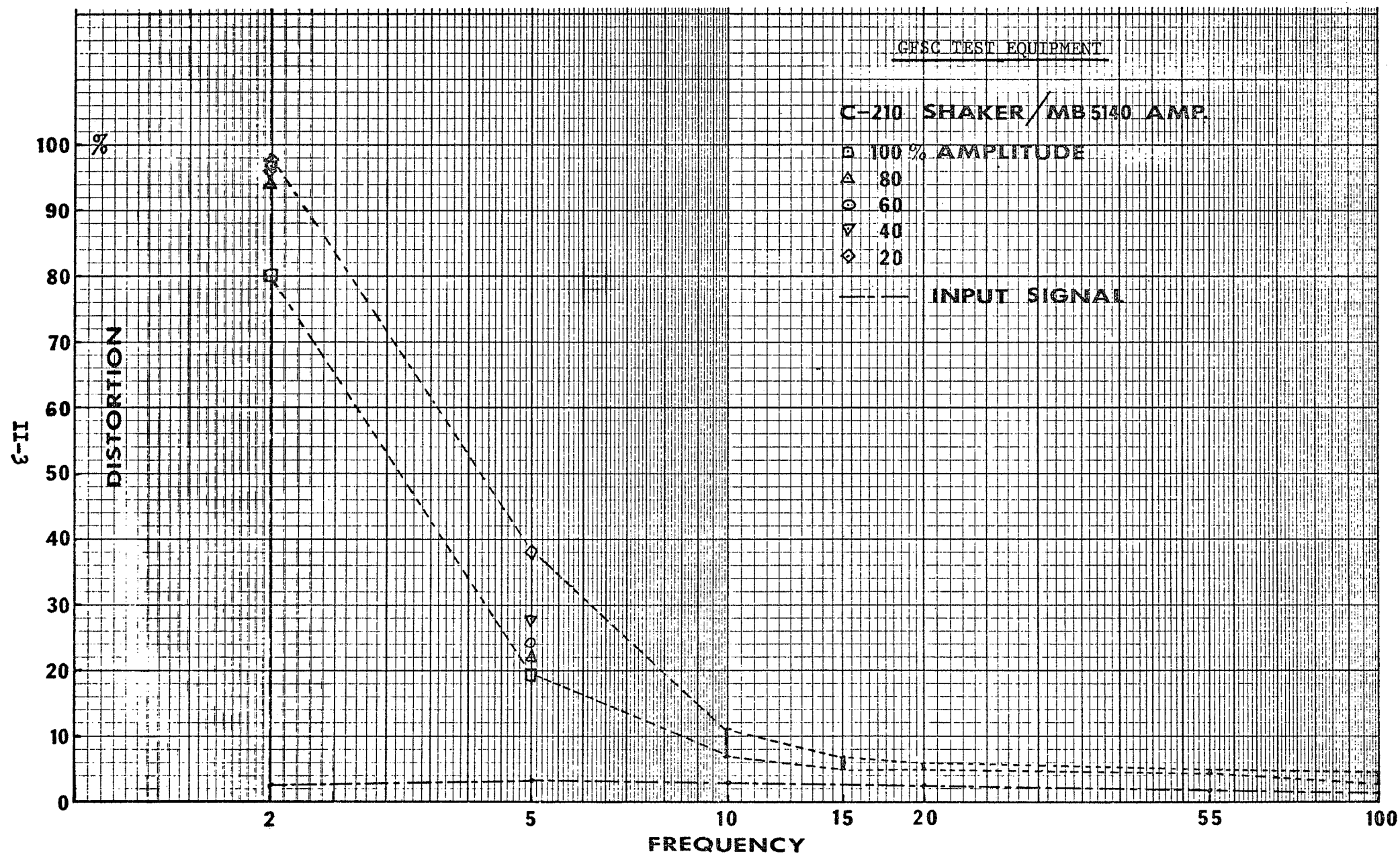



Figure II-2: VIBRATION SYSTEM DISTORTION

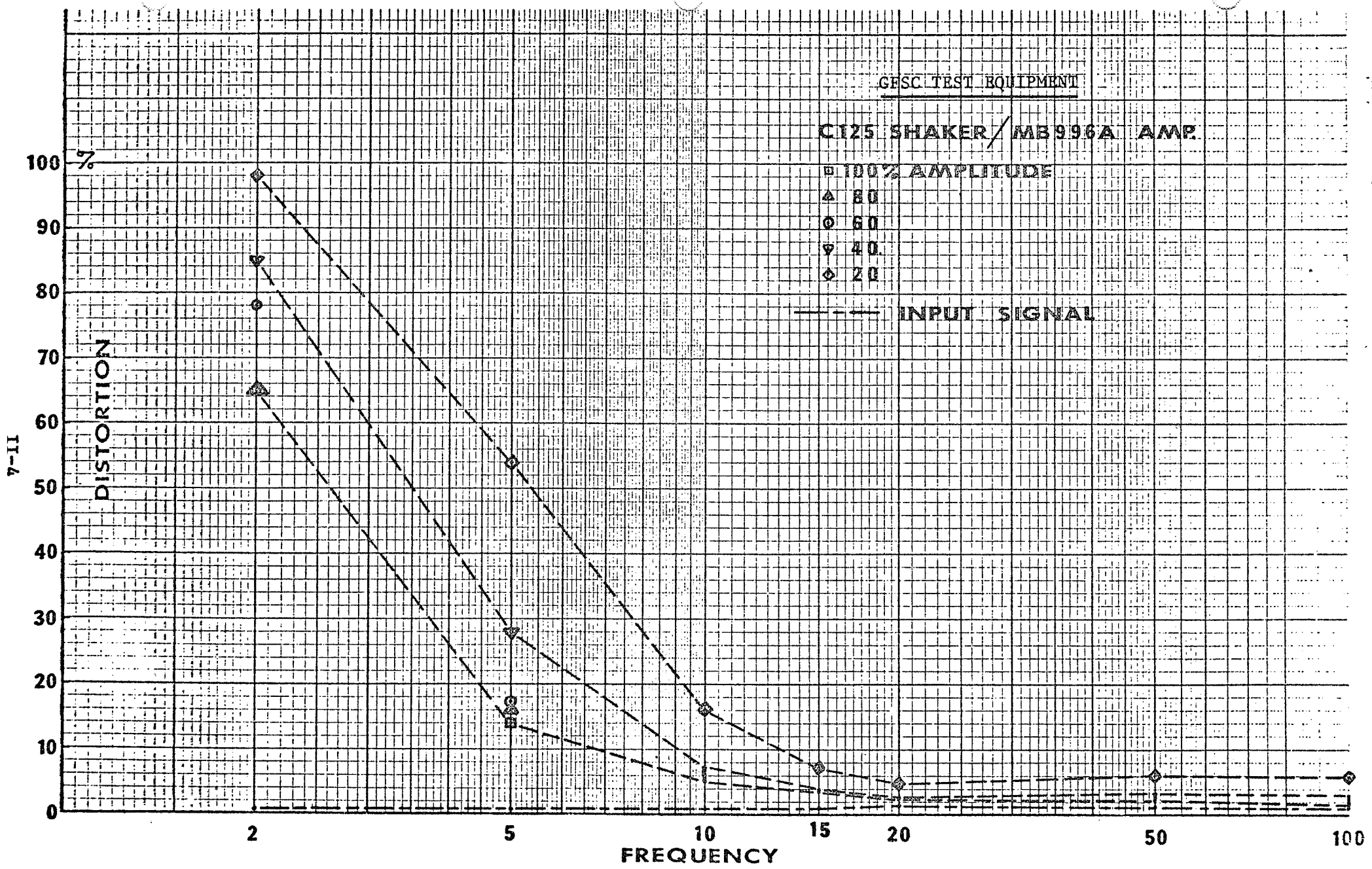



Figure II-3: VIBRATION SYSTEM DISTORTION

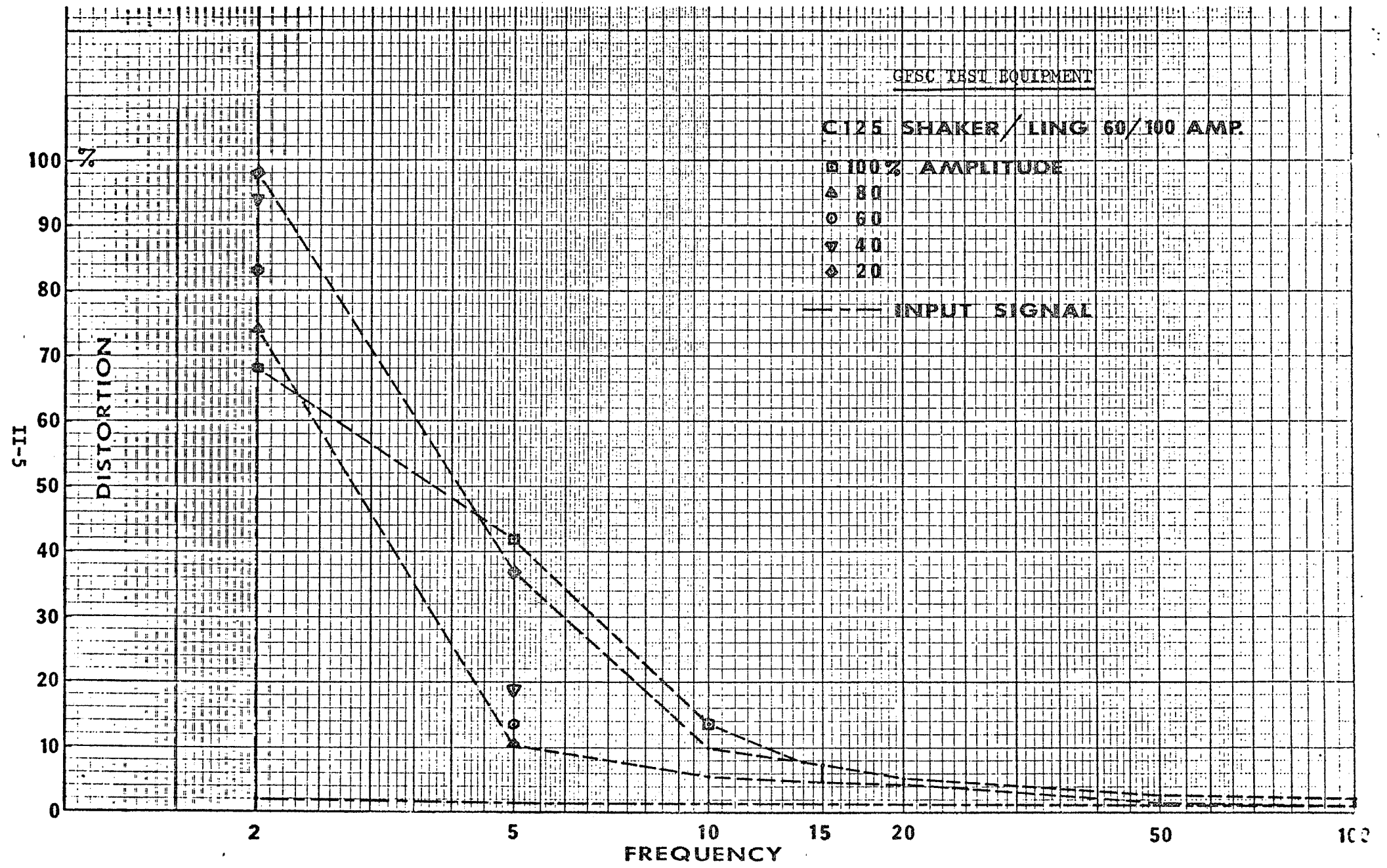



Figure II-4: VIBRATION SYSTEM DISTORTION

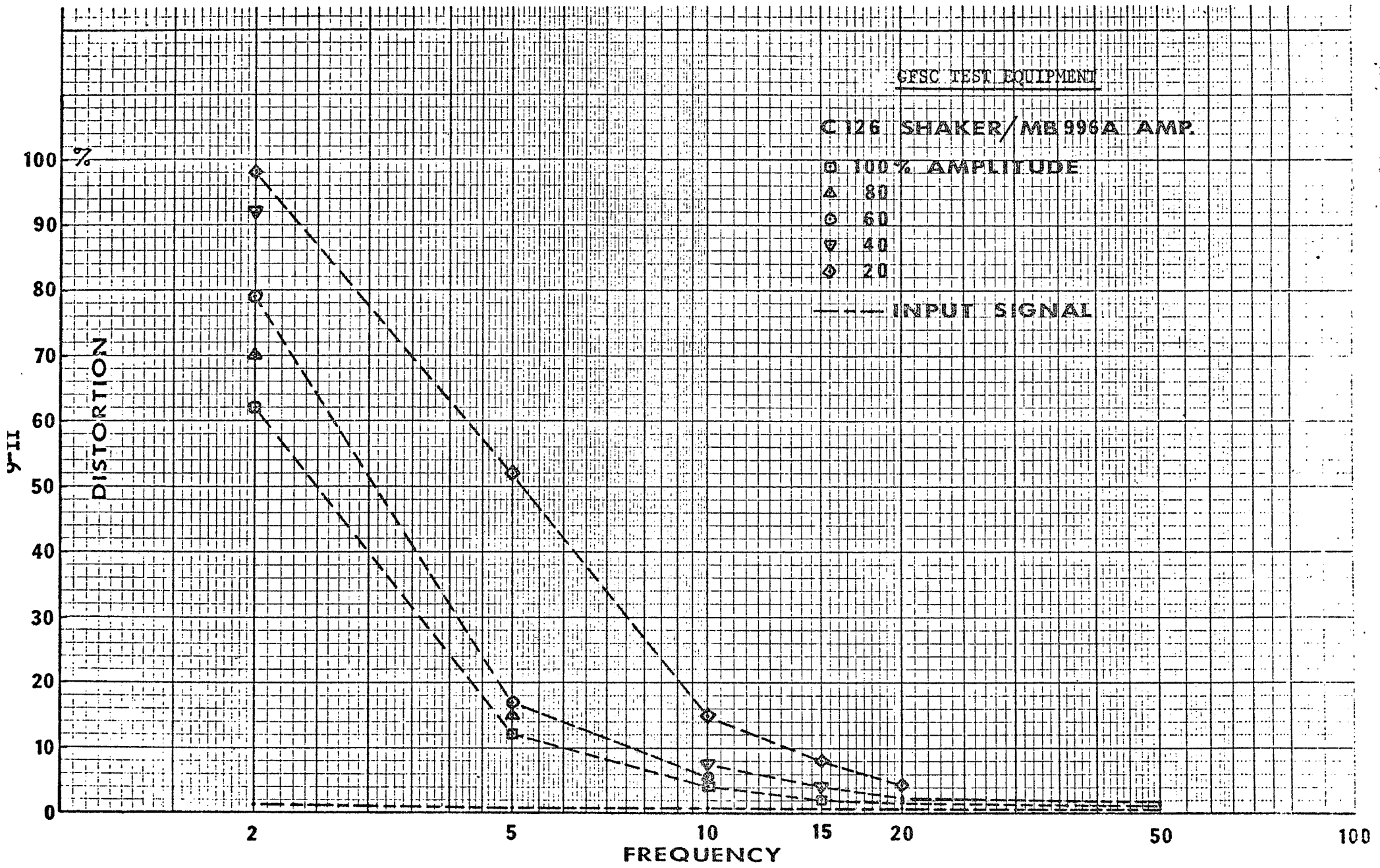



Figure II-5: VIBRATION SYSTEM DISTORTION

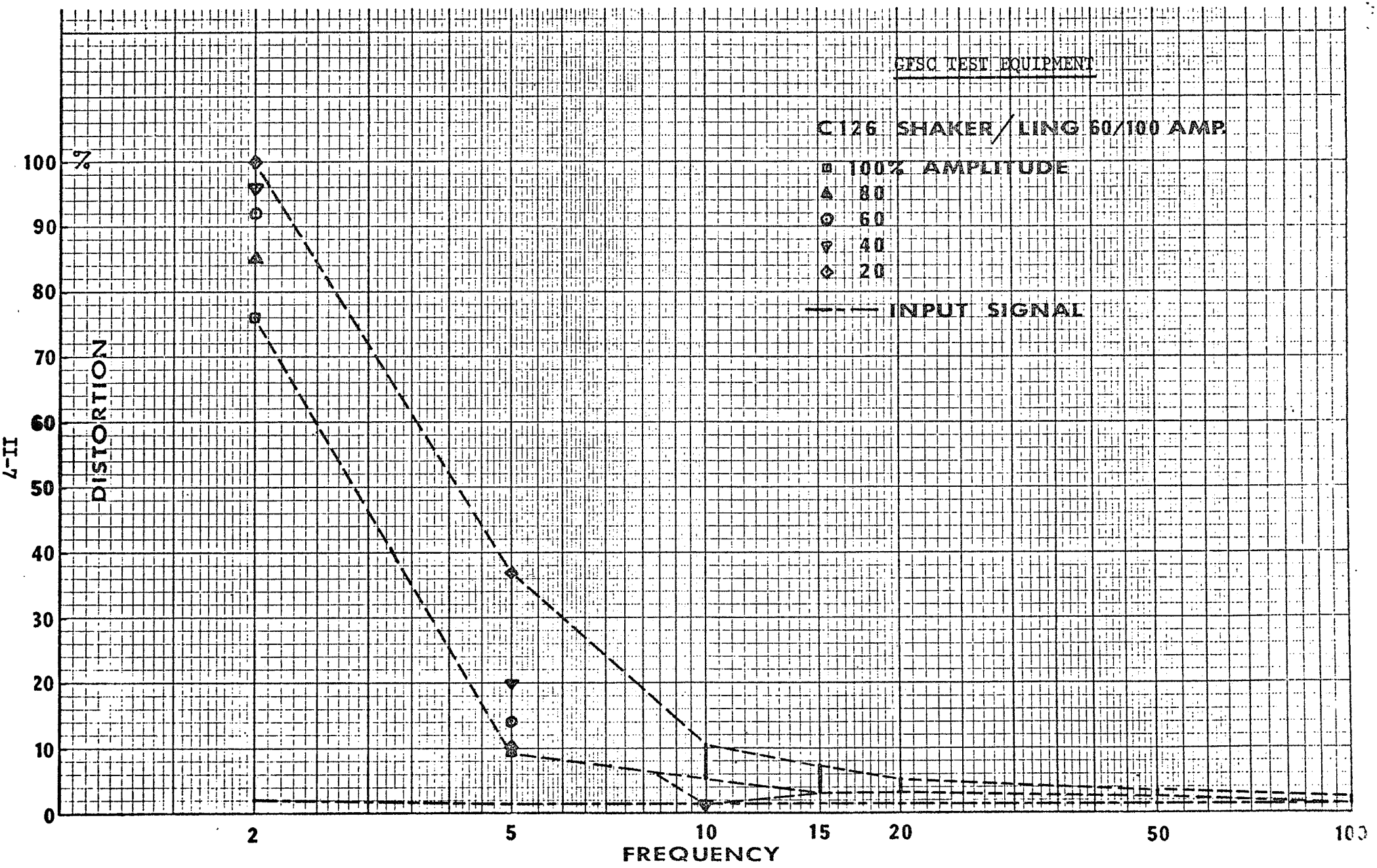



Figure II-6: VIBRATION SYSTEM DISTORTION

# APPENDIX III - STATISTICAL ANALYSIS OF THE PROTOTYPE CONTROL SYSTEM PERFORMANCE

To date, most error studies pertinent to this type of control system have been limited to investigations of errors in the transfer functions of the components comprising the system. In this feasibility study, it was virtually impossible to predict an overall system accuracy analytically (see Appendix I). This appendix presents a statistical assessment of the error bound of the transient waveform control on typical electromagnetic test equipment. The waveforms under consideration are typical transient vibration data from the TAT/Agena-D Launch Vehicle (OGO-D spacecraft):

PL-20 at T+234.5, a typical high-frequency transient, and

PL-30 at T+234.5, a typical low-frequency transient.

The experiment of waveform synthesis (identifying the above transients as "required," $f(t)_R$), was repeated with the "synthesized transient waveforms" displayed as:

1) An expanded time base comparison of the "required" and "synthesized" transient waveform (Figure III-1);
2) Time history plots, $f'(t)_R$ (Figures III-4 and III-6);
3) Frequency domain plots, $F'(\omega)_R$ (Figures III-2, III-3, III-5, and III-7);
4) Numerical listings of the time and frequency domain descriptions of $f'(t)_R$ and $F'(\omega)_R$.

The expanded time domain plots were superimposed on each other such that a visual cross-correlation could be made, and the superimposed plots (Figure III-1) were aligned such that the error, or departure from the ideal of the "required"/"synthesized" relationship, was minimized. This manual alignment of minimizing the mean squared error term between the two plots is discussed from an analytic viewpoint in Appendix I, Page 10.

The statistical error term, $(E_n)$, is defined as the difference in amplitude between the required and synthesized waveform at a discrete point in time.

$$E_n = f(t)_R - f'(t)_R$$

Operating on approximately 400 equally distributed data points, the following statistical parameters are used to further describe the error term $(E_n)$:

The mean of the error term,

$$\mu_e = \frac{1}{N} \sum_{n=1}^{N} E_n$$

indicates the zero frequency or nonalternating component of the error term and the variance of the error term, $E_n$,

$$\sigma_e^2 = \frac{1}{N-1} \sum_{n=1}^{N} (E_n - \mu_e)^2$$

indicates the mean squared value of the alternating component of the error term. The results of this analysis are tabulated below.

| | PL-20 Waveform, N = 314 G's [1] | PL-30 Waveform, N = 408 G's [2] |
|---|---|---|
| Error Mean $\mu_e$ | $-6.4 \times 10^{-4}$ | $2.318 \times 10^{-1}$ |
| Error Variance $\sigma_e^2$ | 2.283 | $8.277 \times 10^{-2}$ |
| Required Waveform Mean $\mu_e$ | $1.177 \times 10^{-1}$ | $2.63 \times 10^{-1}$ |
| Required Waveform Variance $\sigma_R^2$ | $1.887 \times 10^{1}$ | $7.157 \times 10^{-1}$ |
| Test System Noise Variance $\sigma_N^2$ | $2.7 \times 10^{-1}$ | $6.25 \times 10^{-2}$ |
| Time Domain Variance $\frac{\sigma_e^2}{\sigma_R^2} \times 100$ | 12.0% | 11.6% |

[1] Compare Figure 1-B with Figure 1-A

[2] Compare Figure III-6 with Figure III-4

Summarizing the statistical description of the bound on expected performance. A typical high-frequency transient, PL-20, exhibited a time domain variance of 12%.

A typical low-frequency transient, PL-30, exhibited a time domain variance of 11.6%.

These statistics were derived from approximately 400 equally distributed data points over the "transient" interval. Assuming a chi-square distribution of the error term, $E_n$, there is 0.99 probability that the time domain variance of the control system is equal to or less than 13%.

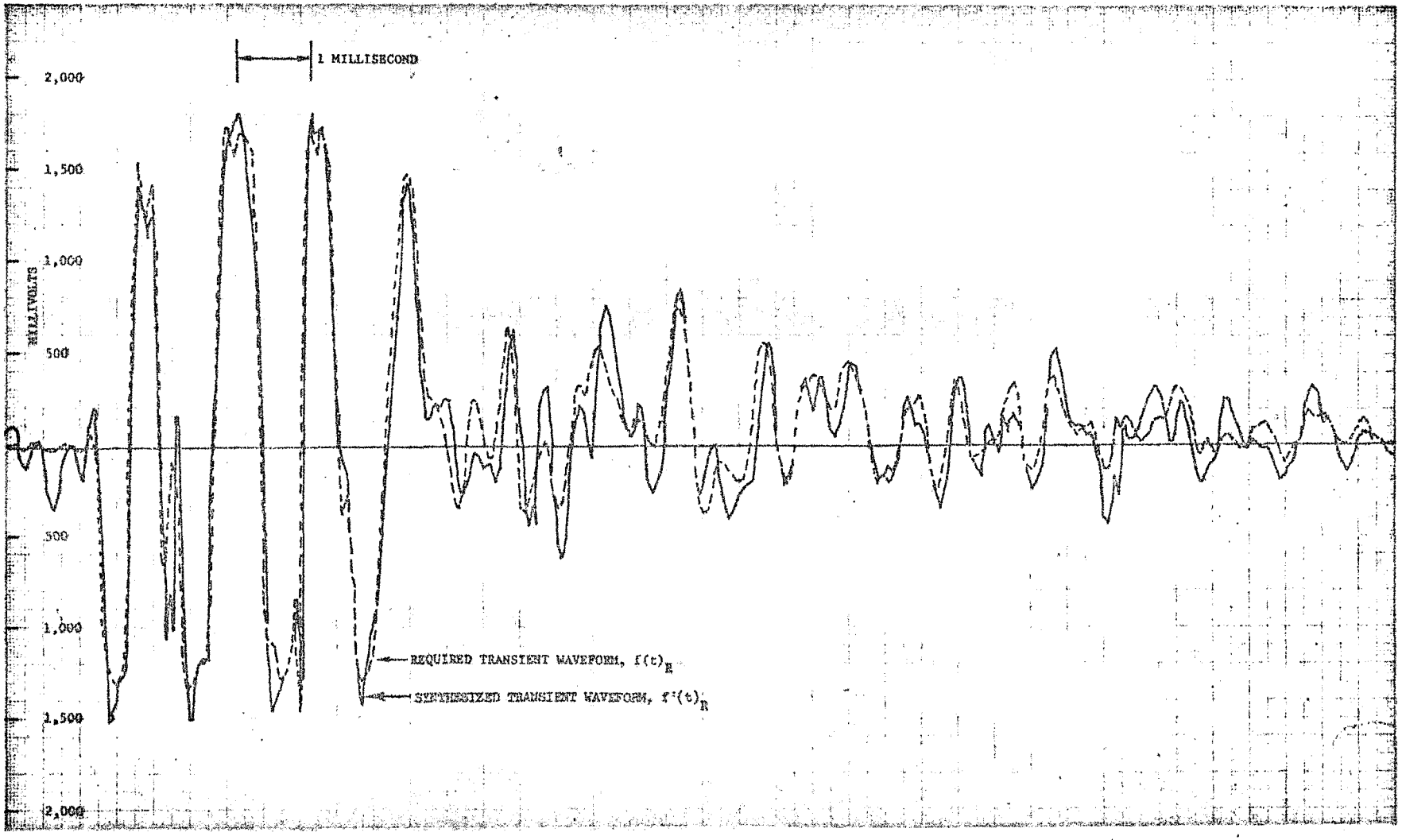



Figure 10-1: 19 MILLISECOND COMPARISON---"REQUIRED" AND "SYNTHESIZED" TRANSIENT WAVEFORM TAT/AGENA-D LAUNCH VEHICLE, (OGO-D SPACECRAFT), PL20 @ T+234.5, (Figure 1-B)

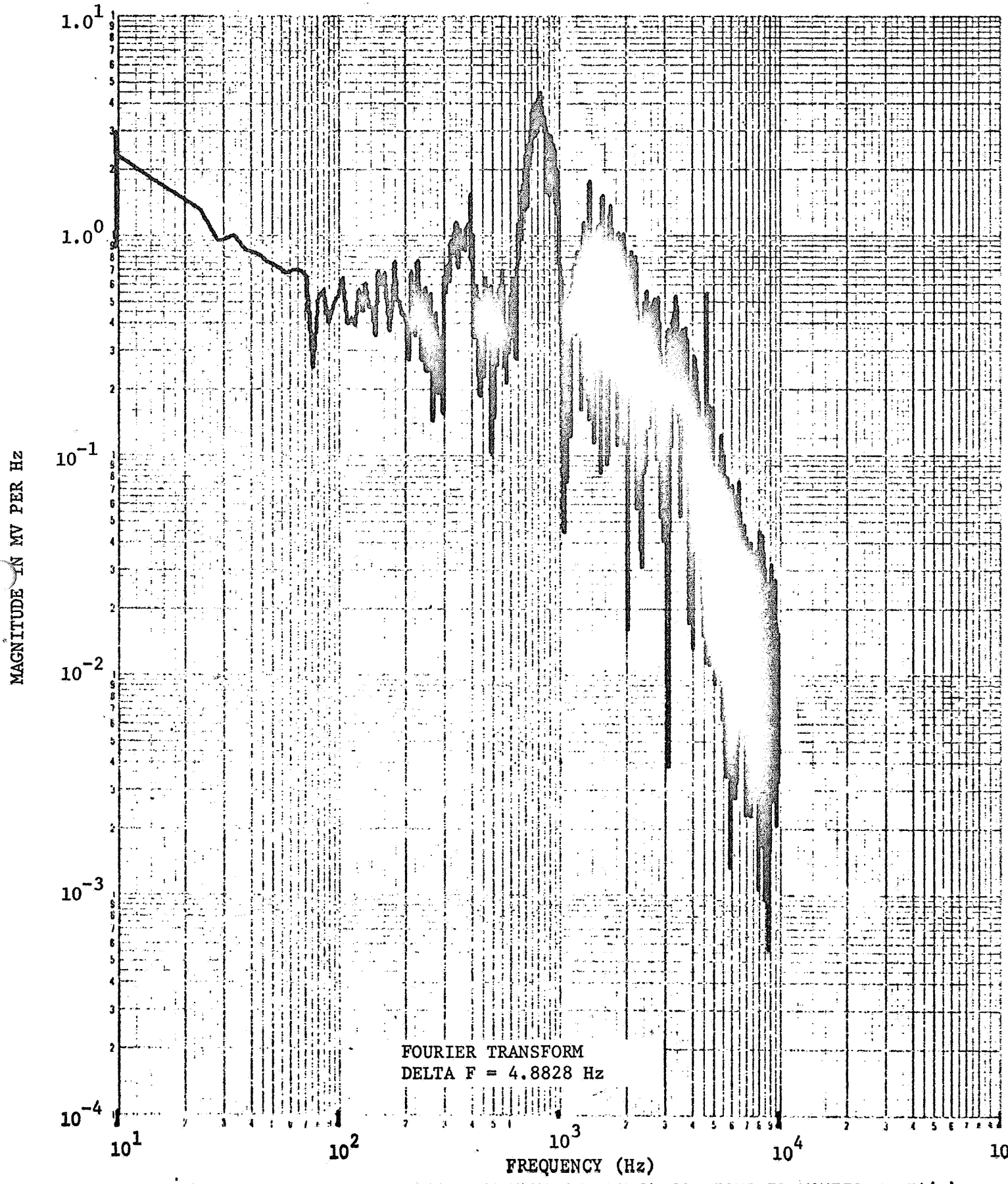



Figure III-2: FOURIER TRANSFORM MODULUS OF THE PL-20 REQUIRED WAVEFORM, $F'(\omega)_R$

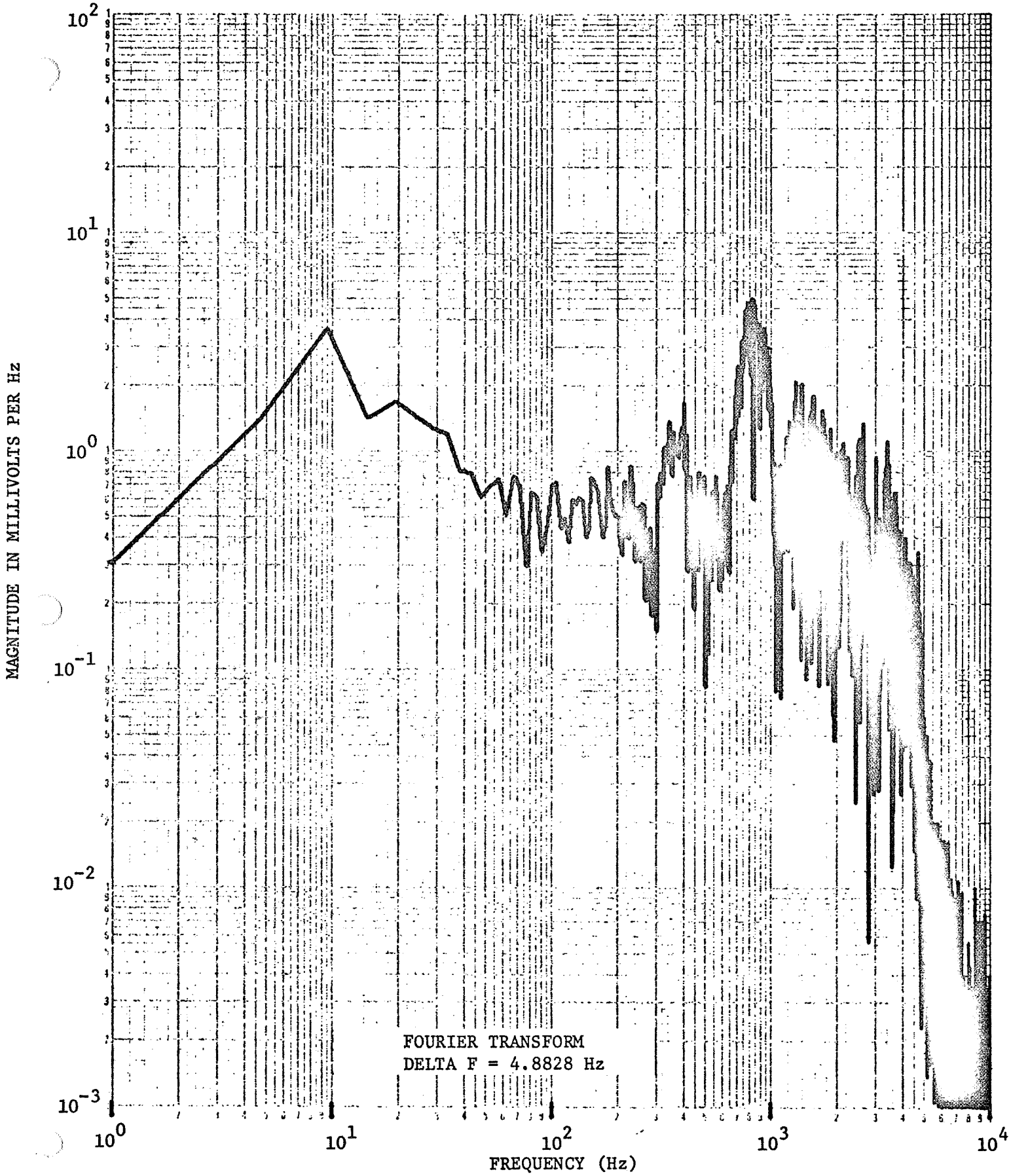



Figure III-3: FOURIER TRANSFORM MODULUS OF SYNTHESIZED WAVEFORM PL-20, $F'(\omega)_R$

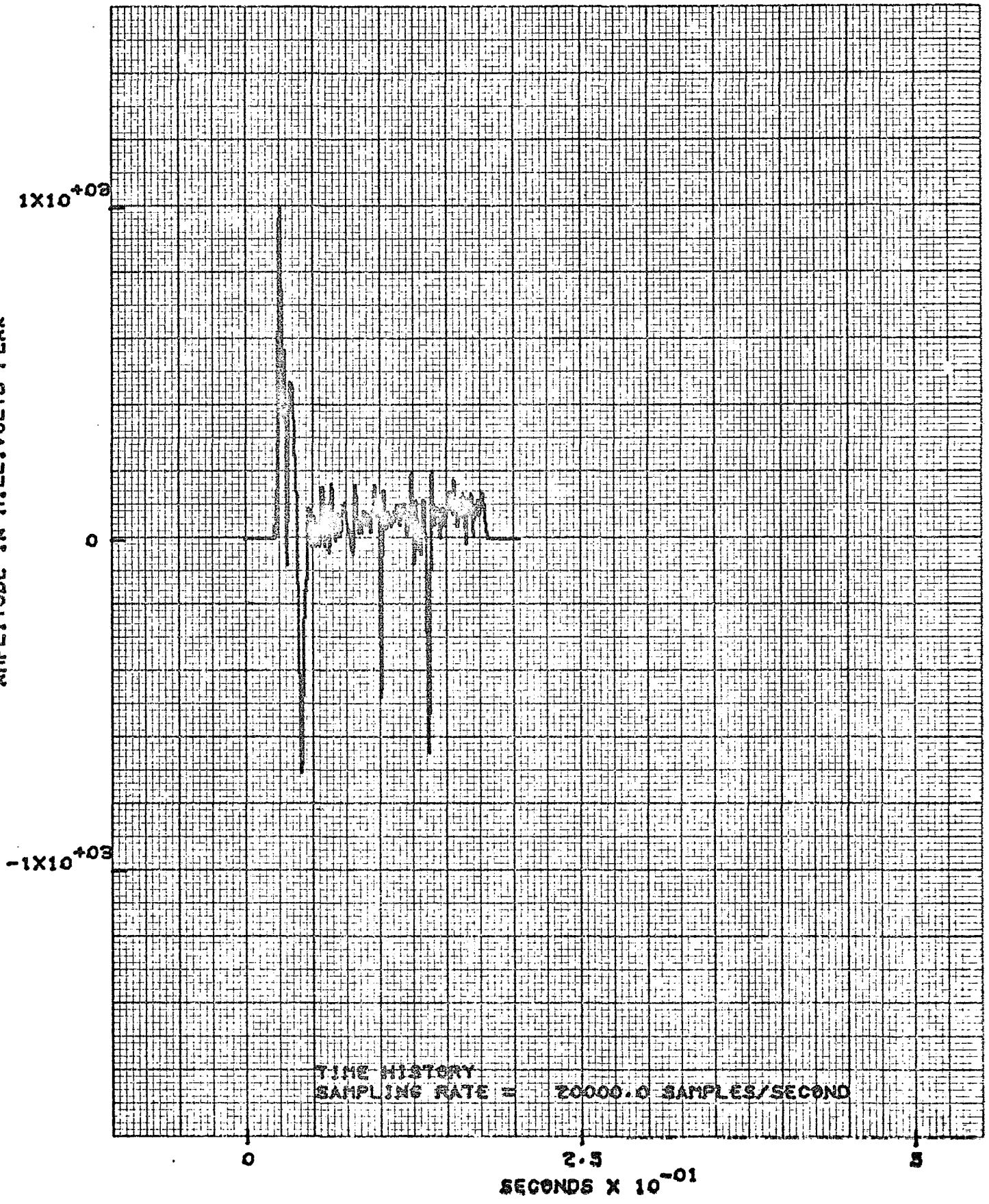



Figure III-4: TIME HISTORY OF REQUIRED WAVEFORM PL-30, $f(t)_R$

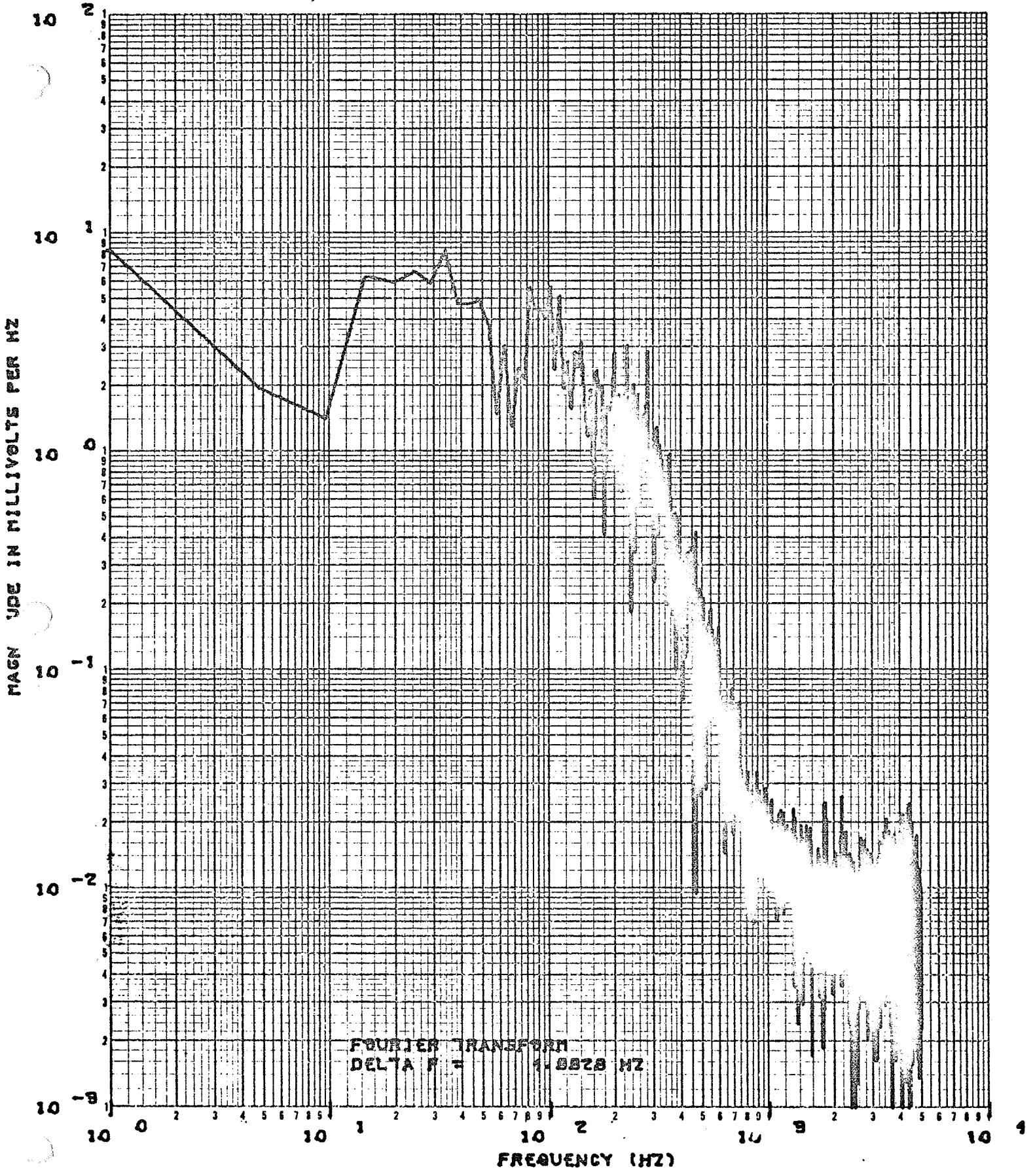



Figure III-5: FOURIER TRANSFORM MODULUS OF REQUIRED WAVEFORM PL-30, $F(\omega)_R$

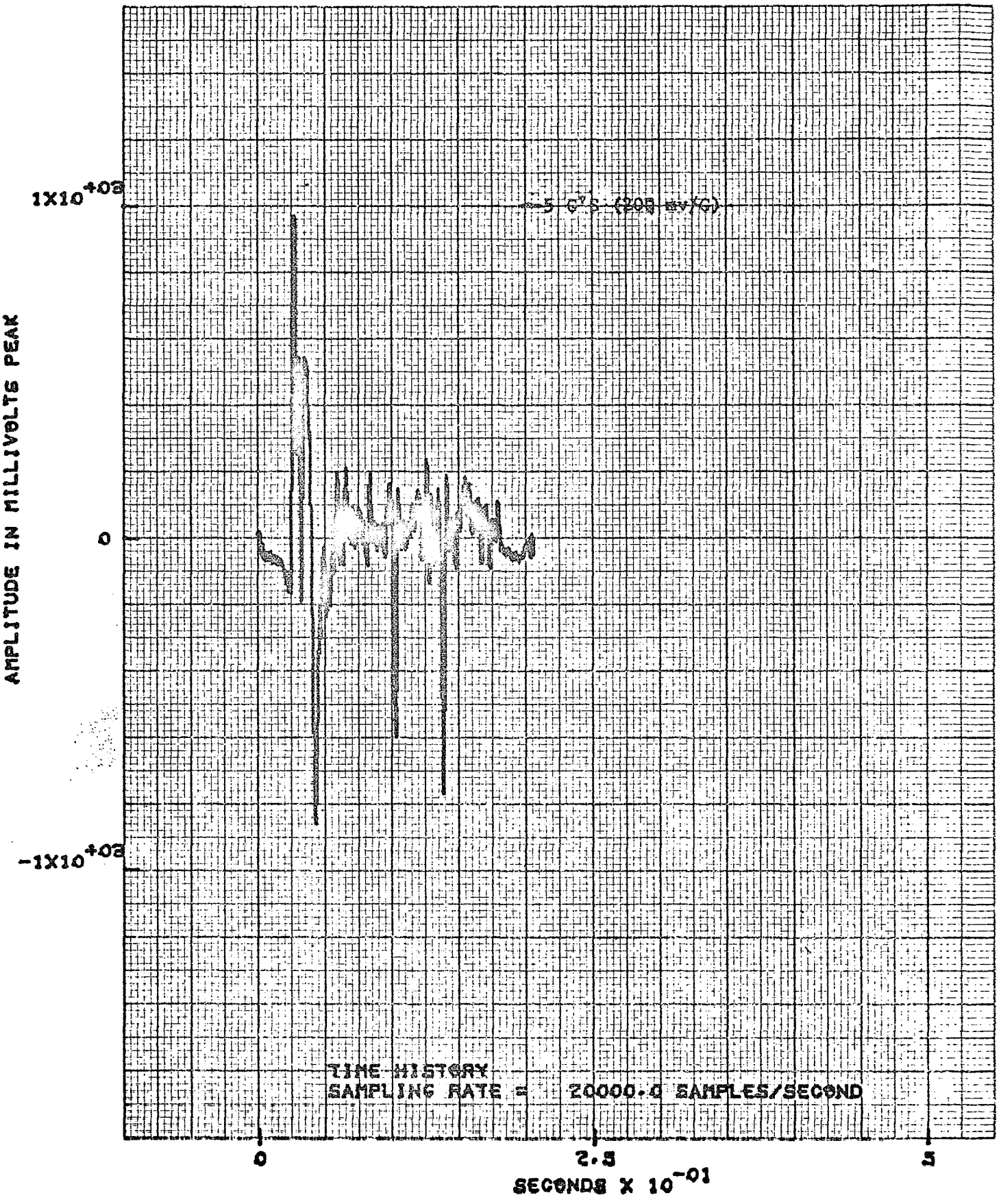



Figure III-6: TIME HISTORY OF SYNTHESIZED WAVEFORM PL-30, $f'(t)_R$

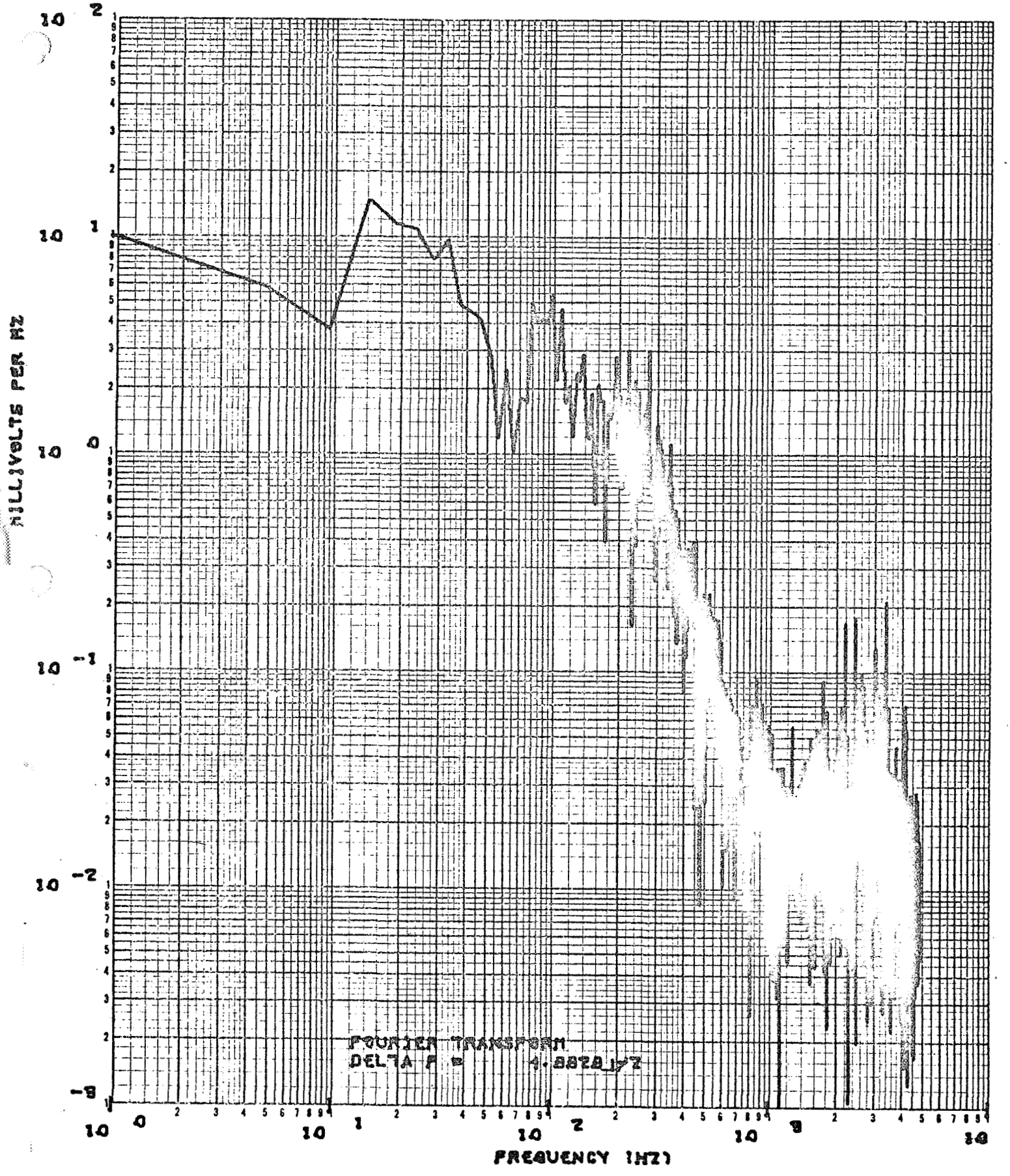



Figure III-7: FOURIER TRANSFORM MODULUS OF SYNTHESIZED WAVEFORM PL-30, $F'(\omega)_R$